



**Characterization and
Prediction of Trace Metal
Bearing Phases in ARD
Neutralization Sludges**

MEND Report 3.44.1

**This work was done on behalf of MEND and funded by The Mining
Association of Canada and MEND**

May 2013



Characterization and Prediction of Trace Metal Bearing Phases in ARD Neutralization Sludges

¹Alan Martin, ²Diana Loomer, ^{1*}Skya Fawcett, ³Andrew Rollo, ⁴Andrew Gault, ⁴Heather Jamieson, ¹Stephanie Simpson and ²Tom Al.

¹*Lorax Environmental Services Ltd., Vancouver, BC*

²*University of New Brunswick, Fredericton, NB*

³*British Columbia Ministry of Energy, Mines and Natural Gas, Victoria, BC*

⁴*Queen's University, Kingston, ON*

**Current address: Golder Associates, Calgary, AB*

Prepared for:

The Mine Environment Neutral Drainage Program

May 22, 2013



2289 Burrard Street
Vancouver, BC, Canada
V6J 3H9
1-604-688-7173

Executive Summary

Lime addition is a common method for the treatment of acid rock drainage (ARD) whereby neutralization promotes a reduction in acidity and the precipitation of metals as voluminous sludges that may contain gypsum, calcite, Fe-oxides and a spectrum of other phases. Due to the extremely fine-grained and often amorphous (*i.e.*, non crystalline) character of sludge solids, the composition of these materials has been difficult to elucidate. Traditional methods such as X-Ray Diffraction (XRD) and optical microscopy, for example, have proved largely ineffective. In order to provide further insight into the solid-phase characterization of neutralization sludges, high density sludge (HDS) materials from seven mine sites across Canada were examined by high resolution microscopy techniques in combination with influent and effluent characterization. The primary objectives of the study were to: 1) define the nature of metal phase associations in sludge materials; 2) define the links between ARD influent/effluent chemistry, treatment process and sludge composition; and 3) provide the basis from which to develop a sludge management framework from the perspective of long-term chemical stability.

High resolution microscopy methods utilized included Scanning Electron Microscopy (SEM), Scanning Transmission Electron Microscopy (STEM), and X-ray Absorption Near Edge Structure (XANES). SEM, and in particular STEM, provided the spatial resolution required to resolve the trace-metal associations in the sludge samples. With respect to XANES, there is a general absence of suitable model compounds analogous to many of the sludge phases examined, and as a result, the applicability of XANES to discern metal-associations in sludge samples is currently limited. However, the XANES data acquired for Zn offer insight into the potential stability of Zn through differentiation of potentially labile and non-labile complexes.

Predictably, SO_4 was a dominant component in all ARD influents. However, considerable variability was observed with respect to other major parameters. Dominant influent chemistries on a molar basis included $\text{SO}_4 > \text{Mg} > \text{Al} > \text{Fe} > \text{Ca} > \text{Cl} > \text{F} > \text{Mn} > \text{Zn}$ (Equity Mine), $\text{SO}_4 > \text{Fe} > \text{Ca} \approx \text{Mg}$ (Geco Mine), $\text{SO}_4 > \text{Ca} > \text{Mg} > \text{Al} > \text{Cl} > \text{Cu} \approx \text{Zn}$ (Britannia Mine), $\text{Na} > \text{SO}_4 > \text{Mg} > \text{Ca} = \text{Cl} > \text{Zn}$ (Brunswick Mine), $\text{Cl} > \text{Na} > \text{Ca} > \text{SO}_4 > \text{Mg} > \text{Zn}$ (Chisel North Mine), $\text{SO}_4 > \text{Mg} > \text{Ca} > \text{Fe} > \text{Zn}$ (Samatosum Mine) and $\text{SO}_4 > \text{Mg} > \text{Ca} > \text{Fe} > \text{Na} = \text{Cl}$ (Sullivan Mine). Outflow compositions showed uniformly circum-neutral pH and greatly reduced values for Fe, Mn, Al and trace elements (*e.g.*, Zn, Cu). In some cases, values for major species also showed pronounced declines through the HDS process, including SO_4 (Equity, Geco, Samatosum) and Mg (Equity, Samatosum and Sullivan).

Treatment sludges show variable elemental compositions, but in all cases, the elemental abundances can be linked to ARD influent chemistry. Crystalline materials identified by XRD include calcite or Mg-calcite (Britannia, Brunswick, Chisel, Samatosum and Sullivan Mines) and gypsum (Equity, Geco, Samatosum and Sullivan). However, none of these phases were shown to be significant repositories for precipitated trace metals.

SEM and STEM data demonstrate that the trace metal-bearing phases in the HDS materials are amorphous or poorly crystalline, and variable in composition (relatively pure to highly heterogeneous). The trace metal host phases are invariably fine-grained, often occurring as oval aggregates ranging in size from <5 to 20 μm , and interspersed with other non-metal-bearing material (*e.g.*, gypsum). Compositional zonation, often in concentric layers, is common, with the zones showing contrasting major ion signatures (*e.g.*, Fe, Mg, Al). Such zonation is predicted to result from the recycling of sludge within the HDS process.

The dominant metal-bearing phases were site-specific, and included relatively pure Fe-oxyhydroxide (Geco Mine), amorphous Mg-Al(Fe) hydroxysulfate (Equity Mine), Zn-Cu oxyhydroxide (Britannia Mine), Zn-Fe-Mn oxyhydroxide (Brunswick and Chisel North Mines), and Fe-Mg oxyhydroxide (Samatosum and Sullivan Mines). For all HDS samples, selected area electron diffraction patterns revealed broad diffuse rings, consistent with poorly crystalline to amorphous phases. Zn K-edge x-ray absorption near-edge structure (XANES) spectra revealed a mixture of labile (outer-sphere complexes) and less labile (structurally incorporated) Zn species.

The data indicate that the nature of the dominant metal-bearing phase in the HDS materials is strongly dependent on ARD influent chemistry, with both the concentrations and relative proportions of Fe, Mg, Mn, Al and SO_4 being dominant variables. In this manner, the results of the assessment highlight the potential for the development of a sludge management framework, which may permit prediction of “sludge type” from the ARD composition. In order to develop a defensible framework, further sludge characterization would be required to assess both within-mine and between-mine variability. A further requirement would also be a detailed understanding of the chemical stability of the various sludge types in varying depositional environments. Currently, there is not sufficient information available from which to assess the chemical stability of the various trace metal-bearing phases identified in this study. Given the substantial contrasts in the nature of the various metal-hosting phases, significant differences in chemical stability can be expected. In order for a potential framework to be applied successfully, sludge chemical stability as a function of varying pH and redox conditions must be established. This would be best achieved through the *in situ* collection of sludge porewaters and laboratory studies designed to assess pH- and pE-dependent solubility controls.

Sommaire

L'ajout de chaux est une méthode courante pour le traitement du drainage rocheux acide (DRA), cette neutralisation favorisant une réduction de l'acidité et la précipitation des métaux dans des boues abondantes pouvant contenir du gypse, de la calcite, des oxydes de fer et toute une gamme d'autres phases. En raison de la granulométrie extrêmement fine et du caractère souvent amorphe (non cristallin) des solides contenus dans ces boues, la composition de ces matières est difficile à élucider. Les méthodes classiques, comme la diffraction X (XRD) et la microscopie optique par exemple, se sont avérées largement inefficaces. Afin d'obtenir plus de renseignements sur la caractérisation de la phase solide des boues de neutralisation, nous avons étudié des boues de haute densité (BHD) provenant de sept sites miniers à travers le Canada, à l'aide de techniques de microscopie haute résolution en combinaison avec la caractérisation de l'influent et de l'effluent. Les principaux objectifs de la présente étude étaient : 1) de définir la nature des associations de phases métalliques présentes dans les boues, et ; 2) de définir les liens entre la chimie de l'influent/effluent du DRA, le procédé de traitement et la composition de la boue; 3) de fournir la base à partir de laquelle développer un cadre de gestion des boues dans la perspective d'une stabilité chimique à long terme.

Parmi les méthodes de microscopie haute résolution utilisées, il y avait la microscopie électronique à balayage (MEB), la microscopie électronique à balayage par transmission (MEBT) et la spectroscopie de structure près du front d'absorption X (XANES pour X ray Absorption Near Edge Structure). La MEB et, en particulier, la MEBT ont permis d'obtenir la résolution spatiale requise pour résoudre les associations trace-métal dans les échantillons de boue. En ce qui concerne la XANES, il y a une absence générale de composés modèles pertinents analogues à la plupart des phases de boue examinées et, en conséquence, l'applicabilité de la XANES pour différencier les associations métalliques dans les échantillons de boue est actuellement limitée. Toutefois, les données acquises en XANES pour le Zn donnent des renseignements sur la stabilité potentielle du Zn grâce à la différenciation de complexes potentiellement labiles ou non.

Comme prévu, SO_4 était un élément dominant de tous les influents de DRA. Toutefois, nous avons pu observer une très grande variabilité des autres paramètres principaux. Parmi les chimies dominantes de l'influent, sur une base molaire, on retrouvait :

$\text{SO}_4 >> \text{Mg} > \text{Al} > \text{Fe} >> \text{Ca} > \text{Cl} > \text{F} > \text{Mn} > \text{Zn}$ (Equity Mine),

$\text{SO}_4 > \text{Fe} >> \text{Ca} = \text{Mg}$ (Geco Mine),

$\text{SO}_4 > \text{Ca} > \text{Mg} >> \text{Al} > \text{Cl} > \text{Cu} \Rightarrow \text{Zn}$ (Britannia Mine),

$\text{Na} > \text{SO}_4 > \text{Mg} > \text{Ca} = \text{Cl} > \text{Zn}$ (Brunswick Mine),

$\text{Cl} > \text{Na} > \text{Ca} > \text{SO}_4 > \text{Mg} > \text{Zn}$ (Chisel North Mine),

SO₄>Mg>Ca>Fe>Zn (Samatosum Mine) et

SO₄>Mg>>Ca>Fe>Na=Cl (Sullivan Mine).

Les compositions de l'écoulement étaient uniformément d'un pH neutre et avaient des valeurs grandement réduites en Fe, Mn, Al et les éléments traces (p. ex. Zn, Cu). Dans certains cas, les valeurs pour les espèces principales ont aussi exhibé des déclinés prononcés avec le procédé BHD, y compris en SO₄ (Equity, Geco et Samatosum) et pour Mg (Equity, Samatosum et Sullivan).

Les boues de traitement ont exhibé des compositions élémentaires variables, mais dans tous les cas les abondances élémentaires peuvent être liées à la chimie de l'influent du DRA. Parmi les matières cristallines identifiées par XRD, nous avons retrouvé la calcite ou la calcite-Mg (Britannia, Brunswick, Chisel, Samatosum et Sullivan) et le gypse (Equity, Geco, Samatosum et Sullivan). Toutefois, aucune de ces phases ne s'est avérée être un dépôt significatif pour les métalliques précipités.

La MEB et la MEBT ont permis de montrer que les phases comportant des métaux traces présentes dans les matières BHD étaient amorphes ou peu cristallisées, et de composition variable (allant de relativement pure à fortement hétérogène). Les phases abritant les métaux traces avaient invariablement une granulométrie fine, souvent sous forme d'agrégats ovales de taille allant de < 5 à 20 µm, et disséminées avec d'autres matières ne comportant pas de métal (p. ex. gypse). La zonalité compositionnelle, souvent en couches concentriques, est commune, les zones comportant des signatures des ions principaux contrastantes (p. ex. Fe, Mg, Al). Nous pensons qu'une telle zonalité est le résultat du recyclage de la boue lors du procédé BHD.

Les phases dominantes comportant des métaux étaient spécifiques au site et comprenaient de l'oxyhydrure de Fe pur (Geco), de l'hydroxysulfate de Mg-Al-(Fe) amorphe (Equity), de l'oxyhydrure de Zn-Cu (Britannia), de l'oxyhydrure de Zn-Fe-Mn (Brunswick et Chisel North) et de l'oxyhydrure de Fe-Mg (Samatosum et Sullivan). Pour tous les échantillons BHD, les diagrammes de diffraction électronique de zones sélectionnées ont révélé de larges anneaux diffus, en accord avec les phases amorphes et peu cristallisées. Les spectres XANES de la structure K du Zn ont révélé un mélange d'espèces du Zn labiles (complexes de sphère extrême) et moins labiles (incorporées dans la structure).

Les données indiquent que la nature de la phase dominante comportant des métaux présente dans les matières BHD est fortement dépendante de la chimie de l'influent de DRA, les concentrations et les proportions relatives de Fe, Mg, Mn, Al et SO₄ étant les variables dominantes. Ainsi, les résultats de la présente évaluation soulignent le potentiel pour le développement d'un cadre de gestion des boues qui peut permettre de prédire le type de boue à partir de la composition du DRA. Afin de développer un cadre défendable, une caractérisation de la boue plus poussée serait requise afin d'évaluer sa variabilité dans une même mine et d'une mine à une autre. Une autre exigence serait aussi d'avoir

une compréhension détaillée de la stabilité chimique des divers types de boue dans des environnements de dépôt variables. Actuellement, nous ne disposons pas d'assez de renseignements pour évaluer la stabilité chimique des diverses phases comportant des métaux traces identifiées dans la présente étude. Étant donné les contrastes marqués entre la nature des diverses phases comportant des métaux traces, on peut s'attendre à des différences significatives de la stabilité chimique. Pour qu'un cadre potentiel puisse être appliqué avec succès, la stabilité chimique de la boue en fonction du pH et des conditions redox doit être établie. À cette fin, il serait préférable de faire la collecte in situ d'eaux interstitielles de boue et des études en laboratoire pour déterminer les paramètres de solubilité dépendants du pH et du pE.

Acknowledgements

This study was based on a collaborative approach involving the Mine Environmental Neutral Drainage (MEND) Program, several Canadian mining companies, Lorax Environmental Services Ltd., the University of New Brunswick, Queens University and the Canadian Light Source. The authors wish to acknowledge the funding provided by the Mine Environmental Neutral Drainage (MEND) Program. Particular thanks go to Gilles Tremblay and Charlene Hogan (Natural Resources Canada/MEND) for their coordination and support, as well as to Janice Zinck (NRCan) for her insight on the topic of neutralization sludges. Completion of this study would not have been possible without the financial support and cooperation of the participating mines. In this regard, we would like to acknowledge: Mike Aziz (Goldcorp Inc., Equity Division); Manon Richard, Rick Schwenger, James Cormier and Robert Prairie (Xstrata Zinc); Christian Madsen (EPCOR); Walter Kuit, Dave Van Dieren, Bruce Dawson and Dana Haggar (Teck); Stephen West and James Dauk (Hudson Bay Mining and Smelting); Brent Hamblin (Inmet); and Geoff Sinnett and Katherine O’Leary (B.C. Ministry of Forests, Lands and Natural Resource Operations). An initial draft of this document also greatly benefited by reviews from Charlene Hogan (MEND), Mike Aziz (Goldcorp) Bill Price (NRCan) and David Chambers (Center for Science in Public Participation).

Table of Contents

EXECUTIVE SUMMARY	I
SOMMAIRE	III
ACKNOWLEDGEMENTS.....	VI
TABLE OF CONTENTS	VII
LIST OF ACRONYMS.....	XIII
1. INTRODUCTION.....	1-1
1.1 OVERVIEW	1-1
1.2 PROJECT BACKGROUND AND OBJECTIVES	1-2
1.3 REPORT STRUCTURE	1-3
2. BACKGROUND AND METHODS	2-1
2.1 OVERVIEW OF LIME TREATMENT.....	2-1
2.1.1 CONVENTIONAL LIME TREATMENT (LDS)	2-1
2.1.2 HIGH DENSITY SLUDGE (HDS) PROCESS.....	2-2
2.2 STUDY SITES.....	2-2
2.2.1 EQUITY MINE	2-4
2.2.2 GECO MINE.....	2-6
2.2.3 BRITANNIA MINE.....	2-7
2.2.4 BRUNSWICK MINE	2-8
2.2.5 CHISEL NORTH MINE.....	2-10
2.2.6 SAMATOSUM MINE	2-11
2.2.7 SULLIVAN MINE	2-12
2.3 SAMPLE COLLECTION	2-14
2.3.1 WATER SAMPLES.....	2-14
2.3.2 SLUDGE SAMPLES	2-15
2.4 ANALYTICAL METHODS.....	2-15
2.4.1 WATER SAMPLES.....	2-15
2.4.2 SLUDGE SOLIDS	2-17
2.4.2.1 BULK CHEMISTRY AND TRACE METALS ANALYSIS	2-18
2.4.2.2 X-RAY DIFFRACTION	2-18
2.4.2.3 SCANNING ELECTRON MICROSCOPY	2-19
2.4.2.4 SCANNING TRANSMISSION ELECTRON MICROSCOPY	2-19
2.4.2.5 X-RAY ABSORPTION SPECTROSCOPY.....	2-20
3. RESULTS AND DISCUSSION	3-1
3.1 WATER SAMPLES.....	3-1
3.1.1 INFLUENT AND EFFLUENT CHEMISTRY	3-1
3.1.1.1 EQUITY MINE.....	3-1
3.1.1.2 GECO MINE.....	3-6
3.1.1.3 BRITANNIA MINE	3-6
3.1.1.4 BRUNSWICK MINE	3-6
3.1.1.5 CHISEL NORTH MINE	3-7
3.1.1.6 SAMATOSUM MINE	3-7
3.1.1.7 SULLIVAN MINE.....	3-8
3.1.2 SATURATION INDICES (PHREEQC).....	3-8
3.2 SLUDGE SOLIDS	3-10
3.2.1 MULTI-ELEMENT CHEMICAL ANALYSES	3-10

3.2.1.1	EQUITY SLUDGE.....	3-13
3.2.1.2	GECO SLUDGE.....	3-13
3.2.1.3	BRITANNIA SLUDGE.....	3-13
3.2.1.4	BRUNSWICK SLUDGE.....	3-14
3.2.1.5	CHISEL NORTH SLUDGE.....	3-14
3.2.1.6	SAMATOSUM SLUDGE.....	3-14
3.2.1.7	SULLIVAN SLUDGE.....	3-15
3.2.2	IDENTIFICATION OF CRYSTALLINE PHASES IN SLUDGE SAMPLES (XRD).....	3-15
3.2.3	IDENTIFICATION OF DOMINANT AND TRACE METAL-BEARING PHASES IN SLUDGE SAMPLES (SEM AND STEM).....	3-16
3.2.3.1	EQUITY SLUDGE.....	3-17
3.2.3.2	GECO SLUDGE.....	3-25
3.2.3.3	BRITANNIA SLUDGE.....	3-29
3.2.3.4	BRUNSWICK SLUDGE.....	3-36
3.2.3.5	CHISEL NORTH SLUDGE.....	3-41
3.2.3.6	SAMATOSUM SLUDGE.....	3-50
3.2.3.7	SULLIVAN SLUDGE.....	3-56
3.2.4	X-RAY ABSORPTION NEAR EDGE STRUCTURE (XANES).....	3-65
3.2.4.1	EQUITY SLUDGE.....	3-66
3.2.4.2	GECO SLUDGE.....	3-68
3.2.4.3	BRITANNIA SLUDGE.....	3-68
3.2.4.4	BRUNSWICK SLUDGE.....	3-69
3.2.4.5	CHISEL NORTH SLUDGE.....	3-69
3.2.4.6	SAMATOSUM SLUDGE.....	3-70
3.2.4.7	SULLIVAN SLUDGE.....	3-70
4.	SUMMARY AND IMPLICATIONS FOR SLUDGE CHEMICAL STABILITY.....	4-1
4.1	SUMMARY OF DATA.....	4-1
4.1.1	EQUITY MINE.....	4-1
4.1.2	GECO MINE.....	4-2
4.1.3	BRITANNIA MINE.....	4-3
4.1.4	BRUNSWICK MINE.....	4-4
4.1.5	CHISEL NORTH MINE.....	4-4
4.1.6	SAMATOSUM MINE.....	4-5
4.1.7	SULLIVAN MINE.....	4-5
4.2	PREDICTION OF SLUDGE TYPE.....	4-6
4.3	GENERAL CONSIDERATIONS FOR SLUDGE CHEMICAL STABILITY.....	4-10
4.3.1	OVERVIEW.....	4-10
4.3.2	EQUITY MINE (OPEN PIT LAKE).....	4-12
4.3.3	GECO, BRUNSWICK AND SAMATOSUM MINES (SUBAERIAL SLUDGE CELLS).....	4-13
4.3.4	BRITANNIA AND SULLIVAN MINES (HOLDING PONDS).....	4-14
4.3.5	CHISEL NORTH MINE (UNDERGROUND SUBMERGED STORAGE).....	4-15
4.4	RECOMMENDATIONS FOR FUTURE WORK.....	4-15
5.	CONCLUSIONS.....	5-1
	REFERENCES.....	R-1

LIST OF APPENDICES:

APPENDIX A: INFLUENT AND EFFLUENT CHEMISTRY

APPENDIX B: SOLID PHASE ELEMENTAL ABUNDANCE

LIST OF FIGURES

FIGURE 2-1	GENERALIZED SCHEMATIC OF CONVENTIONAL LOW DENSITY SLUDGE LIME TREATMENT PLANT (AUBÉ, 2005).....	2-1
FIGURE 2-2	GENERALIZED SCHEMATIC OF CONVENTIONAL HIGH DENSITY SLUDGE (HDS) TREATMENT PROCESS (AUBÉ, 2005).....	2-2
FIGURE 2-3	MAP OF CANADA SHOWING LOCATIONS OF EQUITY, GECO, BRITANNIA, BRUNSWICK, CHISEL NORTH, SAMATOSUM, AND SULLIVAN MINES (MODIFIED FROM NRC, 2001).....	2-3
FIGURE 2-4	GENERALIZED SCHEMATIC OF HEATH STEELE HIGH DENSITY SLUDGE (HDS) TREATMENT PROCESS (AUBÉ, 2005).....	2-5
FIGURE 2-5	GENERALIZED FLOW CHART FOR THE BRITANNIA MINE HDS TREATMENT PROCESS.....	2-7
FIGURE 2-6	GENERALIZED FLOW CHART FOR THE BRUNSWICK MINE ARD LIME TREATMENT PROCESS.	2-9
FIGURE 2-7	GENERALIZED FLOW CHART FOR THE CHISEL NORTH MINE HDS TREATMENT PROCESS..	2-11
FIGURE 2-8	GENERALIZED FLOW CHART FOR THE SAMATOSUM MINE ARD LIME TREATMENT PROCESS.	2-12
FIGURE 2-9	GENERALIZED FLOW CHART FOR THE SULLIVAN MINE ARD LIME TREATMENT PROCESS.	2-14
FIGURE 2-10	PHOTOGRAPHS OF DRIED SLUDGE HDS SAMPLES. PHOTO FOR CHISEL NORTH HDS NOT AVAILABLE.....	2-16
FIGURE 2-11	SCHEMATIC SHOWING INCREASING SPATIAL RESOLUTION ASSOCIATED WITH OPTICAL MICSCROSCOPY, SCANNING ELECTRON MISCROSCOPY (SEM), SCANNING TRANSMISSION ELECTON MICROSCOPY (STEM) AND X-RAY ABSORPTION SPECTROSCOPY (XAS).	2-18
FIGURE 2-12	X-RAY ABSORPTIONS SPECTROSCOPY: ILLUSTRATION (COURTESY OF THE CANADIAN LIGHT SOURCE) OF THE INTERACTION OF THE PHOTOELECTRON WAVE WITH SURROUNDING ATOMS AND THE RESULTING SPECTRA PRODUCED.	2-21
FIGURE 3-1	MAJOR ION PARAMETERS AND pH IN INFLUENT (ARD FEED) AND EFFLUENT (TREATED CLARIFIER) SAMPLES FOR EQUITY MINE, GECO MINE, BRITANNIA MINE (BRIT.), BRUNSWICK MINE (BRUNS.), CHISEL NORTH MINE (CHISEL), SAMATOSUM MINE (SAMAT.) AND SULLIVAN MINE.....	3-4
FIGURE 3-2	DISSOLVED TRACE METALS IN INFLUENT (ARD FEED) AND EFFLUENT (TREATED CLARIFIER) SAMPLES FOR EQUITY MINE, GECO MINE, BRITANNIA MINE (BRIT.), BRUNSWICK MINE (BRUNS.), CHISEL NORTH MINE (CHISEL), SAMATOSUM MINE (SAMAT.) AND SULLIVAN MINE.	3-5
FIGURE 3-3	SOLID PHASE ELEMENTAL ABUNDANCE (BY MASS) FOR SLUDGE SAMPLES FROM EQUITY (HDS AND LDS SAMPLES), GECO, BRITANNIA (BRIT.), BRUNSWICK (BRUNS.), CHISEL NORTH (CHISEL), SAMATOSUM (SAMAT.) AND SULLIVAN (SULL. NEW AND SULL. OLD) MINES.	3-11
FIGURE 3-4	SOLID PHASE ELEMENTAL ABUNDANCE (BY MOLAR CONCENTRATION) FOR SLUDGE SAMPLES FROM EQUITY (HDS AND LDS SAMPLES), GECO, BRITANNIA (BRIT.), BRUNSWICK (BRUNS.), CHISEL NORTH (CHISEL), SAMATOSUM (SAMAT.) AND SULLIVAN (SULL. NEW AND SULL. OLD) MINES.	3-12
FIGURE 3-5	(A) XRD SPECTRA FOR BRUNSWICK MINE SLUDGE. BROAD PEAKS THAT ARE CONSISTENT WITH 2-LINE FERRIHYDRITE (SHOWN IN B) ARE OUTLINED IN RED.....	3-17
FIGURE 3-6	EQUITY MINE HDS: SEM BACK SCATTERED ELECTRON (BSE) IMAGES (LEFT) AND ASSOCIATED EDS SPECTRA (RIGHT) FOR POINTS A THROUGH D.	3-19

FIGURE 3-7	STEM ANNULAR DARK FIELD (ADF) IMAGES OF EQUITY HDS (LEFT) AND ASSOCIATED EDS SPECTRA (RIGHT) FOR POINTS A) THROUGH D) IN EACH IMAGE.	3-20
FIGURE 3-8	SEM BACK SCATTERED ELECTRON (BSE) IMAGE (UPPER LEFT) OF THE EQUITY HDS SHOWING COMPOSITIONAL ZONING OF THE TRACE METAL-BEARING MG-AL-(FE)-HYDROXYSULFATE PHASE. SEM EDS 2-D ELEMENTAL MAPS FOR EQUITY HDS SAMPLE (EQM AREA 8) ARE ALSO SHOWN, SHOWING THE RELATIVE ABUNDANCE OF O, P, CA, S, MN, MG, AL, ZN, FE, SI AND CU.	3-21
FIGURE 3-9	PLOTS OF STEM EDS NET INTENSITIES FOR EQUITY HDS SAMPLE. THE DATA INDICATE A GOOD CORRELATION FOR ZN:MG AND ZN:AL INTENSITIES.	3-22
FIGURE 3-10	STEM HIGH-ANGLE ANNULAR DARK-FIELD (HAADF) IMAGE (UPPER LEFT) OF THE EQUITY LDS TRACE METAL-BEARING MG-AL-(FE)-HYDROXYSULFATE PHASE. STEM EDS 2-D ELEMENT MAPS ARE ALSO SHOWN, SHOWING THE RELATIVE ABUNDANCE OF S, FE, MN, CA MG, AL AND ZN.	3-23
FIGURE 3-11	STEM HIGH-ANGLE ANNULAR DARK-FIELD (HAADF) IMAGE AND ASSOCIATED EDS SPECTRA FOR EQUITY LDS SHOWING (A) FE- AND AL-RICH ZONE, AND (B) MG- AND AL-RICH ZONE OF THE TRACE METAL-BEARING MG-AL-(FE)-HYDROXYSULFATE PHASE.	3-23
FIGURE 3-12	PLOTS OF STEM EDS NET INTENSITIES FOR EQUITY LDS.	3-24
FIGURE 3-13	SEM BACK SCATTERED ELECTRON (BSE) IMAGES OF GECO HDS (LEFT) AND ASSOCIATED EDS SPECTRA.	3-26
FIGURE 3-14	STEM ANNULAR DARK FIELD (ADF) IMAGES OF GECO HDS (LEFT) AND ASSOCIATED EDS SPECTRA (RIGHT) FOR POINTS A) AND B) ON THE CORRESPONDING IMAGE.	3-27
FIGURE 3-15	SEM BACK SCATTERED ELECTRON (BSE) IMAGE (UPPER LEFT) OF GM AREA 1 FROM GECO HDS. EDS 2-D ELEMENTAL MAPS ARE ALSO SHOWN SHOWING THE RELATIVE ABUNDANCE OF O, CA, S, MG, AL, FE AND SI.	3-28
FIGURE 3-16	STEM BRIGHT FIELD IMAGE OF GECO HDS (TOP LEFT), SAED PATTERN (TOP RIGHT) AND EDS SPECTRUM (BOTTOM).	3-29
FIGURE 3-17	(A) SEM BACK SCATTERED ELECTRON (BSE) IMAGES OF THE BRITANNIA HDS AND (B) CORRESPONDING EDS SPECTRA.	3-30
FIGURE 3-18	SEM BACK SCATTERED ELECTRON (BSE) IMAGE (UPPER LEFT) OF BRITANNIA HDS AND SELECTED EDS 2-D ELEMENTAL MAPS SHOWING THE RELATIVE ABUNDANCE OF CA, AL, CU, MG AND ZN. T.	3-31
FIGURE 3-19	STEM HAADF IMAGES OF THE BRITANNIA SLUDGE SAMPLE (A & B), AND (C) SELECTED EDS SPECTRA CORRESPONDING TO POINTS LABELLED IN A & B.	3-33
FIGURE 3-20	STEM HAADF IMAGE OF THE BRITANNIA HDS OF AREA 3 (A) AND (B) SELECTED EDS SPECTRA CORRESPONDING TO POINTS LABELLED IN (A).	3-34
FIGURE 3-21	PLOTS OF STEM EDS NET INTENSITIES FOR THE BRITANNIA HDS.	3-35
FIGURE 3-22	(A) SEM BSE IMAGES OF BRUNSWICK HDS (AREA 1) AND (B) CORRESPONDING EDS SPECTRA OF THE TRACE METAL-BEARING ZN-FE-MN OXYHYDROXIDE PHASE.	3-37
FIGURE 3-23	STEM HAADF IMAGES OF THE BRUNSWICK HDS SAMPLE (A AND B). SELECTED EDS SPECTRA CORRESPONDING TO POINTS LABELLED IN A & B ARE SHOWN IN THE LOWER GRAPHS (C).	3-38
FIGURE 3-24	(A) SEM BACK SCATTER ELECTRON (BSE) IMAGE (UPPER LEFT) OF BRUNSWICK HDS, AND SELECTED EDS 2-D ELEMENTAL MAPS SHOWING RELATIVE ABUNDANCE OF CA, FE, MN, MG AND ZN.	3-39

FIGURE 3-25	(A) STEM HAADF IMAGE (UPPER LEFT) OF BRUNSWICK HDS AND SELECTED EDS 2-D ELEMENTAL MAPS SHOWING RELATIVE ABUNDANCE OF CA, FE, S, MG AND ZN.....	3-40
FIGURE 3-26	PLOTS OF STEM EDS NET INTENSITIES FOR THE BRUNSWICK SAMPLE. COEFFICIENTS OF DETERMINATION (R^2) ≥ 0.6 HAVE BEEN REPORTED.....	3-42
FIGURE 3-27	(A) STEM HAADF IMAGE OF THE BRUNSWICK HDS. (B) BRIGHT-FIELD TEM IMAGE OF THE SAME AREA. (C) DARK-FIELD TEM IMAGE OF THE AREA INDICATED IN (A) AND (B). THE BRIGHT SPOTS IN THE DARK-FIELD IMAGE REPRESENT DIFFRACTION CONTRAST. (D) SAED PATTERN FROM THE FE-ZN OX AREA.	3-43
FIGURE 3-28	(A) SEM BACK SCATTERED ELECTRON (BSE) IMAGES OF THE CHISEL NORTH HDS AND (B) SELECTED EDS SPECTRA CORRESPONDING TO POINTS LABELLED IN (A).....	3-45
FIGURE 3-29	(A) SEM BACK SCATTERED ELECTRON (BSE) IMAGE OF THE CHISEL NORTH HDS (UPPER LEFT) AND SELECTED EDS 2-D ELEMENTAL MAPS SHOWING RELATIVE ABUNDANCE OF CA, FE, MN, MG AND ZN.	3-46
FIGURE 3-30	STEM HAADF IMAGES OF THE CHISEL NORTH HDS (A & B), AND (C) SELECTED EDS SPECTRA CORRESPONDING TO POINTS LABELLED IN A & B.	3-47
FIGURE 3-31	(A) STEM HAADF IMAGE OF CHISEL NORTH HDS AND SELECTED EDS 2-D ELEMENTAL MAPS SHOWING RELATIVE ABUNDANCE OF CA, FE, MN, MG AND ZN.....	3-48
FIGURE 3-32	PLOTS OF STEM EDS NET INTENSITIES FOR THE CHISEL NORTH HDS. COEFFICIENTS OF DETERMINATION (R^2) ≥ 0.6 HAVE BEEN REPORTED.....	3-49
FIGURE 3-33	(A) SEM BACK SCATTERED ELECTRON (BSE) IMAGES OF THE SAMATOSUM HDS, AND (B) SELECTED EDS SPECTRA CORRESPONDING TO POINTS LABELLED IN (A).....	3-51
FIGURE 3-34	(A) SEM BACK SCATTERED ELECTRON (BSE) IMAGE OF THE SAMATOSUM HDS, AND (B) EDS SPECTRUM CORRESPONDING TO THE POINT LABELLED IN (A).....	3-52
FIGURE 3-35	STEM HAADF IMAGES OF THE SAMATOSUM HDS (A & B), AND (C) SELECTED EDS SPECTRA CORRESPONDING TO POINTS LABELLED IN A & B.....	3-53
FIGURE 3-36	(A) STEM HAADF IMAGE OF SAMATOSUM HDS AND SELECTED EDS 2-D ELEMENTAL MAPS, SHOWING RELATIVE ABUNDANCE OF CA, FE, S, MG AND ZN.	3-54
FIGURE 3-37	PLOTS OF STEM EDS NET INTENSITIES FOR THE SAMATOSUM HDS. COEFFICIENTS OF DETERMINATION (R^2) ≥ 0.6 HAVE BEEN REPORTED.....	3-55
FIGURE 3-38	(A) SEM BACK SCATTERED ELECTRON (BSE) IMAGES OF THE SULLIVAN 'NEW' HDS AND (B) SELECTED EDS SPECTRA CORRESPONDING TO POINTS LABELLED IN (A).....	3-57
FIGURE 3-39	(A) SEM BACK SCATTERED ELECTRON (BSE) IMAGE (UPPER LEFT) OF SULLIVAN 'NEW' HDS AND SELECTED EDS 2-D ELEMENTAL MAPS SHOWING RELATIVE ABUNDANCE OF CA, FE, S, MG AND MN.	3-58
FIGURE 3-40	STEM HAADF IMAGES OF THE SULLIVAN (NEW) HDS (A & B), AND (C) SELECTED EDS SPECTRA CORRESPONDING TO POINTS LABELLED IN A & B.	3-59
FIGURE 3-41	(A) STEM HAADF IMAGE OF SULLIVAN 'NEW' HDS AND SELECTED EDS 2-D ELEMENTAL MAPS SHOWING RELATIVE ABUNDANCE OF CA, FE, S, MG AND ZN.....	3-60
FIGURE 3-42	PLOTS OF STEM EDS NET INTENSITIES FOR THE SULLIVAN 'NEW' HDS. COEFFICIENTS OF DETERMINATION (R^2) ≥ 0.6 HAVE BEEN REPORTED.....	3-61
FIGURE 3-43	(A) STEM HAADF IMAGE OF THE SULLIVAN 'NEW' HDS EDS SPECTRUM CORRESPONDING TO THE AREA CIRCLED IN (A) IS PRESENTED IN FIGURE 3-39, POINT II FOR ZN-FE-MG OXYHYDROXIDE. (C) SAED PATTERN CORRESPONDING TO THE AREA CIRCLED IN (A).....	3-62
FIGURE 3-44	(A) SEM BACK SCATTERED ELECTRON (BSE) IMAGES OF THE SULLIVAN 'OLD' HDS AND (B) SELECTED EDS SPECTRA CORRESPONDING TO POINTS LABELLED IN (A).....	3-63

FIGURE 3-45	(A) SEM BACK SCATTERED ELECTRON (BSE) IMAGE (UPPER LEFT) OF SULLIVAN ‘OLD’ HDS AND SELECTED EDS 2-D ELEMENTAL MAPS SHOWING RELATIVE ABUNDANCE OF CA, FE, AL, MG AND MN.....	3-64
FIGURE 3-46	ZN K-EDGE XANES SPECTRA OBTAINED FROM NEUTRALIZATION SLUDGE SAMPLES FROM THE EQUITY, GECO, BRITANNIA, BRUNSWICK, CHISEL NORTH, SAMATOSUM AND SULLIVAN MINES SHOWING BEST 2-COMPONENT AND/OR 3-COMPONENT FITS TO ZN-BEARING STANDARDS.	3-67
FIGURE 4-1	TERNARY DIAGRAMS SHOWING RELATIVE MOLAR PROPORTIONS OF FE-CU-ZN (ABOVE) AND MG-FE-AL (BELOW) IN ARD INFLUENT, AND ASSOCIATED TRACE METAL-BEARING PHASES IN SLUDGE SOLIDS FOR EACH MINE.....	4-9
FIGURE 4-2	SOLUBILITY OF VARIOUS METAL HYDROXIDES (FROM VACHON <i>ET AL.</i> , 1987).	4-11
FIGURE 4-3	DEPTH DISTRIBUTIONS OF TEMPERATURE, DISSOLVED OXYGEN AND % LIGHT TRANSMISSION IN THE MAIN ZONE PIT (JUNE 2001). TEMPERATURE PROFILES FOR OCTOBER 2001 AND JANUARY 2002 ARE ALSO PRESENTED (FROM MCNEE <i>ET AL.</i> , 2003).	4-12

LIST OF TABLES

TABLE 2-1	BACKGROUND INFORMATION ON PARTICIPATING MINES WITH RESPECT TO COMMODITIES, DEPOSIT TYPE, ARD TREATMENT PROCESS AND SLUDGE DEPOSITIONAL ENVIRONMENT.....	2-4
TABLE 2-2	WATER TREATMENT PLANT INFLUENT AND EFFLUENT SAMPLE COLLECTION DETAILS.	2-14
TABLE 2-3	SUMMARY OF MICROSCOPY METHODS.....	2-17
TABLE 3-1	WATER QUALITY SUMMARY FOR ARD TREATMENT PLANT INFLUENT AND EFFLUENT SAMPLES. VALUES ARE ARRANGED IN ORDER OF ABUNDANCE FROM TOP TO BOTTOM TO ILLUSTRATE DOMINANT PARAMETERS. ALL PARAMETERS ARE FOR DISSOLVED SPECIES AND PRESENTED IN MMOL/L.....	3-2
TABLE 3-2	WATER QUALITY SUMMARY FOR ARD TREATMENT PLANT INFLUENT AND EFFLUENT SAMPLES. VALUES ARE ARRANGED IN ORDER OF ABUNDANCE FROM TOP TO BOTTOM TO ILLUSTRATE DOMINANT PARAMETERS. ALL PARAMETERS ARE FOR DISSOLVED SPECIES AND PRESENTED IN MG/L.....	3-3
TABLE 3-3	MINERAL SATURATION INDICES FOR TREATED EFFLUENT SAMPLES - CALCULATED IN PHREEQC (PARKHURST AND APPELO, 1999).....	3-9
TABLE 3-4	SUMMARY OF SOLID PHASE ELEMENTAL COMPOSITION OF SLUDGE SOLIDS. VALUES ARE ARRANGED IN ORDER OF ABUNDANCE FROM TOP TO BOTTOM TO ILLUSTRATE DOMINANT PARAMETERS.....	3-10
TABLE 3-5	CRYSTALLINE PHASES IN SLUDGE SAMPLES IDENTIFIED BY XRD. SHADED BOXES DENOTE PHASES IDENTIFIED	3-16
TABLE 3-6	BEST FITS FOR ZN K-EDGE M-XANES DATA FOR HDS SLUDGE SAMPLES ^A	3-66
TABLE 4-1	SUMMARY OF DOMINANT TRACE METAL-BEARING PHASES FOR SLUDGE SAMPLES AND DOMINANT PARAMETERS IN ARD INFLUENT AND SOLID PHASE ELEMENTS BASED ON MOLAR CONCENTRATIONS.....	4-1

List of Acronyms

ADF - angular dark field
ARD - acid rock drainage
BSE - back scattered electron
EDS - Energy Dispersive X-ray Spectroscopy
HAADF - high angle annual dark field
HDS - high density sludge
LDS - low density sludge
SAED - selected area electron diffraction
SedEx - sedimentary exhalative deposit
SEM - scanning electron microscopy
STEM - scanning transmission electron microscopy
VMS - volcanic massive sulfide
XAFS - x-ray absorption fine structure
XANES - x-ray absorption near-edge structure
XAS - x-ray absorption spectroscopy
XRD - x-ray diffraction

1. Introduction

1.1 Overview

At many mine sites, the management of acid rock drainage (ARD) involves neutralization with lime to reduce levels of acidity and trace elements prior to discharge. Treatment is generally achieved by raising the pH to values greater than 8.5 and separating the resulting precipitates (sludge) from the treated water prior to release to the environment (MEND, 1994). Within Canada alone, it is estimated that approximately 7 million m³ of lime-treated sludges are generated on an annual basis from mining/metallurgical operations (MEND, 1997; MEND, 2005).

Given that neutralization sludges represent significant repositories of metal-rich material, an understanding of their long-term chemical stability in various depositional settings (holding ponds, mined-out stopes, open pits, co-disposal with waste rock, tailings, *etc.*) is required for effective environmental management and planning. Specifically, given that the final conditions of storage may differ markedly from the conditions of formation, there is the potential for the chemical instability (dissolution) of sludge materials. Such considerations have important implications with respect to both waste and water management from the perspectives of potential impacts to aquatic resources, regulatory compliance, and closure liabilities (bonding). In this regard, a thorough understanding of sludge metal-phase associations is a pre-requisite for assessing chemical behaviour.

Due to the extremely fine-grained and often amorphous (*i.e.*, non crystalline) character of sludge solids, the composition of these materials has been difficult to elucidate. Traditional methods such as X-Ray Diffraction (XRD) and optical microscopy have proved ineffective since amorphous and poorly ordered materials are not detected by XRD and since optical microscopy does not provide sufficient spatial resolution to fully differentiate trace element associations associated with extremely fine particle sizes. Early conceptions that metals precipitate solely as their respective hydroxides (*e.g.*, Cu(OH)₂, Zn(OH)₂) during the neutralization process are now known to be overly simplified and largely incorrect. Instead, it is now known that metals may be removed from solution through several pathways in addition to hydroxide formation, including coprecipitation with hydrous ferric oxides (*e.g.*, FeOOH), Mn-oxyhydroxides (MnOOH), Al hydroxides (Al(OH)₃), and other mixed Fe-Mg-Al-hydroxysulfates (Webster *et al.*, 1998; MEND, 2005; Loomer *et al.*, 2007a,b). The current lack of definition of trace element associations in sludge materials is considered a significant information gap in the industry (MEND, 2005). Such trace-element associations must be understood to allow for pE (redox potential) and pH dependent solubility predictions. Further, there is limited

published data on sludge management practices and long-term performance of sludge chemical stability.

1.2 Project Background and Objectives

In order to provide further insight into the composition of neutralization sludges, Lorax Environmental Services Ltd. (Lorax) initiated and funded the characterization of two low-density sludge (LDS) samples in 2006 to build upon previous MEND studies (MEND 1997, 1999, 2005). LDS samples included those from Equity Mine and Mines Selbaie. The particular focus of this work was to elucidate Zn associations within sludge matrices. A range of analyses was performed, including in general order of increasingly refined spatial resolution; bulk chemical analysis, X-ray diffraction (XRD), Scanning Electron Microscopy (SEM) coupled with Energy-Dispersive X-ray Spectroscopy (EDS) and Scanning Transmission Electron Spectroscopy (STEM) coupled with EDS. From this work, it was shown that the dominant association for Zn in both LDS samples was a Mg-Al-(Fe) hydroxysulfate. Lorax presented the results of this assessment in Loomer *et al.* (2007a and 2007b).

In 2008, this work was expanded with support from the MEND program to include examination of high density sludge (HDS) materials from an additional six mines across Canada. This also included the addition of X-ray absorption near edge structure (XANES) in addition to XRD, SEM and STEM as described above. Overall, the report presented herein is based on data collected for seven mines across Canada, including:

- Equity Mine LDS and HDS (Goldcorp Canada);
- Geco Mine HDS (Xstrata Zinc);
- Britannia Mine HDS (EPCOR and BC Ministry of Forests, Lands and Natural Resource Operations);
- Brunswick Mine HDS (Xstrata Zinc);
- Chisel North Mine HDS (Hudson Bay Mining and Smelting);
- Samatosum Mine HDS (Inmet); and
- Sullivan Mine HDS (fresh and aged) (Teck).

The sludge sample from Mines Selbaie was excluded from this report given that influent and effluent water quality data for the lime treatment system were not available.

The program includes direct funding from MEND and the industrial partners, as well as in-kind contributions from the participating mines (collection and analysis of water samples) and Lorax (analysis and reporting). Project management was overseen by senior scientists at Lorax (Alan Martin) and the University of New Brunswick (Diana

Loomer and Dr. Tom Al). To date, data generated from this work have been reported in Martin et al. (2011) and Martin et al. (2012).

Overall, the objectives of the study were to provide greater insight into the characterization of treatment solids generated through the lime neutralization of ARD.

Specific objectives included:

1. To identify the dominant trace metal associations in sludge materials;
2. To assess the links between the dominant trace metal associations in the solid phase and ARD influent chemistry; and
3. To provide a basis from which to assess sludge chemical stability in various depositional environments.

In order build upon the data presented herein, and to potentially develop a sludge management framework, field and/or laboratory studies designed to assess the *in situ* chemical stability of various sludge types in a range of depositional environments will be required. Given that the final storage conditions may differ markedly from the conditions of sludge formation with respect to both pH and pE, there is the potential for chemical instability (dissolution) of sludge materials. For example, pit lakes and impoundments are often characterized by circum-neutral pH that reflects the influence of neutral to acidic water inputs (runoff, groundwater, direct precipitation). With regards to pE, suboxic conditions (as defined by onset to Fe(III) reduction) are predicted to develop within permanently saturated or submerged sludge deposits. In fact, in the long-term, suboxic conditions can be expected to develop in many sludge deposits irrespective of their final mode of storage (subaqueous *versus* subaerial deposition). Specifically, given the fine-grained nature of neutralization sludges, these materials may retain sufficient interstitial saturation to promote suboxia in the foundation/interiors of subaerial deposits. Therefore, an understanding of the sensitivity of sludge materials to low redox potential will be a key element in the subsequent framework development. Such considerations have important implications with respect to both waste and water management from the perspectives of potential impacts to aquatic resources, regulatory compliance, and closure liabilities. Such considerations were not specifically addressed as part of this report.

1.3 Report Structure

A summary of the participating mines, including descriptions of site background, geology and water treatment, is presented in Chapter 2. Also included in Chapter 2 is a description of the field and analytical methods. Chapter 3 presents the results of the assessment relating to influent and effluent chemistry, sludge composition and mineralogy, and dominant trace metal-bearing phases. A results summary and a discussion of considerations for predicting sludge type and sludge chemical stability are provided in Chapter 4. The most salient conclusions of the assessment are provided in Chapter 5.

2. Background and Methods

The following chapter provides background information pertinent to the assessment, including an overview of lime treatment, descriptions of the mine sites of interest (history, treatment methods and sludge management), and an overview of the sampling and analytical methods utilized.

2.1 Overview of Lime Treatment

2.1.1 Conventional Lime Treatment (LDS)

Conventional lime treatment systems involve the neutralization of ARD to a desired pH in a mixing tank through the controlled addition of lime followed by solid/liquid separation in a clarifier or settling pond (Aubé and Zinck, 2003). A conceptual schematic showing the general elements of a LDS system is provided in Figure 2-1 (Aubé, 2005). In these systems, lime is added to attain a pH suitable for the precipitation of the heavy metals targeted for removal from solution, which may range from pH 8.5 to 11. Conventional lime treatment plants produce low-density sludges, typically composed of < 5 wt.% solids.

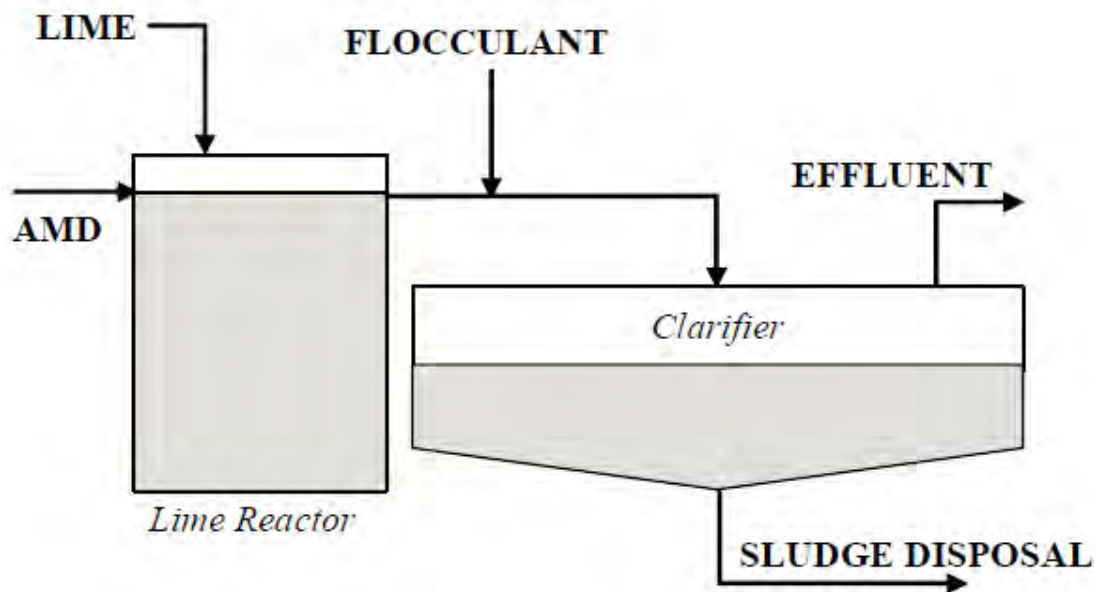


Figure 2-1: Generalized schematic of conventional low density sludge lime treatment plant (Aubé, 2005).

2.1.2 High Density Sludge (HDS) Process

The key difference in the HDS process compared to conventional LDS systems is the recycling of sludge to the head of the process, which fosters increased sludge density (Aubé and Zinck, 2003). Specifically, a portion of the thickened sludge from the clarifier is pumped (and recycled) to a “Lime/Sludge Mix Tank” where the sludge is mixed with additional lime prior to contact with ARD in the “Rapid Mix Tank”. A conceptual illustration of an HDS system is provided in Figure 2-2 (Aubé, 2005). The neutralized slurry feeds the Lime Reactor (LR) where the precipitation reactions are completed. Aeration is generally a feature of the LR to oxidize ferrous iron to ferric iron. The slurry then overflows to a Floc Tank to promote agglomeration and settling of precipitates in the clarifier. In the clarifier, precipitated solids are separated from the liquid phase to produce a clear effluent for discharge and a dense sludge in the underflow that is continuously recycled to the head of the process (*i.e.*, Sludge/Lime Mix Tank). Excess underflow sludge formed by the HDS process typically comprises 20 to 30 wt.% solids.

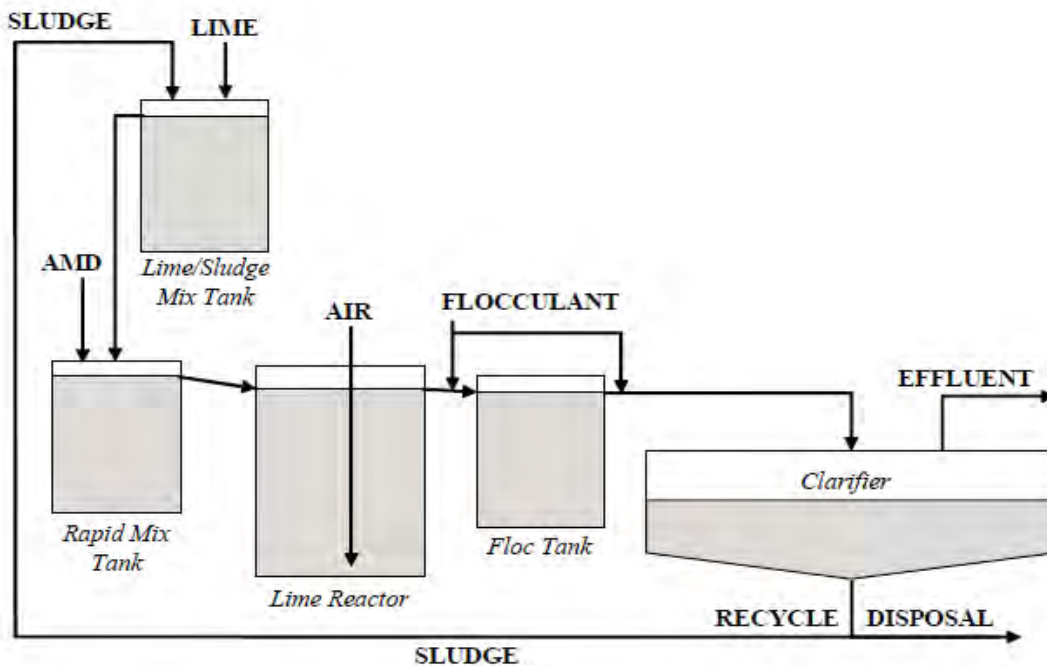


Figure 2-2: Generalized schematic of conventional High Density Sludge (HDS) treatment process (Aubé, 2005).

2.2 Study Sites

Samples of ARD influent, treated effluent, and sludge solids were donated by seven mines across Canada (Figure 2-3), including:

- Equity Mine (Goldcorp Canada);

- Geco Mine (Xstrata Zinc);
- Britannia Mine (EPCOR and BC Ministry of Forests, Lands and Natural Resource Operations);
- Brunswick Mine (Xstrata Zinc);
- Chisel North Mine (Hudson Bay Mining and Smelting);
- Samatosum Mine (Inmet); and
- Sullivan Mine (Teck).

Background information with respect to commodities, deposit type and ARD treatment for each of the sites are summarized in Table 2-1. More detailed descriptions of each mine site, including specific information with respect to site history, treatment system and sludge management, are provided in the sections to follow.



Figure 2-3: Map of Canada showing locations of Equity, Geco, Britannia, Brunswick, Chisel North, Samatosum, and Sullivan mines (modified from NRC, 2001).

Table 2-1:
Background information on participating mines with respect to commodities, deposit type, ARD treatment process and sludge depositional environment.

Mine Site	Stage	Recoverable Elements	Deposit Type	Sample ID	ARD Treatment	Depositional Environment of Sludge
Equity	closed, c/m	Au-Ag-Cu	Intrusion-related hydrothermal	EQM-1	LDS	holding pond
				EQM-2	HDS	open pit lake (subaq.)
Geco	closed, c/m	Cu-Zn	VMS	Geco	HDS	subaerial cells on tailings
Britannia	closed, c/m	Cu (Zn-Pb-Ag)	Massive sulfide	Brit.	HDS	holding pond
Brunswick	operational	Pb-Zn-Cu-Ag	VMS	Brun.	HDS	subaerial cells/cover on tailings
Chisel North	operational	Cu-Zn	VMS	Chisel	HDS	underground workings (subaq.)
Samatosum	closed, c/m	Ag-Cu-Pb-Zn-Au	Stockwork VMS	Samat.	HDS	subaerial storage area
Sullivan	operational	Pb-Zn-Ag-Fe	SedEx	Sull. new	HDS	holding (exfiltration) pond
				Sull. old		

Notes:

VMS = volcanic massive sulfide

HDS = high density sludge

LDS = low density sludge

SedEx = sedimentary exhalative deposit

c/m = care and maintenance

subaq. = subaqueous

2.2.1 Equity Mine

The Equity Silver deposit is an intrusion-related hydrothermal, subvolcanic Cu-Ag-Au (As-Sb) deposit located in the central interior of British Columbia (BC), 35 km southeast of Houston (Figure 2-3; Table 2-1). The Equity Mine was operated by Placer Dome Inc. between 1980 and 1994, producing over 33.8 Mt of ore at an average grade of 0.4 % Cu, 65 g/t Ag and 0.46 g/t Au (MINFILE, 2009). Approximately 85 Mt of waste rock were also generated. Ore was mined from three open pits and underground workings, and processed by conventional grinding and flotation followed by cyanidation. The site is currently under care and maintenance by Goldcorp Canada Ltd., Equity Division, who acquired the site in 2006. Primary closure activities are associated with the collection and treatment of ARD.

The deposit is hosted by Mesozoic volcanic and sedimentary beds which have been uplifted, brecciated, and mineralized by intrusion of the Goosly syenomonzonite-gabbro stock (Church and Barakso, 1990). Mineralization is found as both sulfide disseminations and replacement sulfide lenses, with disseminations forming the bulk of the mineralized zones. Massive sulfide replacement bodies, which can be up to 3 m thick, are irregularly distributed throughout the disseminated zone.

Prior to December 2003, the Equity Mine used a conventional ARD lime treatment process to treat acidic drainage collected from this site, which produced low density sludges (LDS) (Figure 2-1). Since December 2003, the Equity Mine has used an HDS process similar to that employed at Heath Steele (Figure 2-4). The Heath Steele Process

provides the same physical and chemical advantages as the conventional HDS process, but eliminates the Rapid Mix Tank and the Floc Tank (Figure 2-4; Aubé, 2005; Aubé and Zinck, 2003). Rather, the lime/sludge mixture overflows directly to a lime reactor where ARD is added and the mixture is aerated and agitated to allow for complete oxidation and neutralization reactions to occur. Overflow from the lime reactor is then fed directly to the clarifier. A diluted polymer flocculant is added either to the clarifier or directly to the clarifier feed to flocculate suspended solids and produce agglomerates that settle out in the clarifier.

In the current operation at Equity, the amount of lime (delivered as quick lime (CaO)) required to treat the volume of ARD in the feed depends on the acidity, but ranges from 3,000 to 5,000 t/yr to maintain an average effluent pH of 8 to 8.5. The concentrated flocculant (Ciba Magnafloc 10) solution, composed of approximately 0.3 g dry flocculant/kg solution (0.03%), is added at a rate that varies according to final effluent turbidity and visual observation of the condition of the flocs in the clarifier feed well. The plant is designed for flow rates of 568 m³/h, but has the potential to handle up to 1,136 m³/h.

Sludge from ARD treatment prior to 1986 was pumped to the tailings pond as LDS, but records on the volumes were not kept. From 1986 to 1992, ~974,000 m³ of neutralization sludge was stored in a tailings pond. Since 1993, sludge produced at Equity has been pumped to the flooded Main Zone open pit for final storage (permanently saturated environment).

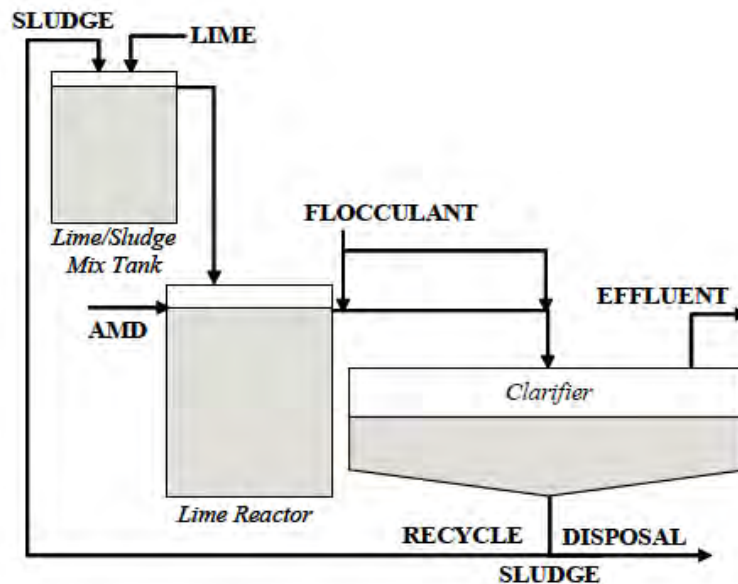


Figure 2-4: Generalized schematic of Heath Steele High Density Sludge (HDS) treatment process (Aubé, 2005).

2.2.2 Geco Mine

The Geco Mine is a metamorphosed volcanogenic Cu-Zn-Ag (Au-Pb-Cd) massive sulfide deposit located approximately 400 km East of Thunder Bay, Ontario, near Manitouwadge (Figure 2-3, Table 2-1). Mining commenced at the Geco site in 1957 under the General Engineering Company (Geco), which became the Geco Division of Noranda Mines Ltd. in 1964. Operations ceased in August 1995, having produced over 53 Mt of ore (containing on average 1.8% Cu, 3.8% Zn, 1.6 oz/t Ag, and 0.0004 oz/t Au) and approximately 50 Mt of tailings (Jamieson *et al.*, 1995). Ore was extracted from underground workings and processed by conventional grinding and differential flotation. The site is currently being reclaimed under care and maintenance of Xstrata Zinc, who acquired the site in 2006. The major focus of closure activities is the collection and treatment of ARD.

The deposit is hosted by a small complexly deformed greenstone sequence within the Abitibi-Wawa metavolcanic belt (Petersen, 1986). A mineable envelope of disseminated chalcopyrite encloses the main massive sulfide ore body, which is comprised of pyrite, pyrrhotite, sphalerite, chalcopyrite and minor galena.

In 2005, a new HDS treatment plant began operating at the Geco site to treat ARD collected from both the Willroy and Geco mines. The plant is similar in design to that of the Britannia Mine (Figure 2-5). The Geco plant uses two reactor tanks in addition to the Lime/Sludge Mix Tank and clarifier for a total hydraulic retention time of approximately 97 minutes (SNC-Lavalin, 2004). A controlled amount of lime/sludge slurry is added to the first reactor tank where it is contacted with untreated acidic solution from the holding pond. A portion of sludge from the clarifier is also recycled to the Lime/Sludge Mix Tank. Solution pH is controlled to achieve a range of $8.0 < \text{pH} < 9.5$ to precipitate ferric iron, zinc and other trace metals. Air is also added to the first reactor tank to oxidize ferrous iron to ferric iron. The overflow from first reactor tank discharges to the second reactor tank where secondary aeration and liming may take place if required. Flocculant is added directly to the clarifier to aid in solid-liquid separation.

ARD is collected from both mines sites then pumped to a holding pond for storage prior to being treated through the HDS plant. The plant is designed to operate at a continuous flow rate of 500-930 m³/h (depending on metal loading). The amount of lime required to treat the volume of ARD in the feed at Geco varies according to water chemistry; average annual lime consumption is approximately 2,000-3,000 t/y. ARD is batch treated three times per year between spring and fall, with each treatment episode lasting from 1 to 2 months. The plant is shut down in the winter months. Flocculant (high molecular weight anionic polymer) is applied to the clarifier at a rate of approximately 3 g/m³ under

maximum treatment capacity conditions. Sludge that is not recirculated in the Geco treatment process is pumped to storage cells in the existing tailings storage facility, where sludges are deposited subaerially.

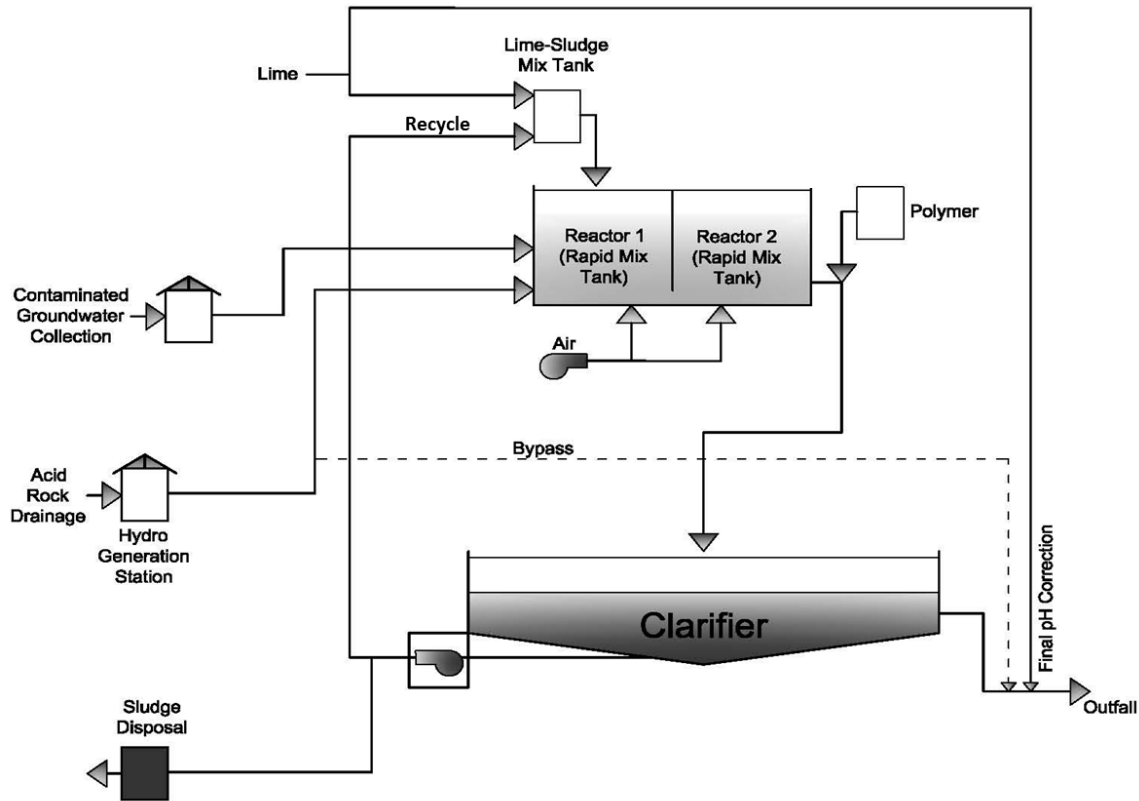


Figure 2-5: Generalized flow chart for the Britannia Mine HDS treatment process.

2.2.3 Britannia Mine

The Britannia Mine is a Kuroko type volcanic Cu-Zn massive sulfide deposit located at Britannia Beach on the east shore of Howe Sound, 48 km north of Vancouver, BC (Figure 2-3, Table 2-1). The Britannia Mine was operated by the Howe Sound Company and subsidiary Britannia Mining and Smelting Company from 1904 until 1963 and subsequently by the Anaconda Copper Company until closure in 1974 (Britannia Mine Museum, 2012). In the 70 years of mining, 210 km of underground workings and five open pits were excavated producing over 50 Mt of Cu ore (and lesser amounts of Ag, Zn, Cd, Pb and Au) (Price *et al.*, 1995). Since the mine ceased operations, surface water continues to enter the mine workings through the open pits and glory holes in the Jane Basin area. Drainage is routed through the underground workings, eventually discharging at the 4100 Level. The site is currently under care and maintenance by the

B.C. Ministry of Forests, Lands and Natural Resource Operations (plant operated by EPCOR).

The deposit is located in the volcanic and sedimentary rocks of the Cretaceous Gambier Group within the Coast Crystalline tectonic belt. Specifically, the Britannia sulfide orebodies are hosted in a roof pendant structure of Gambier Group rocks isolated by a plutonic intrusion of quartz diorite and granodiorite. The Gambier stratigraphy is intruded by several generations of intermediate to mafic dykes, some of which are highly deformed and mineralized. The Britannia shear zone, which strikes northwesterly across the roof pendant, is host to all ore bodies at the site (Price *et al.*, 1995). Sulfides, including pyrite and lesser amounts of chalcopyrite, sphalerite, pyrrhotite, galena, tennantite and tetrahedrite, occur as stringer deposits or as massive deposits that are widely disseminated or concentrated along bedding and fracture planes.

HDS treatment of ARD and contaminated groundwater at the Britannia Mine began in 2005 (EPCOR, 2005). The HDS system at Britannia is similar to a conventional HDS system with exclusion of a Floc Tank (Figure 2-5). The Britannia plant uses a dual reactor tank system which includes a Rapid Mix Tank (Reactor 1), where ARD is neutralized with partially recycled slurry from the Lime/Sludge Mix Tank. A polymer (Ciba Magnafloc 10 Flocculant) is added to the clarifier feed to enhance particle flocculation. The pH of the clarified water is typically corrected to a pH of 9 prior to discharge.

The sludge that settles to the bottom of the tank is collected and pumped to recycle, with a portion pumped to a sludge holding tank for dewatering and disposal. Dewatering of sludge is achieved by means of a filter press at the treatment plant. The sludge cake produced by the dewatering process is transported for storage to a holding pond in the Glory Holes of the Jane Basin.

2.2.4 Brunswick Mine

The Brunswick Mine is a Pb-Zn-Cu (Ag) massive-sulfide deposit located approximately 30 km southwest of Bathurst, New Brunswick (Figure 2-3; Table 2-1). The underground mine has operated for nearly half a century (since 1964) and generated more than 134 million tonnes of ore. The Brunswick Mine has been a fully-owned division of Xstrata Zinc Canada since 2007. The site is scheduled for closure in March of 2013.

The Brunswick No. 12 ore body lies within the upper part of the Nepisiguit Falls Formation of the Tetagouche Group. The Tetagouche Group is a bimodal volcano-sedimentary back-arc basin sequence within the complexly deformed Cambro-Ordovician volcano-sedimentary and plutonic sequence (Pers. Comm. Xstrata, 2010). The ore

consists mainly of chalcopyrite and variable assemblages of pyrite, pyrrhotite, sphalerite and galena. Minor arsenopyrite and tetrahedrite are disseminated throughout the massive sulfides as are secondary or supergene sulfide minerals, including covellite, chalcocite, bornite, native copper and native silver.

In 1993, a conventional HDS plant was commissioned to treat contaminated water at the Brunswick site (Figure 2-6). Waters from the open pit (No.6 Mine), underground workings (No. 12 Mine) and tailings area are collected and mixed through a series of water management ponds before being pumped at an average rate of 30,500 L/min to the treatment plant. Acidic drainage from the open pit is pumped seasonally (May to October) while drainage from underground workings is pumped year-round into the existing quarry to reduce high levels of dissolved sulfide (via metal sulphide precipitation) in the reclaim water stream (since Feb 22, 2010).

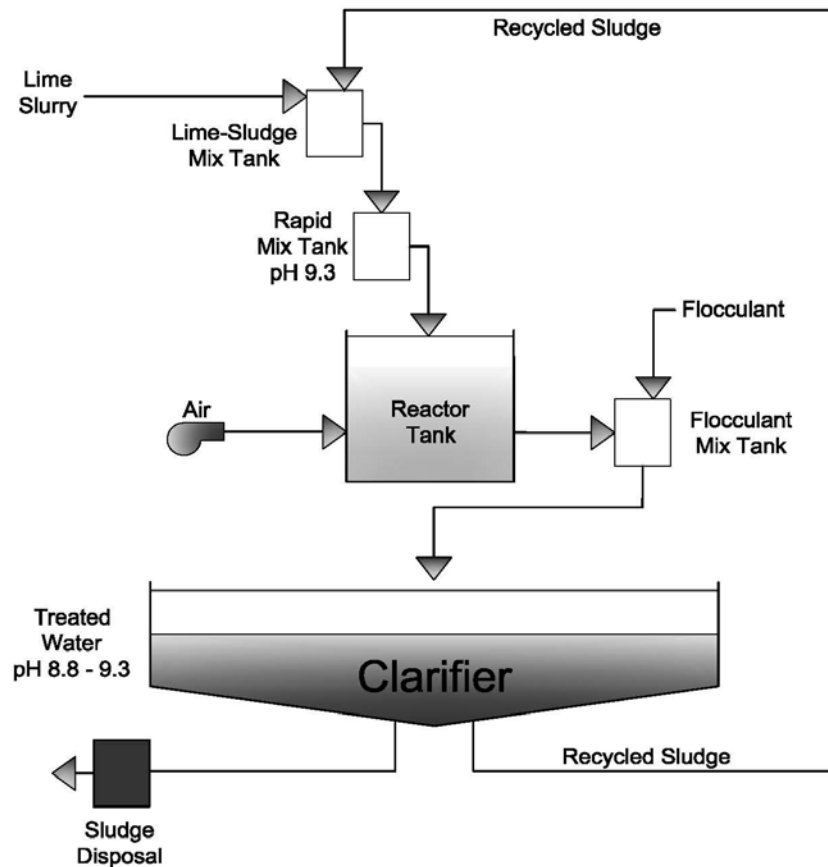


Figure 2-6: Generalized flow chart for the Brunswick Mine ARD lime treatment process.

Lime consumption at the Brunswick HDS plant varies from 0.3 kg/m³ to 1.3 kg/m³, depending on the pH and metal concentrations of the ARD influent. A 50% hydrogen

peroxide (5 to 80 mg/L) solution is pumped into the buffer pond seasonally (May to October), when thiosalt concentrations exceed 25 mg/L. The addition of hydrogen peroxide promotes oxidation of thiosalts to produce sulfate.

Up until 2010, sludge was stored in cells on the tailings pond and used as a cover for the closed tailings basin. The closure plan for the Brunswick Mine includes final storage of sludge in the Reclaim Quarry.

2.2.5 Chisel North Mine

The Chisel North Mine is a volcanic massive sulfide deposit located near the town of Snow Lake, 120 km east of Flin Flon, Manitoba (Figure 2-3; Table 2-1). Hudson Bay Mining & Smelting Co. Limited (HBMS) began mining in the Snow Lake area in 1960 and continues to operate at the present time (Pers. Comm HBMS, 2010). The Chisel North Mine opened in 2000, but was placed on care and maintenance in February 2009 due to depressed world Zn prices, having produced approximately 2.9 Mt of ore during its nine years of operation. The mine returned to full production in March 2010, and is currently still in operation. All ore mined from HBMS operations in the Snow Lake area are processed in the Snow Lake Mill.

The deposit comprises a series of shallowly northeast-dipping massive sulfide lenses hosted within a highly deformed tholeiitic island arc assemblage located on the eastern edge of the Flin Flon volcanic belt, 300 m down-plunge from the Chisel Lake orebody (Gagne *et al.*, 2007). The Chisel North deposit typically consists of up to 20 m of silicate-dolomite-rich, semi-massive sphalerite rich ore, with thin, massive sphalerite-pyrite or sphalerite bands containing up to 100% sulfide minerals. Pyrite is typically more abundant near the base of the ore horizon and locally massive pyrrhotite occurs near the hanging wall. The ore horizon is locally underlain by discordant zones of disseminated and vein sulfides, comprising mostly chalcopyrite and pyrrhotite. Throughout the deposit, the hanging wall is locally variably enriched in Au, Ag and Pb with values reaching as high as 7-10 g/t Au, 300 g/t Ag and 1% Pb over a few metres.

In 2008, an HDS water treatment plant was constructed at Chisel Lake to treat contaminated water from the underground workings at the Chisel North Mine and from the Chisel Open Pit. Notable differences between the Chisel Lake HDS process and the conventional HDS process are that the Chisel Lake plant includes two reactor tanks in addition to a rapid mix tank (Figure 2-7). Further, the lime/sludge slurry from the Lime/Sludge Mix Tank is fed to both reactor tanks and the rapid mix tank, as is lime and recycled sludge from the clarifier. Therefore, the slurry from Reactor 1 is transferred to the Rapid Mix Tank where it is mixed with additional lime and recycled sludge prior to aeration in Reactor 2 and reaction with more lime and recycled sludge. The addition of

lime increases the pH of the influent water from 4.7 to ~10.5. The pH is then reduced to ~8.5 by CO₂ injection before discharge to the environment. A polymer is added to the slurry as it is transferred to the Floc Tank before being transferred to the clarifier. Sludge that is not recycled within the treatment process is pumped into the underground workings and stored subaqueously.

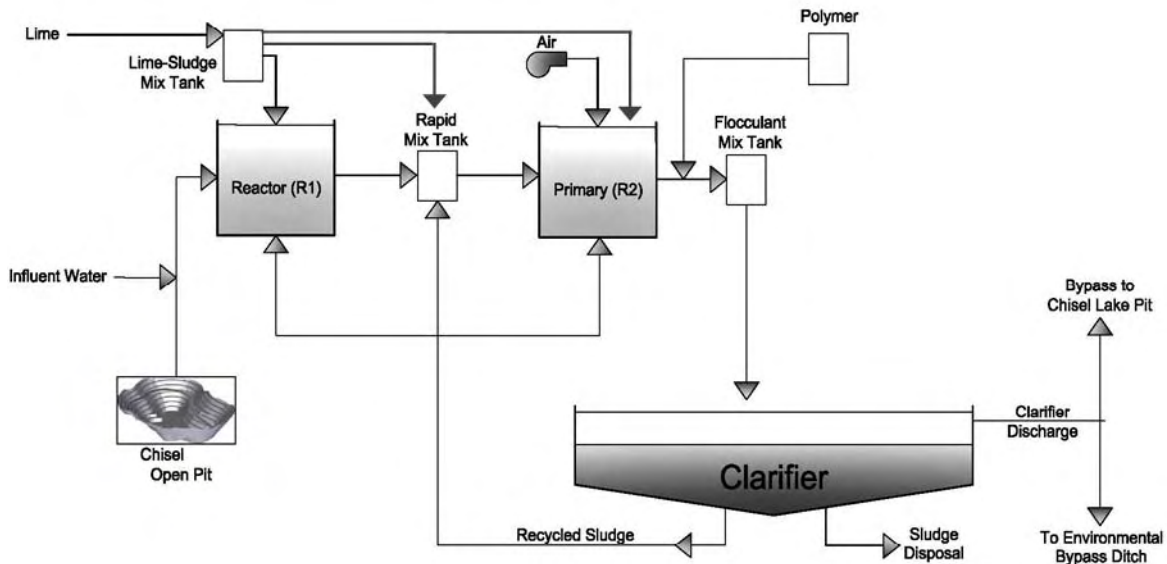


Figure 2-7: Generalized flow chart for the Chisel North Mine HDS treatment process.

2.2.6 Samatosum Mine

The Samatosum Mine is a stockwork type Cu-Pb-Zn massive sulfide deposit located approximately 80 km northeast of Kamloops, in the Adams Lake area of south-central BC (Figure 2-3; Table 2-1). The site operated from 1989 until 1992 by Inmet Mining Corporation, producing nearly 635 kt of ore grading 1035 g/t Ag, 1.2% Cu, 1.7% Pb, 3.6% Zn and 1.9 g/t Au from an open pit and underground workings (Bailey *et al.*, 2000). Upon closure, an estimated 8.14 Mt of layered waste rock and 542 kt of sub-aqueous tailings had accumulated. The site has been under closure maintenance since 1992.

The Samatosum deposit is hosted by the low-grade metamorphic sedimentary and volcanic rocks of the Eagle Bay Assemblage (Bailey *et al.*, 2000). The deposit is a stratabound sulfide-rich quartz-vein system contained within an overturned metasedimentary sequence of greenschist-grade sericitized, silicified, and carbonaceous argillites structurally overlain by mafic volcanoclastic rocks and flows. Massive to disseminated tetrahedrite, sphalerite, galena, and chalcopyrite are contained within the roughly stratabound, highly deformed, quartz vein system.

In 1998, a HDS water treatment plant was constructed to treat mine drainage associated with waste rock and open pit (Figure 2-8). The Samatosum HDS plant is similar to that of the Britannia Mine, including two reactors and no Flocc Tank. ARD from the site is directed into Reactor 1 where it is mixed with slurry from the Lime/Sludge Mix Tank and aerated by air spargers to enhance neutralization/precipitation reactions. Overflow from Reactor 1 is directed to Reactor 2 (Primary Tank) for additional residence time. Flocculant is added to the clarifier feed. In the clarifier, the sludge settles out from the water, where a portion is recycled back to Reactor 1. Overflow from the clarifier is piped to settling ponds before eventual release to the local watershed.

Sludge that is not recirculated in the HDS plant is transferred to holding cells for drying for four to six years before being excavated and hauled to the mill site storage facility (Pers. Comm. Inmet, 2010). Final sludge disposal is currently planned to be subaerial stockpiles that will be capped and vegetated.

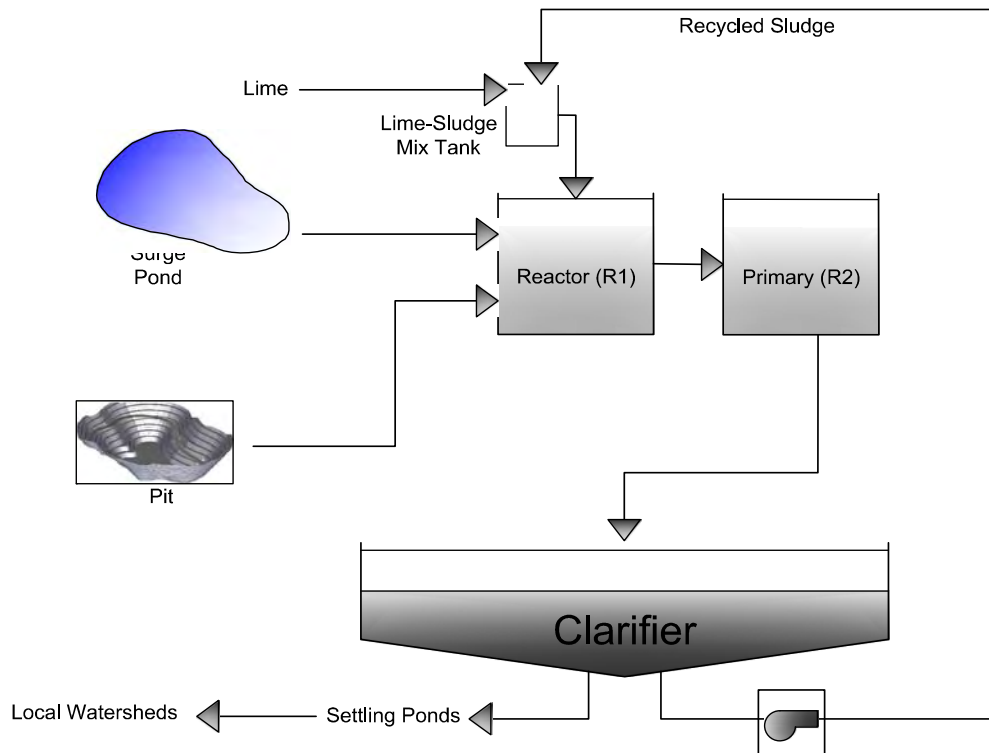


Figure 2-8: Generalized flow chart for the Samatosum Mine ARD lime treatment process.

2.2.7 Sullivan Mine

The Sullivan Mine is a sedimentary exhalative (Sedex) Fe-Pb-Zn sulfide deposit located in Kimberley, BC (Figure 2-3; Table 2-1). The Sullivan deposit was discovered in 1892

and acquired by Cominco Ltd. (now Teck) in 1909. The underground mine closed in December 2001, after nearly 100 years of operation, producing 9 Mt of Pb, 8 Mt of Zn and more than 285 million oz. of Ag.

The mine is situated within the Belt-Purcell Supergroup, in siliciclastic rocks at the boundary of the lower and middle Aldridge Formation turbidites (Taylor, 2003). The Sullivan deposit lies at the intersection of the Sullivan–North Star Corridor, a northerly trending, fault-bounded Proterozoic graben, and the roughly east–west trending Kimberley fault. The Sullivan deposit comprises a lenticular body consisting of laminated pyrrhotite–pyrite–sphalerite–galena-rich layers with intervening siliciclastic layers that are locally replaced by massive pyrrhotite and/or pyrite.

In 1979, an HDS water treatment plant was put into operation at the Sullivan site to treat ARD seepage from the tailings and waste impoundments (Figure 2-9) (Pers. Comm. Teck, 2010). As with the conventional HDS system, lime/sludge slurry is oxidized in a reactor to enhance the conversion of ferrous iron to ferric iron and a pH of >9.0 is maintained to precipitate heavy metals. Flocculant is added in multiple stages to optimize the settling characteristics. Overflow from the clarifier is discharged to the St. Mary River and the underflow is recycled to the Lime/Sludge Mix Tank.

Reclamation work on the tailings and waste impoundments is complete; however, the water treatment plant continues to operate in the spring and fall to treat ARD produced from the waste rock and tailings storage facilities. Sludge that is not recirculated within the treatment process is disposed of in an exfiltration pond located in a former oxbow of a river that is dyked at both ends.

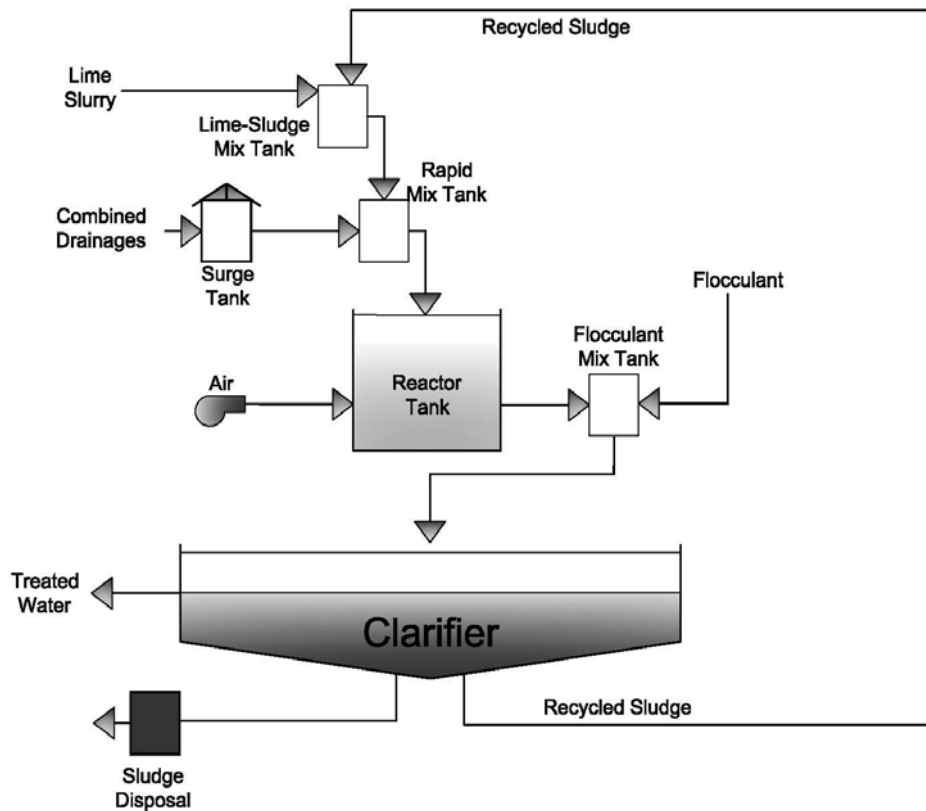


Figure 2-9: Generalized flow chart for the Sullivan Mine ARD lime treatment process.

2.3 Sample Collection

2.3.1 Water Samples

For each treatment system, influent and effluent water sample collection was timed to coincide with sludge sample collection. At several sites, influent and effluent samples were collected on multiple days before and after sludge collection. All water samples were collected according to the details outlined in Table 2-2.

**Table 2-2:
Water treatment plant influent and effluent sample collection details.**

Bottle Volume	Analytes	Filtered	Preservation
500 mL	pH, conductivity, alkalinity, Br, Cl, F, SO ₄ , NO ₃ , NO ₂	No	None
125 mL	Total Metals	No	HNO ₃
125 mL	Dissolved Metals	Yes	HNO ₃

2.3.2 Sludge Samples

Nine neutralization sludge samples were collected from seven Canadian mine sites for solid phase analysis (Table 2-1). Mine site personnel collected seven fresh sludge samples in 4 L HDPE jugs from the access point closest to “end-of-pipe” at their respective HDS treatment plants. Two aged samples, were also collected: 1) from the Sullivan Mine (Sull. old), which was collected from a previous sub-aerial deposition site in the holding pond and could be up to 30 years old; and 2) LDS sample from the Equity Mine (EQM-1), which was collected from the moist surface layers of the sludge deposited in the diversion pond. Sludge was last deposited in the Equity diversion pond in 2002; therefore, since the aged Equity sample was collected in 2007, the sample represents sludge that is between 5 and 10 years old. No water samples were collected in conjunction with the aged samples. Photographs of the sludge samples are shown in Figure 2-10.

All samples were delivered to the Lorax office in Vancouver, BC for processing. All sludge samples were centrifuged to separate the treatment solids from the supernatant. Solid and liquid samples were then sent out for various analyses (described below).

2.4 Analytical Methods

2.4.1 Water Samples

Influent and effluent samples were analyzed for a comprehensive suite of physical and chemical parameters (Table 2-2) in the laboratories of ALS Environmental or Maxxam Analytics Inc. Dissolved metals were determined by Inductively Coupled Plasma Mass Spectrometry (ICP-MS).

Effluent chemistry data were also incorporated into PHREEQC, a geochemical equilibrium modeling program capable of simulating a variety of low-temperature aqueous geochemical reactions for natural and experimental systems (Parkhurst and Appelo, 1999). PHREEQC modelling was used to support the XRD results, and specifically, to provide an indication of the mineral phases that may control the solubility of various elements in solution.



Figure 2-10: Photographs of dried sludge HDS samples. A photo for the Chisel North HDS was not available.

2.4.2 Sludge Solids

Sludge materials were analyzed using a combination of traditional solid-phase analysis and high-resolution microscopy methods. Total elemental analysis was conducted via aqua-regia digestion (HCl and HNO₃ acids) followed by ICP-MS analysis. Given the fine-grain size and amorphous nature of sludge materials, aqua regia digestion is predicted to result in near-quantitative dissolution of all metal-bearing phases. X-Ray Diffraction (XRD) was used to assess the relative abundance of crystalline phases present in the sludge samples. The sludge solids were then subjected to increasingly higher resolution microscopic methods, including scanning electron microscopy (SEM), scanning transmission electron microscopy (STEM) and X-ray absorption near-edge structure (XANES) (Table 2-3, Figure 2-11). These methods were required to determine the mineral/trace-element associations in the sludge materials. Due to the fine-grained condition of the samples, and the amorphous nature of the materials, traditional methods such as XRD and optical microscopy could not be used to differentiate trace element associations. The following sections provide further details of the analytical instruments and techniques used in the solid-phase investigation.

**Table 2-3:
Summary of microscopy methods.**

Technique	Working Scale	Information Provided
Optical Microscopy	Millimetre to micron	Bulk texture Mineralogical identification of large crystalline particles (<i>e.g.</i> , gypsum blades)
Scanning Electron Microscopy (SEM)	Micron	Back scattered electron (BSE) imaging: - Texture, particle size - Relative atomic number (grey scale) Identification of elemental phase associations using: - Point Energy Dispersive X-ray Spectroscopy (EDS) - 2D elemental mapping
Scanning Transmission Electron Microscopy (STEM)	Nanometre	High Angle Angular Dark Field (HAADF) imaging: - Texture, particle size - Relative atomic number (grey scale) Identification of elemental phase associations using: - Point Energy Dispersive X-ray Spectroscopy (EDS) - 2D elemental mapping Selected-Area Electron Diffraction (SAED): - Mineralogy - Degree of crystallinity
X-Ray Absorption Near Edge Structure (XANES)	Atomic	Speciation Oxidation state Bonding characteristics (weakly sorbed or structurally incorporated)

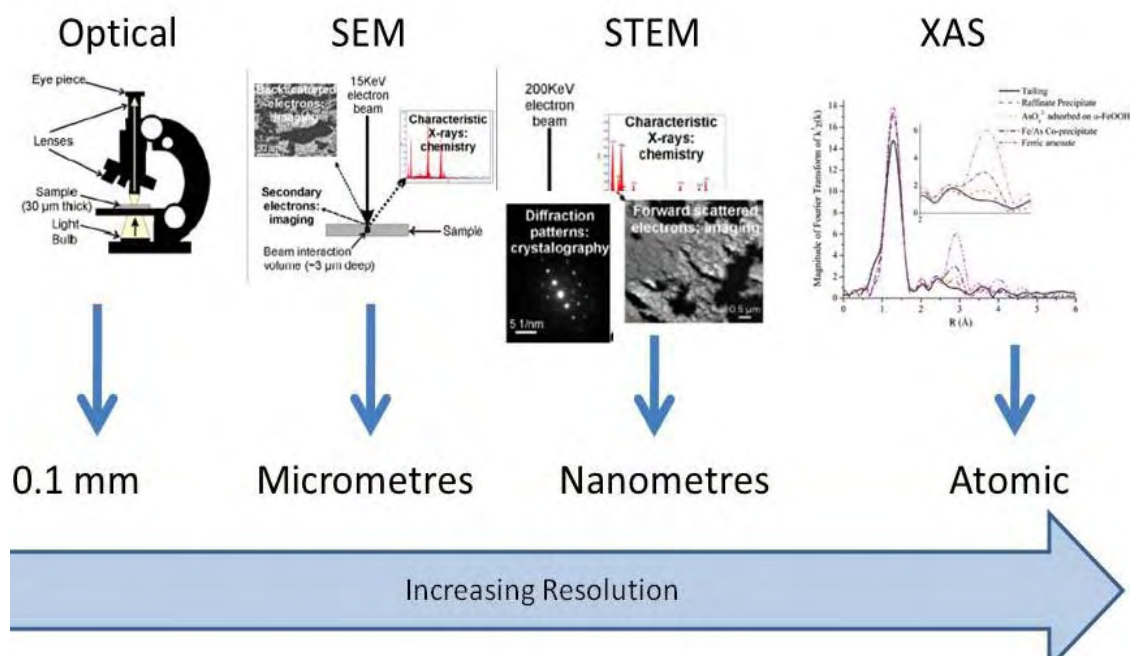


Figure 2-11: Schematic showing increasing spatial resolution associated with optical microscopy, scanning electron microscopy (SEM), scanning transmission electron microscopy (STEM) and x-ray absorption spectroscopy (XAS, that encompasses X-ray absorption near-edge structure).

2.4.2.1 Bulk Chemistry and Trace Metals Analysis

100 mL of each of the HDS samples were sent to SGS-Canadian Environmental & Metallurgical Inc. in Vancouver, BC for solid phase element determination via aqua-regia digestion followed by ICP-MS. Bulk elemental composition for the aged LDS sample from Equity Mine that was collected as part of Phase I of this project was determined by X-Ray Fluorescence (XRF) spectrometry at the University of British Columbia using a Philips PW2400 wavelength-dispersive spectrometer.

2.4.2.2 X-Ray Diffraction

X-ray diffraction analysis identifies minerals by measuring the angle at which a mineral diffracts incident X-rays, which is in turn dependent on the arrangement of atoms within the crystal lattice of minerals. Due to the fact that amorphous materials contain no regularly ordered crystal lattice, these materials do not diffract X-rays and are therefore unidentifiable by XRD.

One sludge sample from each site was submitted for XRD analysis. The samples were dried in an oven at 40°C in the Geology Department at the University of New Brunswick

(UNB). Bulk mineralogy of each sludge sample was determined using a Bruker D8 Advance Powder X-Ray Diffractometer equipped with a solid-state detector. The X-ray diffractograms were interpreted using the International Centre for Diffraction Database PDF-4 and the Search-Match analytical software program Jade.

2.4.2.3 Scanning Electron Microscopy

Scanning electron microscopy (SEM) is used to gain both physical and chemical information of solid materials. Imaging on the SEM provides information on grain size, texture, and mineralogical associations. In addition, the relative greyscale intensity shown in back scatter electron (BSE) images corresponds to the average atomic number such that bright areas indicate relatively high atomic numbers (*e.g.*, CuS₂) while darker areas indicate low atomic numbers (*e.g.*, SiO₂). Elemental analysis is conducted using point energy dispersive X-ray spectroscopy (EDS) and by producing 2-D elemental maps. Under optimized EDS experimental setups, the volume of beam interaction can be as small as 1 x 1 x 3 μm. Point EDS analyses produce spectra which are processed to reveal the elements that are present within the volume of beam interaction as well as their relative quantity. While not quantitative, the production of 2-D elemental maps is useful in visualizing elemental distributions and elemental associations over a given area.

One sample from each mine site was submitted for microscopy investigations. A sample from both the old and new Sullivan treatment plants was included. Grain mounts of the sludge samples submitted for SEM analysis were prepared by mixing the dried material with epoxy and compressing the mixture onto a glass slide. Electron microscopy investigations of the grain mounts were carried out at the University of New Brunswick Microscopy and Microanalysis Facility using a JEOL JSM6400 Scanning Electron Microscope equipped with an EDAX Genesis Energy Dispersive X-ray Spectroscopy system. For each sample, nine areas were analysed by SEM BSE imaging, with up to nine points in each area analyzed by EDS for elemental abundance. Three elemental maps were produced for each sample.

2.4.2.4 Scanning Transmission Electron Microscopy

Scanning transmission electron microscopy (STEM) provides higher resolution information for both imaging and analysis in comparison to SEM, thereby improving the assessment of discrete trace element mineral phase associations. It can also provide information concerning the mineral structure of individual grains. However, with the increase in resolution, the amount of sample material analyzed is consequently reduced. For example, the thickness of the STEM sample is only ~0.1 μm, compared to ~3 μm for SEM.

STEM offers the ability for high resolution imaging (texture and grain size), selected-area electron diffraction (SAED), and qualitative EDS. When in STEM mode, a Gatan Annular Dark Field (ADF) detector, which produces High Angle Angular Dark Field (HAADF) images, is used for imaging. In these images, the brightness reveals information with respect to atomic number, sample thickness, and diffraction contrast (related to the crystallinity of the grains). Similar to SEM, point EDS analyses and 2-D elemental maps are possible using STEM. Unique to the STEM setup is the SAED component. SAED produces a pattern that can be used to derive d-spacings and hence mineral identification. Also, the nature of the pattern (*i.e.*, spotty, narrow smooth rings, broad diffuse rings, *etc.*) provides information on the degree of crystallinity of the mineral phase (*i.e.*, coarsely crystalline, nanocrystalline or amorphous).

One sludge sample from each site was prepared by embedding dried sludge grains in epoxy and sectioning with an ultramicrotome. Glycol was used during ultramicrotoming to minimize the risk of dissolving water-soluble phases. The ultramicrotomed sections were 100 to 150 nanometres in thickness and placed onto 200 mesh Cu or Ni TEM grids with a carbon support film. Analysis was conducted at the University of New Brunswick Microscopy and Microanalysis Facility using a JEOL 2011 STEM. For each sample, up to 18 areas were analyzed by STEM HAADF imaging, with several points within each area analyzed by EDS for elemental abundance. Several points were also analyzed using the SAED feature to assess the degree of crystallinity. One or two elemental maps were produced for each sample.

2.4.2.5 X-Ray Absorption Spectroscopy

X-ray absorption spectroscopy (XAS) is a spectroscopic technique that uses X-rays to probe the chemical and physical structure around an element. X-ray absorption near edge structure (XANES) is a type of XAS technique that examines the structure closest to the atom of the element being analysed. Using this technique, x-rays penetrate the atom and in doing so, cause an electron close to the core of the atom to be ejected. The ejection of this core electron causes a photoelectron wave to emanate from around the atom (Figure 2-12). The nature of the photoelectron wave reveals information about the chemistry (what element it is) as well as its oxidation state. For this study, XANES spectra for Zn were collected for the sludge samples as well as a range of Zn-bearing model phases. This information allowed for the distinction between Zn adsorbed onto the surface of Fe-oxyhydroxide, and structurally-incorporated Zn, as in a Zn-oxyhydroxide, for example.

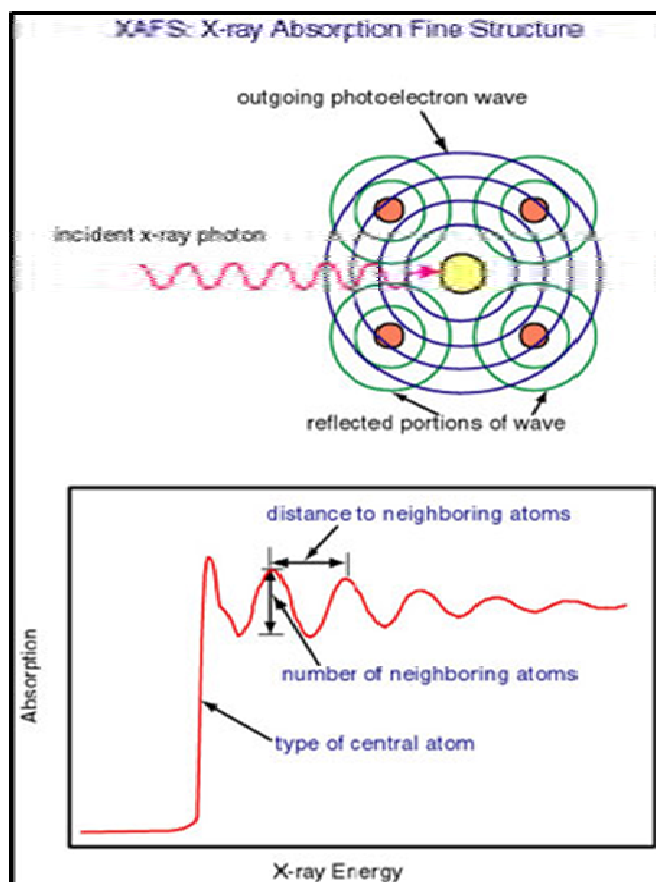


Figure 2-12: X-ray absorptions spectroscopy: Illustration (courtesy of the Canadian Light Source) of the interaction of the photoelectron wave with surrounding atoms and the resulting spectra produced.

Zn K-edge XANES spectra for the seven HDS samples and two Zn-bearing model mineral phases (franklinite (ZnFe_2O_4) and zincite (ZnO)) were collected at the Canadian Light Source (CLS) in Saskatoon, SK. The data were sent to Queen's University for processing and linear combination fitting against XANES spectra collected at the CLS and Advanced Photon Source (APS) for a range of Zn-bearing mineral assemblages. All XANES data processing was performed in SIXpack (Webb, 2005), a software program dedicated to XAS analysis. In order to determine the maximum number of components (or standards) required to adequately describe the data, principal component analysis (PCA) was applied to the CLS sample spectra. The reference XANES spectra collected were then related to the principal components by target transformation to identify which could be considered as appropriate end-members for linear combination fitting. Linear combination fitting of the reference standards to the sample data was performed by minimizing a least squares residual. This was done between 9640 and 9740 eV, which encompassed the primary features of the Zn K-edge XANES region.

3. Results and Discussion

3.1 Water Samples

3.1.1 Influent and Effluent Chemistry

Influent (*i.e.*, raw ARD feed) and effluent (*i.e.*, clarifier outflow) waters were sampled at each study site on multiple days before and after sludge collection to: 1) assess variability in the influent and effluent streams; and 2) ensure that the process waters were representative of the sludges generated. Overall, all influent and effluent waters show a high level of consistency over the daily time scales of sample collection. A summary of the influent and effluent water chemistry data for the mine site treatment plants is presented in Table 3-1 (values as mmol/L), Table 3-2 (values as mg/L), Figure 3-1 (dominant parameters) and Figure 3-2 (trace elements). Note that all parameters are for dissolved species. The complete influent and effluent chemistry data sets are provided in Appendix A. Water quality data for each site are discussed in the sections to follow.

3.1.1.1 Equity Mine

The Equity Mine ARD influent samples are dominated on a molar basis by $\text{SO}_4 >> \text{Mg} > \text{Al} > \text{Fe} >> \text{Ca} > \text{Cl} > \text{F} > \text{Mn} > \text{Zn}$ (Table 3-1; Appendix A1). With respect to cations, the combined molar concentration of Mg+Al is greater than four times the concentration of Fe. Manganese (~140 mg/L), Zn (~120 mg/L) and Cu (~60 mg/L) represent the dominant trace elements in the ARD feed, with lesser amounts of As (~6 mg/L), Co (~4 mg/L) and Cd (~1 mg/L) (Appendix A-1). The composition of the clarifier outflow is dominated by $\text{SO}_4 > \text{Mg} > \text{Ca} > \text{Na} > \text{Mn}$. Through the treatment process, the pH increases from 2.7 to 7.0, and concentrations of As, Cd, Co, Cr, Cu, Ni and Zn are reduced by ~ 90%, with the majority of trace elements at values below the analytical limits of detection (Figure 3-1 and Figure 3-2). Of the major cations, Al and Fe are removed completely during treatment while Mg is reduced in concentration by ~60%. Sulfate concentrations are reduced by >70% during the treatment process, from ~9,000 mg/L in the ARD feed to ~2,800 mg/L in the outflow. Concentrations of Ca and Sr increase in concentration in the effluent, reflecting the dissolution of Sr-bearing quick lime (CaO) applied during water treatment. Concentrations of SO_4 , Al, Mg, Mn, Zn and Cu are highest in the feed at Equity compared to all other influent samples in the study. The concentration of Fe in the Equity feed is also notably higher than concentrations in all other influent samples except for that of Geco.

Table 3-1:
Water quality summary for ARD treatment plant influent and effluent samples.
Values are arranged in order of abundance from top to bottom to illustrate
dominant parameters. All parameters are for dissolved species and presented in
mmol/L.

<i>Equity Silver Mine</i>		<i>Geco Mine</i>		<i>Britannia Mine</i>		<i>Brunswick Mine</i>									
Influent	Effluent	Influent	Effluent	Influent	Effluent	Influent	Effluent								
pH	2.7	pH	7.0	pH	3.0	pH	8.1	pH	4.1	pH	7.5	pH	6.8	pH	8.5
SO ₄	103	SO ₄	29.4	SO ₄	47.7	SO ₄	35.5	SO ₄	13.7	SO ₄	13.6	Na	80.0	Na	79.6
Mg	37.8	Mg	15.5	Fe	19.4	Ca	21.6	Ca	10.3	Ca	12.5	SO ₄	36.6	SO ₄	37.0
Al	28.7	Ca	15.4	Ca	8.39	Mg	7.80	Mg	2.62	Mg	2.17	Mg	4.53	Ca	5.32
Fe	16.5	Na	1.31	Mg	7.23			Al	0.704	Na	0.787	Ca	2.94	Mg	4.18
Ca	8.15	Mn	0.05	Zn	0.19			Cl	0.526	Cl	0.737	Cl	2.88	Cl	2.82
Cl	7.05			Mn	0.13			Cu	0.275			Zn	1.11	Mn	0.12
F	3.05							Zn	0.274			Fe	0.57		
Mn	2.49							Mn	0.0764			Mn	0.46		
Zn	1.88											Cu	0.012		
Cu	0.93														
		<i>Chisel North Mine</i>		<i>Samatosum Mine</i>		<i>Sullivan Mine</i>									
		Influent	Effluent	Influent	Effluent	Influent	Effluent	Influent	Effluent	Influent	Effluent	Influent	Effluent	Influent	Effluent
		pH	4.8	pH	7.4	pH	2.9	pH	8.8	pH	3.2	pH	8.6		
		Cl	43.3	Cl	43.0	SO ₄	42.7	SO ₄	30.2	SO ₄	42.8	SO ₄	38.6		
		Na	17.95	Ca	18.90	Mg	16.7	Ca	19.8	Mg	26.4	Ca	19.0		
		Ca	16.33	Na	17.86	Ca	8.56	Mg	13.9	Ca	8.14	Mg	18.7		
		SO ₄	14.33	SO ₄	14.09	Fe	6.63			Fe	4.60	Na	1.49		
		Mg	7.75	Mg	7.52	Zn	0.980			Na	1.57	Cl	1.41		
		Zn	1.07			Al	0.437			Cl	1.41	Mn	0.02		
		Fe	0.812			Mn	0.208			Mn	0.82				
		Mn	0.090			Cu	0.061			Zn	0.81				
										Al	0.75				

Note: Data presented for Equity, Geco, Brunswick and Chisel North mines are mean values based on three influent and effluent samples. Data presented for the Sullivan Mine is are mean values based on five samples. Data presented for the Britannia and Samatosum mines are based on a single sample.

Table 3-2:
Water quality summary for ARD treatment plant influent and effluent samples.
Values are arranged in order of abundance from top to bottom to illustrate
dominant parameters. All parameters are for dissolved species and presented in
mg/L.

<i>Equity Silver Mine</i>		<i>Geco Mine</i>		<i>Britannia Mine</i>		<i>Brunswick Mine</i>									
Influent	Effluent	Influent	Effluent	Influent	Effluent	Influent	Effluent								
pH	2.6	pH	7.0	pH	3.0	pH	8.1	pH	4.1	pH	7.5	pH	6.8	pH	8.5
SO ₄	9,877	SO ₄	2,823	SO ₄	4,587	SO ₄	3,410	SO ₄	1,320	SO ₄	1,310	SO ₄	3,513	SO ₄	3,553
Fe	924	Ca	616	Fe	1,082	Ca	868	Ca	411	Ca	502	Na	1,840	Na	1,830
Mg	919	Mg	378	Ca	336	Mg	190	Mg	63.7	Mg	52.8	Ca	118	Ca	213
Al	776	Na	30.0	Mg	176	K	51.8	Al	19.0	Na	18.1	Mg	110	Mg	102
Ca	327	Cl	25.0	K	47.7	Na	33.8	Zn	17.9	Cl	14.0	Cl	102	Cl	99.8
Cl	250	Mn	2.53	Na	29.9			Cu	17.5			Zn	72.9	K	21.0
Mn	137			Zn	12.4			Mn	4.20			Fe	32.0	Mn	6.36
Zn	123			Al	10.6							Mn	25.1		
Cu	58.9														
Fe	58.0														
<i>Chisel North Mine</i>		<i>Samatosum Mine</i>		<i>Sullivan Mine</i>											
Influent	Effluent	Influent	Effluent	Influent	Effluent	Influent	Effluent	Influent	Effluent	Influent	Effluent	Influent	Effluent	Influent	Effluent
pH	4.8	pH	7.4	pH	2.9	pH	8.8	pH	3.2	pH	8.6				
Cl	1,537	Cl	1,523	SO ₄	4,100	SO ₄	2,900	SO ₄	4,110	SO ₄	3,708				
SO ₄	1,377	SO ₄	1,353	Mg	405	Ca	793	Mg	641	Ca	761				
Ca	654	Ca	757	Fe	370	Mg	339	Ca	326	Mg	455				
Na	413	Na	411	Ca	343			Fe	257	Na	34.2				
Mg	188	Mg	183	Zn	64.1			Zn	52.7	K	25.0				
Zn	69.9			Al	11.8			Mn	45.2						
Fe	45.3			Mn	11.4			Na	36.1						
Mn	4.96			Cu	3.88			K	26.1						
								Al	20.3						

Note: Data presented for Equity, Geco, Brunswick and Chisel North mines are mean values based on three influent and effluent samples. Data presented for the Sullivan Mine is are mean values based on five samples. Data presented for the Britannia and Samatosum mines are based on a single sample.

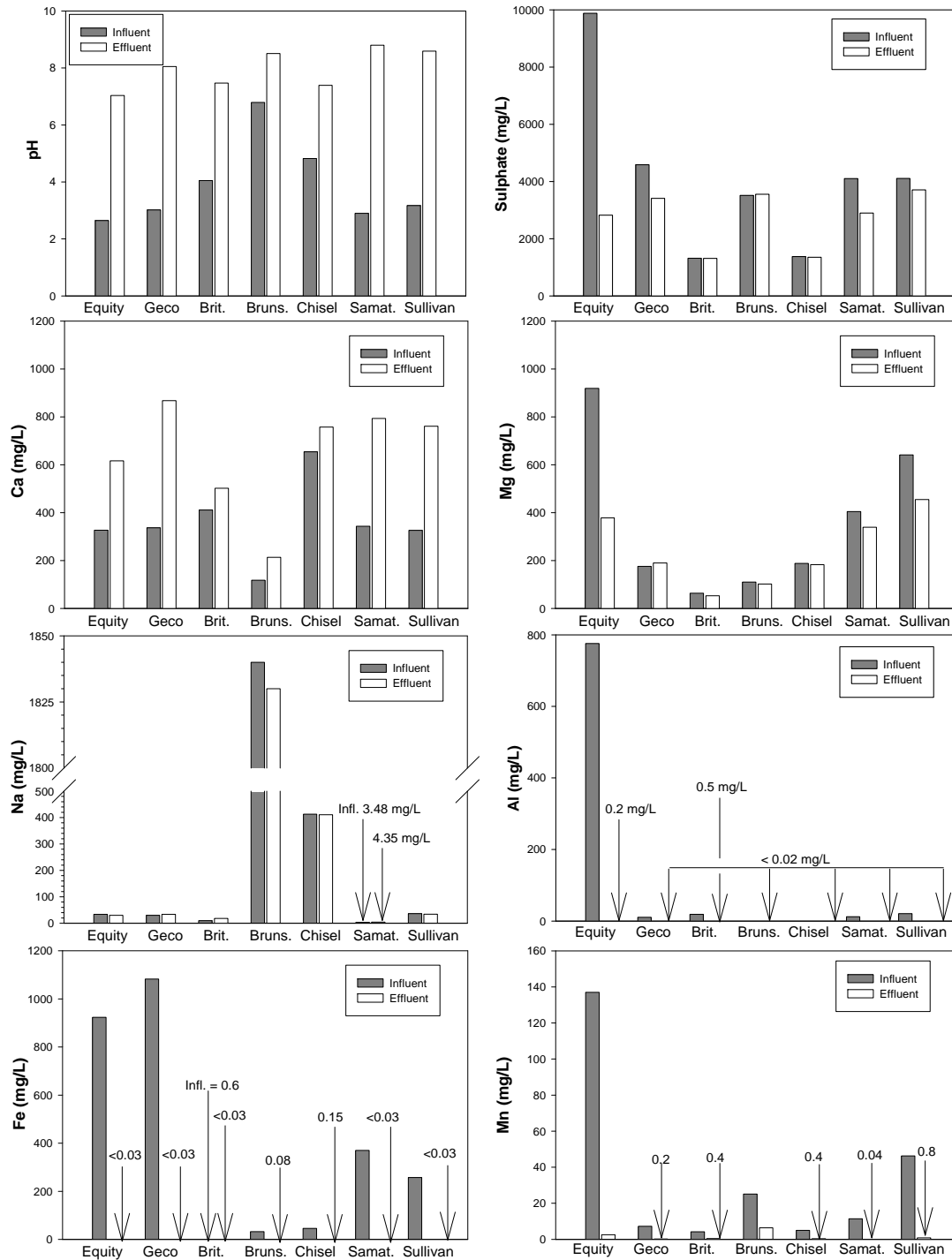


Figure 3-1: Major ion parameters and pH in influent (ARD feed) and effluent (treated clarifier) samples for Equity Mine, Geco Mine, Britannia Mine (Brit.), Brunswick Mine (Bruns.), Chisel North Mine (Chisel), Samatosum Mine (Samat.) and Sullivan Mine. All labeled values represent effluent values unless indicated. All values are for dissolved species.

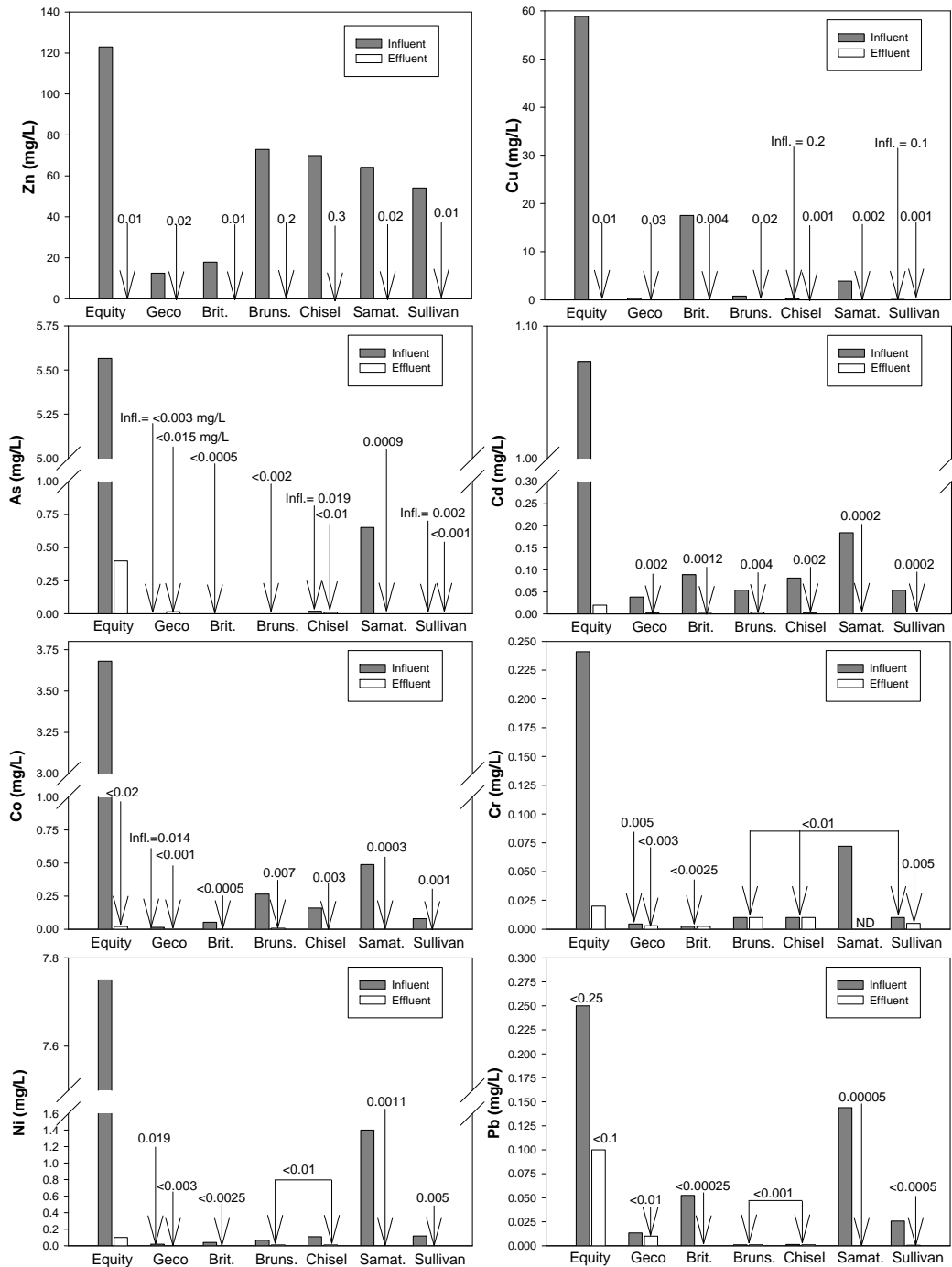


Figure 3-2: Dissolved trace metals in influent (ARD feed) and effluent (treated clarifier) samples for Equity Mine, Geco Mine, Britannia Mine (Brit.), Brunswick Mine (Bruns.), Chisel North Mine (Chisel), Samatosum Mine (Samat.) and Sullivan Mine. All labeled values represent effluent values unless indicated.

3.1.1.2 Geco Mine

On a molar basis, the Geco Mine ARD influent samples are dominated by $\text{SO}_4 > \text{Fe} \gg \text{Ca} = \text{Mg}$ (Table 3-1; Appendix A2). Based on molar proportions, the average concentration of Fe (1,082 mg/L) is greater than the combined contribution from Ca and Mg. Zinc (~12 mg/L), Mn (~7 mg/L), and to a lesser degree Cu (~0.3 mg/L) and Cd (~0.04 mg/L), represent the dominant trace elements in Geco ARD. Through the treatment process, the pH increases from 3.0 to 8.1 and concentrations of trace elements are reduced in the outflow by an average of >90% relative to the composition of the inflow (Figure 3-1 and Figure 3-2). Sulfate concentration decreases only marginally through the HDS process (4,590 mg/L to 3,400 mg/L). The concentration of Fe, which is highest in the Geco feed compared to all other samples in the study, is reduced to levels near or below the analytical detection limit. An increase in Mg and Sr concentrations (along with Ca) in the effluent likely reflects the dissolution of Mg- and Sr-bearing lime during the treatment process.

3.1.1.3 Britannia Mine

On a molar basis, the Britannia Mine ARD influent is dominated by $\text{SO}_4 > \text{Ca} > \text{Mg} \gg \text{Al} > \text{Cl}$ (Table 3-1; Appendix A3). Unlike influent composition at the other study sites, the concentration of dissolved Fe in Britannia feed is particularly low (0.55 mg/L). The dominant trace elements in the Britannia ARD feed are Cu (~18 mg/L) and Zn (~18 mg/L), with lesser amounts of Mn (4.2 mg/L). SO_4 , Ca and Mg dominate the composition of the clarifier outflow (Figure 3-1 and Figure 3-2). Through the HDS treatment process, pH increases from 4.1 to 7.5 and concentrations of Cu and Zn are reduced to <15 ppb. Sulfate shows a negligible change in concentration through the treatment circuit, with concentrations decreasing from ~1,320 mg/L in the influent to 1,310 mg/L in the treated effluent. The difference between these latter values is within the limit of the measurement precision.

3.1.1.4 Brunswick Mine

The Brunswick Mine ARD influent samples are dominated by $\text{Na} > \text{SO}_4 > \text{Mg} > \text{Ca} = \text{Cl} > \text{Zn}$ on a molar basis (Table 3-1; Appendix A4). Zinc (~70 mg/L) represents the dominant trace element of concern in the ARD feed. The concentrations of Fe (~32 mg/L), Mn (25 mg/L), and to a lesser extent, Cu (0.8 mg/L) and Co (0.3 mg/L) are also elevated in the ARD feed (Figure 3-1 and Figure 3-2). A rationale to explain the elevated Fe concentrations in the Brunswick influent is not clear, given the near-neutral pH of the plant feed ($\text{pH} \approx 6.8$). It is possible the high Fe values represent the effect of colloidal Fe that can pass through a 0.45 micron filter, or conversely suboxic waters originating from

the Mine 12 underground. Sulfate, Na, Ca, Mg and Cl represent the main solutes in the clarifier outflow, with many trace elements at values below the analytical limits of detection. Through the HDS process, pH increases from 6.8 to 8.5. Concentrations of SO₄, Mg, and Ca are not appreciably affected through the treatment system. SO₄, for example, shows a marginal increase in concentration from an average of 3,510 mg/L in the ARD feed to an average of 3,550 mg/L in the treated effluent. Trace element concentrations, including Cd, Co, Cu, Fe, Mn, Ni and Zn are reduced in the outflow by >75% relative to the composition of the feed water (Figure 3-1 and Figure 3-2). Zn levels are effectively reduced in the HDS process to an average effluent concentration of 0.2 mg/L.

3.1.1.5 Chisel North Mine

The Chisel North Mine ARD influent samples are dominated by Cl>Na>Ca>SO₄>Mg>Zn on a molar basis (Table 3-1; Appendix A-5). Zinc (~70 mg/L) represents the dominant trace element of concern in ARD feed, with concentrations of Fe (~45 mg/L), Mn (~5 mg/L), Al (~0.8 mg/L), Cu (0.2 mg/L), Co (~0.2 mg/L) and Ni (0.1 mg/L) present in lesser amounts. Dominant solutes in the clarifier outflow include Cl>Ca>Na>SO₄>Mg, all of which show negligible changes in concentration through the HDS process. In particular, SO₄ remains high (>1,350 mg/L) in the effluent. Through the treatment process, the pH of the influent water increases from 4.8 to 7.4 and concentrations of Zn and Mn are reduced to ~0.3 mg/L. Concentrations of Al, Cd, Co, Cu Fe and Ni in the treated effluent are reduced by an average of >90%, with many trace elements reduced to below the limits of analytical detection.

3.1.1.6 Samatosum Mine

On a molar basis, the Samatosum Mine ARD influent sample is dominated by SO₄>Mg>Ca>Fe>Zn (Table 3-1; Appendix A-6). Zinc (~64 mg/L) represents the dominant trace element in the ARD feed; however, appreciable concentrations of Al (11.8 mg/L), As (0.7 mg/L), Cd (0.2 mg/L), Co (0.5 mg/L), Cu (3.9 mg/L), Mn (11.4 mg/L), Ni (1.4 mg/L) and Pb (0.14 mg/L) are also present (Figure 3-1 and Figure 3-2). The composition of the clarifier outflow is dominated by SO₄>Ca>Mg (on a molar basis), with SO₄ concentrations reduced from ~4,100 mg/L in the influent to 2,900 mg/L in the effluent. Through the HDS treatment process, pH increases from 2.9 to 8.8 and most trace elements are reduced to below detection limits (Figure 3-2).

3.1.1.7 Sullivan Mine

The Sullivan Mine ARD influent samples are dominated by $\text{SO}_4 > \text{Mg} \gg \text{Ca} > \text{Fe} > \text{Na} = \text{Cl}$ on a molar basis (Table 3-1; Appendix A-7). With respect to cations, the molar concentration of Mg is more than three times that of Ca. Zinc (53 mg/L), Mn (~46 mg/L) and Al (~20 mg/L) represent the most abundant trace elements in the ARD feed, with lesser amounts (~0.1 mg/L) of Cu and Ni also identified. Through the treatment process, the pH of the influent water increases from ~3.2 to 8.6 and soluble Zn and Mn levels are reduced to <0.01 mg/L and 0.8 mg/L, respectively (Figure 3-1 and Figure 3-2). Of the major cations, Al and Fe are quantitatively removed, while Mg is reduced in concentration by ~30%. The composition of the clarifier outflow is dominated by $\text{SO}_4 > \text{Ca} = \text{Mg} \gg \text{Na} = \text{Cl}$ on a molar basis. Only a minor reduction in SO_4 concentration (~10%) is observed through the HDS process (~ 4,100 to 3,700 mg/L).

3.1.2 Saturation Indices (PHREEQC)

The effluent compositions from each water treatment plant were used as input data to PHREEQC (Parkhurst and Appelo, 1999) to calculate saturation indices (SI) and determine what mineral phases may be close to saturation or oversaturated in the effluent solutions. In brief, saturation indices (SI) are calculated according to:

$$\text{SI} = \log (\text{IAP}/\text{Ksp})$$

where IAP is the ion activity product and Ksp is the solubility constant. SI values for a given mineral phase are generally interpreted in the following manner:

- $\text{SI} < 0$ (*i.e.*, $\text{IAP} \ll \text{Ksp}$): mineral phase is undersaturated and is not predicted to precipitate in solution;
- $\text{SI} > 0$ (*i.e.*, $\text{IAP} \gg \text{Ksp}$): mineral phase is supersaturated and stable if present, indicating that the phase may act as a secondary mineral control. It may also be an indication of some kinetic inhibition in solid precipitation; and
- $\text{SI} \cong 0$ (*i.e.*, $\text{IAP} \cong \text{Ksp}$): mineral phase is at equilibrium and provides strong evidence of a mineral solubility control.

Calculated SIs for each site are presented in Table 3-3. The data show near-saturation with respect to gypsum at all sites ($\text{SI} = 0.0 \pm 0.3$, Table 3-3), with Equity, Geco, Samatosum and Sullivan effluent showing slightly positive values. These results suggest that gypsum is a likely solubility control for both dissolved Ca and SO_4 in treated effluents. This result is not unexpected since lime is predicted to be added in excess to some degree in all treatment systems. XRD data (Section 3.2.2) confirmed the presence of secondary gypsum in all sites showing slightly positive SI values.

The SI values for calcite also provide evidence of a solubility control for dissolved Ca and CO₃. Effluents from Geco and Britannia, for example, show near-saturation with respect to calcite, while effluents from Brunswick, Samatosum and Sullivan mines are slightly supersaturated. The effluent from the Equity Mine is the only solution to show pronounced undersaturation with respect to calcite. XRD data (Section 3.2.2) confirmed the presence of calcite and/or Mg-calcite in all sludge solids with the exception of Equity and Geco mines.

Effluents from all sites are supersaturated with respect to ferrihydrite (5Fe₂O₃·9H₂O) and goethite [FeO(OH)], indicating that these phases are stable if present. Such results are expected given the circum-neutral pH and oxidizing conditions of the final effluents. Indeed, secondary Fe oxide phases are observed at all sites showing appreciable dissolved Fe values in the ARD feed. Effluents from the Geco, Britannia, Brunswick, Chisel North and Sullivan sites are also supersaturated with respect to gibbsite [Al(OH)₃]. Effluent from each site except Equity and Britannia are also supersaturated with respect to barite (BaSO₄). Only the Equity and Geco effluent samples show supersaturation with respect to fluorite.

Table 3-3:
Mineral saturation indices for treated effluent samples - calculated in PHREEQC
(Parkhurst and Appelo, 1999).

Mine	Gypsum CaSO ₄ ·2H ₂ O	Fluorite CaF ₂	Calcite CaCO ₃	Quartz SiO ₂	SiO _{2(am)}	Goethite FeO(OH)	Ferrihydrite 5Fe ₂ O ₃ ·9H ₂ O	Barite BaSO ₄	Gibbsite Al(OH) ₃
Equity	0.08	0.8	-0.87	NC	NC	NC	NC	NC	NC
	0.11	0.08	-1.03	NC	NC	NC	NC	NC	NC
	0.08	0.74	-0.95	NC	NC	NC	NC	NC	NC
Geco	0.3	0.96	0.34	-1.2	-2.53	5.2	2.38	1.29	NC
	0.28	0.88	0.54	-1.2	-2.52	5.69	2.87	0.2	0.5
	0.29	0.94	-0.17	-0.97	-2.29	NC	NC	1.27	NC
Britannia	-0.09	-0.72	-0.31	-0.52	-1.85	4.65	1.83	0.13	2.52
Brunswick	-0.31	-1.37	0.79	-0.42	-1.74	6.01	3.19	1.05	0.38
	-0.31	-1.45	0.75	-0.41	-1.73	6	3.18	0.94	0.39
	-0.32	-1.42	0.88	-0.41	-1.74	6	3.18	0.82	0.26
Chisel North	-0.07	-0.84	NC	-0.7	-2.02	4.51	1.69	1.5	1.15
	-0.09	-0.84	NC	-0.7	-2.03	4.5	1.68	1.15	1.15
	-0.1	-0.75	NC	-0.72	-2.04	4.64	1.82	1.46	1.1
Samatosum	0.19	-0.53	0.91	NC	NC	4.75	1.93	3.24	-0.62
Sullivan	0.21	-0.7	0.84	-0.41	-1.74	5.6	2.78	0.72	0.5
	0.21	-0.72	0.85	-0.41	-1.73	5.6	2.78	0.71	0.42
	0.21	-0.74	0.86	-0.39	-1.71	5.59	2.77	0.72	0.37
	0.23	-0.78	0.76	-0.69	-2.02	5.61	2.79	0.75	0.12
	0.23	-0.15	0.82	-0.69	-2.01	5.6	2.79	0.78	-1.02

Notes: NC = not calculated, effluent parameters below the analytical limit of detection

3.2 Sludge Solids

3.2.1 Multi-Element Chemical Analyses

Sludge samples were analyzed for major and minor element concentrations. These data are summarized in Table 3-4, and presented graphically by mass (Figure 3-3) and by molar concentration (Figure 3-4). The complete solid phase chemistry data set is provided in Appendix B. In general, the dominant solid phase elements in the sludge samples are closely related to the dominant dissolved species in the influent waters. Solid phase composition of each sludge sample is discussed in the subsequent sections.

Table 3-4:

Summary of solid phase elemental composition of sludge solids. Values are arranged in order of abundance from top to bottom to illustrate dominant parameters. Note that a large proportion of the Ca in the solid-phase is from the addition of lime during treatment. Values are presented as mmol/kg and ppm.

<i>mmol/kg</i>															
<i>Equity</i>		<i>Geco</i>		<i>Britannia</i>		<i>Brunswick</i>		<i>Chisel North</i>		<i>Samatosum</i>		<i>Sullivan</i>			
HDS	LDS											new	old		
S	3618	ND	Fe	4692	Ca	3294	Ca	3942	Ca	3643	Ca	2869	Mg	2790	2818
Ca	3468	4117	Ca	2495	Al	2061	Fe	1968	Zn	2016	Mg	2526	Ca	2118	853
Al	1490	704	S	2295	Mg	1419	Zn	1875	Fe	1687	Fe	1903	Fe	2057	2742
Mg	1024	576	Mg	140	Zn	808	Mn	504	Mg	950	S	1877	S	1092	511
Fe	777	734	Si	125	Cu	792	S	502	S	331	Zn	312	Al	537	1390
Mn	127	116	Al	96.4	S	352	Mg	387	Mn	166	Al	193	Zn	445	820
Zn	96.6	115			Mn	208	Na	174					Mn	395	375
					Fe	124									
<i>ppm</i>															
<i>Equity</i>		<i>Geco</i>		<i>Britannia</i>		<i>Brunswick</i>		<i>Chisel North</i>		<i>Samatosum</i>		<i>Sullivan</i>			
HDS	LDS											new	old		
Ca	139,000	165,000	Fe	262,000	Ca	132,000	Ca	158,000	Ca	146,000	Ca	115,000	Fe	114,900	153,100
S	116,000	ND	Ca	100,000	Al	55,600	Zn	122,600	Zn	131,800	Fe	106,300	Ca	84,900	34,200
Fe	43,400	41,000	S	73,600	Zn	52,800	Fe	109,900	Fe	94,200	Mg	61,400	Mg	67,800	68,500
Al	40,200	19,000	Si	3,500	Cu	50,340	Mn	27,700	Mg	23,100	S	60,200	S	35,000	16,400
Mg	24,900	14,000	Mg	3,400	Mg	34,500	S	16,100	S	10,600	Zn	20,400	Zn	29,100	53,600
Mn	6,956	6,400	Zn	2,743	Mn	11,400	Mg	9,400	Mn	9,140	Al	5,200	Mn	21,700	20,600
Zn	6,317	7,500	Al	2,600	S	11,300	Na	4,000			Mn	4,435	Al	14,500	37,500
Cu	2,693	4,900	Mn	1,880	Fe	6,900	Cu	1,470			Cu	1,430			

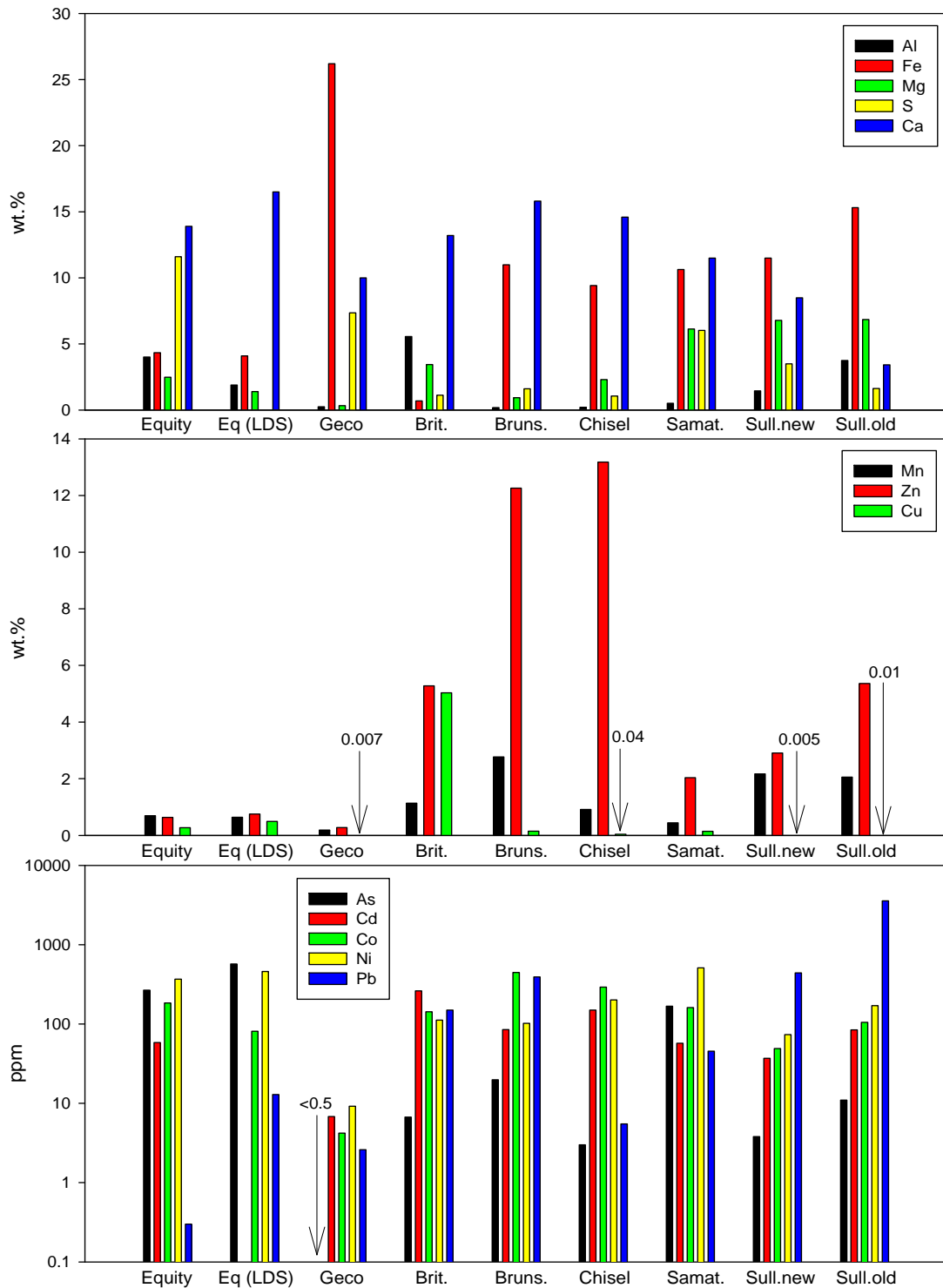


Figure 3-3: Solid phase elemental abundance (by mass) for sludge samples from Equity (HDS and LDS samples), Geco, Britannia (Brit.), Brunswick (Bruns.), Chisel North (Chisel), Samatosum (Samat.) and Sullivan (Sull. new and Sull. old) mines.

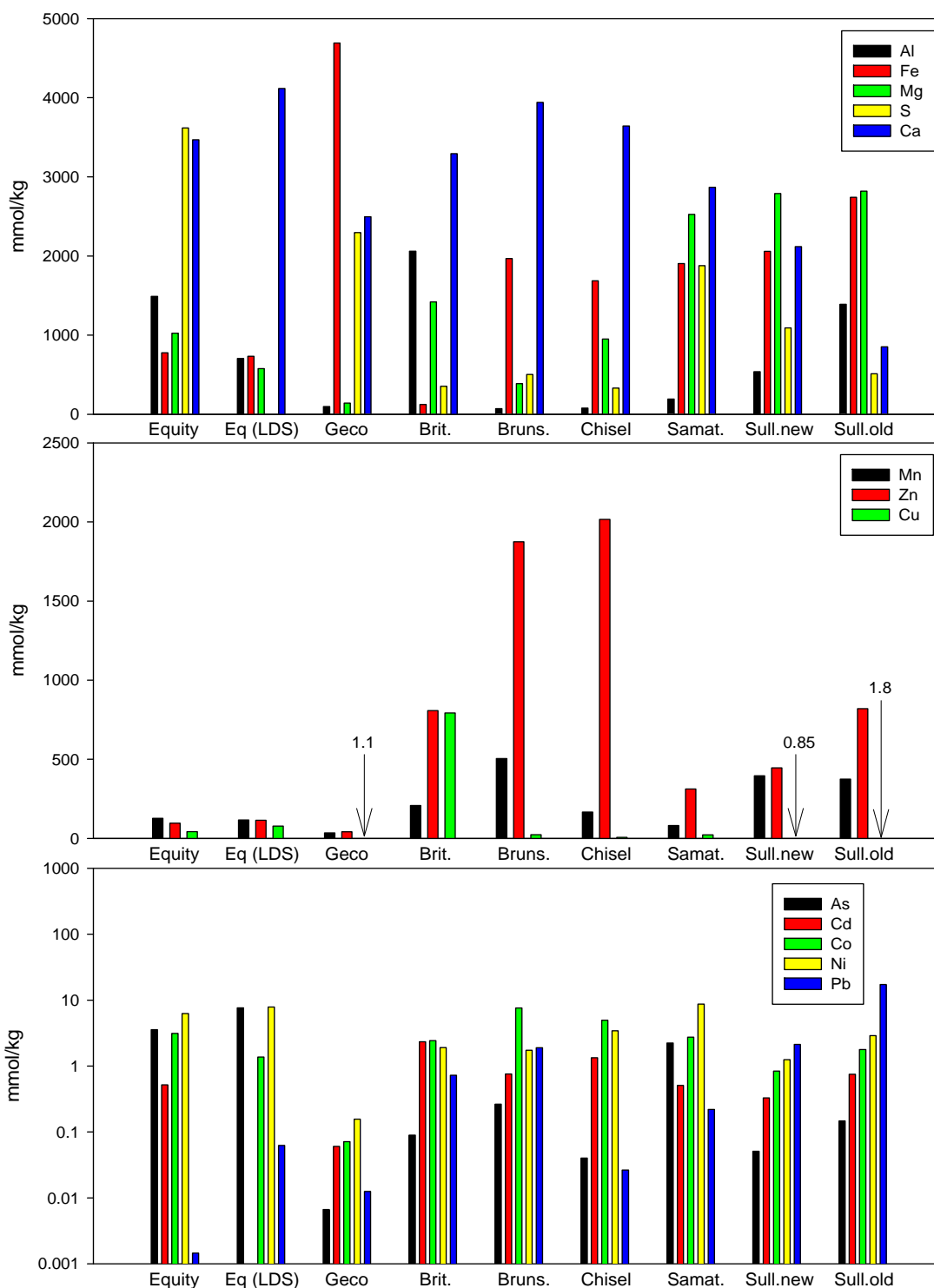


Figure 3-4: Solid phase elemental abundance (by molar concentration) for sludge samples from Equity (HDS and LDS samples), Geco, Britannia (Brit.), Brunswick (Bruns.), Chisel North (Chisel), Samatosum (Samat.) and Sullivan (Sull. new and Sull. old) mines.

3.2.1.1 Equity Sludge

The Equity HDS sample is composed primarily of Ca, S, Fe, Al, and Mg (13.9, 11.6, 4.3, 4.0 and 2.5 wt. %, respectively) (Table 3-4 and Figure 3-3) and is consistent with the high proportions of these elements in the ARD feed (Table 3-4). The LDS and HDS samples show similar compositions, with the exception of As, Cu and Pb, which are noticeably higher in the LDS sample compared to the HDS. Further, Al and Mg are notably higher in the HDS sample relative to the LDS. The variation in sludge composition from the different treatment processes may be due to compositional differences of the ARD feed, variable conditions of the treatment processes, and/or the different analyses employed for the two samples (*i.e.*, bulk elemental composition for the LDS sample was determined by XRF spectrometry, while aqua-regia digestion followed by ICP-MS was used for the HDS sample; Section 2.2.2.1). Concentrations of As are highest in the Equity LDS (572 ppm) and HDS (267 ppm) samples compared to the other sludge samples in the study (Figure 3-3).

3.2.1.2 Geco Sludge

The Geco sludge sample is composed primarily of Fe, Ca and S (26, 10, and 7.4 wt. %, respectively) with considerably lower concentrations of Al and Mg (0.26 and 0.34 wt. %, respectively) (Table 3-4 and Figure 3-3). The composition of the Geco sludge is consistent with the high concentrations of Fe and S in the ARD influent and high rates of removal for these constituents during the neutralization process.. The concentration of Fe, in particular, is higher in the Geco sludge compared to all other sludge samples in the study. Mn (1,880 ppm) and Zn (2,743 ppm) are the dominant trace metals in the Geco sludge; however, concentrations of these metals are significantly lower than those measured in the other study samples.

3.2.1.3 Britannia Sludge

The Britannia sludge sample is composed primarily of Ca, Al, Zn, Cu, Mg and Mn (13, 5.6, 5.3, 5.0, 3.5 and 1.14 wt. %, respectively) (Table 3-4 and Figure 3-3). The abundance of these elements in the solid phase is reflected by high values for these constituents in the ARD influent (Figure 3-1). In addition, solid phase concentrations of Cd, Co, Pb and Ni are also relatively high in the Britannia sludge (262, 143, 150 and 112, respectively; Figure 3-3) despite the relatively low concentrations in the ARD feed (<0.09 mg/L). Overall, solid phase concentrations of Cd and Cu are highest in the Britannia sludge compared to the other study samples. Note that the solid phase concentration of Fe (0.7 wt. %) is lowest in the Britannia sludge compared to the other samples, which is consistent with low levels measured in Britannia ARD influent (0.6 mg/L).

3.2.1.4 Brunswick Sludge

The Brunswick sludge sample is composed primarily of Ca, Fe, Zn and Mn (16, 11, 12 and 2.8 wt. %, respectively) (Table 3-4 and Figure 3-3). Despite the relatively low concentration of Fe in the ARD feed (~30 mg/L), Fe is one of the dominant solid phase constituents. This reflects: 1) the low solubility of dissolved Fe in the treated effluent, and its quantitative removal during treatment; and 2) the negligible removal of the dominant ARD solutes within the treatment system (S, Na and Mg). The concentration of Al (0.19 wt. %) is lower than the other major cations and is the lowest of all the sludge samples in the study. This is consistent with the low levels of dissolved Al present in the ARD feed (<0.02 mg/L). Solid phase concentrations of Cd, Co, Cu, Pb, Ni, and Ag are also elevated in the Brunswick sludge (85, 447, 1,470, 392, 102, and 109 ppm, respectively). However, with the exception of Co and Cu, these metals are not particularly abundant in the ARD feed water (< 0.07 mg/L).

3.2.1.5 Chisel North Sludge

The Chisel North sludge sample is composed primarily of Ca, Zn, Fe and Mg (14.6, 13.2, 9.4 and 2.3 wt. %, respectively) (Table 3-4 and Figure 3-3). The concentration of Al is considerably lower than the other major cations (0.21 wt. %), consistent with the low dissolved Al content in the ARD feed (<1 mg/L). The solid-phase value for Zn (~13 wt.%) is the highest measured in all the sludge materials sampled in the study. Though concentrations of Zn are elevated in the Chisel North ARD feed, concentrations of Zn in the Equity and Brunswick influent are higher (Figure 3-2). The lower Zn values in the solid phase in the Equity and Brunswick sludge, despite higher Zn in the mine drainage, indicates that the final solid phase concentration is also influenced by dilution with other phases that form within the treatment system.

Similar to the Brunswick Mine, the concentration of solid phase Fe is relatively high in relation to its proportion in the ARD feed (45 mg/L). This can be related to the complete removal of Fe during treatment, in conjunction with negligible rates of removal for the dominant ions (Cl, S, Ca and Mg). Ba, Cd, Co, Cu and Ni (152, 150, 292, 430 and 201 ppm, respectively) are also present in moderate quantities.

3.2.1.6 Samatosum Sludge

The Samatosum sludge sample is composed primarily of Ca, Fe, Mg, S and Zn (11.5, 10.6, 6.1, 6.0 and 2.0 wt. %, respectively) (Table 3-4 and Figure 3-3). Concentrations of Al are considerably lower than the other major cations in the Samatosum sludge (0.52 wt. %), consistent with the relatively-low dissolved Al content in the ARD feed (~12 mg/L). Zn represents the dominant trace metal in the solid phase,

which is consistent with elevated concentration in the ARD feed. The abundance of Fe, Mg and S in the solid phase is also reflected by high values for these elements in ARD influent. After Zn, the highest solid-phase abundances are shown by Mn (0.44 wt. %) and Cu (0.14 wt. %), followed by As, Cd, Co and Ni (168, 57.1, 161 and 511 ppm, respectively).

3.2.1.7 Sullivan Sludge

The ‘new’ Sullivan sludge sample is composed primarily of Fe, Ca, Mg, Zn and Mn (11.5, 8.5, 6.8, 2.9 and 2.2 wt. %, respectively) and to a lesser extent Al (1.45 wt. %) (Table 3-4 and Figure 3-3). Overall, the solid-phase concentration of Mg in the ‘new’ Sullivan sludge sample is higher compared to the other study samples. This relates to the high Mg concentration in the ARD feed, as well as to the lower concentrations of other competing phase-forming elements (*e.g.*, Al). At Equity Mine, for example, Mg concentrations in the solid phase are lower despite higher values in the ARD feed. This can be attributed to the dilution of the Mg signature with other phase forming elements (Al and S) that are present in much higher proportions in the Equity ARD.

Zinc and Mn represent the dominant trace metals in the solid phase of the ‘new’ sludge, which is consistent with elevated concentrations of these metals in the ARD feed. Other trace elements of note in the solid phase include Pb, Cd, Co and Ni (440, 37.0, 49.2 and 73.5 ppm, respectively). The ‘old’ Sullivan sludge sample shows similar trace element content compared to the ‘new’ sample, but differs somewhat with respect to the major cation composition (Table 3-4 and Figure 3-3). Specifically, the ‘old’ sludge sample shows higher concentrations of Fe (15.3 wt. %) and Al (3.8 wt. %) and lower concentrations of Ca (3.5 wt. %) and S (1.6 wt. %). The ‘old’ Sullivan sludge sample also hosts higher concentrations of Zn (5.4 wt. %) compared to the ‘new’ Sullivan sample. Such differences may be related to both differences in the ARD feed and treatment process.

3.2.2 Identification of Crystalline Phases in Sludge Samples (XRD)

A sub-sample of each of the HDS samples was analyzed by XRD to identify detectable crystalline phases. A summary of the minerals identified by XRD is presented in Table 3-5. Gypsum is the only crystalline phase confirmed by XRD in both the Equity and Geco HDS samples, while Mg-calcite is the only crystalline phase identified in the Britannia HDS sample. Two phases, calcite and Mg-calcite, were identified in the Brunswick and Chisel North HDS samples; and three crystalline phases, calcite, Mg-calcite and gypsum, were identified in the Samatosum HDS sample. XRD analysis identified different crystalline assemblages in the two Sullivan HDS samples; calcite and

gypsum were identified in the “new” Sullivan sludge sample; however, only calcite was identified in the “old” Sullivan sludge sample. The identification of Ca-bearing phases by XRD analysis is consistent with saturation indices calculated from effluent chemistry data (Table 3-3) and dominant solid phase elements measured in sludge samples (Table 3-4).

Table 3-5:
Crystalline phases in sludge samples identified by XRD. Shaded boxes denote phases identified.

Mineral	Ideal Formula	Mine Site							
		Equity	Geco	Brit.	Bruns.	Chisel	Samat.	Sull. new	Sull. old
Calcite	CaCO ₃								
Mg-Calcite	(Mg _{0.03} Ca _{0.97})(CO ₃)								
Gypsum	CaSO ₄ ·2H ₂ O								

Further review of the XRD spectra revealed a broad unidentified peak near 34-36 degrees 2θ and another broad peak at 60-63 degrees 2θ (that may be overlapping with calcite peaks) in the Brunswick, Chisel North, Samatosum and Sullivan mine sludge samples which are consistent with the poorly crystalline 2-line ferrihydrite (Fe₂O₃·0.5(H₂O)) (Figure 3-5). The presence of ferrihydrite in these samples is further supported by the absence of ferrihydrite peaks in the Britannia HDS sample, which contained the lowest Fe content in influent and solid phase relative to the other study samples. Collectively, the available evidence suggests that the sludge samples from the Brunswick, Chisel North, Samatosum and Sullivan mines host ferrihydrite.

3.2.3 Identification of Dominant and Trace Metal-Bearing Phases in Sludge Samples (SEM and STEM)

Investigations using XRD and optical microscopy have proved ineffective in identifying trace-element associations within lime neutralization sludges. This relates to: 1) amorphous or poorly crystalline materials are not detected by XRD; and 2) optical microscopy does not provide sufficient spatial resolution to fully differentiate trace element associations in fine-grained, heterogeneous sludge matrices. In order to provide further insight into the nature of neutralization sludges, a combination of high-resolution microscopy methods was utilized to characterize the controls governing metal sequestration. These methods include, in order of increasing resolution; SEM, STEM and XANES. A summary of the major, minor and trace metal-bearing phases identified in the sludge samples by XRD and microscopic investigations are provided in Table 3-5. Substantiation of these phases is outlined and discussed in the following sections.

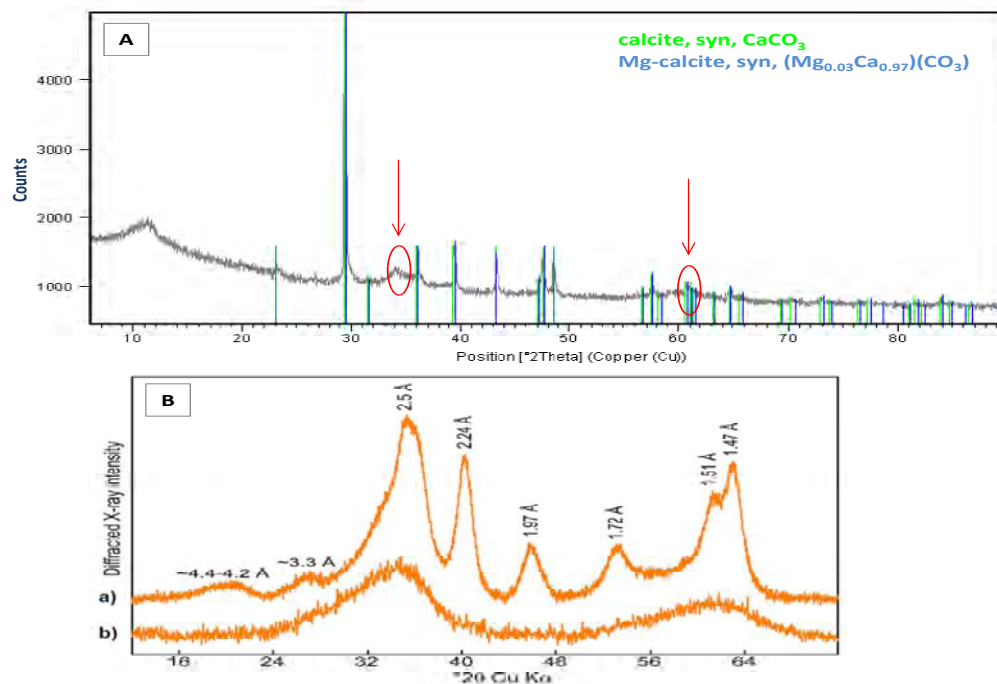


Figure 3-5: (A) XRD spectra for Brunswick Mine sludge. Broad peaks that are consistent with 2-line ferrihydrite (shown in B) are outlined in red.

(B) X-ray diffraction patterns for 6-line (a) and 2-line (b) ferrihydrite, modified from A. Manceau (2009), after Drits *et al.* (1993) in *Clay Minerals* (vol. 28, 185-207).

3.2.3.1 Equity Sludge

Equity HDS Sample

Five main phases were identified in the Equity HDS sample by SEM analysis: 1) gypsum, as confirmed by XRD (Table 3-5); 2) Al-(oxy)hydroxide; 3) Fe-Al (oxy)hydroxide; 4) Mg-Al-(Fe) hydroxysulfate (Figure 3-6); and 5) a Ca- and Sr-bearing carbonate, likely calcite (Figure 3-7). SEM and STEM analyses demonstrate that Zn and Cu are predominantly associated with the Mg-Al-(Fe) hydroxysulfate phase rather than the Al or Fe-Al (oxy)hydroxide phases (Figure 3-6 and Figure 3-7). Other elements detected in the Mg-Al-(Fe) hydroxysulfate phase include As and Pb. Due to the fact that As and Pb peaks overlap in EDS, the presence of these two elements cannot be determined definitively based on EDS alone. However, bulk chemical analyses indicate that As is present in considerably higher concentrations compared to Pb in both Equity sludge samples (Figure 3-3). Therefore, it is likely that As was detected in the STEM analyses.

Table 3-5:
Summary major, minor and trace metal-bearing phases identified in sludge samples.

Mine	Major Phases (XRD, SEM and/or STEM)	Minor Phases (SEM and/or STEM)	Trace Metal Bearing Phase (SEM and/or STEM)
Equity	gypsum Mg-Al(Fe) hydroxysulfate	Al-(oxy)hydroxide Fe-Al (oxy)hydroxide calcite	Mg-Al(Fe) hydroxysulfate
Geco	gypsum Fe oxyhydroxide	Al-(oxy)hydroxides calcite	Fe oxyhydroxide
Britannia	Mg-calcite Cu oxyhydroxide	quartz Fe oxyhydroxide	Cu oxyhydroxide
Brunswick	calcite Mg-calcite Zn-Fe-Mn oxyhydroxide	quartz Al-silicates Fe oxyhydroxide	Zn-Fe-Mn oxyhydroxide
Chisel	calcite Mg-calcite Zn-Fe-Mn oxyhydroxide	pyrite quartz barite Al and Ca-Fe silicate	Zn-Fe-Mn oxyhydroxide
Samatosum	calcite, Mg-calcite (altered) Al-silicates gypsum Fe-Mg oxyhydroxide	Fe oxyhydroxide	Fe-Mg oxyhydroxide
Sullivan	calcite gypsum Fe-Mg oxyhydroxide	Ca silicates Fe oxyhydroxides barite Ca-Fe oxyhydroxide/carbonate Ca Ti-oxide	Fe-Mg oxyhydroxide

Note: method of identification is in parentheses

The Mg-Al(Fe) hydroxysulfate phase occurs as spherical to oval aggregates that typically display concentric layers and irregular particle boundaries (Figure 3-8). The aggregates range in size from <1 μm to approximately 15 μm and are composed of wispy fibres measuring <0.01 by 0.2 μm (Figure 3-7). The Mg-Al(Fe) hydroxysulfate in the Equity HDS did not produce discernible diffraction patterns or rings when analyzed by SAED, suggesting that it is amorphous. Of particular note for the Mg-Al(Fe) hydroxysulfate grains in the Equity HDS, is the compositional zoning in concentric layers alternating between: 1) Mg- and Al-rich (Fe-poor); and 2) Fe-rich zones (Figure 3-8). Such zonation can be attributed to the recycling of sludge within the HDS process, and the contrasting solution chemistries between the beginning and end of the system.

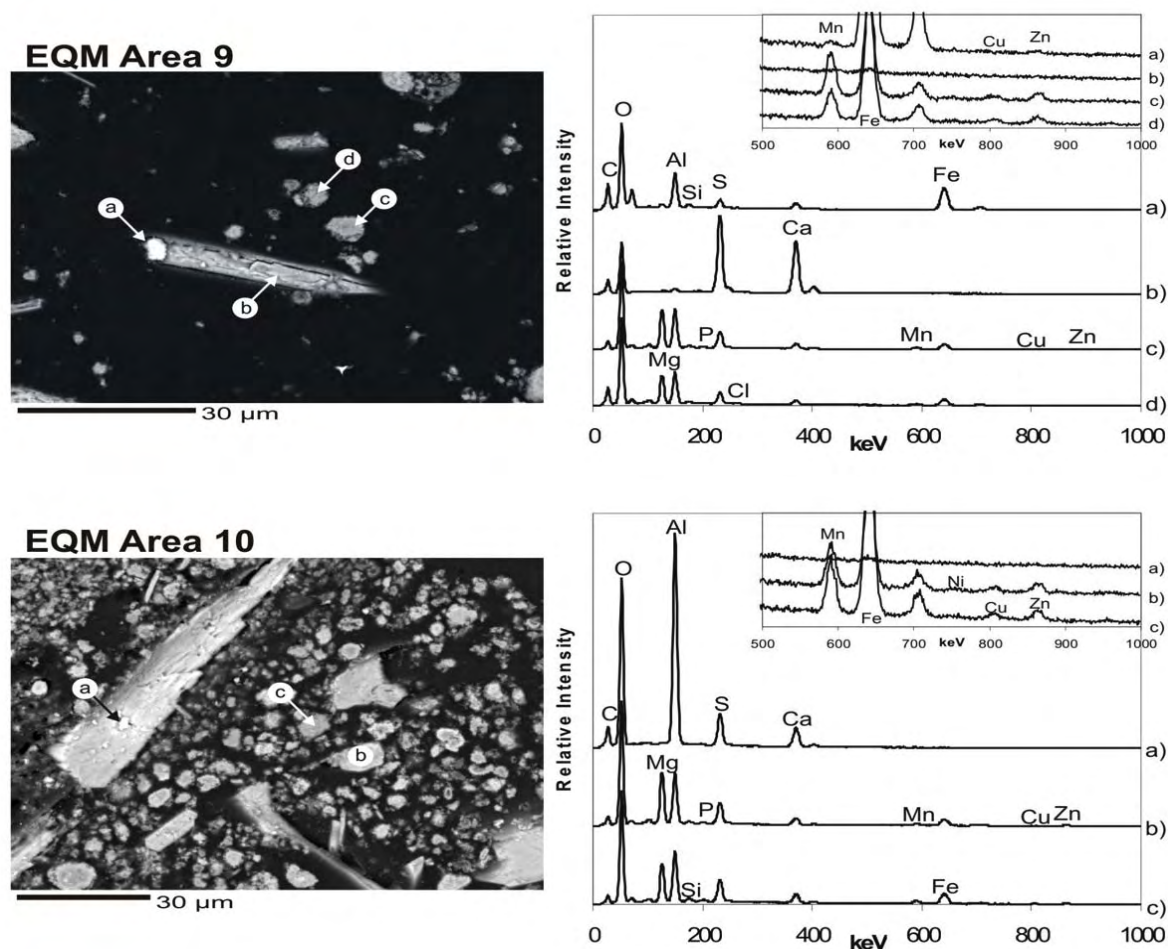


Figure 3-6: Equity Mine HDS: SEM back scattered electron (BSE) images (left) and associated EDS spectra (right) for points a through d. The inset spectra have been vertically expanded to show trace element peaks.

EQM Area 9: Gypsum (b) with Al-Fe (oxy)hydroxide (a) and Mg-Al-(Fe) hydroxysulfate (c and d). Note that there is relatively more Cu and Zn associated with the Mg-Al-(Fe) hydroxysulfate than the Al-Fe hydroxide (shown on expanded scale in inset).

EQM Area 10: Gypsum with Al-(oxy)hydroxide (a) and Mg-Al-(Fe) hydroxysulfate (b and c), illustrating the Cu and Zn association with the Mg-Al-(Fe) hydroxysulfate and the Al (oxy)hydroxide (shown on expanded scale in inset).

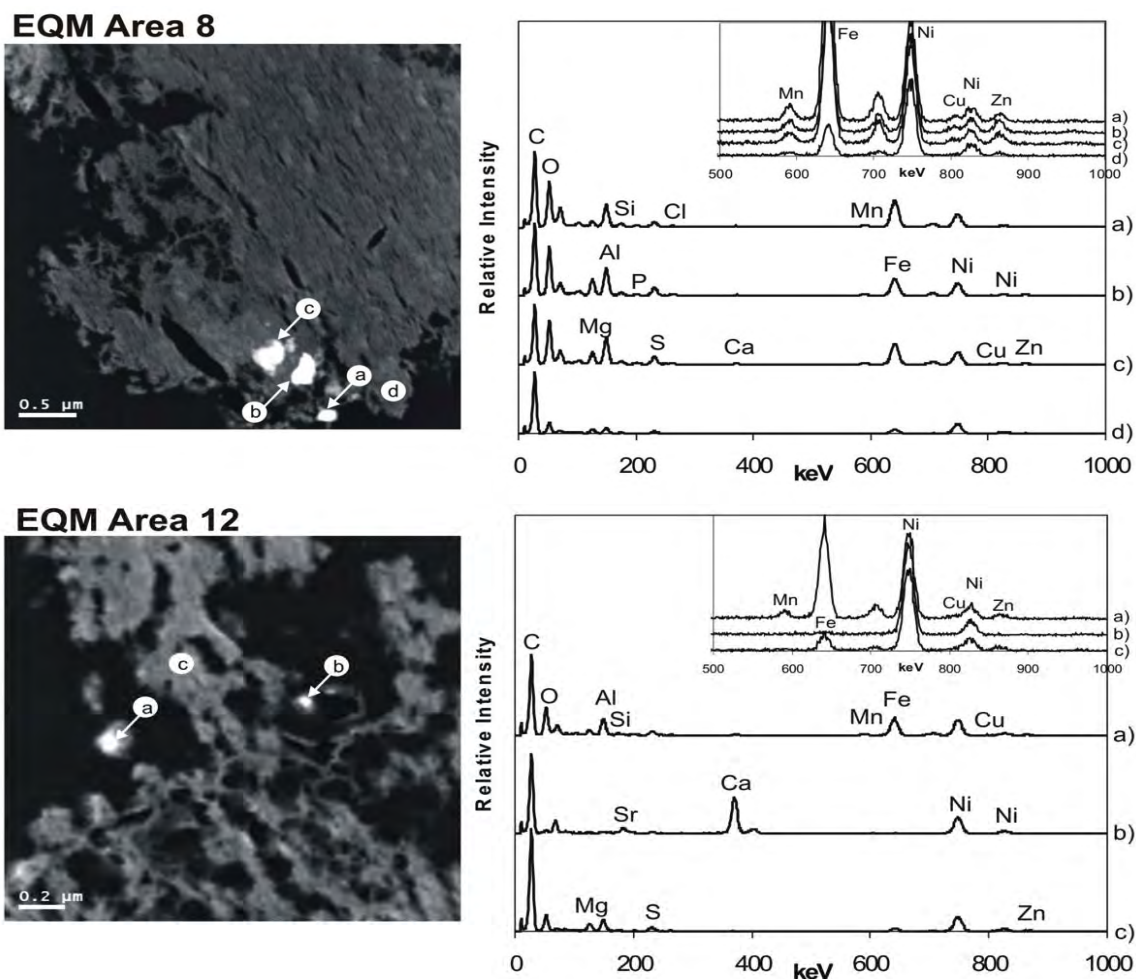


Figure 3-7: STEM annular dark field (ADF) images of Equity HDS (left) and associated EDS spectra (right) for points a) through d) in each image. The inset spectra have been vertically expanded to show trace element peaks. The Ni peaks result from the Ni support grid used in STEM analysis, and do not represent Ni content in the sample.

EQM Area 8: Four point spectra of the Mg-Al-(Fe) hydroxysulfate (a through d) showing presence of Cu and Zn. The spectra illustrate that the difference in brightness in the ADF image is most likely a result of variation in sample thickness rather than major compositional differences (brighter image for a through c compared to d).

EQM Area 12: Spectra of the Mg-Al-(Fe) hydroxysulfate (a and c) illustrating variable Mg, Al, and Fe content and presence Zn; and a Ca-bearing carbonate (b) containing trace Sr (likely calcite) and no Cu or Zn (inset).

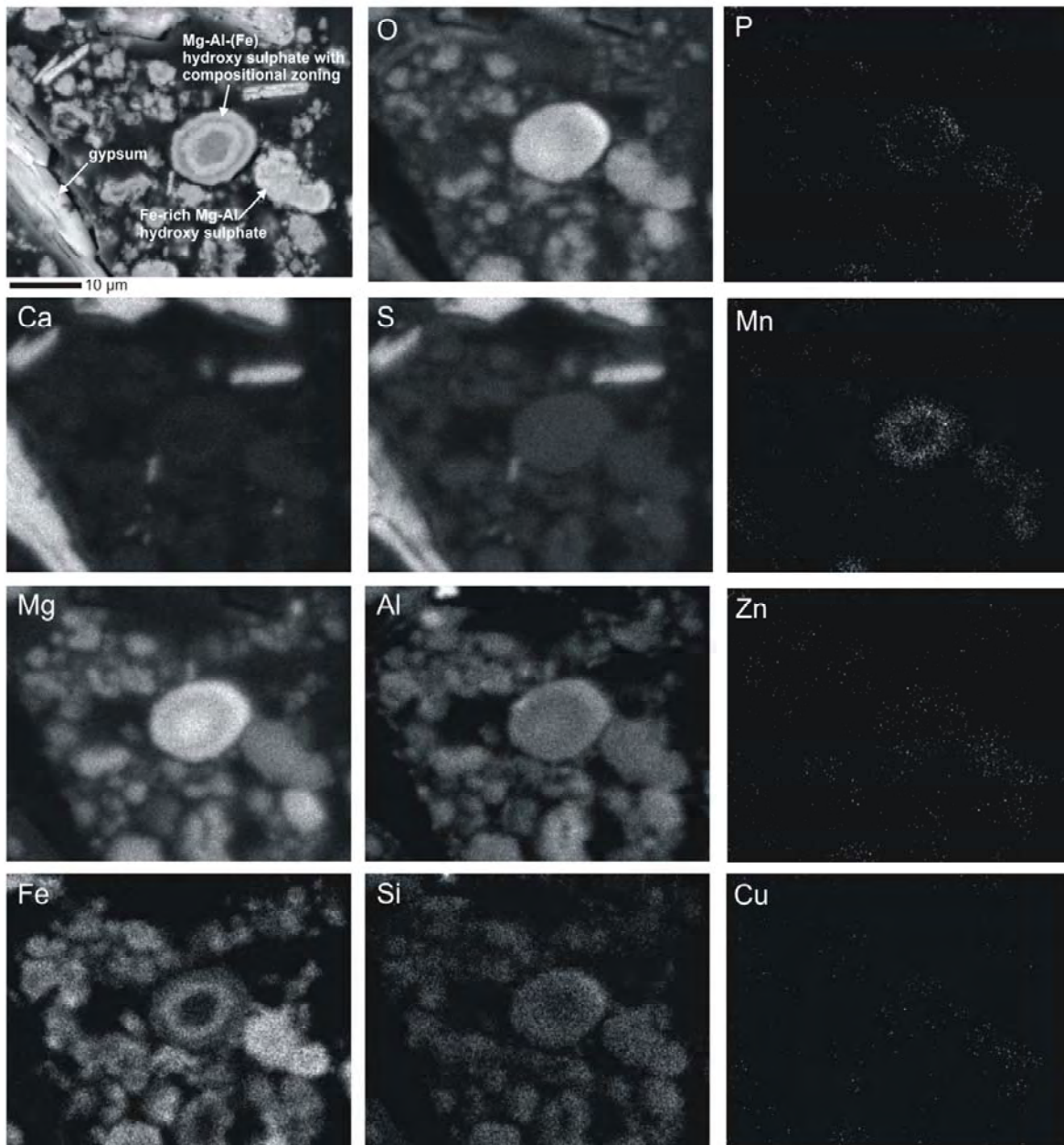


Figure 3-8: SEM back scattered electron (BSE) image (upper left) of the Equity HDS showing compositional zoning of the trace metal-bearing Mg-Al-(Fe)-hydroxysulfate phase. SEM EDS 2-D elemental maps for Equity HDS sample (EQM Area 8) are also shown, showing the relative abundance of O, P, Ca, S, Mn, Mg, Al, Zn, Fe, Si and Cu.

EDS elemental maps indicate that Mn and P are associated with the Fe-rich components of the sludge matrix (Figure 3-8). The specific associations of Cu and Zn with the Mg-Al-(Fe) hydroxysulfate phase are more difficult to determine in SEM EDS element maps due to the low concentrations of these elements (Figure 3-7). However, plots of EDS relative intensities for Zn:Mg, Zn:Al and Zn:Fe for the Equity HDS indicate that Zn is better correlated with Mg and Al in comparison to Fe (Figure 3-9), suggesting a preferential association of Zn with the Mg and Al.

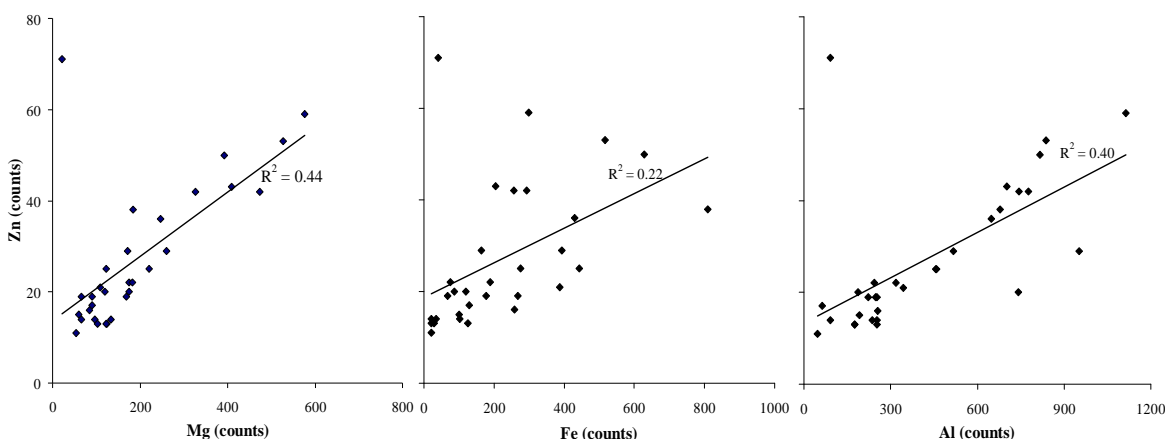


Figure 3-9: Plots of STEM EDS net intensities for Equity HDS sample. The data indicate a good correlation for Zn:Mg and Zn:Al intensities.

While SEM analyses indicate that Ca may also be a component of the Mg-Al-(Fe) hydroxysulfate (Figure 3-8), STEM shows that, although Ca may be included at trace levels in discrete locations, it is not a major component of the Mg-Al-(Fe) hydroxysulfate phase (Figure 3-7). The relatively high Ca peaks in the SEM analyses (Figure 3-8) are likely a result of the close spatial association of the Mg-Al-(Fe) hydroxysulfate phase with gypsum, rather than from the inclusion of Ca in the hydroxysulfate matrix. Further, it is unlikely that the S detected in the Mg-Al-(Fe) hydroxysulfate phase is related to the presence of fine-grained gypsum because the Ca/S ratios are lower than would be expected for gypsum.

Equity LDS Sample

Consistent with the Equity HDS, an amorphous Mg-Al-(Fe) hydroxysulfate was identified as the main trace metal-bearing phase in the Equity LDS (Loomer *et al.*, 2007a and Lorax, 2009). Similar to the HDS sample, the LDS sample demonstrates zonation of Mg-Al-(Fe) hydroxysulfate grains with Fe- and Al-rich zones and Mg- and Al-rich (Fe-poor) zones, though not in concentric layers as observed in the HDS (Figure 3-10 and Figure 3-11).

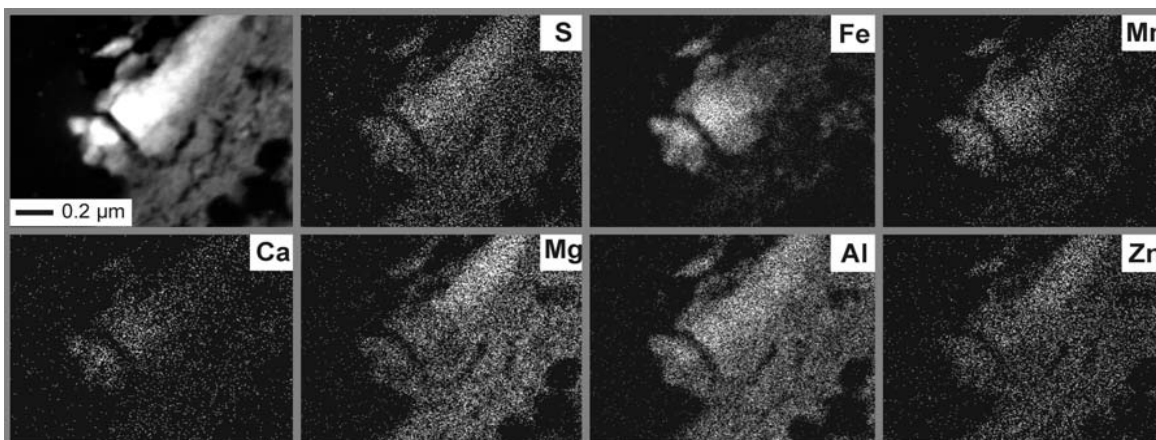


Figure 3-10: STEM high-angle annular dark-field (HAADF) image (upper left) of the Equity LDS trace metal-bearing Mg-Al-(Fe)-hydroxysulfate phase. STEM EDS 2-D element maps are also shown, showing the relative abundance of S, Fe, Mn, Ca Mg, Al and Zn.

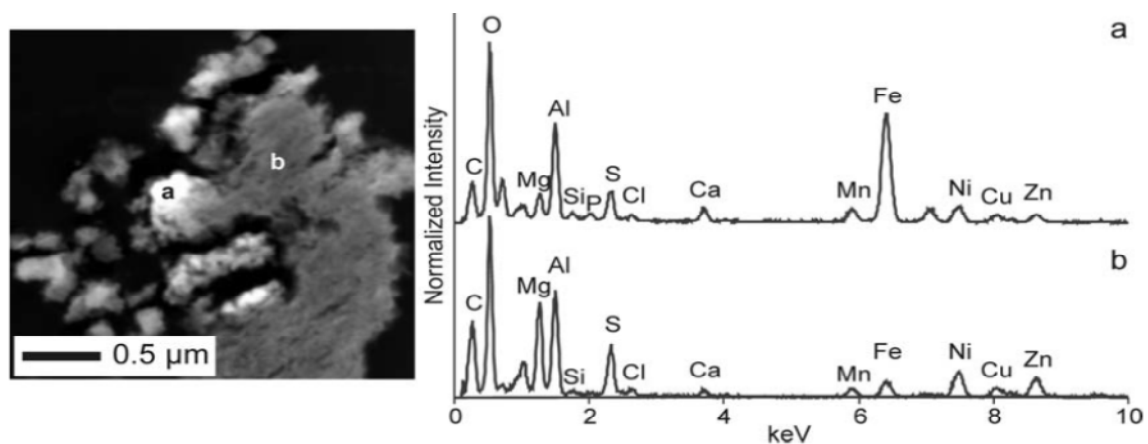


Figure 3-11: STEM high-angle annular dark-field (HAADF) image and associated EDS spectra for Equity LDS showing (a) Fe- and Al-rich zone, and (b) Mg- and Al-rich zone of the trace metal-bearing Mg-Al-(Fe)-hydroxysulfate phase. The Ni peaks are from the Ni TEM grid used in the analysis and do not represent Ni in the sample.

Overall, notable differences between the Equity HDS and LDS samples include: 1) larger Mg-Al-(Fe) hydroxysulfate grains in the HDS; and 2) presence of concentric layers alternating in composition between Mg- and Al-rich (Fe-poor) and Fe-rich zones in the HDS sample (Figure 3-8). The larger grains and concentric layers observed for the HDS hydroxysulfate phase are most likely a result of sludge recycling within the treatment system. Another difference identified between the two samples from Equity is demonstrated by the EDS relative intensity plots for Zn correlations (Figure 3-12). Moderately positive correlations for Zn:Mg and Zn:Al are evident for the HDS sample (Figure 3-9); however, only Zn:Mg shows a noticeably positive correlation for the LDS sample (Figure 3-12). This may also reflect a function of sludge recycling within the HDS system.

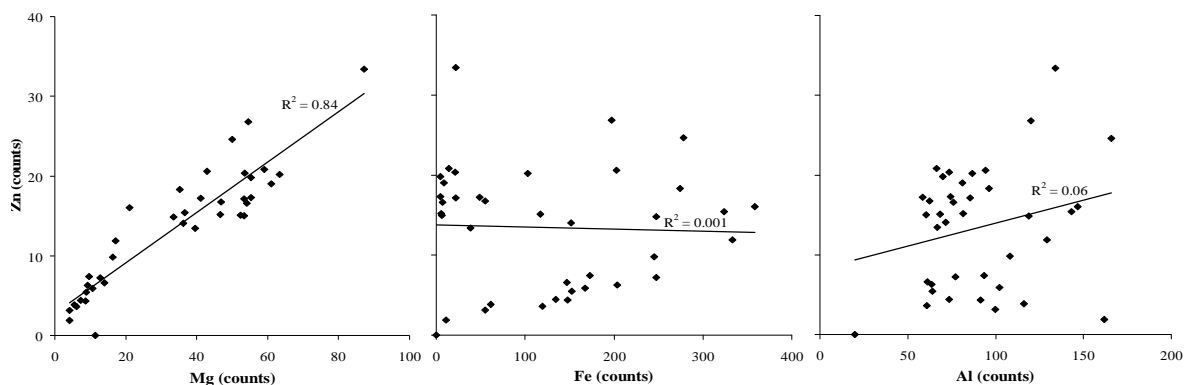


Figure 3-12: Plots of STEM EDS net intensities for Equity LDS sample. The data indicate a good correlation for Zn:Mg intensities, but not for Zn:Al intensities as observed in the HDS sample.

Crystalline trace metal-bearing phases were not detected in the ‘aged’ LDS sample, which is between 5-10 years old. This contrasts with the HDS material which hosts gypsum as confirmed by XRD. This indicates that the amorphous phases in the LDS may take a significant amount of time to recrystallize (*i.e.* >10 years). Alternatively, the differences may relate purely to contrasts in the precipitation environments between the LDS and HDS systems. Future investigations of the ‘aged’ LDS to assess the degree of crystallinity of the trace metal-bearing phases may provide further insight into the long-term changes in stability of the neutralization sludge.

3.2.3.2 Geco Sludge

Four main phases were identified in the Geco HDS sample by SEM analysis: 1) gypsum, as confirmed by XRD (Table 3-5); 2) Fe-(oxy)hydroxides; 3) Al-(oxy)hydroxides; and 4) calcite (Figure 3-13). Zinc and Mn in the Geco HDS are predominantly associated with the Fe-(oxy)hydroxide phase (Figure 3-13 and Figure 3-14). Minor associations of Al, Mg and S are also indicated for this phase. With the exception of Zn, most trace elements in the Geco HDS are below the limit of detection by SEM/EDS methods.

The Fe-(oxy)hydroxide phase occurs as spherical to oval aggregates that typically display concentric layers and irregular particle boundaries (Figure 3-13). The aggregates range in size from $<1 \mu\text{m}$ to approximately $20 \mu\text{m}$ and are composed of wispy fibres measuring <0.01 by $0.3 \mu\text{m}$ (Figure 3-14). The compositional zoning is less pronounced in the Geco sludge compared to the hydroxysulfate phase in the Equity HDS sample, which may be due to the lower Mg content of the Geco influent compared to the Equity influent. The Al-(oxy)hydroxide phase generally occurs as aggregated masses of very fine-grained particles interstitial between the gypsum and Fe-(oxy)hydroxide phases.

High resolution EDS collected during STEM indicates that the Fe-(oxy)hydroxide phase is essentially pure with only minor amounts of other constituents (Mg, Al and SO_4) (Figure 3-14). Consistent with SEM analysis, Zn and Mn are primarily associated with the Fe-(oxy)hydroxide phase. EDS 2-D elemental maps demonstrate that the sample is dominated by gypsum and Fe (oxy)hydroxides with lesser amounts of Al (oxy)hydroxide (Figure 3-15).

The Fe-(oxy)hydroxide in the Geco HDS sample produced broad diffuse rings when analyzed by SAED (Figure 3-16), consistent with poorly crystalline to amorphous mineral phases. The rings are too few and too diffuse to accurately determine representative d-spacings, and therefore an absolute mineralogical identification is not possible. However, d-spacings obtained from one SAED pattern are consistent with ferrihydrite ($\text{Fe}_2\text{O}_3 \cdot 0.5\text{H}_2\text{O}$) while d-spacings obtained from another SAED pattern are consistent with lepidocrocite [$\text{FeO}(\text{OH})$], a polymorph of goethite. Collectively, these data indicate that while a majority of the Fe-(oxy)hydroxide material present within the Geco sludge sample is amorphous, crystallization of Fe-(oxy)hydroxides is occurring, which may result from the lack of competition from other co-precipitating and competing metal phases (Aubé and Zinck, 1999). Sludge crystallinity is an indication of effective supersaturation/crystallization control during precipitation. Incorporation of trace metals into crystalline Fe-(oxy)hydroxides is favourable from the perspective of long term chemical stability.

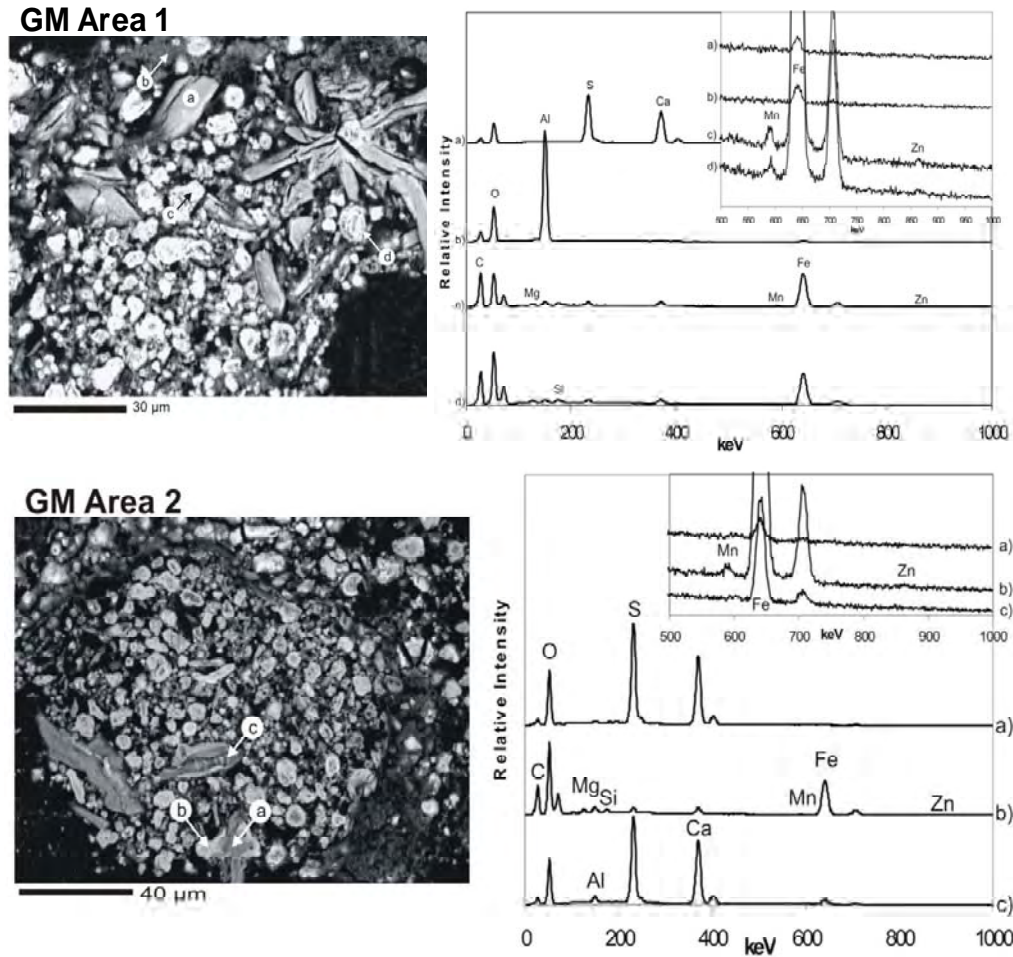


Figure 3-13: SEM back scattered electron (BSE) images of Geco HDS (left) and associated EDS spectra. The inset spectra have been vertically expanded to show trace element peaks.

GM Area 1: Data illustrate that Zn and Mn are associated with Fe-(oxy)hydroxides (c and d) and not with gypsum (a) or Al-(oxy)hydroxide (b).

GM Area 2: Data show gypsum (a and c) and correlation of Zn with the Fe-(oxy)hydroxide (b).

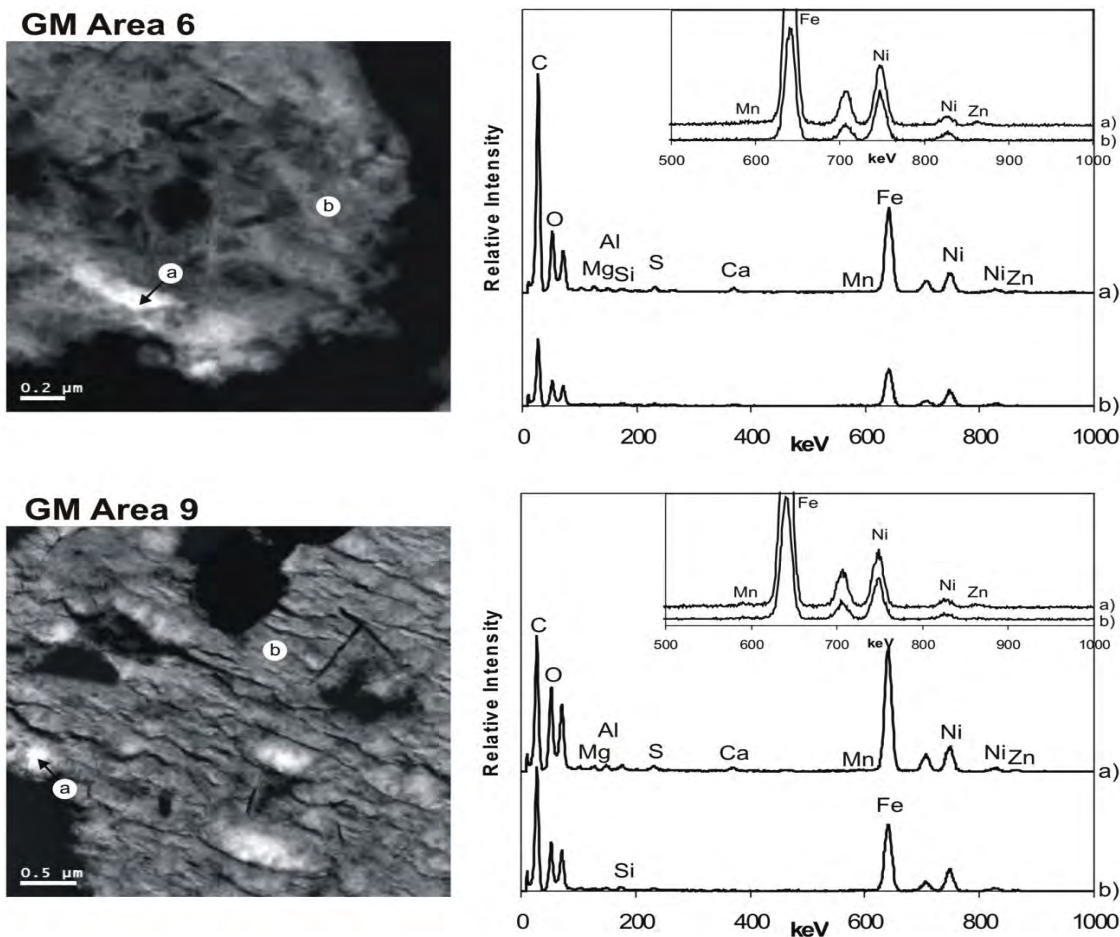


Figure 3-14: STEM annular dark field (ADF) images of Geco HDS (left) and associated EDS spectra (right) for points a) and b) on the corresponding image. The inset spectra have been vertically expanded to show trace element peaks. The Ni peaks are from the Ni support grid and do not reflect Ni content in the sample.

GM Areas 6 and 9: Spectra of Fe-(oxy)hydroxide phase present within the Geco sludge. Note that points (a) and (b) in both areas have almost identical elemental compositions; however, the intensity of the Fe peak is greater at point (a) relative to point (b), most likely indicating a thicker sample at point (a).

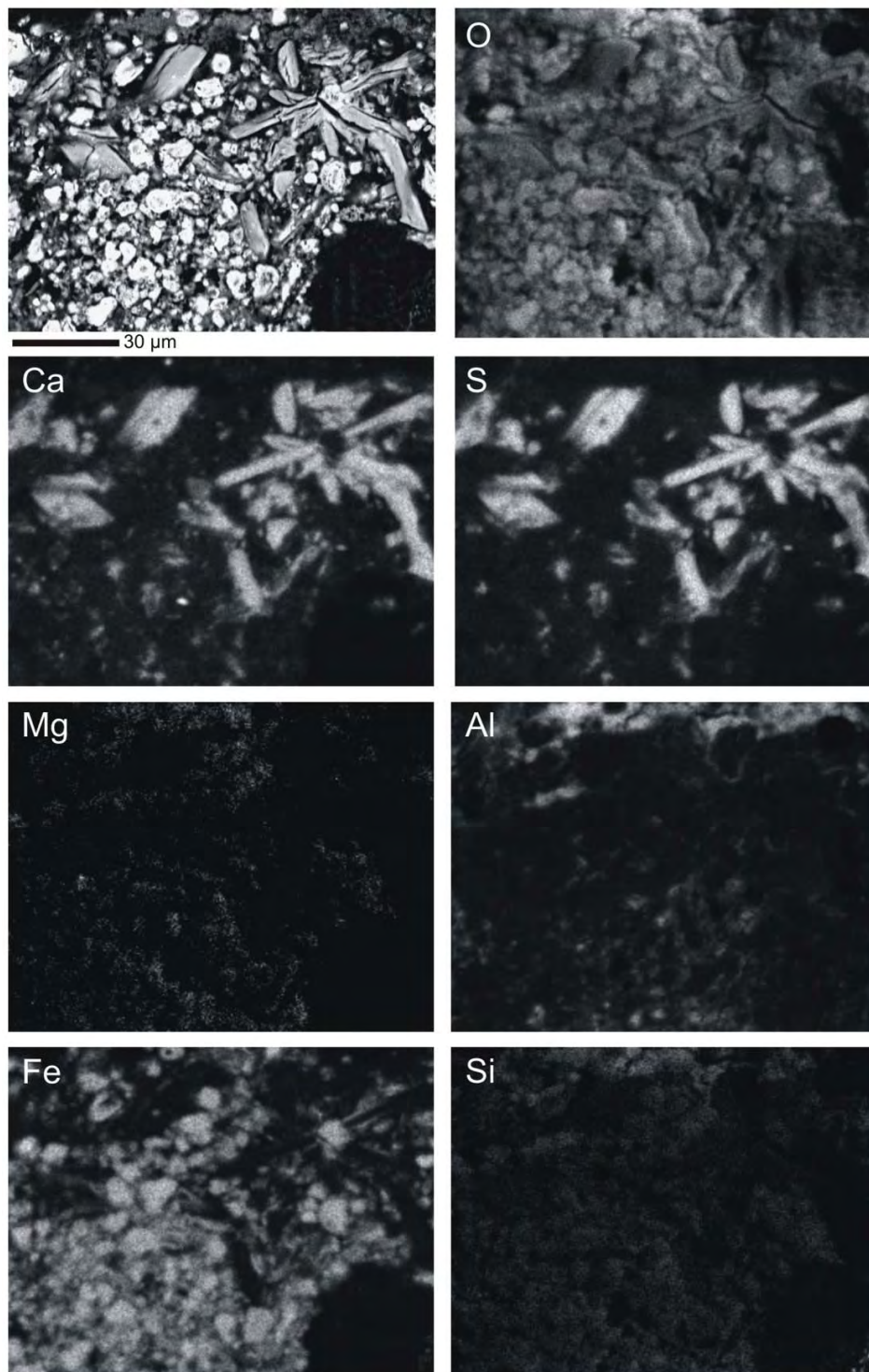


Figure 3-15: SEM back scattered electron (BSE) image (upper left) of GM Area 1 from Geco HDS. EDS 2-D elemental maps are also shown showing the relative abundance of O, Ca, S, Mg, Al, Fe and Si. These maps demonstrate how the sample is dominated by gypsum and Fe (oxy)hydroxides with lesser amounts of Al (oxy)hydroxide.

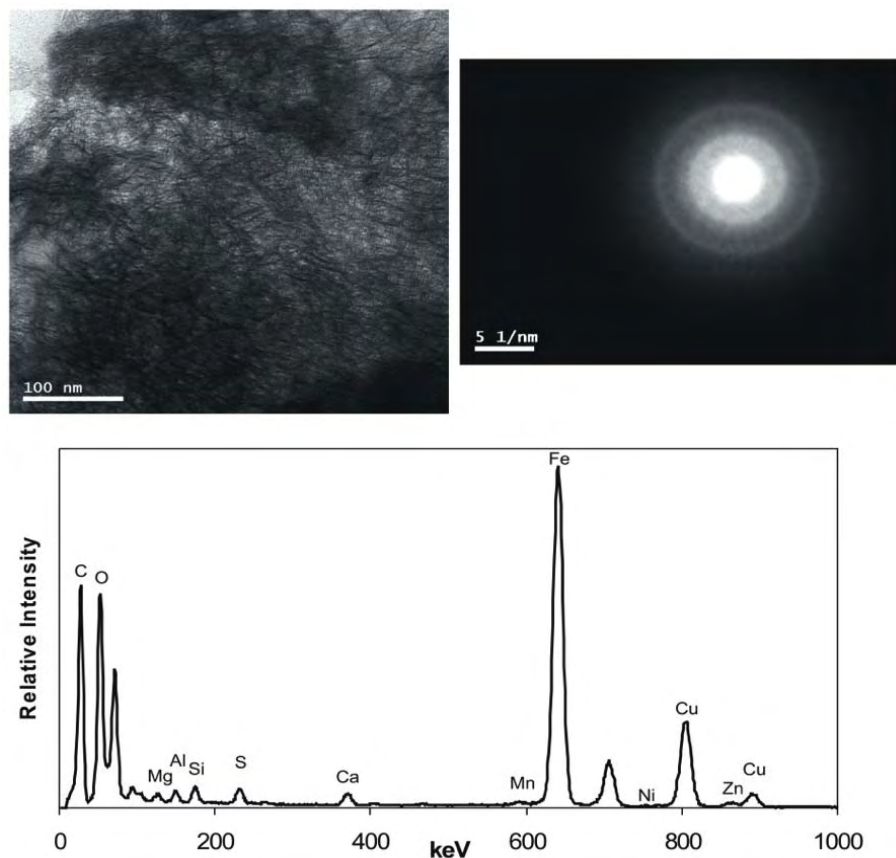


Figure 3-16: STEM bright field image of Geco HDS (top left), SAED pattern (top right) and EDS spectrum (bottom). The Cu peaks result from the Cu support grid and do not reflect Cu content in the sample. The diffuse rings of the SAED pattern suggest the presence of a poorly crystalline material, while the d-spacings measured from the rings suggest the presence of lepidocrocite [FeO(OH)].

3.2.3.3 *Britannia Sludge*

The main phases identified in the Britannia HDS sample by SEM are: 1) a Ca-rich phase, likely calcite or Mg-calcite as confirmed by XRD analysis (Table 3-5); and 2) a Cu-Zn rich Mg-Al-Si oxyhydroxide (Figure 3-17). The Mg-Al-Si oxyhydroxide phase is the dominant repository for Cu and Zn, the two elements of primary concern. Other elements associated with the Mg-Al-Si phase include S, Mn, and possibly Ca and Fe. It should be noted that a close association between the calcite and Mg-Al-Si phases is apparent in the data, and given the spatial resolution of the SEM, overlap of the two phases is likely apparent in the EDS spectra (Figure 3-18). In two examples, grains of pure calcite (>50 μm) were identified in proximity to quartz and smaller grains (<2 μm) of Fe-oxyhydroxides (Figure 3-17 and Figure 3-18). Considering the relatively low Fe content of the HDS in general, sequestration of trace metals by the Fe-oxyhydroxides is likely

limited. The small size of the Fe-oxyhydroxides also places a limit upon EDS analysis since overlap with other minerals is almost certain. Regardless, Cu and Zn associations with the Fe-oxide phases were not apparent. The source of the quartz and Fe-oxyhydroxides is suspected to be detrital (*i.e.*, transported in with the wastewater during treatment).

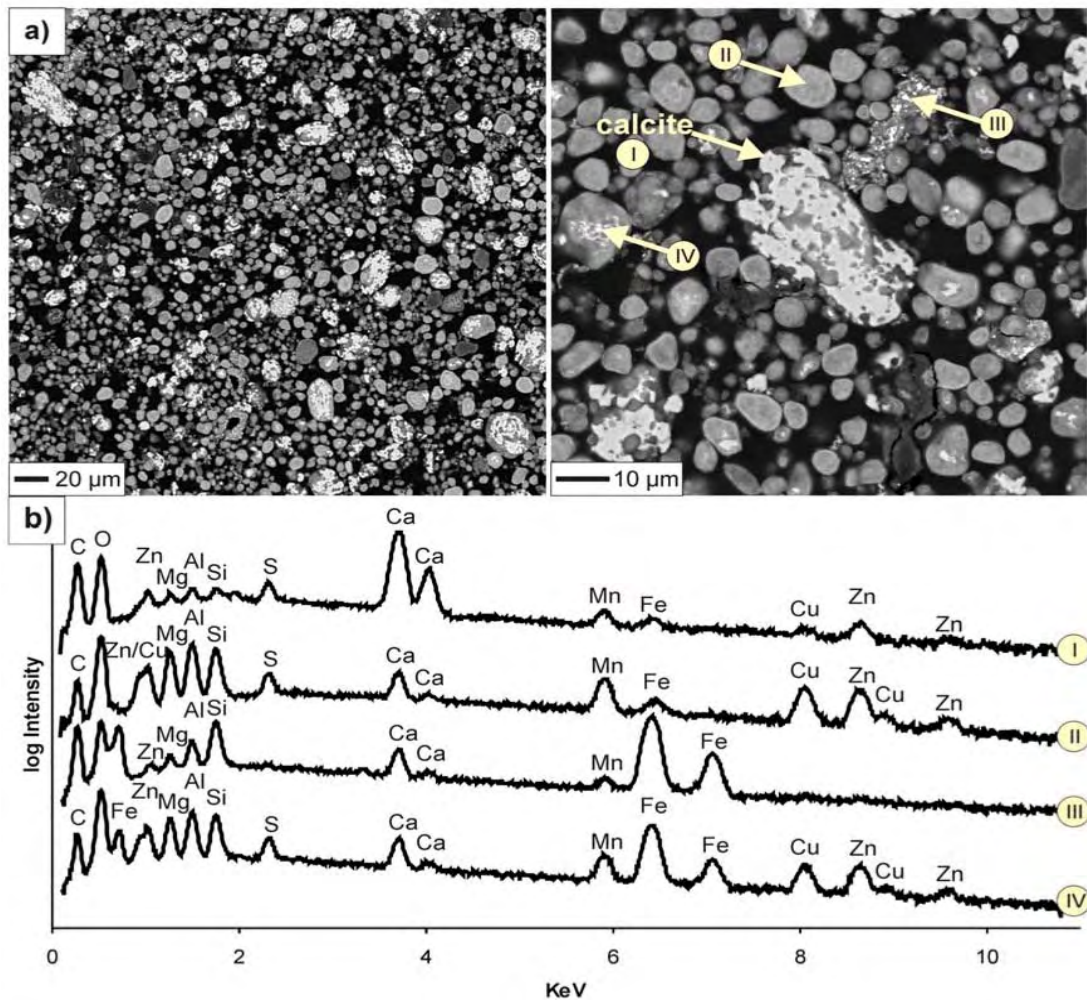


Figure 3-17: (a) SEM back scattered electron (BSE) images of the Britannia HDS and (b) corresponding EDS spectra. Log intensities have been plotted to highlight trace metal peaks. Point II is the Cu-Zn rich Mg-Al-Si oxyhydroxide, while points III and IV represent Fe-oxyhydroxides although overlap with neighbouring phases is likely.

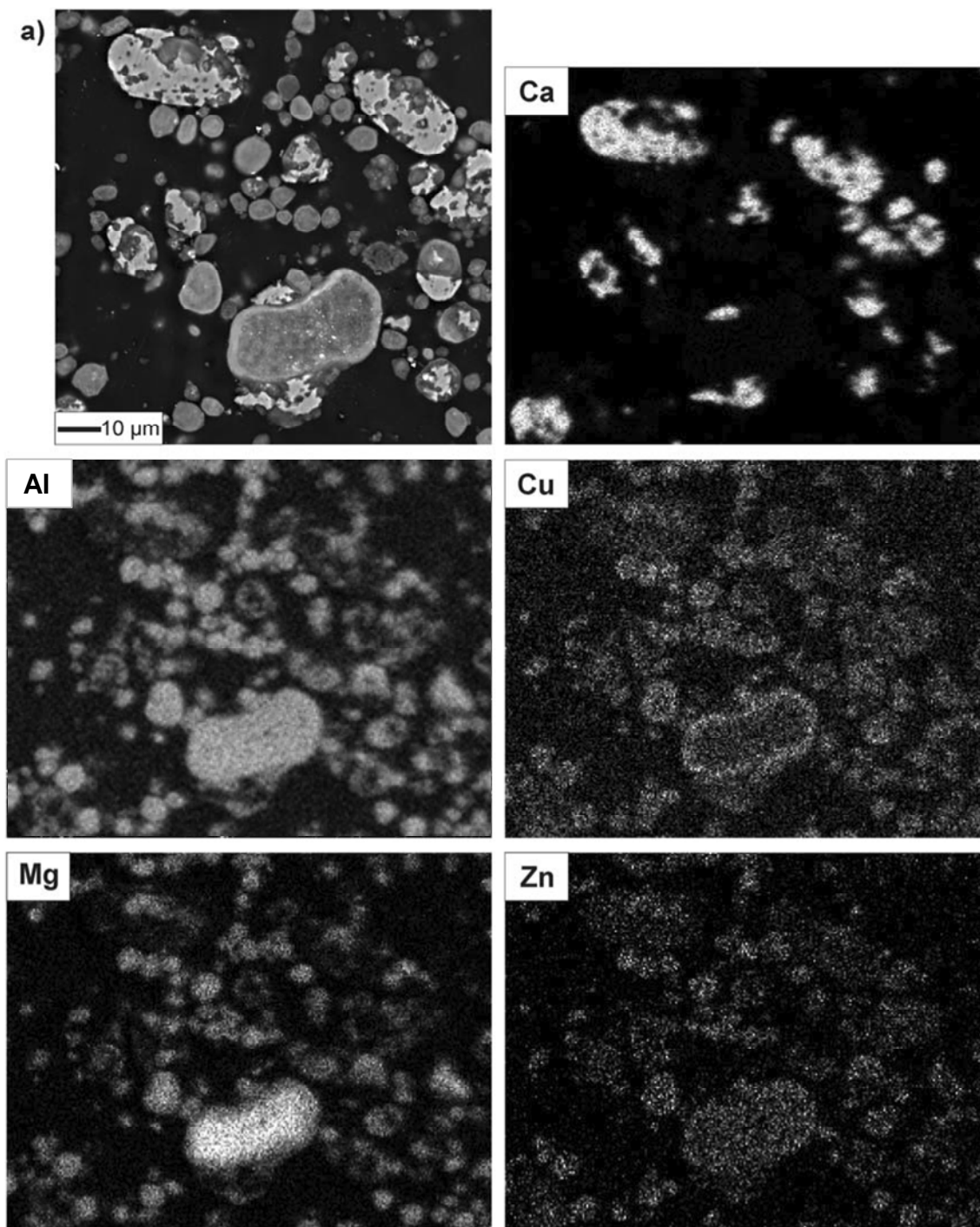


Figure 3-18: SEM back scattered electron (BSE) image (upper left) of Britannia HDS and selected EDS 2-D elemental maps showing the relative abundance of Ca, Al, Cu, Mg and Zn. The Ca map shows the calcite distribution.

Combined analysis using STEM HAADF images and higher spatial resolution point EDS analyses indicate that the Mg-Al-Si phase identified in SEM has higher molar concentrations of Cu than Mg, Al or Si. In addition, the abundance of Zn is equal to Al and Si, and slightly higher than Mg. Hence, a better description for the trace metal-bearing phase is a Cu-Zn-oxyhydroxide. The Cu-Zn oxyhydroxide phase occurs as well rounded to more irregularly shaped aggregates that display concentric layers and relatively sharp particle boundaries (Figure 3-18). The aggregates range in size from <10 μm to 25-35 μm in size and are composed of wispy fibres measuring <0.01 by 0.2 μm .

Zones of varying brightness were identified by HAADF (Figure 3-19), with Zn being more abundant in the darker zones. Commonly found within the centre of the fibrous Cu-Zn-oxyhydroxide are zones of Fe-rich features ($\leq 0.3 \mu\text{m}$) (Figure 3-20). Small amounts of Ca, S, Cl, Mn and Fe were also consistently detected in the Cu-Zn-oxyhydroxide phase, as were sporadic trace amounts of Cr and Sn. Analysis with a Cu-TEM support grid was used to confirm that Ni was not associated with the Cu-oxyhydroxides. The calcite phase was associated with significant amounts of Cu, trace amounts of Zn, and lesser amounts of Mn (Figure 3-19, point I). High Cu abundances associated with calcite were confirmed by SAED analysis.

An EDS net intensity comparison between Zn and Cu *versus* Mg, Al, Fe, Mn, Ca and S did not result in strong correlations ($R^2 \leq 0.6$; Figure 3-21), which is indicative of considerable heterogeneity in the composition of the sludge sample. Note that a single R^2 may not be representative of the variability in the material. For, example, the Zn *versus* Ca plot suggests a bimodal control (*e.g.*, Zn-rich calcite and Ca-poor phase) (Figure 3-21).

Analysis of the Cu-, Zn- and Fe-rich phases using SAED generated patterns consisting of diffuse rings, and spotty rings, which is consistent with amorphous or nanocrystalline material. Only 2 to 4 d-spacings were identifiable in the patterns exhibiting rings. The d-spacings were compared with known materials including 2 and 6-line ferrihydrite, goethite, hematite, Cu-oxyhydroxides, Cu-hydroxycarbonates and a range of hydrotalcite-type minerals (*e.g.*, $\text{Mg}_6\text{Al}_{12}(\text{OH})_{16}\text{CO}_3 \cdot 4\text{H}_2\text{O}$). Of these, the best fit occurred with 6-line ferrihydrite. Analysis of one of the spotty ring SAED patterns would suggest that two phases are present since d-spacings consistent with calcite and possibly ferrihydrite were identified. As reflected by the data, most of the Cu/Zn-rich and Fe-rich oxyhydroxide mass is amorphous.

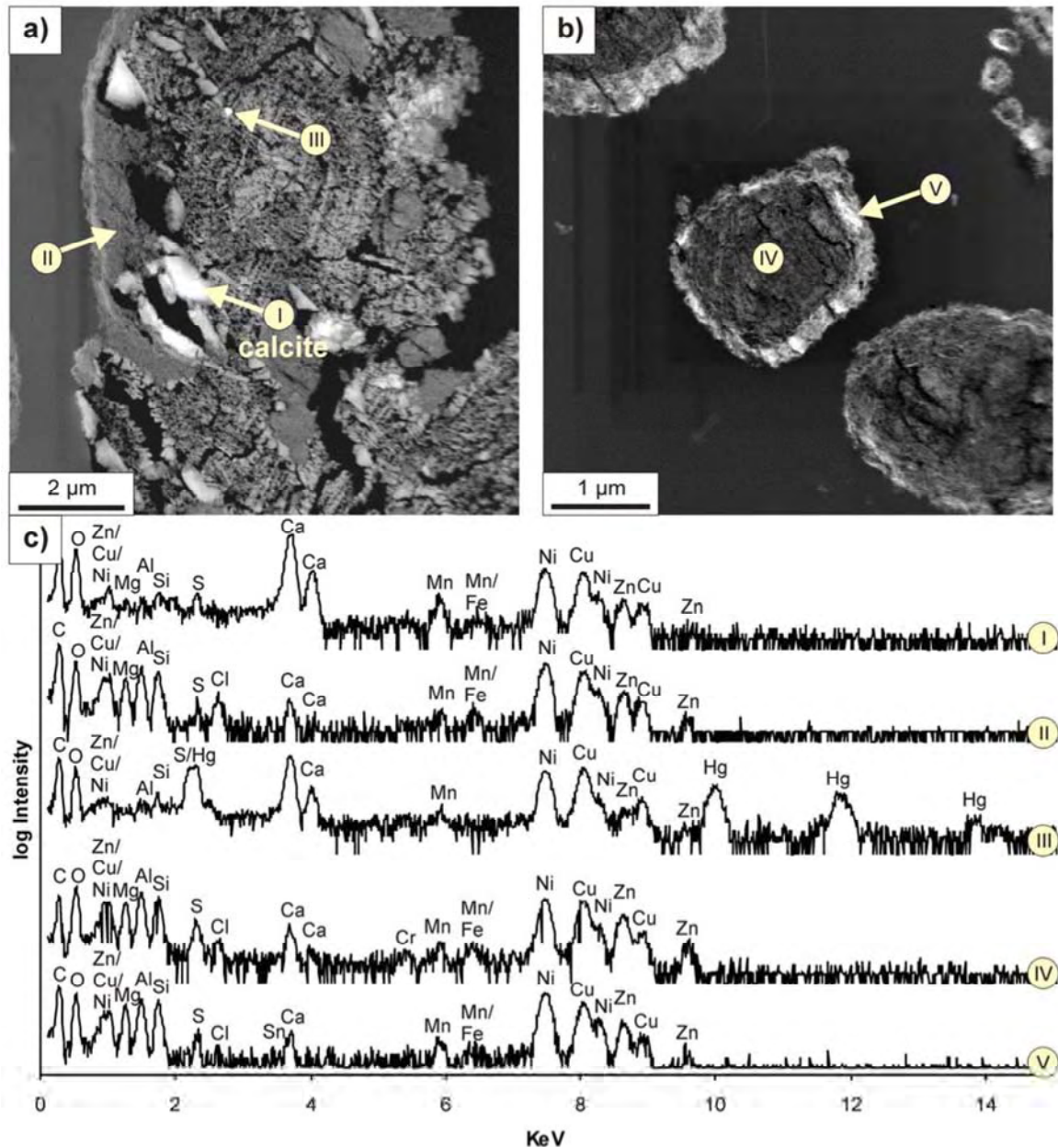


Figure 3-19: STEM HAADF images of the Britannia sludge sample (a & b), and (c) selected EDS spectra corresponding to points labeled in a & b. Log intensities have been plotted to highlight trace metal peaks (if present). The Ni peaks result from the support grid and do not reflect Ni content in the sample. Points II, IV and V represent Cu-Zn-oxyhydroxide, and point III is a Hg-Cu-S phase.

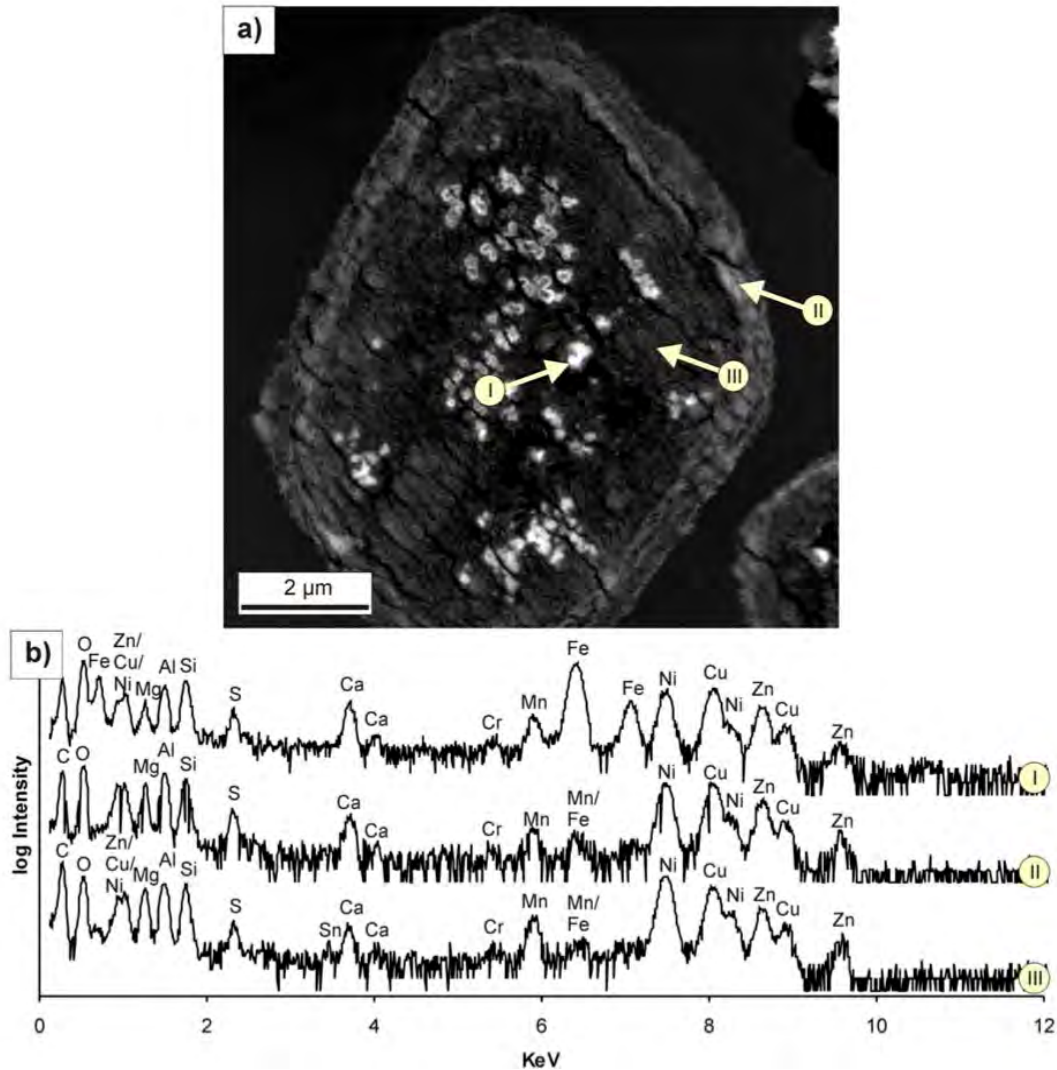


Figure 3-20: STEM HAADF image of the Britannia HDS of Area 3 (a) and (b) selected EDS spectra corresponding to points labeled in (a). Log intensities have been plotted to highlight trace metal peaks, if present. The Ni peaks result from the Ni-TEM support grid and do not reflect Ni content in the sample. The bright grains (point I) are Fe-rich while the darker material (points II and III) is Fe-poor Cu-Zn-oxyhydroxide.

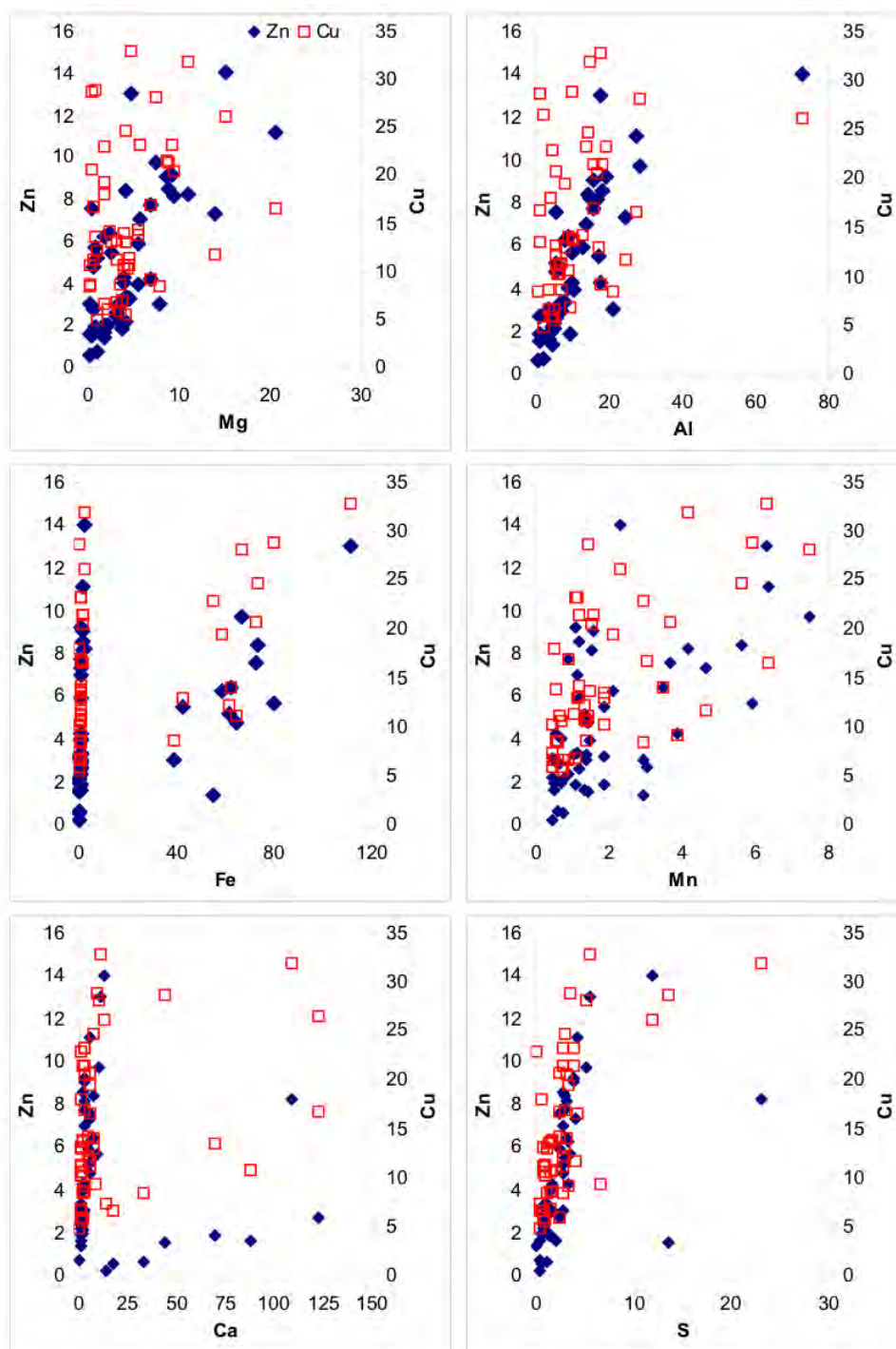


Figure 3-21: Plots of STEM EDS net intensities for the Britannia HDS sample. No coefficients of determination (R^2) were ≥ 0.6 and have not been reported. Note that a single R^2 may not be representative of the variability in the material. For, example, the Zn versus Ca plot suggests a bimodal material; perhaps Zn-rich calcite, and Ca-poor phase.

Two small grains ($<0.1\mu\text{m}$) containing Hg, Cu and S were identified by STEM HAADF-EDS (Figure 3-19, point III). Solid solutions that contain a combination of Hg and Cu are typically unexpected in sulfides. SAED analysis of the spotty ring pattern collected from point III in Figure 3-19 was inconclusive; however, it is possible that the SAED pattern represents a mixture of calcite, metacinnabar and a Cu sulfide (*i.e.*, chalcocite, Cu_2S).

3.2.3.4 Brunswick Sludge

Two dominant phases were identified in the Brunswick HDS sample: 1) a Ca-rich phase, likely calcite, as supported by XRD analysis (Table 3-5); and 2) a Fe-Mn-Zn-rich oxyhydroxide phase. The Zn-Fe-Mn oxyhydroxide phase is the dominant host for Zn and occurs as well rounded to irregularly shaped aggregates that display concentric layers and irregular particle boundaries (Figure 3-22). The aggregates range from $<5\mu\text{m}$ to up to 10 by 15 μm in size and are composed of wispy fibres measuring 0.05 by 0.2 μm (Figure 3-23). The data indicate that while Fe and Mn proportions in the Zn-Fe-Mn oxyhydroxide phase are variable, Zn abundance is more uniform. Specifically, BSE imaging indicates that there is variation between the relative amounts of Fe and Mn throughout the sample, with brighter zones within the fibrous aggregates being relatively Mn-rich and darker zones within the aggregates more Fe-rich (Figure 3-23). Zinc peaks, on the other hand, are relatively similar between the bright and dark zones. Other elements consistently detected in the oxyhydroxide phase include Si, S, Cl, Mg and trace amounts of Al and Cu. Calcium was variably detected in the oxyhydroxide phase as well.

Calcite was also identified (Figure 3-24 and Figure 3-25), and confirmed via XRD. Fe, Zn and Mn were also detected at lower levels in association with the calcite. Due to the close association between calcite and Zn-Fe-Mn oxyhydroxide phases at the spatial resolution of the SEM, many of the EDS spectra likely reflect overlap of the phases. Even with the increased spatial resolution of the STEM, it is apparent in the HAADF image that the Zn-Fe-Mn oxyhydroxide phase overlaps (or coats) the calcite grain (Figure 3-25). Duplicate analysis of large ($>20\mu\text{m}$), relatively pure calcite grains using SEM shows that Zn and calcite are not associated (Figure 3-22, point I), a result that is consistent with the elemental mapping (Figure 3-24 and Figure 3-25). Collectively, the data suggest that the calcite phase is, at most, a minor host for Zn in comparison to the Zn-Fe-Mn oxyhydroxide.

A Mg-Al-S-rich oxyhydroxide or hydroxycarbonate phase was also identified in association with Zn, Fe and Mn. In addition, quartz and Al-silicate phases were identified in the sample. The elemental maps suggest that the Zn-Fe-Mn oxyhydroxide is more abundant than the Mg-Al-rich phase (Figure 3-24). A large (274 μm diameter) and relatively pure Fe-oxyhydroxide was also identified, but showed no associated Zn. The

source of the quartz, Al-silicates and relatively pure Fe-oxyhydroxide may reflect a detrital origin, having possibly been carried in as particles with the wastewater during treatment, or as impurities in the lime.

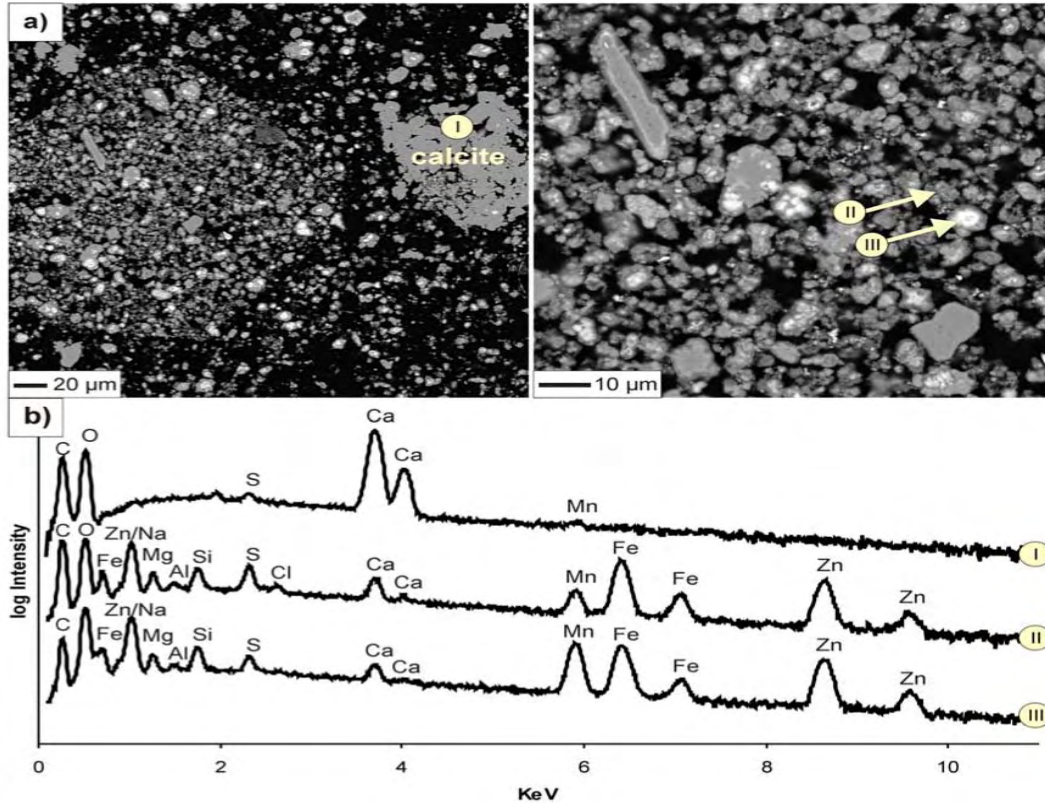


Figure 3-22: (a) SEM BSE images of Brunswick HDS (Area 1) and (b) corresponding EDS spectra of the trace metal-bearing Zn-Fe-Mn oxyhydroxide phase. Log intensities have been plotted to highlight trace metal peaks. Point II is a relatively Mn-poor example of the Zn-Fe-Mn oxyhydroxide while point III is a Mn-rich example.

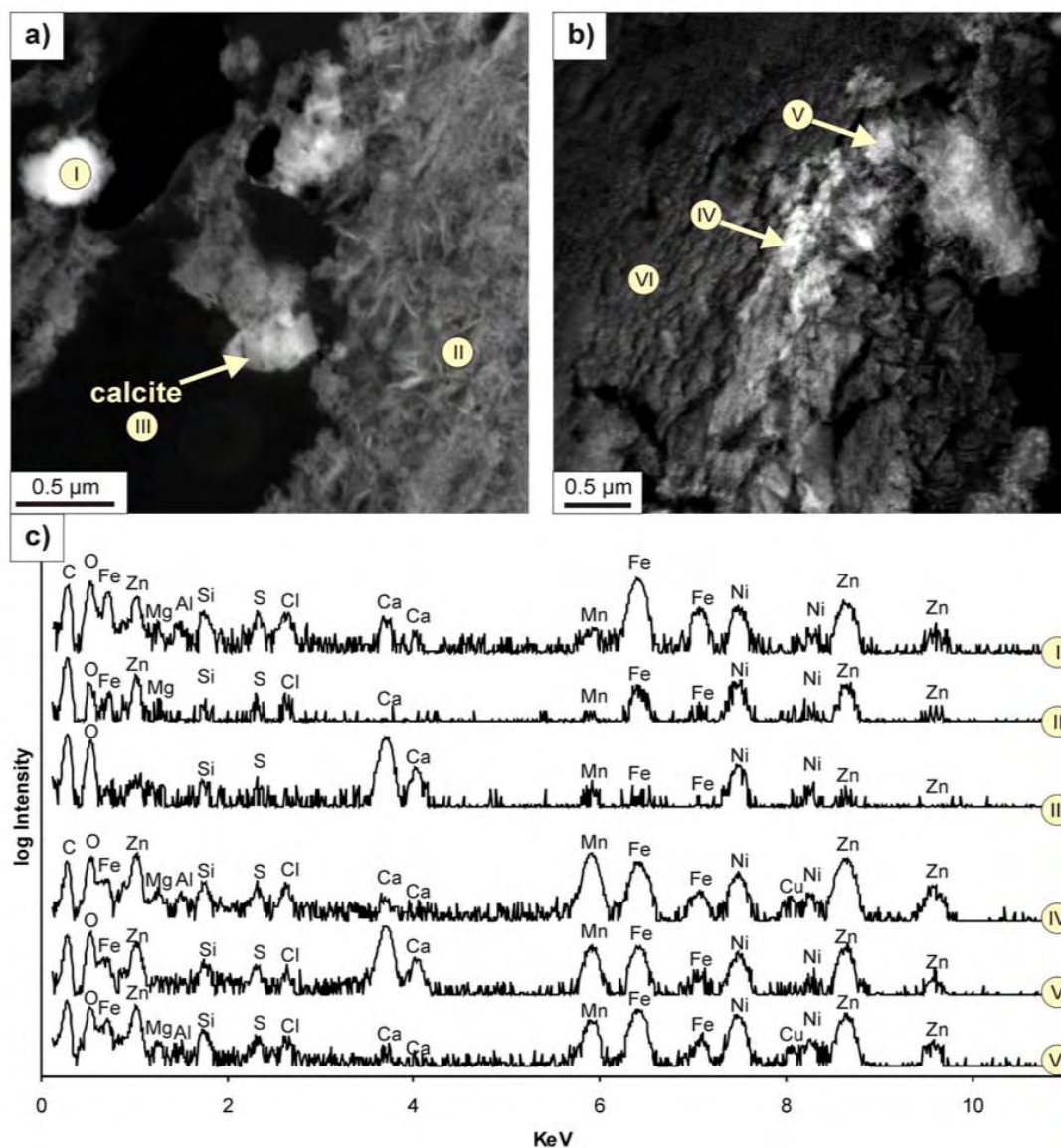


Figure 3-23: STEM HAADF images of the Brunswick HDS sample (a and b). Selected EDS spectra corresponding to points labeled in a & b are shown in the lower graphs (c). Log intensities have been plotted to highlight trace metal peaks, if present. The Ni peaks result from the Ni-TEM support grid and do not reflect Ni content in the sample. Point I is an example of the discrete Fe-rich oxyhydroxides. Points II, IV and VI represent zones of variable Mn content in the Zn-Fe-Mn oxyhydroxide. Point V is likely calcite within the Zn-Fe-Mn oxyhydroxide aggregate.

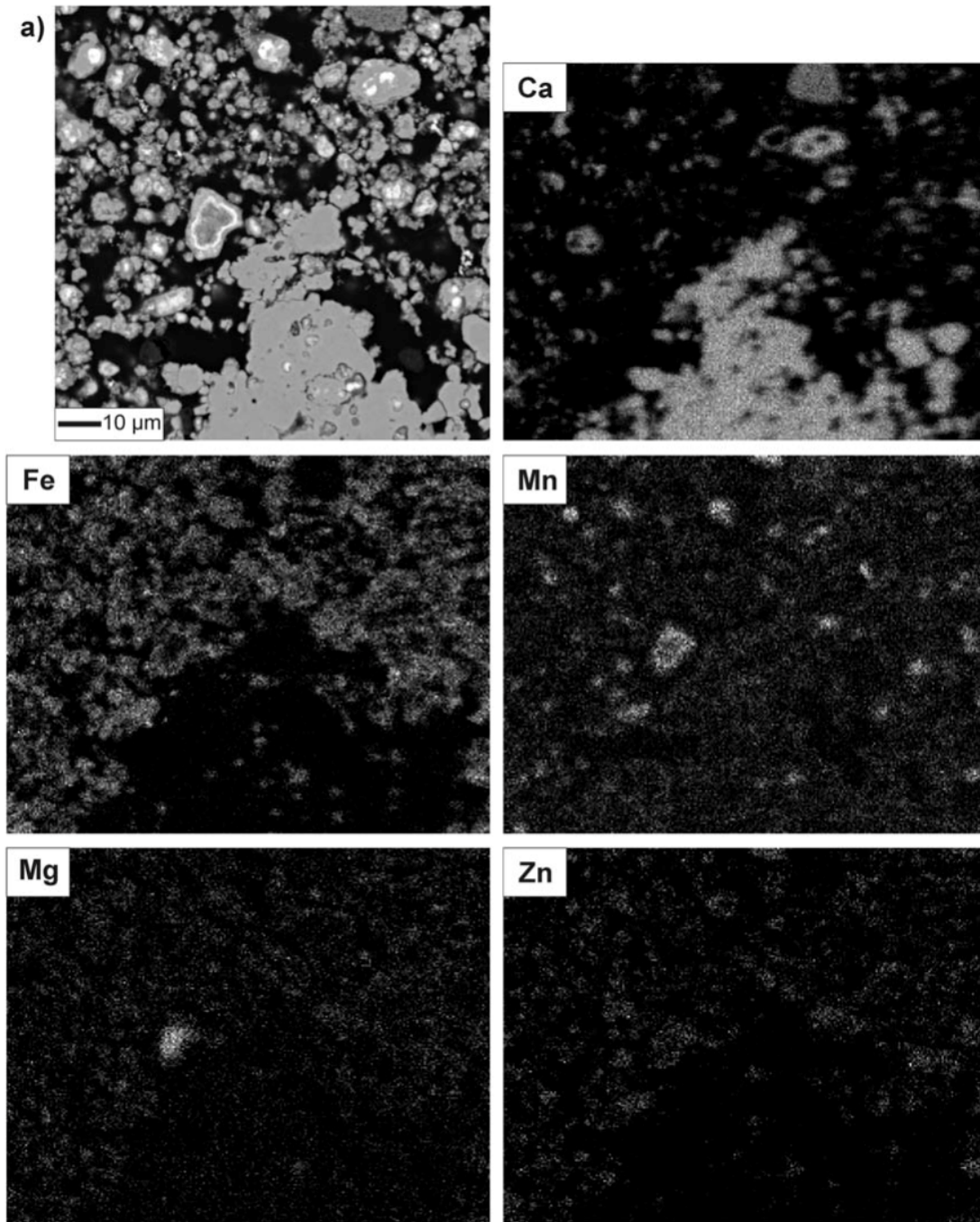


Figure 3-24: (a) SEM back scatter electron (BSE) image (upper left) of Brunswick HDS, and selected EDS 2-D elemental maps showing relative abundance of Ca, Fe, Mn, Mg and Zn. The elemental maps indicate that Fe and Zn are not associated with the calcite (Ca map). Mn shows some degree of association with the calcite although it is present in grains of the Zn-Fe-Mn oxyhydroxide at higher concentrations.

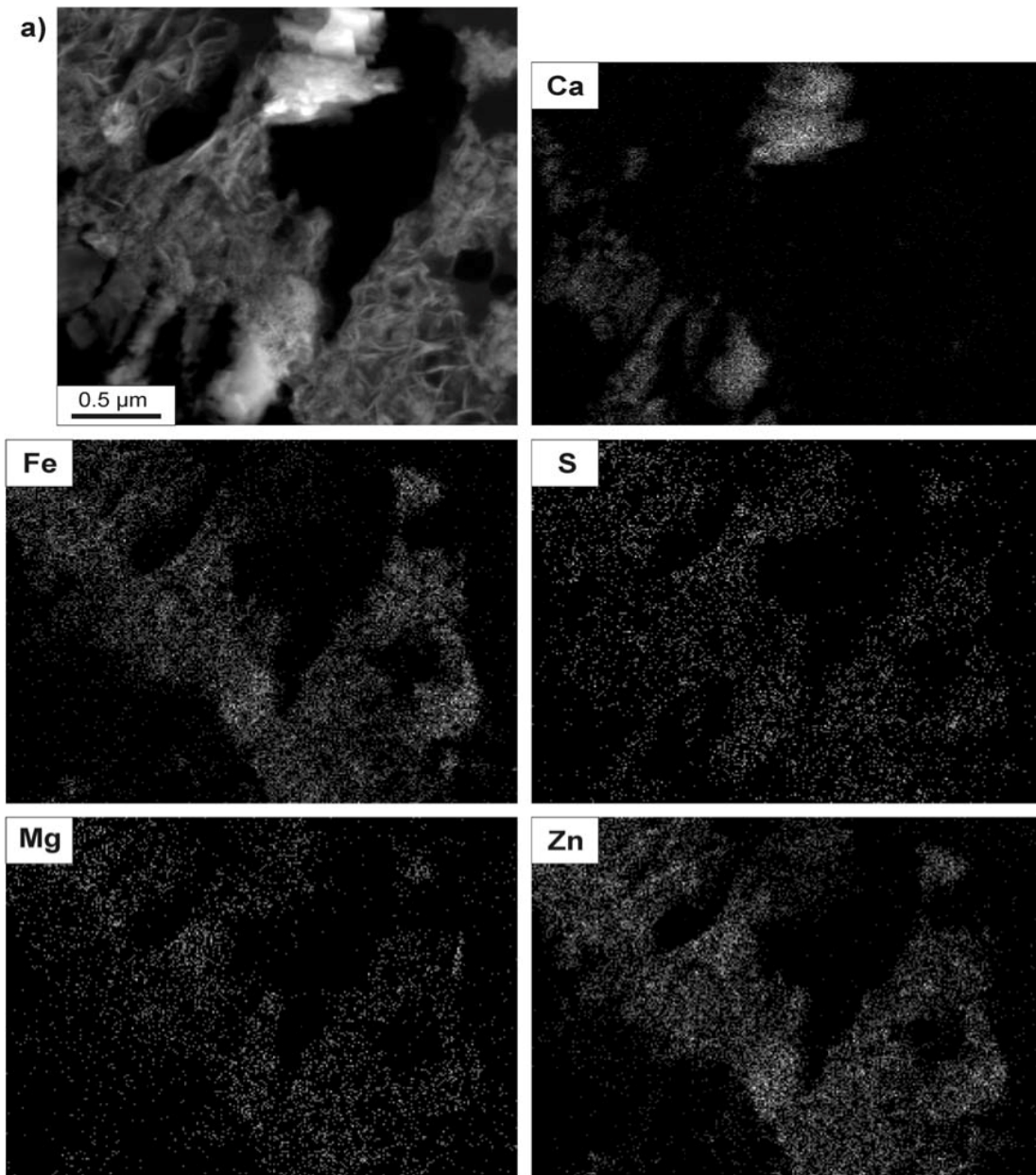


Figure 3-25: (a) STEM HAADF image (upper left) of Brunswick HDS and selected EDS 2-D elemental maps showing relative abundance of Ca, Fe, S, Mg and Zn. The maps illustrate the nature of the spatial relationship between calcite and Zn-Fe-Mn oxyhydroxides.

Net EDS intensities for Zn and Cu versus Mg, Al, Fe, Mn, Ca and S (Figure 3-26) indicate that both Cu and Zn have good correlations with Fe and S. However, a lack of correlation for Zn and Cu with Ca at high intensities indicates that Zn and Cu are not structurally incorporated in the calcite.

The Zn-Fe-Mn phase generated diffuse ring and spotty ring diffraction patterns when analyzed by SAED (Figure 3-27d), consistent with amorphous or nanocrystalline material. Unfortunately, the crystallites had measured d-spacings (4.03, 2.60, 1.95, and 1.53 Å) that could not be satisfactorily fit to plausible mineral phases. Although 6-line ferrihydrite appears to have the best fit, the strongest d-spacing for 6-line ferrihydrite is not observed; therefore, this determination is not conclusive. Overall, the results are indicative of a largely amorphous, heterogeneous sludge matrix.

3.2.3.5 Chisel North Sludge

Two major phases were identified in the Chisel North HDS sample by SEM analysis: 1) a Ca-rich phase, likely calcite, as supported by XRD analysis (Table 3-5); and 2) a Fe-Mn-Mg-Si-Zn-rich oxyhydroxide phase (Figure 3-28 and Figure 3-29). The Fe-Mn-Mg-Si phase represents the dominant host for Zn. The STEM-EDS spectra indicate that Fe, Mn and Zn are more abundant than Mg and Al in the Fe-Mn-Mg-Si-Zn phase identified by SEM (Figure 3-30 and Figure 3-31). This observation is supported by the elemental analysis (Figure 3-3). In fact, Zn is present in roughly equal proportions to the combined Fe and Mn content; therefore, the trace metal-bearing phase is better identified as a Zn-Fe-Mn oxyhydroxide.

The Zn-Fe-Mn oxyhydroxide phase occurs as irregularly shaped aggregates that display concentric layering with irregular particle boundaries. The aggregates appear to be smaller than the other HDS samples, measuring up to 10 µm in diameter and are composed of wispy fibres measuring <0.01 by 0.5 µm. The Zn-Fe-Mn oxyhydroxide aggregates are interspersed with what are likely calcite grains which appear as bright regions in STEM HAADF images (Figure 3-30, point I). In other instances, the bright zones that appear within the fibrous masses are concentrations of elements with high atomic number (U and Pb) (Figure 3-30, point III).

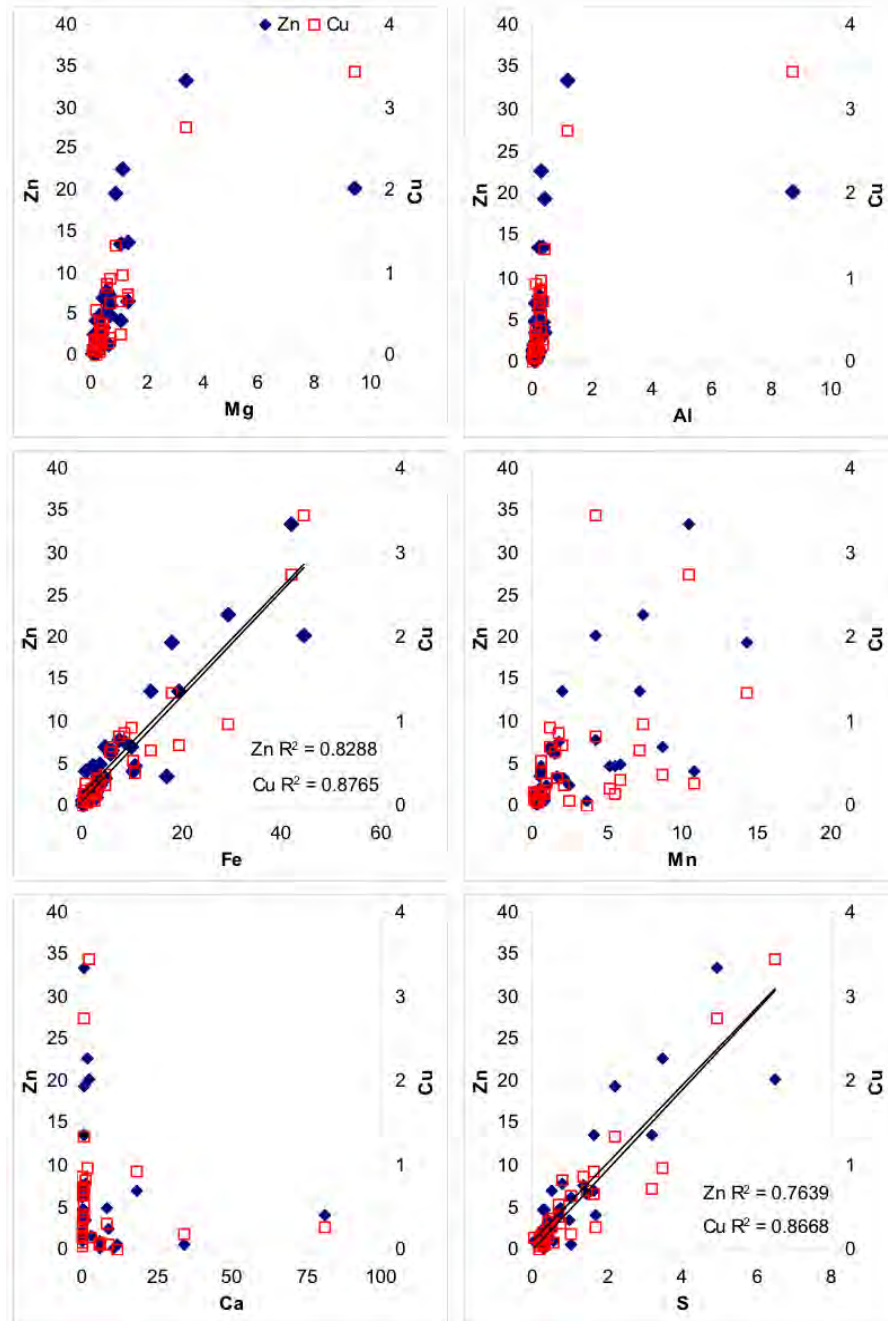


Figure 3-26: Plots of STEM EDS net intensities for the Brunswick sample. Coefficients of determination (R^2) ≥ 0.6 have been reported. The data indicate a good correlation between Fe and Cu or Zn intensities and between S and Cu or Zn intensities. Note that a single R^2 may not be representative of the variability in the material.

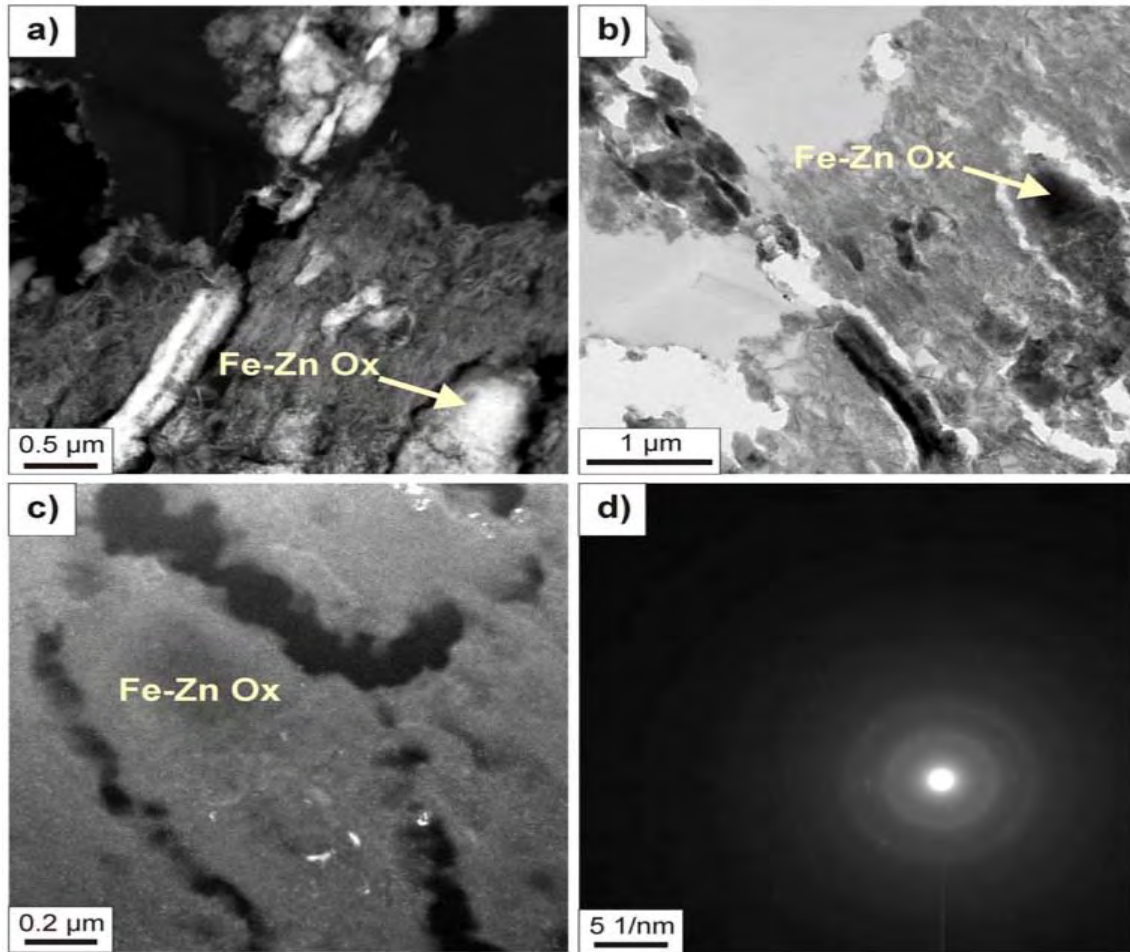


Figure 3-27: (a) STEM HAADF image of the Brunswick HDS. (b) Bright-field TEM image of the same area. (c) Dark-field TEM image of the area indicated in (a) and (b). The bright spots in the dark-field image represent diffraction contrast. (d) SAED pattern from the Fe-Zn Ox area identified in a, b & c. The spots in the ring pattern represent diffraction from the bright spots in (c). The SAED pattern could not be satisfactorily matched to known, plausible minerals.

Other elements detected consistently in the Fe-Mn-Mg-Si-Zn oxyhydroxide phase include Si, S, Ca and trace amounts of Al. It is apparent that the calcite and Fe-Mn-Mg-Si-Zn oxyhydroxide phases are closely associated, forming sub-spherical mixed-phase agglomerations (Figure 3-28 and Figure 3-29). Many of the phases in the EDS spectra are overlapping due to limitations of the spatial resolution of the SEM. Sulfur, and trace amounts of Mg, Fe and Zn, were consistently detected with the calcite phase by SEM. Other mineral phases identified in the Chisel North HDS were pyrite, quartz, small barite grains (BaSO_4 : $\leq 4 \mu\text{m}$) and Al and Ca-Fe silicates (Figure 3-29). The source of these latter minerals may be detrital, having been carried in with the wastewater during treatment. Zinc was not associated with any of these detrital mineral phases.

The net EDS intensities of Zn, Cu and U versus Mg, Al, Fe, Mn, Ca and S are plotted in Figure 3-32. The data indicate a good correlation between Mg, Al and Fe with Cu or Zn intensities. The relatively low Mg and Al content in the EDS spectra suggest an Al and Mg correlation with the Zn-Fe-Mn oxyhydroxide phase rather than the presence of a separate Mg-Al phase. The lack of correlation between Zn and Ca at high Ca intensities (calcite) suggests that Zn is not structurally incorporated with the calcite lattice.

Calcite grains were identified, and in all cases Zn was detected, even when elements such as Fe and Mn were very low, indicating possible analytical interference from adjacent grains (Figure 3-30, point IV). However, the combination of higher Zn and lower Fe content in the spectra suggests that some Zn carbonate is structurally incorporated in the calcite grains. Small amounts of S and Si were also consistently detected with the calcite, while Pb and U were not. Overall, calcite is predicted to represent a minor host for Zn in comparison to the Zn-Fe-Mn oxyhydroxide phase.

The Zn-Fe-Mn oxyhydroxide phase generated diffuse rings when analyzed by SAED, consistent with amorphous or nanocrystalline material. Two to five d-spacings were identifiable in the patterns. Comparison of the measured d-spacings with known materials indicates that 6-line ferrihydrite provides the best fit. Two areas in particular have SAED patterns that match well with 6-line ferrihydrite. These two points are discreet bright zones (in HAADF images) within the amorphous mass of Zn-Fe-Mn oxyhydroxide. It is concluded that the bulk of the Zn-Fe-Mn oxyhydroxide phase is likely amorphous but contains discrete crystallites of ferrihydrite ($\sim 0.5 \mu\text{m}$ in size).

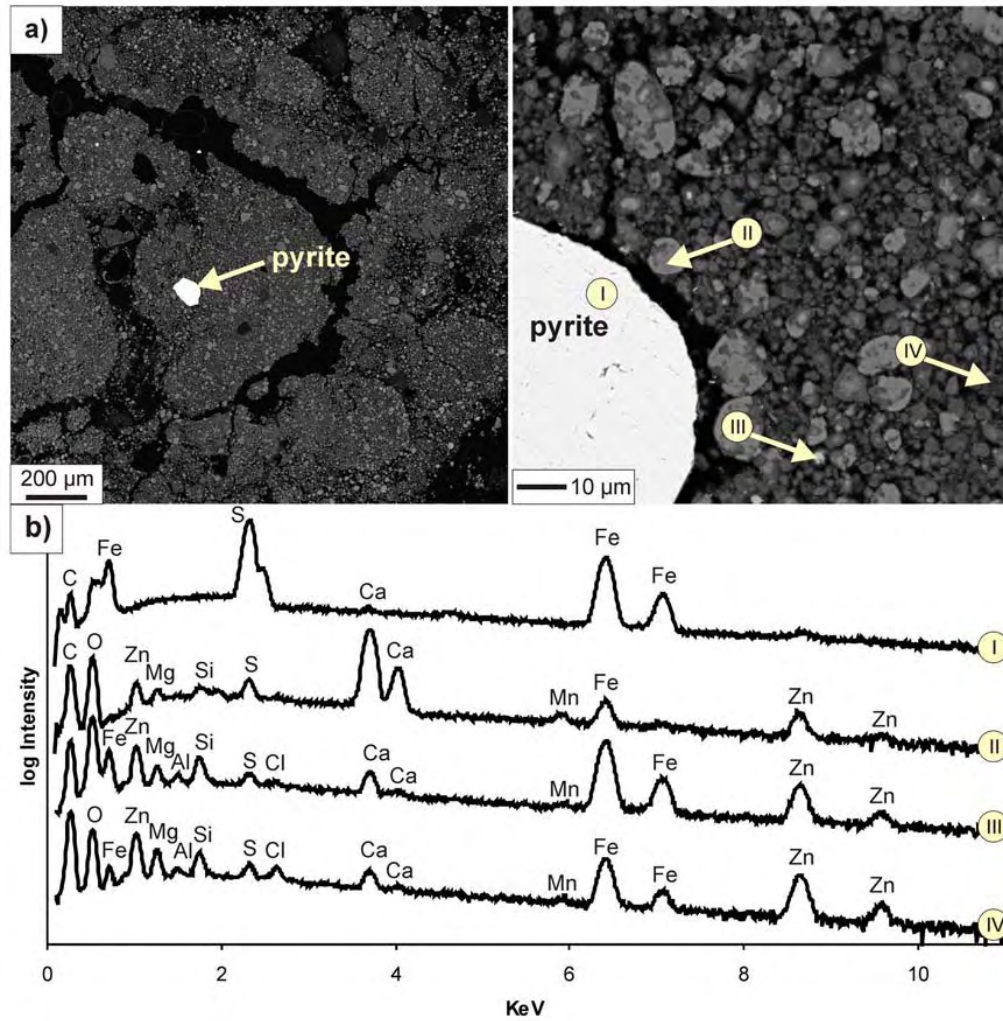


Figure 3-28: (a) SEM back scattered electron (BSE) images of the Chisel North HDS and (b) selected EDS spectra corresponding to points labeled in (a). Log intensities have been plotted to highlight trace metal peaks, if present. The pyrite grain indicated in (a) is shown at a higher magnification in the image to the right. Point II is calcite with overlap from the Zn-Fe-Mn oxyhydroxide. Points III and IV are examples of the Zn-Fe-Mn oxyhydroxide.

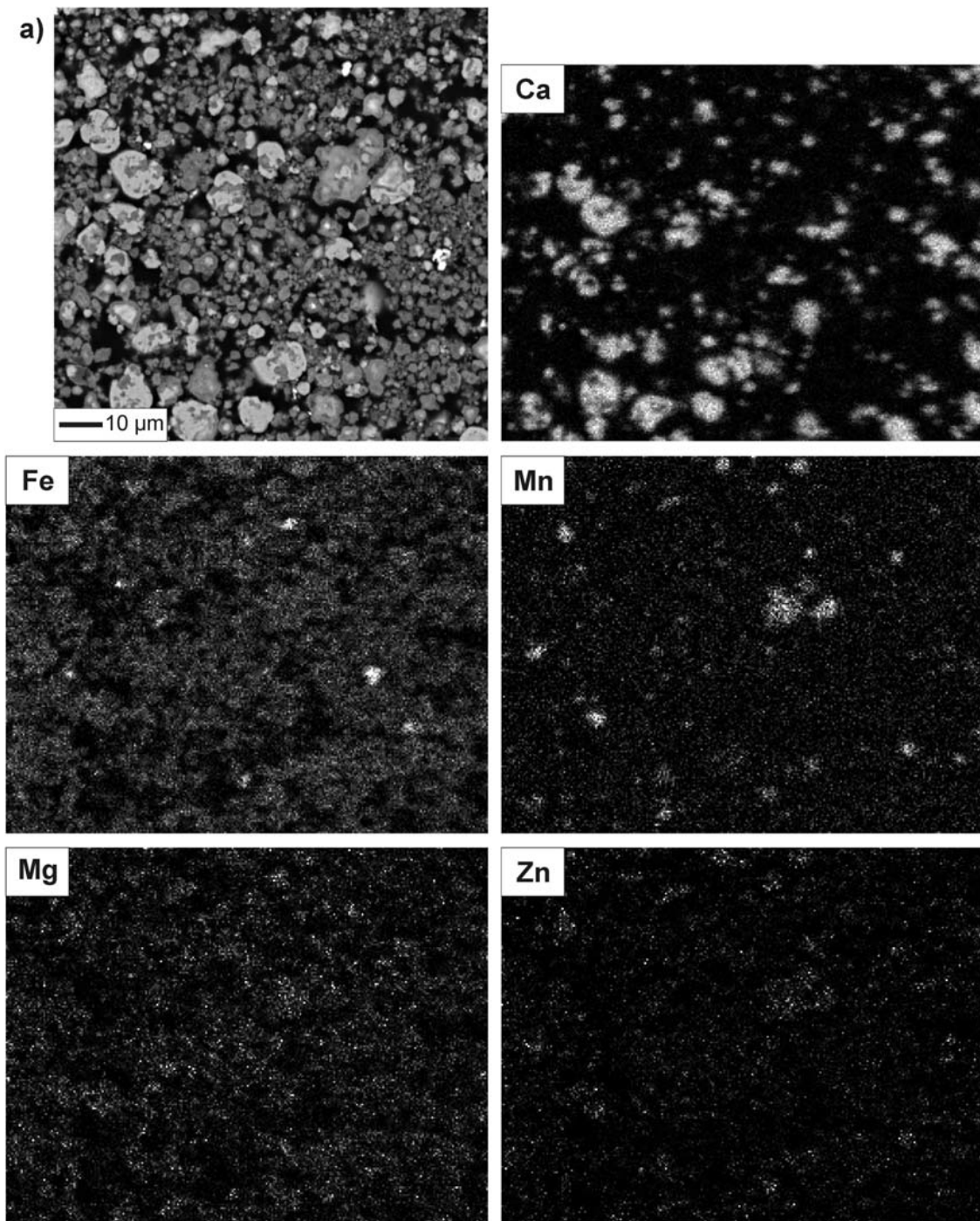


Figure 3-29: (a) SEM back scattered electron (BSE) image of the Chisel North HDS (upper left) and selected EDS 2-D elemental maps showing relative abundance of Ca, Fe, Mn, Mg and Zn.

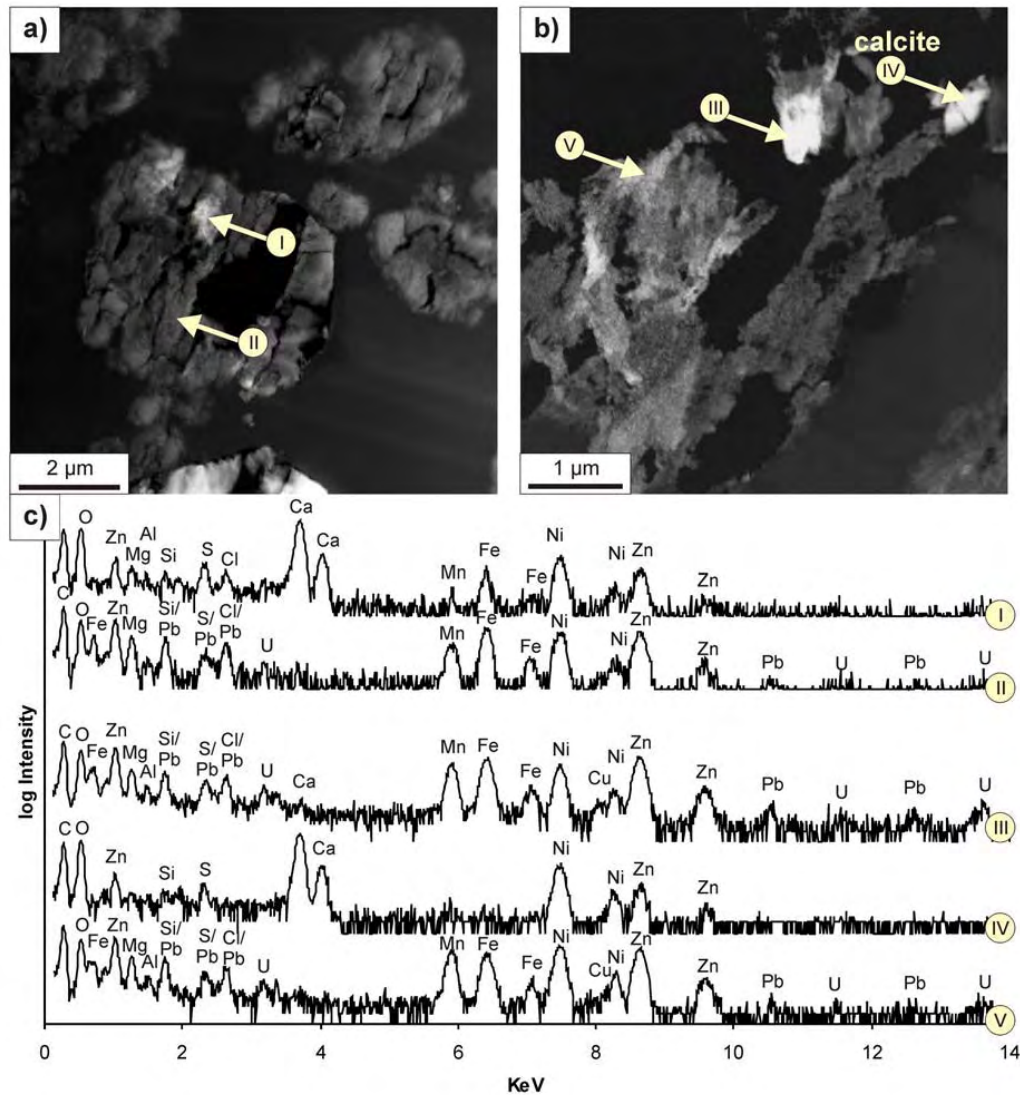


Figure 3-30: STEM HAADF images of the Chisel North HDS (a & b), and (c) selected EDS spectra corresponding to points labeled in a & b. Log intensities have been plotted to highlight trace metal peaks, if present. The Ni peaks result from the Ni-TEM support grid and do not reflect Ni content in the sample. Point I reflects calcite within the Zn-Fe-Mn oxyhydroxide aggregate. Points II, III and V are examples of the Zn-Fe-Mn oxyhydroxide with associated Pb and U.

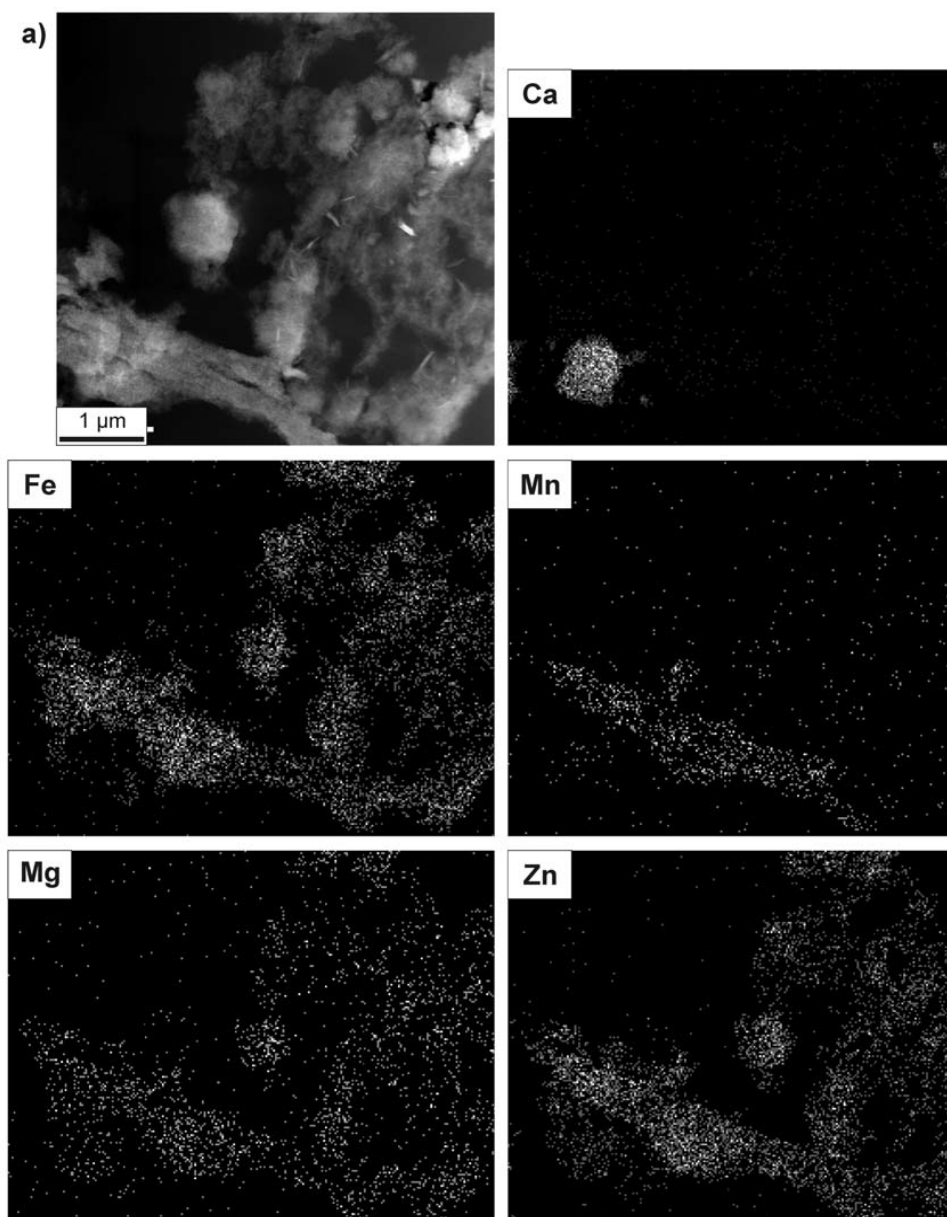


Figure 3-31: (a) STEM HAADF image of Chisel North HDS and selected EDS 2-D elemental maps showing relative abundance of Ca, Fe, Mn, Mg and Zn. The maps illustrate the presence of calcite within the Zn-Fe-Mn oxyhydroxide and show an example of a Mn-rich zone in the Zn-Fe-Mn oxyhydroxide. The overlap of calcite and the Zn-Fe-Mn oxyhydroxide is apparent by comparing the Ca-rich grain in the Ca map with the HAADF image and the Fe map. It can be difficult to identify pure Zn-Fe-Mn oxyhydroxides or calcite grains using HAADF imaging.

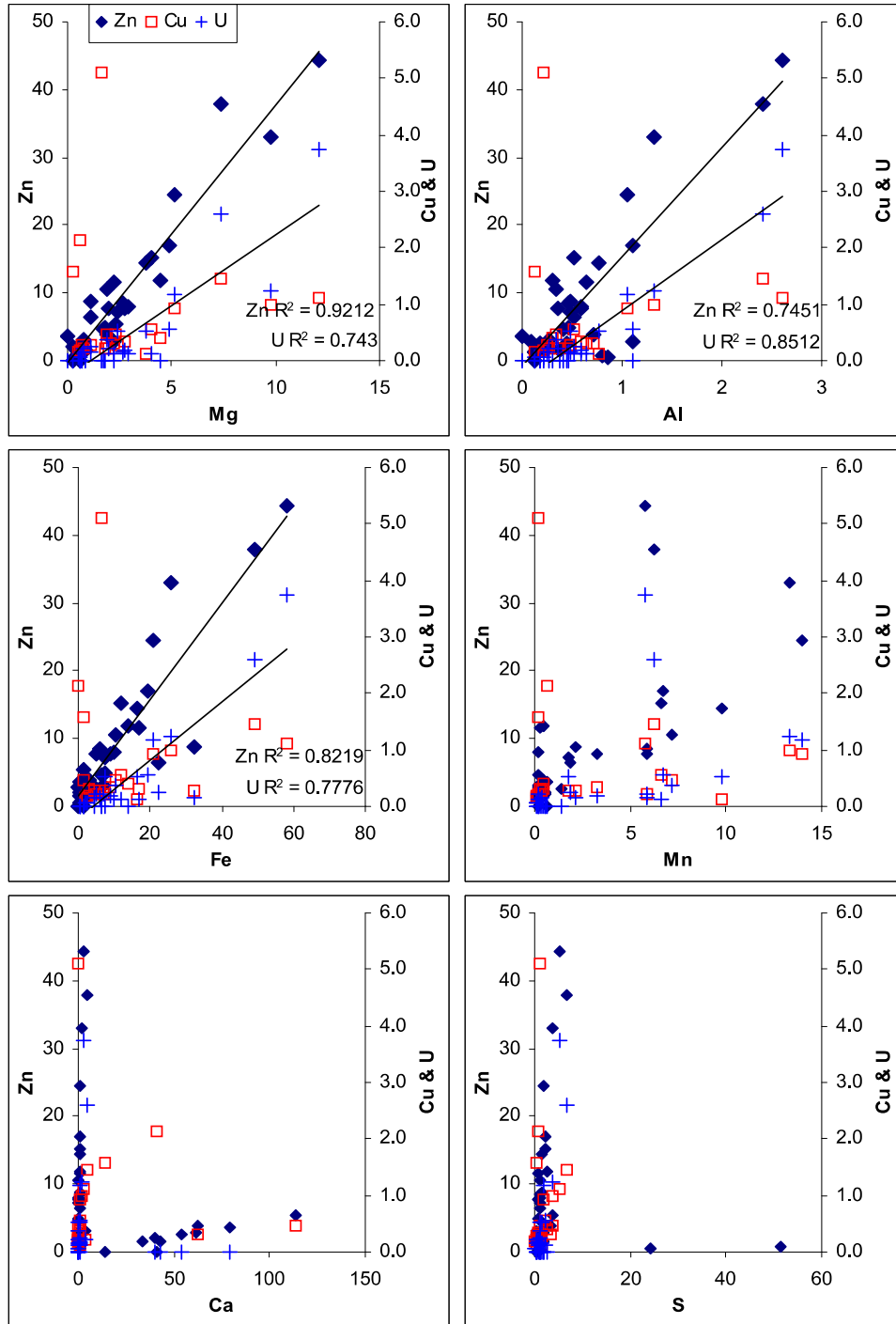


Figure 3-32: Plots of STEM EDS net intensities for the Chisel North HDS. Coefficients of determination (R^2) ≥ 0.6 have been reported. The data indicate good correlations for Zn and U with Mg, Al and Fe. Note that a single R^2 may not be representative of the variability in the material. For, example, the Zn versus Ca plot suggests a bimodal mineral control; perhaps Zn-rich calcite, and a Ca-poor phase.

3.2.3.6 Samatosum Sludge

Four major phases were identified in the Samatosum HDS sample by SEM analysis: 1) a calcium-rich phase, likely calcite as confirmed by XRD analysis (Table 3-5); 2) (altered) Al-silicates; 3) gypsum (also identified by XRD); and 4) a Zn-bearing Mg- and Fe-rich oxyhydroxide or hydroxycarbonate phase (Figure 3-33). Pure Fe-oxyhydroxide grains were also identified, but in low abundance. Zinc is primarily associated with the Mg- and Fe-rich phase and was not found in association with calcite, the Al-silicates, gypsum or the pure Fe-oxyhydroxides. Other elements detected consistently in the Mg-Fe phase include Al, Si, P, S, Cl, Ca and Mn. A Cu-Zn phase was also identified (Figure 3-34), which contained lesser amounts of Si, S, Ca, Cr, Mn, Fe and Ni.

The STEM EDS spectra in Figure 3-35 indicate that the relative proportions of Fe and Mg vary considerably within the Zn-rich Mg-Fe phase with either Fe or Mg being the major cation depending on the area analyzed. The Mg-Fe phase forms rounded irregularly shaped aggregates that display concentric layers and irregular particle boundaries (Figure 3-33). The aggregates range from <5 μm up to 10 μm in diameter and are composed of wispy fibres measuring 0.02 by 0.5 μm (Figure 3-36). The fibrous aggregates may be chemically zoned, with brighter areas in STEM HAADF images being dominated by Fe and darker areas by Mg (Figure 3-36). Little variation in the Zn content was observed between the Fe- and Mg-rich zones.

The net EDS intensities of Zn, Cu and P *versus* Mg, Al, Fe, Mn, Ca and S are plotted in Figure 3-37. The data indicate a good correlation for Fe with P, Zn and to a lesser extent Cu as well as for Mg and S with Zn. The correlation of S with Zn is likely a result of the consistent detection of S in the Zn-bearing Mg-Fe phase. In general, a trend of increasing trace-element intensities with Mg, Al, and Mn intensities is observed. The lack of correlation between Zn and Ca at high Ca intensities (calcite) suggests that Zn is not structurally incorporated with the calcite. This is consistent with the SEM and STEM results.

The Zn-bearing Fe-Mg oxyhydroxide phase generated diffuse rings when analyzed by SAED, consistent with amorphous or nanocrystalline material. Typically, only 2 to 3 d-spacings were identifiable in the patterns. Comparison of the measured d-spacings with known materials indicates that 6-line ferrihydrite provides the best fit. However, it is not conclusive because the strongest d-spacing for 6-line ferrihydrite (2.47 \AA) was not observed.

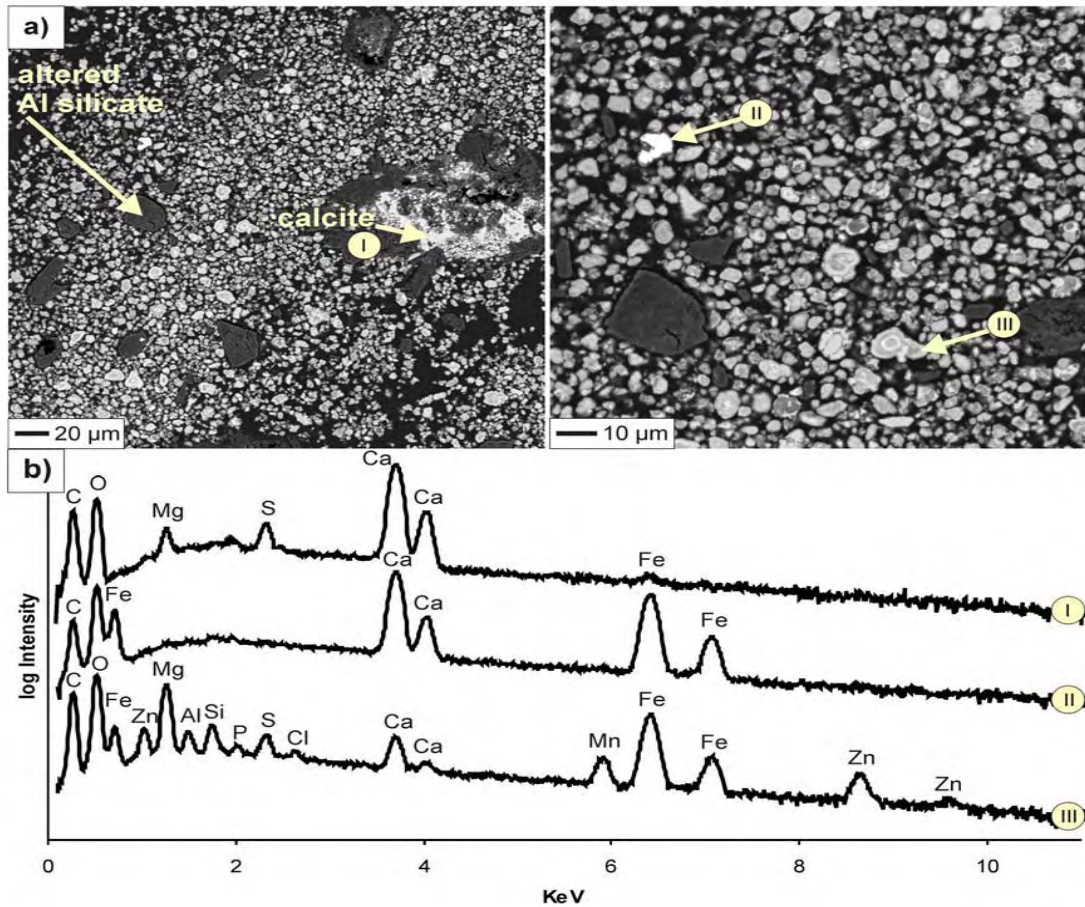


Figure 3-33: (a) SEM back scattered electron (BSE) images of the Samatosum HDS, and (b) selected EDS spectra corresponding to points labeled in (a). Log intensities have been plotted to highlight trace metal peaks, if present. Point II is a Ca-Fe rich oxide or carbonate and point III is an example of the Zn-bearing Fe-Mg oxyhydroxide.

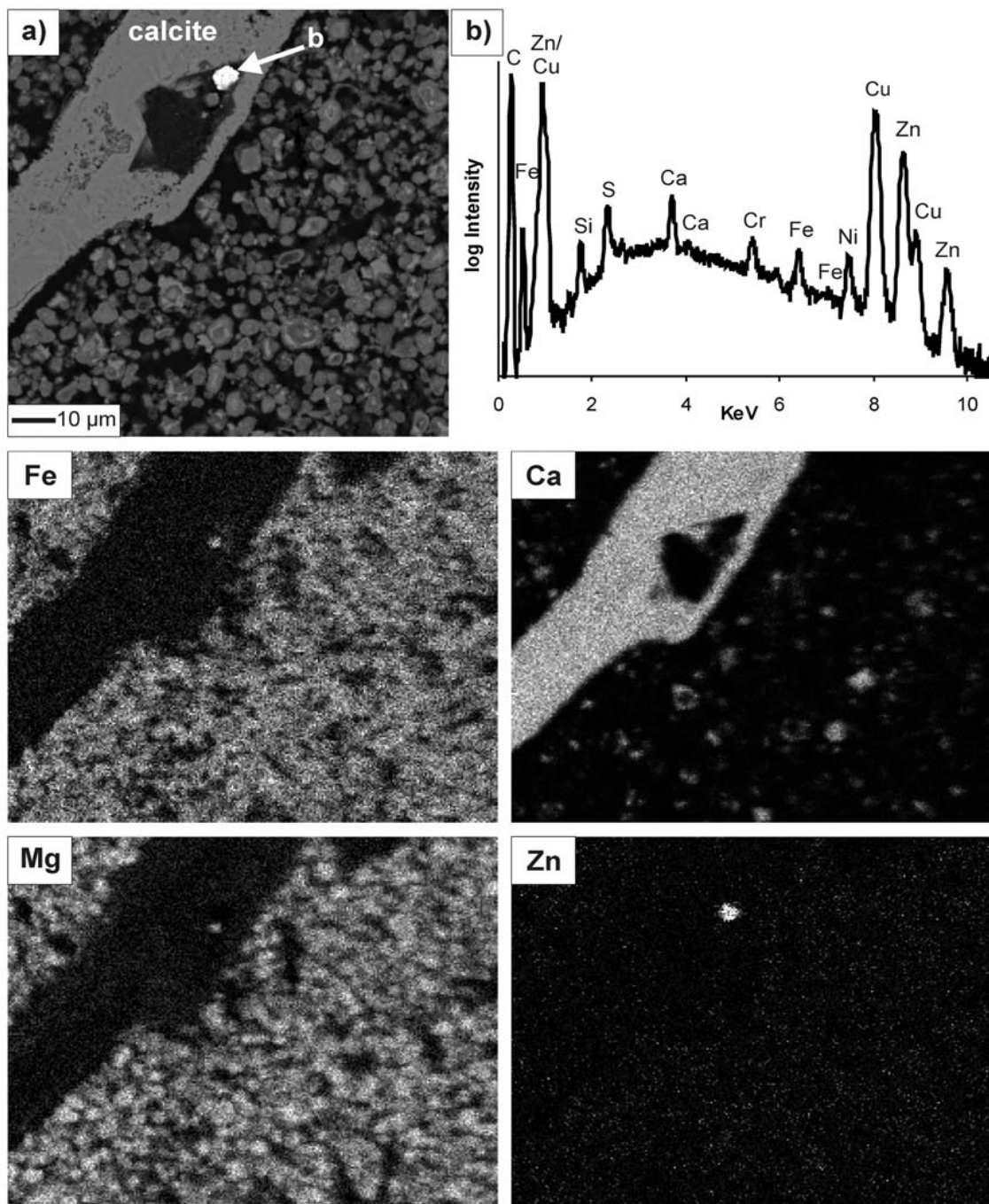


Figure 3-34: (a) SEM back scattered electron (BSE) image of the Samatsum HDS, and (b) EDS spectrum corresponding to the point labeled in (a). Selected EDS 2-D elemental maps are also provided to show the relative abundance of Fe, Ca, Mg and Zn.

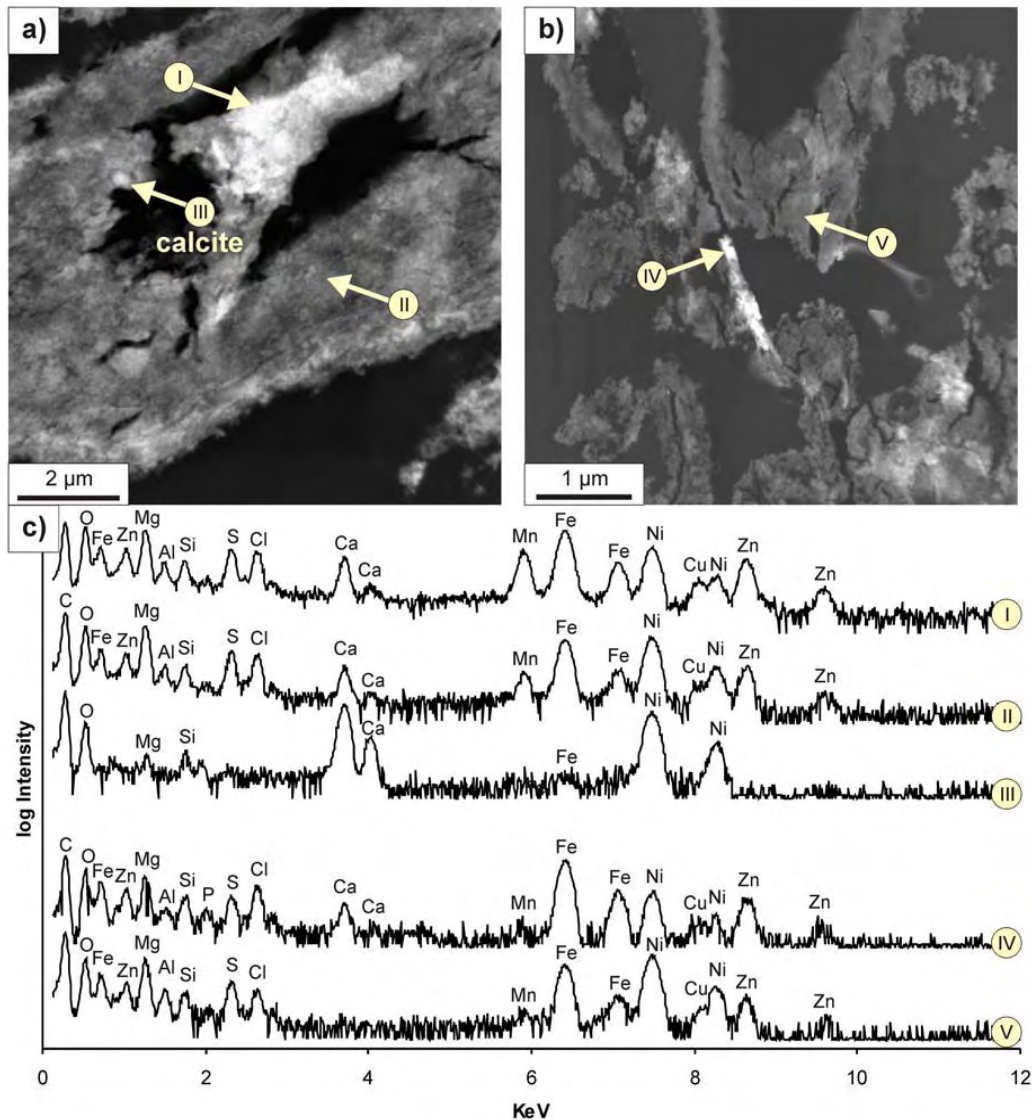


Figure 3-35: STEM HAADF images of the Samatosum HDS (a & b), and (c) selected EDS spectra corresponding to points labeled in a & b. Log intensities have been plotted to highlight trace metal peaks, if present. The Ni peaks result from the Ni-TEM support grid and do not reflect Ni content in the sample. All points show the Zn-Mg-Fe oxyhydroxide. Point I is an example of a Mn-rich Fe-Mg oxyhydroxide. Points II and V represent relatively Mg-rich zones of the Fe-Mg oxyhydroxide and point IV is relatively Mg-poor.

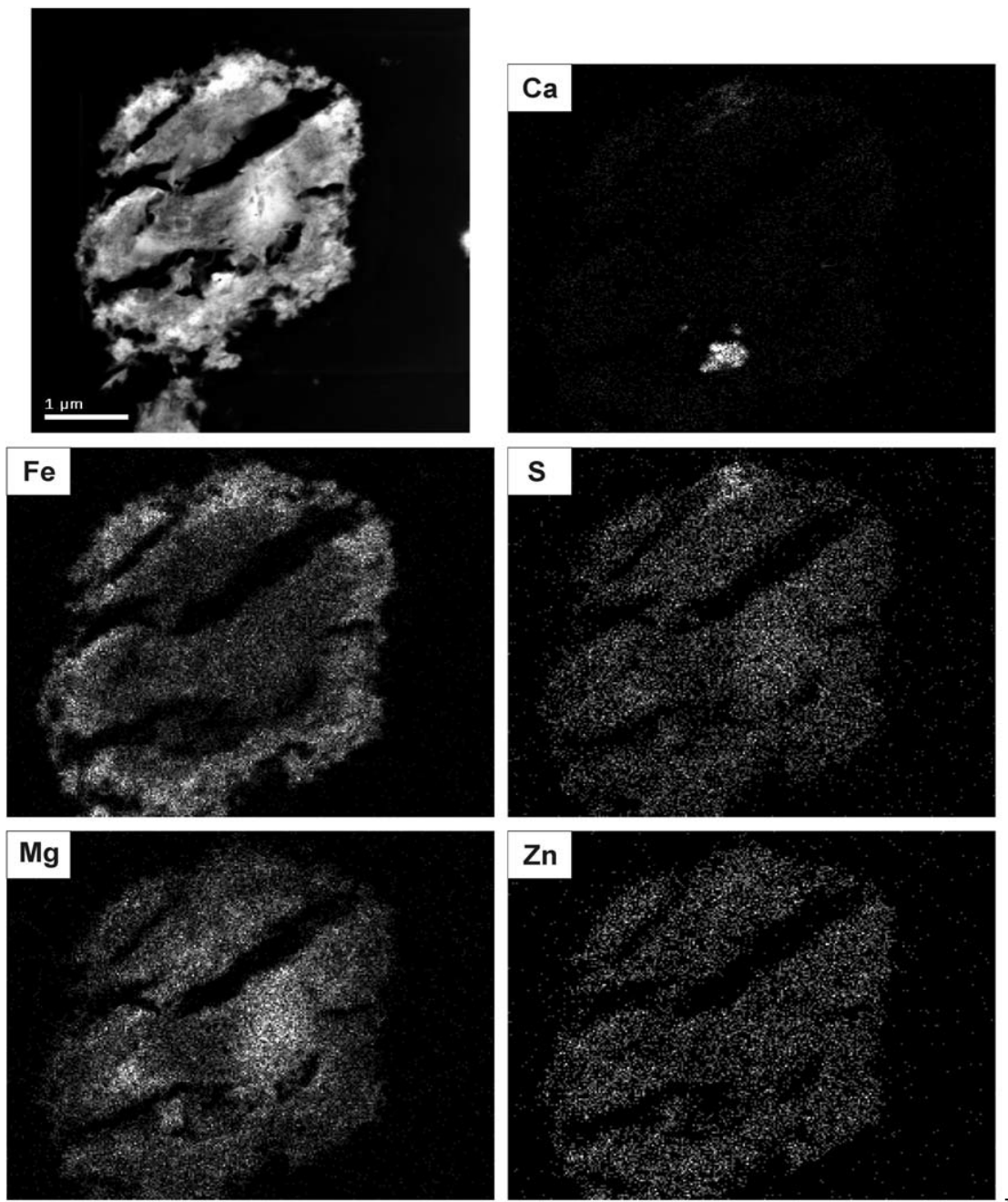


Figure 3-36: (a) STEM HAADF image of Samatosum HDS and selected EDS 2-D elemental maps, showing relative abundance of Ca, Fe, S, Mg and Zn. The Fe *versus* Mg zonation in the aggregate is apparent from the Fe and Mg maps. There does not appear to be corresponding Zn zonation (*i.e.*, relatively uniform).

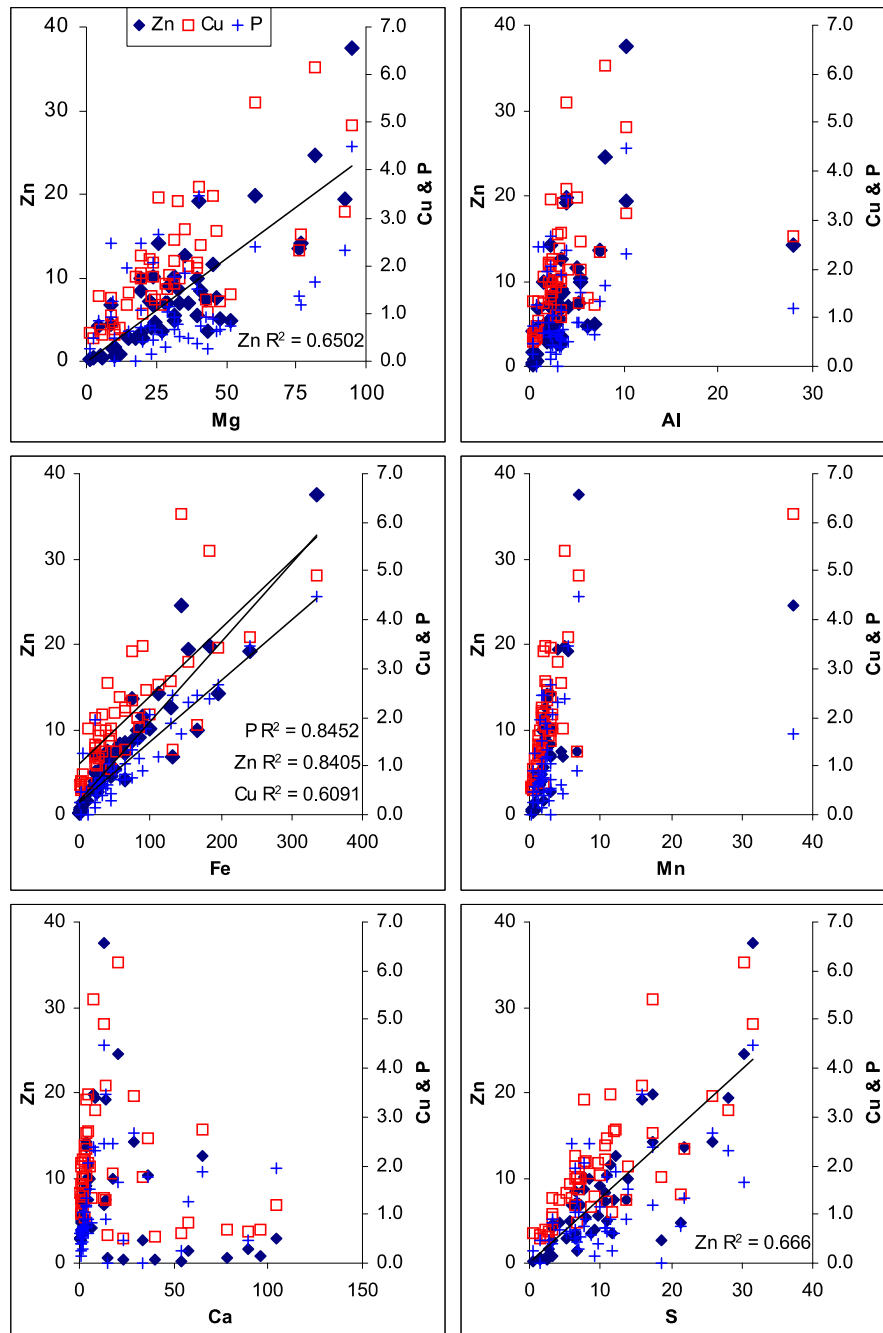


Figure 3-37: Plots of STEM EDS net intensities for the Samatosum HDS. Coefficients of determination (R^2) ≥ 0.6 have been reported. There is good correlation for Zn with Mg, Fe and S; and good correlations for Cu and P with Fe. A single R^2 may not be representative of the variability in the material. For, example, the Zn versus Ca plot may suggest a bimodal mineral control.

3.2.3.7 Sullivan Sludge

Sullivan ‘new’ HDS sample

Three major phases were identified in the Sullivan ‘new’ HDS sample by SEM analysis: 1) a Ca-rich phase, likely calcite as indicated by XRD analysis (Table 3-5); 2) gypsum (also identified by XRD); and 3) a Mg- and Fe-rich oxyhydroxide or hydroxycarbonate phase (Figure 3-38, Figure 3-39 and Figure 3-40). Overall, the analysis indicates Zn is primarily observed in association with the Mg-Fe phase. The Mg-Fe phase forms rounded, irregularly shaped aggregates that display clear concentric layers and irregular to sharp particle boundaries (Figure 3-39). The aggregates measure up to 15 x 20 µm in size and are composed of wispy fibres that measure 0.02 by 0.5 µm (Figure 3-41).

The STEM EDS spectra demonstrate that there is considerable variation in the relative proportions of Fe and Mg within the Mg-Fe phase (Figure 3-40 and Figure 3-41). Specifically, the fibrous aggregates appear to display chemical zonation with brighter areas in STEM HAADF images dominated by Fe and darker areas by Mg. Calcium associated with this phase is generally present in minor amounts except in locations where the S content is relatively high, suggesting that gypsum occurs intermixed with the Mg-Fe oxyhydroxide phase. Despite variability in the Fe and Mg content, the Zn content is relatively constant (Figure 3-41).

Other elements detected consistently in the Mg-Fe phase include Al, Si, P, S, Cl, Ca, Mn and occasionally Ti. A considerable amount of Ca was detected in some of the Mg-Fe phases, and is attributed to either a Ca-Mg-Fe phase or overlap between the Mg-Fe phase and calcite. SEM analysis did not detect a pure calcite phase. Calcite grains in the Sullivan ‘new’ HDS sample consistently contained Mg and S, and trace amounts of Fe, Al, Si, Mn and Zn (Figure 3-38). Other mineral phases identified include Ca-silicates, relatively pure Fe-oxyhydroxides, barite (BaSO₄), Ca-Fe oxyhydroxide or carbonate, and a Ca Ti-oxide. Zinc was not observed in association with these mineral phases. It is thought that these minerals may represent detrital phases, and were carried in with the wastewater during treatment.

The net EDS intensities for Zn and Cu versus Mg, Al, Fe, Mn, Ca and S are plotted in Figure 3-42. The data indicate an excellent correlation for Zn with Mg, Fe and Mn. The same correlations are not as clear for Cu; however, Cu is near the detection limit in these analyses, which may affect the coherence of the relationships.

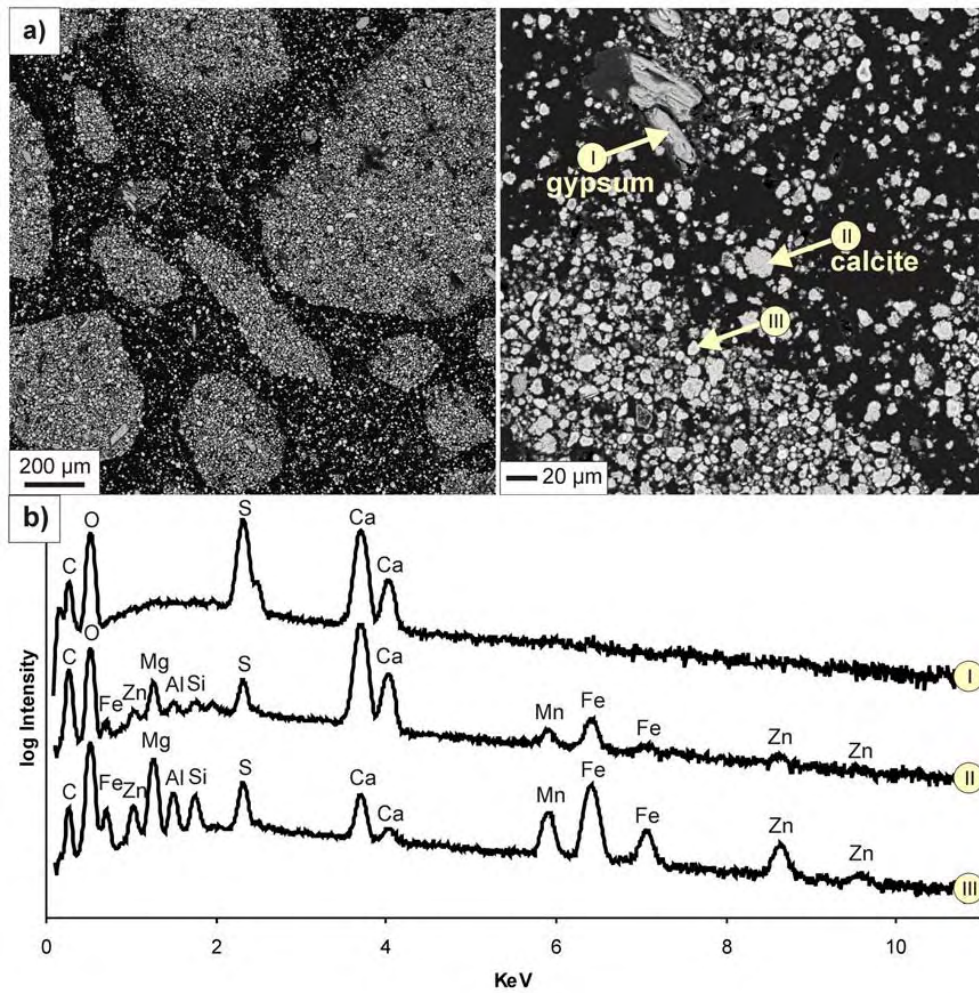


Figure 3-38: (a) SEM back scattered electron (BSE) images of the Sullivan ‘new’ HDS and (b) selected EDS spectra corresponding to points labeled in (a). Log intensities have been plotted to highlight trace metal peaks, if present. Point III is an example of the Zn- and Mn-rich Fe-Mg oxyhydroxide.

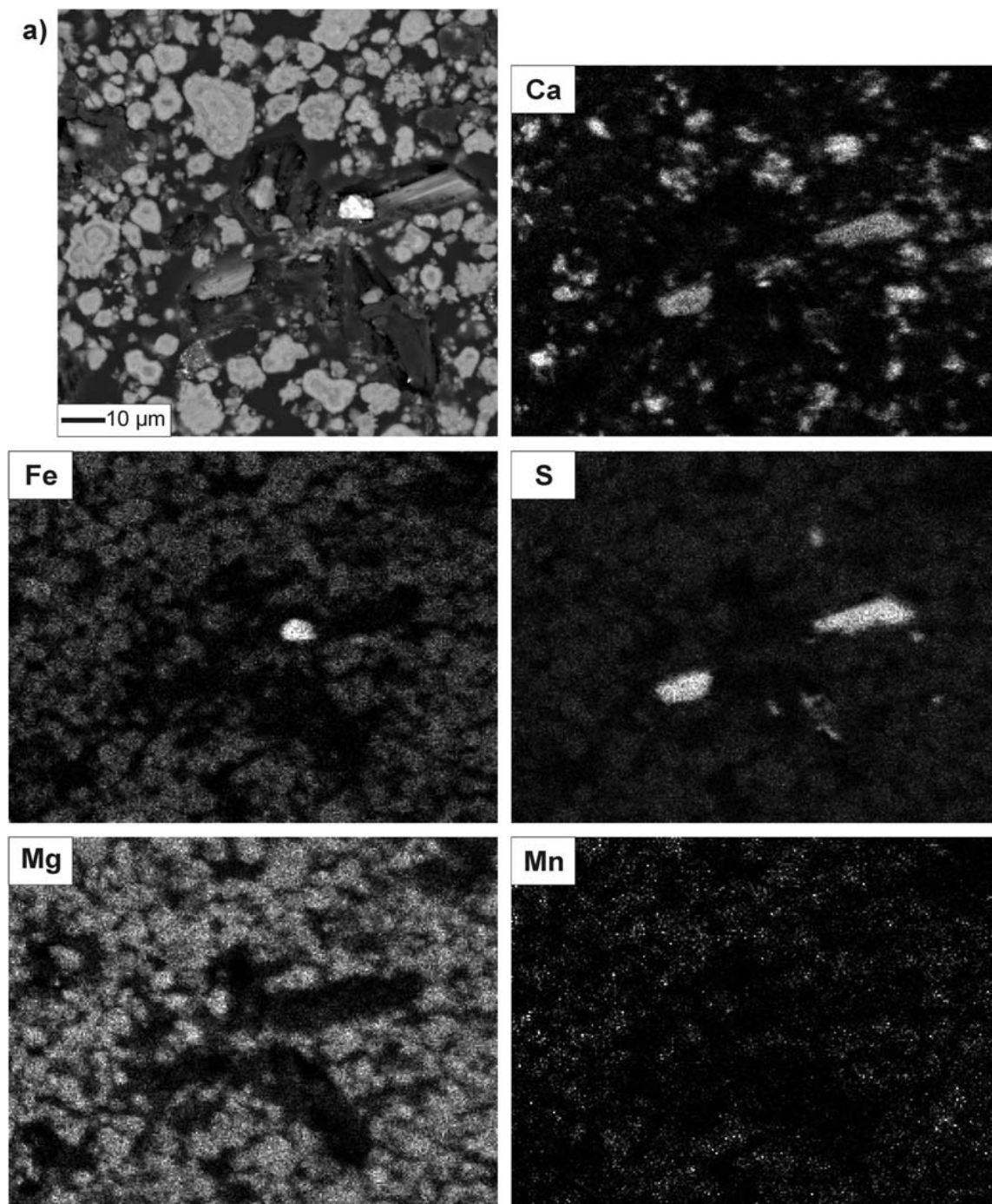


Figure 3-39: (a) SEM back scattered electron (BSE) image (upper left) of Sullivan ‘new’ HDS and selected EDS 2-D elemental maps showing relative abundance of Ca, Fe, S, Mg and Mn. The Zn concentration in the Fe-Mg oxyhydroxide is too low to be detected in EDS mapping with the instrument conditions used for this work.

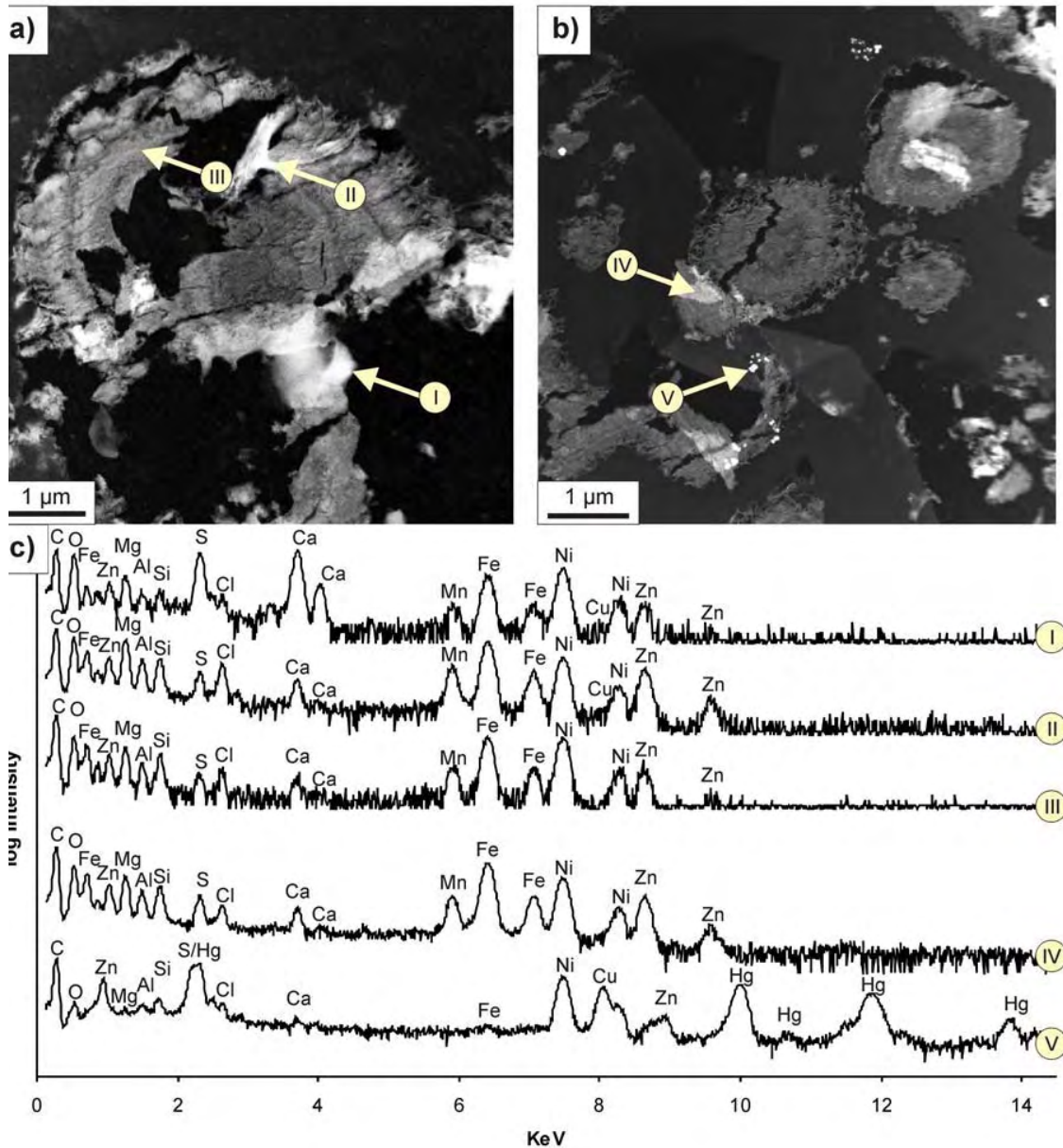


Figure 3-40: STEM HAADF images of the Sullivan (New) HDS (a & b), and (c) selected EDS spectra corresponding to points labeled in a & b. Log intensities have been plotted to highlight trace metal peaks, if present. The Ni peaks result from the Ni-TEM support grid and do not reflect Ni content in the sample. Point I is an example of a Ca-SO_4 phase overlapping the Zn-Fe-Mg oxyhydroxide. Points II, III and IV are examples of the Zn-Fe-Mg oxyhydroxide. Point V is a Hg-Cu-S material.

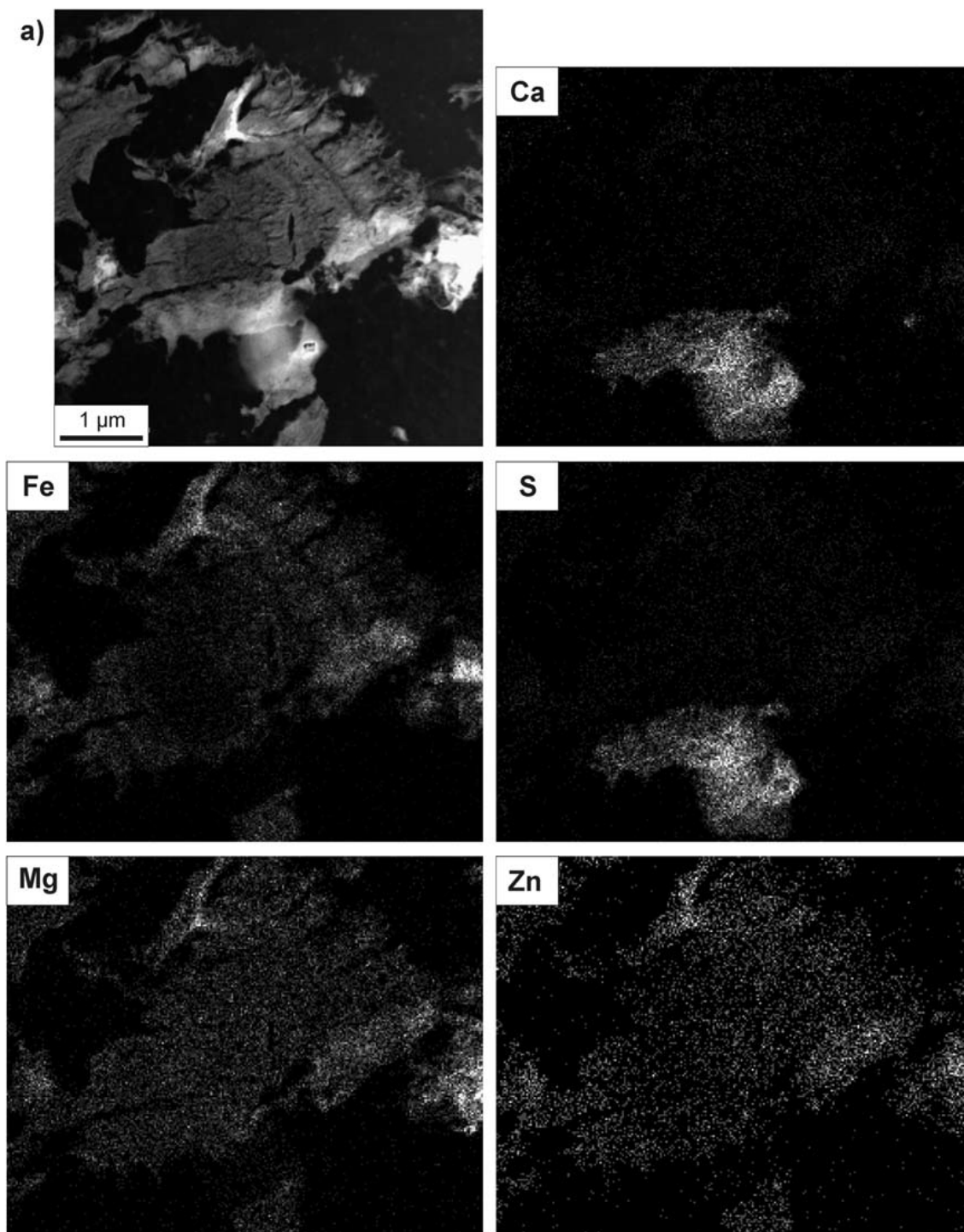


Figure 3-41: (a) STEM HAADF image of Sullivan 'new' HDS and selected EDS 2-D elemental maps showing relative abundance of Ca, Fe, S, Mg and Zn.

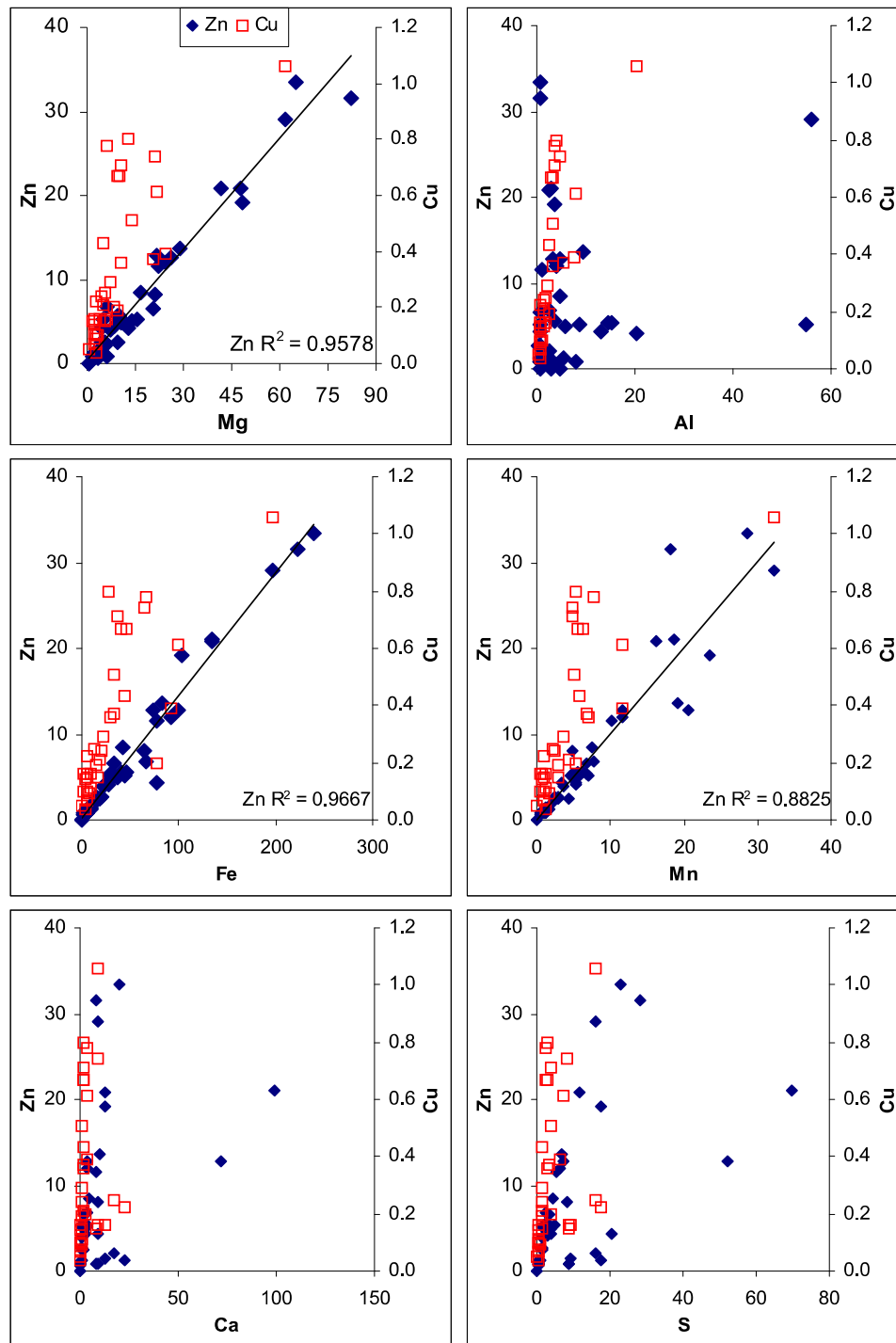


Figure 3-42: Plots of STEM EDS net intensities for the Sullivan ‘new’ HDS. Coefficients of determination (R^2) ≥ 0.6 have been reported. There are excellent correlations for Zn with Mg, Fe and Mn. A single R^2 may not be representative of the host-phase relationships. For, example, the Zn versus Ca plot may suggest a bimodal mineral control.

The Zn-Fe-Mg oxyhydroxide phase generated diffuse rings when analyzed by SAED (Figure 3-43), consistent with amorphous or nanocrystalline material. Typically, only 2 to 3 d-spacings were identifiable in the patterns. Comparison of the measured d-spacings with known materials indicates that 6-line ferrihydrite provides the best fit. However, this interpretation is not conclusive because the strongest d-spacing for 6-line ferrihydrite, 2.47Å (I/I0 100%), was not observed.

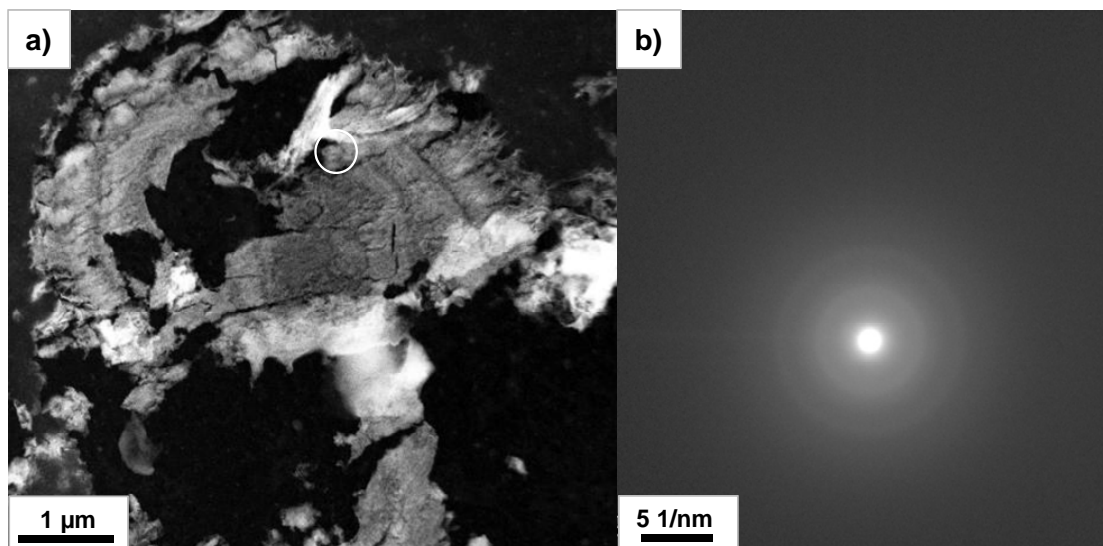


Figure 3-43: (a) STEM HAADF image of the Sullivan ‘new’ HDS EDS spectrum corresponding to the area circled in (a) is presented in Figure 3-39, point II for Zn-Fe-Mg oxyhydroxide. (c) SAED pattern corresponding to the area circled in (a). SAED pattern are consistent with amorphous or nano-crystalline material.

Sullivan ‘old’ HDS sample

SEM identified two major phases in the Sullivan ‘old’ HDS sample: 1) a Ca-rich phase, likely calcite, as indicated by XRD analysis; and a 2) Mg- and Fe-rich oxyhydroxide or hydroxycarbonate phase (Figure 3-44). Unlike the Sullivan ‘new’ HDS sample, gypsum was not detected in the ‘old’ sample by SEM. Consistent with the ‘new’ sample, Zn was primarily observed to be associated with the Mg-Fe phase.

Similar to the Sullivan ‘new’ HDS sample, the Mg-Fe phase in the Sullivan ‘old’ sample forms rounded irregularly shaped aggregates measuring <10 x 20 μm in size that display clear concentric layers and relatively sharp particle boundaries (Figure 3-44 and Figure 3-45). Unlike the Sullivan ‘new’ sample, large grains of calcite measuring 18 to 134 μm were commonly observed in the Sullivan ‘old’ HDS sample (Figure 3-44). Aggregate size range and distribution appears to be consistent for the ‘new’ and ‘old’ Sullivan samples based on qualitative comparison of SEM images.

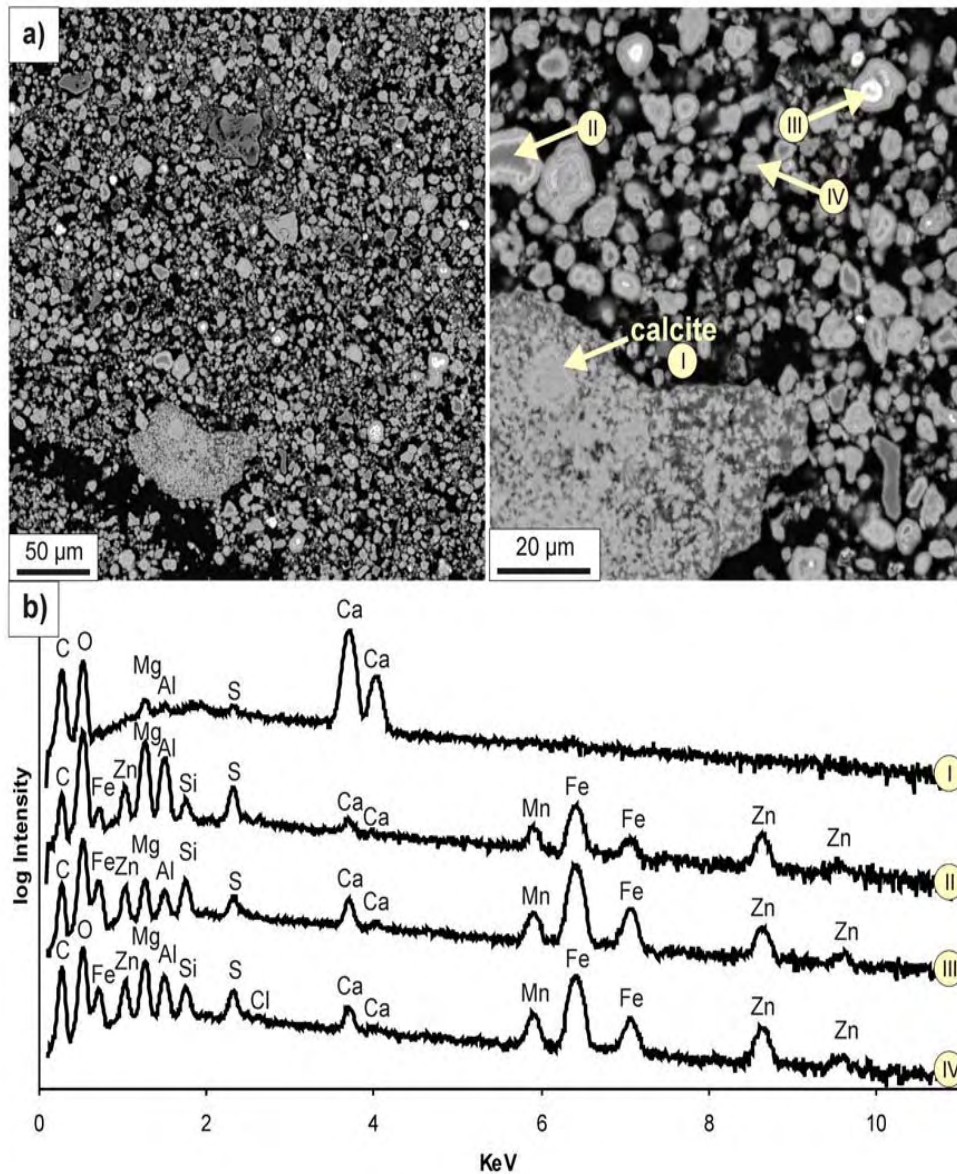


Figure 3-44: (a) SEM back scattered electron (BSE) images of the Sullivan 'old' HDS and (b) selected EDS spectra corresponding to points labeled in (a). Log intensities have been plotted to highlight trace metal peaks, if present. Point II represents a relatively Mg-rich zone of the Zn-bearing Mg-Fe oxyhydroxide while points III and IV represent relatively Fe-rich grains of the Zn-bearing Mg-Fe oxyhydroxide.

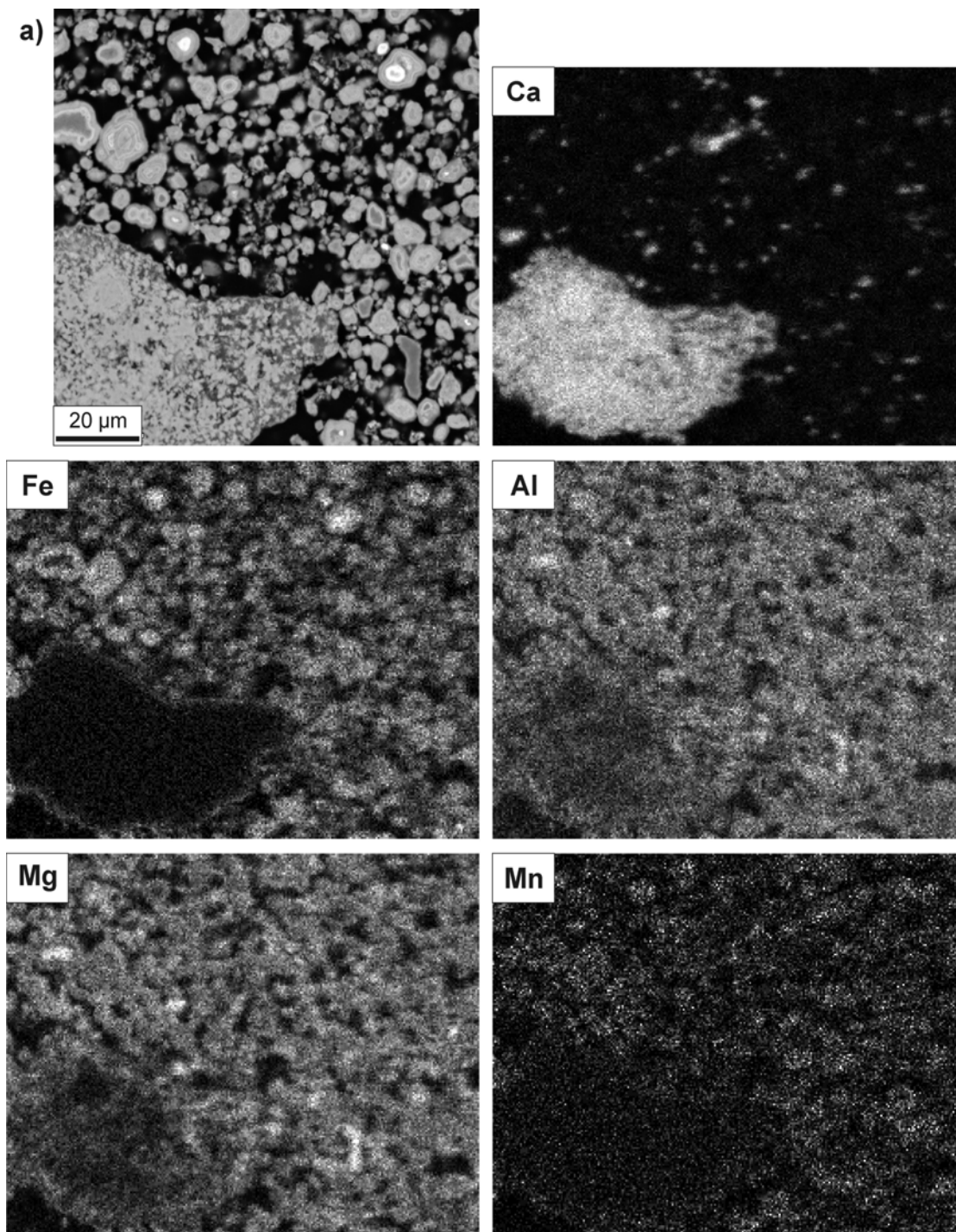


Figure 3-45: (a) SEM back scattered electron (BSE) image (upper left) of Sullivan ‘old’ HDS and selected EDS 2-D elemental maps showing relative abundance of Ca, Fe, Al, Mg and Mn. The Zn concentration in the Fe-Mg oxyhydroxide is too low to be detected in EDS mapping with the instrument conditions used for this work. Zoning of some of the Fe-Mg oxyhydroxide grains is apparent from the Fe and Mg maps.

Other elements detected consistently in the Mg-Fe phase include Al, Si, S, Ca and Mn. In some analyses Mg and Al were the dominant cations, with Fe present at trace levels. The elements P and Cl were also detected sporadically in the Mg-Fe phase. Other mineral phases identified include relatively pure Fe-oxyhydroxides, a Ca-P rich phase (likely hydroxyl-apatite, $\text{Ca}_5(\text{PO}_4)_3\text{OH}$), Al-silicates, and pyrite (<5 μm in size). Zinc was not detected with these phases nor with the calcite. It is likely that these minerals represent detrital phases associated with the treatment plant influent. No STEM analysis was conducted for the Sullivan 'old' HDS sample.

3.2.4 X-Ray Absorption Near Edge Structure (XANES)

In order to assess the nature of Zn associations in sludge solids, XANES spectra were collected at the Canadian Light Source, with the data being sent to Queens University (Drs. Andrew Gault and Heather Jamieson) for processing and linear combination fitting against XANES spectra collected at the Canadian Light Source as well as the Advanced Photon Source for a range of Zn-bearing mineral assemblages. The best fits for Zn K-edge XANES data for the neutralization sludge samples are summarized in Table 3-6. Figure 3-46 presents the Zn K-edge XANES spectrum obtained from the sludge samples showing the best 2-component and/or 3-component fits to Zn-bearing standards provided in Table 3-6.

The standards utilized, and their relevance to Zn sequestration and stability, can be summarized as follows:

- Zn coprecipitated with ferrihydrite (Zn coppt 2LF; Table 3-6: represents Zn incorporated in the Fe-oxide matrix during formation. Indicative of relatively-stable complexes;
- Zn nitrate - $\text{Zn}(\text{NO}_3)_2$ (Table 3-6): representative of Zn present as labile, hydrated outer sphere complexes that will be relatively labile;
- Mg-bearing $\text{Zn}_{0.8}\text{Mg}_{0.2}$ -kerolite (-talC) (Table 3-6): included since provided spectral fits for peaks in data for Brunswick, Chisel North, Sammatosum and Sullivan samples. Zn present as a relatively stable complex;
- Gahnite (ZnAl_2O_4 ; Table 3-6): included in model fits since provided closest spectral fit for peaks in Britannia, Brunswick and Chisel North data. Zn present as a relatively stable complex; and
- Zn sorbed to ferrihydrite (Zn sorbed 2LF; Table 3-6): Zn adsorbed to the surface of Fe-oxides. Indicative of potentially labile complexes.

Overall, given the general absence of suitable model compounds analogous to the sludge phases, the applicability of XANES to discern metal-associations in certain sludge samples is currently limited. However, the data offer insight into the potential stability of Zn through differentiation of potentially labile and non-labile forms. The data can also be used to qualitatively evaluate the shape of the spectra and determine or confirm similar/different complexes from site to site. For example, STEM analyses suggested that the Brunswick and Chisel North samples host comparable Zn-bearing phases (Zn-Fe-Mn oxyhydroxide). Similarly, the Samatosum and Sullivan samples show similar Zn-bearing phases (Fe-Mg oxyhydroxide). This is confirmed by the shape of the XANES spectra.

Table 3-6:
Best fits for Zn K-edge μ -XANES data for HDS sludge samples^a.

Sample	Proportion of Zn present as:					Energy shift	χ^2
	Zn coppt 2LF ^b	Zn(NO ₃) ₂	Zn _{0.8} Mg _{0.2} -kerolite (-talc)	Gahnite (ZnAl ₂ O ₄)	Zn sorbed 2LF		
Equity	60	41	-	-	-	-0.11	3.14
Geco	81	21	-	-	-	0.1	0.8
	48	16	-	-	37	0.09	0.71
Britannia	27	72	-	-	-	0.01	4.04
	-	79	-	21	-	0.01	3.83
Brunswick	59	41	-	-	-	-0.32	0.64
	51	37	13	-	-	-0.36	0.54
	44	44	-	12	-	-0.32	0.5
Chisel North	64	37	-	-	-	-0.02	0.5
	55	33	14	-	-	-0.07	0.38
	47	40	-	13	-	-0.03	0.33
Samatosum	69	-	31	-	-	-0.24	0.92
Sullivan	52	-	48	-	-	0.07	1.43
	57	13	30	-	-	0.2	0.98

Notes: a) components were not forced to sum to 100% during the fitting process (typically 100 – 103%). All fit combinations that yielded comparably low χ^2 values are reported. Although principal component analysis indicated two components are adequate to describe the data, three component fits are also reported where significant improvements in the least squares residuals were obtained.

b) "2LF" denotes 2-line ferrihydrite; "coppt" indicates "co-precipitated with".

c) χ^2 = sum of the squared differentials (*i.e.*, the goodness of fit of the standard to the significant principal components). The lower the number, the better the fit.

3.2.4.1 Equity Sludge

The Zn K-edge XANES spectrum obtained for the Equity HDS sample is best fit with 60% Zn co-precipitated with ferrihydrite and 41% zinc nitrate (Table 3-6, Figure 3-46). The Zn nitrate fit indicates that a proportion of the Zn in the Equity HDS is present as labile, hydrated outer sphere complexes that will be relatively mobile, whereas, the Zn co-precipitated with ferrihydrite is likely to be less mobile.

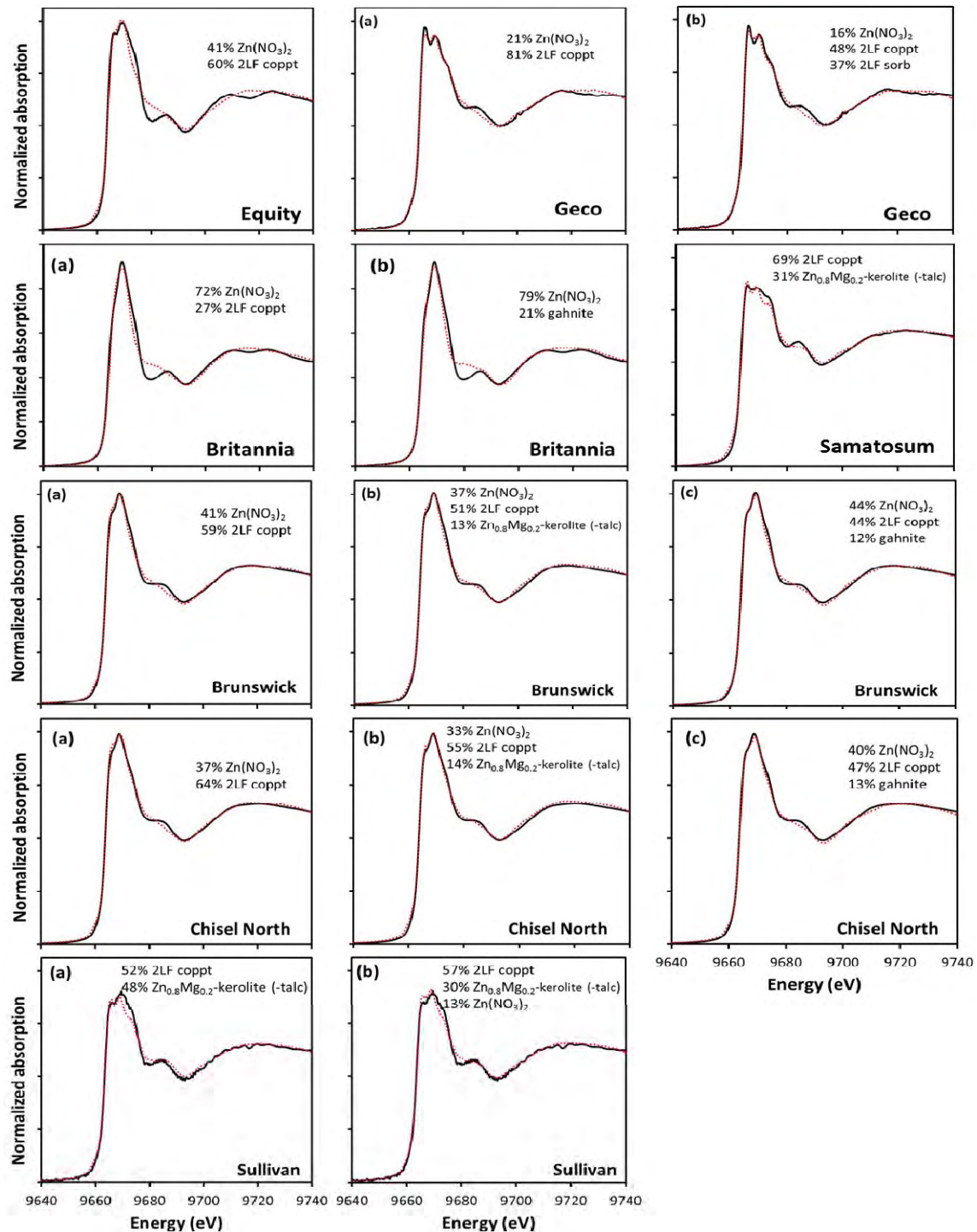


Figure 3-46: Zn K-edge XANES spectra obtained from neutralization sludge samples from the Equity, Geco, Britannia, Brunswick, Chisel North, Samatosum and Sullivan mines showing best 2-component and/or 3-component fits to Zn-bearing standards. Dotted red line shows best match of reference Zn phases listed in Table 3-6. Percentage fits for each phase are shown in graphs. 2LF coppt = co-precipitated with 2-line ferrihydrite; sorb 2LF = adsorbed to 2-line ferrihydrite.

It should be noted that significant discrepancies are visible between the sample and reconstructed fit XANES spectra (Figure 3-46) for the Equity HDS, reflected in the rather high χ^2 value (Table 3-6). Such observations indicate other unidentified Zn phases are present in this sample. Indeed, the Equity sludge sample contains other Zn phases that are not present in the standard library, including the dominant Mg-Al-(Fe) hydroxysulfate indicated by SEM and STEM (Section 3.2.3.1). The absence of a suitable model compound for this phase limits application of the XANES data.

It is interesting to note that the Equity HDS shows a marked post-edge peak at *ca.* 9,686.5 eV. Of all the standard phases collected, only the Mg-bearing Zn_{0.8}Mg_{0.2}-kerolite (-talc) shares this feature, suggesting the XANES spectra for other Zn-bearing Mg-rich phases should be collected for future data fitting (Gault and Jamieson, 2012). Further work should also consider collecting the Zn K-edge X-ray absorption spectra for other Zn-bearing phases that might be expected to be present in mine neutralization sludges such as Zn(OH)₂ and Zn sorbed and/or co-precipitated with hydrous oxides of Al and Mg.

3.2.4.2 Geco Sludge

The Zn K-edge XANES spectrum obtained for the Geco HDS sample is best fit with 81% Zn co-precipitated with ferrihydrite and 21% zinc nitrate (Table 3-6; Figure 3-46, Geco a). The least squares residual for this fit is marginally improved by adding 37% Zn sorbed to ferrihydrite in the fit, mainly at the expense of Zn co-precipitated with ferrihydrite (Table 3-6; Figure 3-46, Geco b). This indicates that Zn is likely associated with ferrihydrite (either co-precipitated or sorbed) and a certain proportion (16~21%) of the Zn is relatively labile in this sample. The fact that the best fits of this sludge sample are obtained with Zn co-precipitated with ferrihydrite (or Zn sorbed to ferrihydrite) is consistent with the results of the SEM and STEM analyses indicating the association of Zn with Fe-bearing oxyhydroxides (Section 3.2.3.2).

3.2.4.3 Britannia Sludge

Two sets of Zn K-edge XANES spectra produced best matches for the Britannia HDS sample (Table 3-6, Figure 3-46). Zinc nitrate is the dominant fitted phase, comprising >70% of the Zn; and the remainder fit well with either Zn co-precipitated with ferrihydrite (27%; Figure 3-46, Britannia a) or gahnite (ZnAl₂O₄; 21%; Figure 3-46 Britannia b). Because the Zn nitrate accounts for the bulk of the Zn speciation in the Britannia sample, a portion of the Zn is indicated to be in a labile form, perhaps as weakly sorbed outer sphere complexes. The formation of outer sphere complexes has been observed for Zn sorption studies on amorphous hydrous ferric oxide at relatively

high aqueous Zn loadings (10^{-2} to 10^{-3} M), while lower Zn loadings tend to form inner sphere complexes with ferrihydrite (Gault and Jamieson, 2012). Data fits for more crystalline (*e.g.*, gahnite) and less labile Zn compounds (*e.g.*, Zn co-precipitated with ferrihydrite) also suggest that a portion of the Zn is in less available forms.

Similar to the Equity sludge sample, it is evident that the best fits could not reproduce all the structural features of the sample XANES spectra, reflected in the rather high χ^2 values (Table 3-6). The marked post-edge peak at *ca.* 9,686.5 eV suggests possible presence of Zn-bearing Mg-rich phases. This is consistent with indications of Mg-bearing Cu-Zn oxyhydroxides as revealed by SEM and STEM analyses (Section 3.2.3.3).

3.2.4.4 Brunswick Sludge

The best two component fit for the Zn K-edge XANES spectrum obtained from the Brunswick HDS sample is a mixture of Zn co-precipitated with ferrihydrite (59%) and zinc nitrate (41%) (Table 3-6; Figure 3-46, Brunswick (a)). Although principal component analysis indicates that just 2 standards are necessary to adequately describe the data, the inclusion of a third component to better match the shape of the post-edge shoulder at *ca.* 9,686 eV results in a 16% or 22% improvement in the fit quality when $\text{Zn}_{0.8}\text{Mg}_{0.2}$ -kerolite (-talc) (13%) or gahnite (12%) are included (Table 3-6; Figure 3-46, Brunswick b) and c), respectively). This suggests a portion of the Zn is associated with less labile complexes. Overall, the fitting of Zn nitrate suggests that up to 44% of the Zn in the Brunswick HDS sample is relatively labile. The remainder is likely much less labile as a ferrihydrite co-precipitate, with perhaps a minor (12 to 13%) proportion of Zn structurally incorporated into other less labile phases.

3.2.4.5 Chisel North Sludge

The best two component fit for the Zn K-edge XANES spectrum obtained from the Chisel North HDS sample is a combination of 64% Zn co-precipitated with ferrihydrite and 37% zinc nitrate (Table 3-6, Figure 3-46 Chisel (a)), potentially indicating a mixing of labile and less labile species. This is consistent with the XANES spectrum obtained for the Brunswick sample and consistent with STEM analysis which identified Zn-Fe-Mn oxyhydroxide as the main trace metal-bearing phase in both the Chisel North and Brunswick samples. The Zn nitrate fit indicates that a proportion of the Zn is present as labile, hydrated outer sphere complexes that will be relatively labile, whereas the fit with Zn co-precipitated with ferrihydrite suggests a more chemically-stable component. The fit is considerably improved by the addition of 14% $\text{Zn}_{0.8}\text{Mg}_{0.2}$ -kerolite (-talc) (Figure 3-46, Chisel (b)), which is a better match with the post-edge shoulder at *ca.* 9,686 eV, or 13% gahnite (Figure 3-46, Chisel (c)); however, these fits cannot be distinguished given their similar reduced squares residuals (χ^2 of ~ 0.35 , Table 3-6

3.2.4.6 Samatosum Sludge

The best two component fit for the Zn K-edge XANES spectrum obtained for the Samatosum HDS sample is a mixture of 69% Zn co-precipitated with ferrihydrite and 31% $Zn_{0.8}Mg_{0.2}$ -kerolite (-talc) (Table 3-6, Figure 3-46). This is consistent with the indication of a Zn-bearing Fe-Mg oxyhydroxide phase by SEM and STEM analyses (Section 3.2.3.6). Of all the standard phases collected in the XANES analyses, only the Mg-bearing $Zn_{0.8}Mg_{0.2}$ -kerolite (-talc) shares the marked post edge peak at *ca.* 9,686.5 eV with the Samatosum sample (Gault and Jamieson, 2012). The fit with Zn-kerolite suggests almost a third of the Zn is incorporated within more structurally (and chemically) stable complexes.

3.2.4.7 Sullivan Sludge

The best two component fit for the Zn K-edge XANES spectrum obtained for the Sullivan HDS sample is a combination of 52% Zn co-precipitated with ferrihydrite and 48% $Zn_{0.8}Mg_{0.2}$ -kerolite (-talc) (Table 3-6; Figure 3-46 Sullivan a)). This is consistent with the XANES spectrum obtained for the Samatosum sample and the predominance of a Zn-bearing Fe-Mg-oxyhydroxide phase in both the Sullivan and Samatosum samples as revealed by SEM and STEM. The fit is significantly improved with the inclusion of 13% zinc nitrate (Figure 3-46 Sullivan b), also indicating the presence of more labile species. Similar to the Samatosum HDS sample, the fits with $Zn_{0.8}Mg_{0.2}$ -kerolite (-talc) and Zn co-precipitated with ferrihydrite suggest that a sizeable proportion of the Zn may be structurally sequestered within less labile complexes.

4. Summary and Implications for Sludge Chemical Stability

4.1 Summary of Data

The most salient results for the influent and effluent water chemistry, solid phase sludge composition and high-resolution microscopy are summarized below for the seven HDS samples. The dominant parameters in the ARD influent, solid phase elements in sludge samples and the primary trace metal-bearing phases are summarized in Table 4-1. A potential management model tool to predict the trace metal-bearing phases in neutralization sludges is presented in Section 4.2, followed by a discussion of the implications for *in situ* sludge chemical stability in various depositional environments (Section 4.3).

Table 4-1:
Summary of dominant trace metal-bearing phases for sludge samples and dominant parameters in ARD influent and solid phase elements based on molar concentrations.

Mine	Dominant Parameters in Influent (mmol/L)	Dominant Solid-Phase Elements (mmol/kg)	Trace Metal Hosting Phase
Equity	SO ₄ >>Mg>Al>Fe>>Ca>Cl>F>Mn>Zn	S=Ca >>Al>Mg >Fe >Mn >Zn	Mg-Al(Fe) hydroxysulphate
Geco	SO ₄ >Fe >>Ca=Mg	Fe >Ca >S >>Mg	Fe-oxhydroxide
Britannia	SO ₄ >Ca >Mg >>Al>Cl	Ca >Al>Mg >>Zn >Cu >S >Mn >Fe	Cu-Zn oxyhydroxide
Brunswick	Na >SO ₄ >Mg >Ca=Cl>Zn	Ca >Fe >Zn >>Mn >S >Mg >Na	Zn-Fe-Mn oxyhydroxide
Chisel North	Cl>Na >Ca >SO ₄ >Mg >Zn	Ca >Zn >Fe >>Mg >S >Mn	Zn-Fe-Mn oxyhydroxide
Samatosum	SO ₄ >Mg >Ca >Fe >Zn	Ca >Mg >Fe >S >>Zn >Al	Fe-Mg oxyhydroxide
Sullivan	SO ₄ >Mg >>Ca >Fe >Na=Cl	Mg >Ca >Fe >S >>Al>Zn >Mn	Fe-Mg oxyhydroxide

4.1.1 Equity Mine

The Equity Mine ARD influent samples are dominated on a molar basis by SO₄>Mg>Al>Fe>Ca>F (Table 3-1 Appendix A-1). With respect to cations, the combined molar concentration of Mg and Al was greater than four times the concentration of Fe. Zn (~120 mg/L) and Cu (~60 mg/L) represent the dominant trace elements in the ARD feed. Through the treatment process the pH increased from 2.6 to 7.0. The composition of the clarifier outflow (*e.g.*, treated effluent) was dominated by SO₄, Ca, Mg, Mn, Na and Sr, with the majority of trace elements at values below the limits of analytical detection. Sulfate concentrations were reduced considerably during the treatment process from ~9,000 mg/L in the influent to ~2,800 mg/L in the outflow.

Saturation indices indicate that the treated effluent is supersaturated with respect to gypsum and fluorite.

Consistent with influent chemistry, the Equity Mine HDS and LDS samples are composed primarily on a molar basis of $S > Ca >> Al > Mg > Fe > Mn > Zn$ (Figure 3-4, Appendix B). Gypsum (also supported by XRD), Al-(oxy)hydroxide, Fe-Al (oxy)hydroxide are the main sludge phases identified based on SEM imaging of composition and morphology. SEM and STEM analyses indicate that the main Zn-bearing phase is a Mg-Al-(Fe) hydroxysulfate that forms fine-grained fibrous aggregates (<15 μm). SAED analysis conducted on the Mg-Al-(Fe) hydroxysulfate did not produce any discernible diffraction patterns, suggesting that this phase is amorphous. Qualitative assessment of the SEM images indicates the Mg-Al-(Fe) hydroxysulfate particles are fibrous aggregates that range in size from <1 μm to approximately 15 μm . Larger grains of the Mg-Al-(Fe) hydroxysulfate show compositional zoning in concentric layers alternating between Mg and Al-rich (Fe-poor) and Fe-rich zones, which can be attributed to dissolution and re-precipitation reactions that occur during sludge recycling in the HDS process.

The Equity HDS and LDS samples are compositionally similar. Both samples are composed predominantly of gypsum and an amorphous trace metal-bearing phase, Mg-Al-(Fe) hydroxysulfate, and lesser amounts of Al (oxy)hydroxides, Fe-Al (oxy)hydroxides and calcite (Table 3-5). Due to limitations associated with sample standards for XANES, the Zn K-edge XANES spectrum for the Equity HDS offers only limited utility. However, the XANES data suggest that a proportion of Zn in the Equity HDS is present as labile, hydrated outer sphere complexes while another proportion of Zn demonstrates bonding characteristics consistent with the ferrihydrite standard used for the testwork. It is unclear whether one or both of these modes applies to the trace metal-bearing Mg-Al-(Fe) hydroxysulfate identified in the Equity sludge.

4.1.2 Geco Mine

The Geco Mine ARD influent samples are dominated on a molar basis by $SO_4 > Fe >> Ca = Mg$ (Table 3-1, Appendix A-2). Based on molar proportions, the average concentration of Fe was greater than the combined contribution of Ca and Mg. Zinc (~12 mg/L), and to a lesser degree Cu (~0.3 mg/L) and Cd (~0.04 mg/L), are the dominant trace elements in Geco ARD. Through the treatment process, the concentrations of Zn, Cu and Cd were reduced in the outflow by an average of greater than 90%. Sulfate concentrations decreased only moderately through the HDS process (4,590 mg/L to 3,400 mg/L). Saturation indices indicate that the Geco effluent is supersaturated with respect to gypsum, calcite, fluorite, ferrihydrite and gibbsite.

The Geco HDS sample is composed primarily on a molar basis of $Fe > Ca > S >> Mg$ (Figure 3-4, Appendix B). The Fe content of the Geco HDS is the highest of all sludges analyzed, while the Mg concentration is the lowest. Phases identified by SEM include dominant gypsum (also supported by XRD), Fe-(oxy)hydroxide, Al-(oxy)hydroxide and calcite. Zn and Cu in the Geco sludge sample are predominantly associated with the

Fe-(oxy)hydroxide that forms fine-grained fibrous aggregates (<20 μm). High resolution EDS collected during STEM indicates that the Fe-(oxy)hydroxide phase is essentially pure with only minor amounts of other constituents (Mg, Al and SO₄). SAED analysis of the Fe (oxy)hydroxide suggests that this phase is poorly crystalline to amorphous, with d-spacings consistent with ferrihydrite (Fe₂O₃•0.5H₂O) and lepidocrocite [FeO(OH)]. The Zn K-edge XANES spectrum obtained for the Geco HDS sample indicates that a large proportion (>81%) of the Zn is relatively chemically stable (co-precipitated or sorbed to ferrihydrite), with a relatively-small proportion (16 to 21%) of the Zn being relatively labile (*i.e.*, weakly complexed outer sphere complexes).

4.1.3 Britannia Mine

Britannia Mine ARD influent sample is dominated on a molar basis by SO₄>Ca>Mg>>Al>Cl (Table 3-1, Appendix A-3), with Zn (~18 mg/L) and Cu (~18 mg/L) being the dominant trace elements of concern in ARD. Through the HDS process, pH increases from 4.0 to 7.5 and concentrations of Zn and Cu are reduced to <10 ppb. The composition of the clarifier outflow is dominated by SO₄, Ca and Mg. Sulfate shows a negligible change in concentration through the treatment circuit. Saturation indices indicate that the effluent solution is near equilibrium with respect to gypsum, undersaturated with respect to calcite and supersaturated with respect to goethite, ferrihydrite and gibbsite.

The Britannia HDS sample is composed primarily on a molar basis of Ca>Al>Mg>>Zn>Cu>S>Mn>Fe (Figure 3-4, Appendix B). The Cu content measured in the Britannia sludge represents the highest of all the nine sludge samples analyzed while the Fe concentration is the lowest. Zinc and Cu are associated with a Cu-Zn oxyhydroxide that forms fine-grained fibrous aggregates (<35 μm) which include significant but variable concentrations of Mg, Al and Si. STEM spectra show variable metal content in the Cu-Zn oxyhydroxide, indicating significant heterogeneity. The results of SAED analysis indicate that the Cu-Zn-oxyhydroxide phase is mostly amorphous. As per the Equity HDS, the XANES data offer limited application owing to a lack of suitable model compounds analogous to the phases present in the Britannia HDS. However, the Zn K-edge XANES spectrum indicates that a significant proportion (>70%) of the Zn is in a labile form, perhaps as outer sphere complexes. The remaining Zn is likely much less labile, as suggested by XANES fits for more structurally stable complexes.

4.1.4 Brunswick Mine

The Brunswick Mine ARD influent samples are dominated on a molar basis by Na>SO₄>Mg>Ca=Cl>Zn (Table 3-1, Appendix A-4). Zn (~70 mg/L) represents the dominant trace element of concern in ARD feed waters. Through the HDS process, most trace elements are reduced to values below the limits of analytical detection. Sulfate, Na, Ca, and Mg represented the main solutes in the clarifier outflow with concentrations of SO₄, Mg, and Ca not appreciably affected by the process. Solubility calculations indicate that the effluent solution is undersaturated with respect to gypsum and supersaturated with respect to calcite, goethite, ferrihydrite and gibbsite.

The Brunswick HDS sample is composed primarily on a molar basis of Ca>Fe>Zn>>Mn>S>Mg>Na (Figure 3-4, Appendix B). Phases identified by high-resolution microscopy include calcite (also supported by XRD) and a Fe-Mn-Zn-rich oxyhydroxide phase. STEM elemental maps show that Zn is dominantly associated with the Fe-Mn-Zn oxyhydroxide phase. The Fe-Mn-Zn oxyhydroxide forms fine-grained fibrous aggregates (<15 μm) and is heterogeneous in its elemental proportions. The results of SAED analysis indicate that the Fe-Mn-Zn oxyhydroxide is amorphous or nanocrystalline. The Zn K-edge XANES spectrum obtained for the Brunswick HDS sample indicates that <44% of the Zn is potentially labile. The remainder is likely much less labile as a ferrihydrite co-precipitate, with perhaps a minor (12 to 13%) proportion of Zn structurally incorporated into other less labile phases.

4.1.5 Chisel North Mine

The Chisel North Mine ARD samples are dominated on a molar basis by Cl>Na>Ca>SO₄>Mg >Zn (Table 3-1, Appendix A-5). Zn (~65 mg/L) represents the dominant trace element of concern in ARD feed waters. Through the treatment process, the pH of the influent water increased from ~4.8 to 7.4 and concentrations of Zn are reduced to 0.3 mg/L. Dominant solutes in the clarifier outflow include SO₄, Ca, Mg, and Na, all of which show negligible changes in concentration through the HDS process. Calculated saturation indices indicate that the effluent solution is near equilibrium with respect to gypsum and supersaturated with respect to goethite, ferrihydrite and gibbsite.

The Chisel North HDS sample is composed primarily of Ca>Zn>Fe>>Mg>S>Mn on a molar basis (Figure 3-4, Appendix B). Phases identified by SEM include calcite (also supported by XRD) and a trace metal-bearing Fe-Mn-Zn oxyhydroxide phase that forms fine-grained fibrous aggregates (<10 μm). Elements consistently detected with the Fe-Mn-Zn oxyhydroxide include Mg, Si, S, Ca and trace amounts of Al, Cu and S. The results of SAED analysis indicate that the Fe-Mn-Zn oxyhydroxide is amorphous or nanocrystalline. Zn was repeatedly detected in calcite grains, even when Fe and Mn were

low, indicating that that some Zn carbonate is structurally incorporated into calcite. The Zn inventory hosted by calcite is inferred to be small in comparison to that hosted by the Fe-Mn-Zn oxyhydroxide. The Zn K-edge XANES spectrum obtained from the Chisel North HDS sample indicates that 64% of Zn is co-precipitated with ferrihydrite (less labile) while the remainder is present as labile, hydrated outer sphere complexes and will be more labile.

4.1.6 Samatosum Mine

The Samatosum Mine ARD influent sample is dominated on a molar basis by $\text{SO}_4 > \text{Mg} > \text{Ca} > \text{Fe} > \text{Zn}$ (Table 3-1, Appendix A-6). With respect to cations, the molar concentration of Mg is nearly twice that of Ca. Zn (~64 mg/L) represents the dominant trace element in ARD feed waters. Through the HDS treatment process pH increased from 2.9 to 8.8 and Zn decreased to near detection limit values. SO_4 , Ca and Mg dominate the composition of the clarifier outflow, with SO_4 concentrations showing a significant decrease through the treatment process (~4,100 mg/L to 2,900 mg/L). Solubility calculations indicate that the effluent solution is supersaturated with respect to gypsum, calcite, goethite and ferrihydrite.

The Samatosum HDS is composed primarily on a molar basis of $\text{Ca} > \text{Mg} > \text{Fe} > \text{S} > \text{Zn} > \text{Al}$ (Figure 3-4, Appendix B). Phases identified by high-resolution microscopy include calcite and gypsum (also supported by XRD), Al-silicate, relatively-pure Fe oxyhydroxide and a Zn-bearing Mg- and Fe-rich oxyhydroxide phase that forms fine-grained fibrous aggregates (<10 μm). The SAED results show that the Mg-Fe oxyhydroxide phase is amorphous or nanocrystalline. The Zn K-edge XANES spectrum obtained for the Samatosum HDS sample indicates a The XANES fit with Zn-kerolite and Zn co-precipitated with ferrihydrite suggests a significant portion of Zn is incorporated within more structurally (and chemically) stable complexes.

4.1.7 Sullivan Mine

The Sullivan Mine ARD influent samples are dominated on a molar basis by $\text{SO}_4 > \text{Mg} > \text{Ca} > \text{Fe} > \text{Na} = \text{Cl}$ (Table 3-1, Appendix A-7). With respect to cations, the Mg concentration is more than three times that of Ca. Zn (54 mg/L) represents the most abundant trace element of concern in the ARD feed. Through the HDS treatment process, the pH of the influent water increases from ~3.2 to 8.6 and Zn is reduced to <0.01 mg/L. Of the major cations, Al and Fe are removed completely while Mg is reduced in concentration by ~30%. SO_4 , Ca, and Mg dominate the composition of the clarifier outflow, with a minor reduction in sulfate concentration (~4100 to 3,700 mg/L). Calculated saturation indices indicate that the effluent is supersaturated with respect to gypsum, calcite, goethite, ferrihydrite and gibbsite.

The Sullivan HDS samples ('new' and 'old') are composed primarily on a molar basis of Mg>Ca>Fe>S>>Al>Zn>Mn (Figure 3-4, Appendix B). Phases identified in the HDS samples by SEM analysis include calcite, gypsum and a Zn-bearing Mg-Fe-oxyhydroxide that forms fine grained fibrous aggregates (<20 µm). The main difference observed for the two Sullivan HDS samples is the absence of gypsum in the 'old' sample. STEM analyses indicated that Al, Si, P, S, Cl, Ca, Mn and Cu are also consistently detected in the Mg-Fe oxyhydroxide phase of the 'new' and 'old' samples. The results of SAED analysis conducted on the 'new' sample indicate that the Zn-bearing Mg-Fe oxyhydroxide is amorphous or nanocrystalline. Similar to the Samatosum HDS sample, the fits with Zn-kerolite and Zn co-precipitated with ferrihydrite suggest that a sizeable proportion of the Zn may be structurally sequestered within less labile complexes.

4.2 Prediction of Sludge Type

The results of high-resolution microscopy on seven HDS samples have yielded five dominant trace metal-bearing phases (summarized in Table 4-1):

- 1) Mg-Al-(Fe) hydroxysulfate (Equity);
- 2) Fe oxyhydroxide (Geco);
- 3) Zn-Cu oxyhydroxide (Britannia);
- 4) Zn-Fe-Mn oxyhydroxide (Brunswick and Chisel North); and
- 5) Fe-Mg oxyhydroxide (Samatosum and Sullivan).

The results of the analyses also demonstrate that the nature of the trace-metal phase associations in neutralized sludge materials is strongly dependent on the raw ARD influent composition, and specifically, the molar concentrations of the major phase-forming elements (S, Al, Fe, Mg, Mn).

The dominance of Fe, Al and Mg in the Equity HDS, for example, is consistent with the high concentrations of these elements in the ARD influent (Figure 3-1). The Equity HDS is also the only example of a dominant trace metal-bearing hydroxysulfate phase. This agrees with the extremely high sulfate concentration in the ARD feed (~10,000 mg/L), and the marked reduction in sulfate concentration through the treatment process. In addition to gypsum, the pH-dependent solubility of sulfate at Equity is further governed through associations with Al and Mg with the formation of the Mg-Al-(Fe) hydroxysulfate. Al and Mg are also present in high concentrations in the Equity ARD influent compared to the other mines included in the study. Solubility constants for the Mg-Al-(Fe) hydroxysulfate phase have not been proposed, and therefore threshold values for SO₄, Mg and Al cannot be defined with regards to an ion-activity product. However, based on the results presented here, values for SO₄, Mg and Al must be sufficiently high

in the ARD feed to foster this solubility control. Mg is also a significant component of the Zn-bearing phases in the Samatosum and Sullivan (Fe-Mg oxyhydroxide) HDS samples, for which Mg concentrations in ARD were 405 and 641 mg/L, respectively (Figure 3-1). Like the Equity example, Mg shows a significant decrease in concentration between the influent and effluent samples at Samatosum and Sullivan (Figure 3-1). In contrast, Mg behaves conservatively at Geco, Britannia, Chisel North and Brunswick where Mg concentrations in ARD feed are considerably lower (64 to 188 mg/L; Figure 3-1). Such observations suggest the pH-dependent solubility of Mg is minimally influenced at these lower Mg concentrations.

The precipitation of Fe exhibits slightly more complex solubility controls. Fe is a significant component of the Zn-bearing sludge phase in six of the seven samples, precipitating with four different phases. Given the pH dependent solubility of ferric Fe, near complete removal of Fe is expected in all HDS systems. The Geco ARD exhibits the highest Fe concentrations (1,082 mg/L) and the Zn-bearing phase that forms in the neutralization process is a relatively pure Fe-oxyhydroxide. In this regard, the formation of a relatively pure Fe phase can be linked to the high concentration in the ARD feed, and relatively low levels of other ions (*e.g.*, Mg, Al), thereby minimizing competition from other competing metal phases (Aubé and Zinck, 1999). Although the Equity ARD exhibits comparable Fe content, competition by other phase-forming elements (*e.g.*, Al, Mg, and S) does not allow the formation of a pure Fe oxyhydroxide.

Fe is also relevant for the Samatosum, Sullivan, Chisel and Brunswick HDS samples, with ARD influent values ranging from 32 to 370 mg/L. Of the samples analyzed, only the Britannia HDS did not show appreciable Fe in the metal-bearing phase. This can be attributed to the very low Fe content (<0.6 mg/L) in the ARD feed at this site. In this regard, the predominance of a trace metal-bearing Cu-Zn oxyhydroxide at Britannia can be linked to the high concentrations of both Cu and Zn, in concert with the very low values for other phase-forming elements (S, Al, Fe, Mg, and Mn). Mn was also found to be a significant component in the trace metal-bearing phases for Brunswick and Chisel North (Fe-Mn-oxyhydroxide). In the case of Mn, the importance for the Brunswick and Chisel North sludge samples also appears to relate to the higher proportion of Mn in comparison to other phase-forming elements (*e.g.*, Al, Mg).

Overall, the results of this assessment highlight the potential for the development of a sludge management framework, which may permit prediction of “sludge type” from the ARD composition. This is highlighted in the ternary plots in Figure 4-1, which show the location of the various sludge phases as a function of the relative proportions of Mg-Fe-Al and Fe-Cu-Zn in the ARD influent. For most sludge types, including Fe-oxyhydroxide (Geco), Mg-Al(Fe) hydroxysulfate (Equity), Cu-oxyhydroxide (Britannia), and Zn-Fe-

Mn oxyhydroxide (Brunswick and Chisel North), the ARD influent composition occupies a distinct zone in one or both of the Mg-Fe-Al and Fe-Cu-Zn ternary plots. In contrast, the Mg-Fe oxyhydroxide (Samatosum and Sullivan) shows some degree of overlap with Mg-Al-(Fe) hydroxysulfate (Fe-Cu-Zn ternary) and Zn-Fe-Mn oxyhydroxide (Mg-Fe-Al ternary) (Figure 4-1).

If such a framework could be developed, it could be applied in the pre-mine development phase to identify the likely sludge-type to be generated should lime treatment be required in the future. This information could then be used to highlight potential environmental liabilities associated with sludge storage in various depositional environments (subaerial disposal in discrete impoundments, subaqueous disposal in pit lakes, co-disposal with tailings, *etc.*). In order to build a credible sludge management framework that would adequately characterize thresholds for precipitated phases in sludge, characterization of further sludge materials is required to assess both between-mine and within-mine variability. Furthermore, information regarding the chemical stability of sludge materials is required to link sludge type to metal solubility in varying depositional environments (subaerial storage, saturated storage, in-pi storage, *etc.*).

Currently, there is not sufficient information available from which to assess the chemical stability of the various trace metal-bearing phases identified in this study. Given the marked contrasts between sludge types, and the wide spectrum of metal-phase associations, the sludge materials would be expected to show varying degrees of chemical stability under a range of pH and pE conditions. In order for a potential framework to be applied successfully, sludge chemical stability as a function of varying pH and pE conditions must be established. This would require the collection of *in situ* porewaters for each sludge type, and possibly laboratory testwork to quantify pH- and pE-dependent solubility controls.

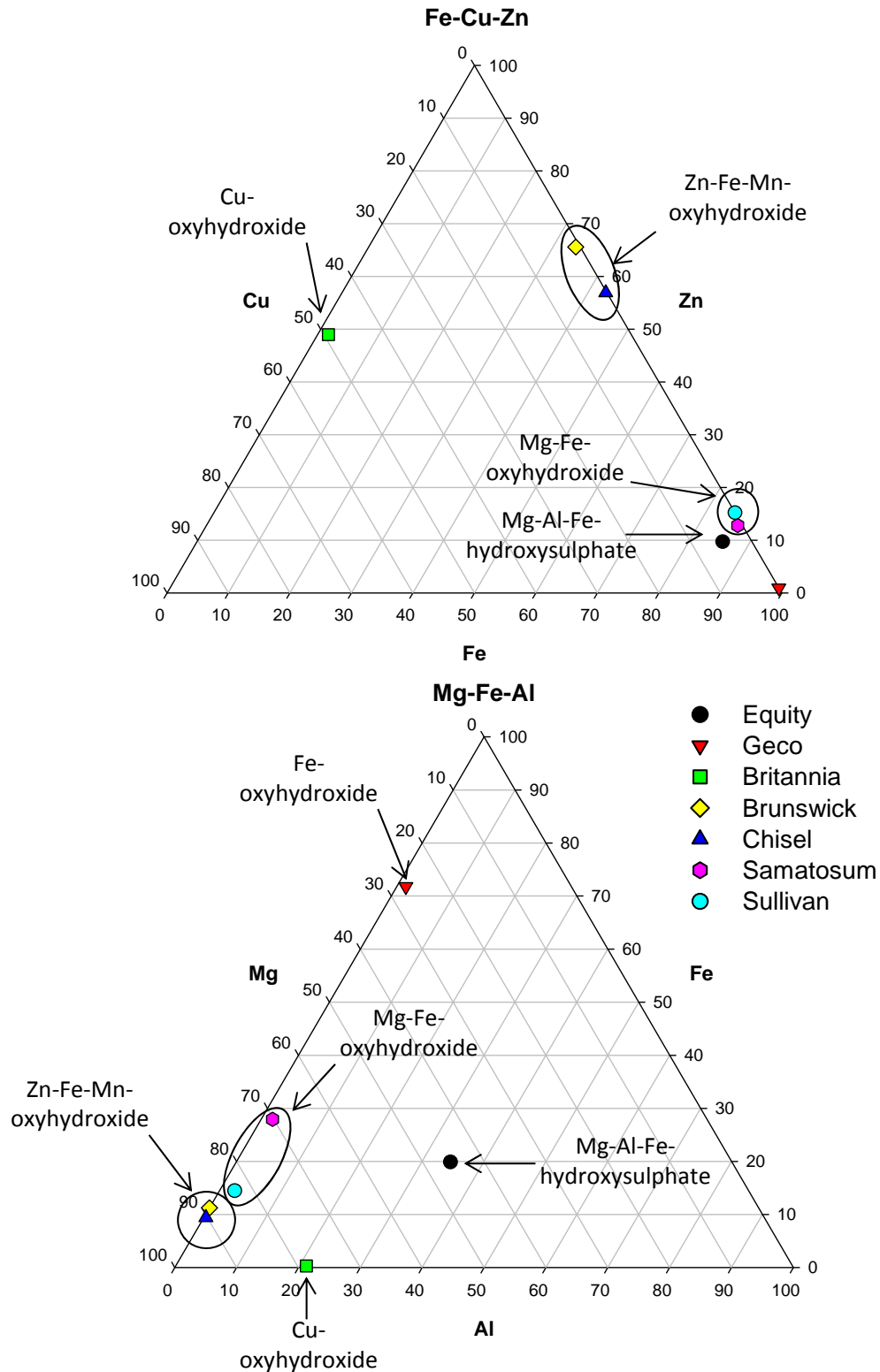


Figure 4-1: Ternary diagrams showing relative molar proportions of Fe-Cu-Zn (above) and Mg-Fe-Al (below) in ARD influent, and associated trace metal-bearing phases in sludge solids for each mine.

4.3 General Considerations for Sludge Chemical Stability

4.3.1 Overview

Treatment process parameters such as agitation rate, flocculant type and concentration, recycle rate (proportion of total flow comprised of recycled sludge), recycle ratio (ratio of mass of sludge recycled per mass produced), ratio of ferric to ferrous iron, and rate of neutralization have been shown to affect various physical properties of neutralization sludges including particle size, percent solids, bulk density, viscosity, and sludge settleability. Similarly, such process variables have been shown to influence chemical stability in terms of both degree of crystallinity and metal leachability (MEND, 1997; 1999; Aubé and Zinck, 1999).

Studies that have assessed the chemical stability of neutralization sludges have primarily examined the pH-dependent solubility of synthetic ARD and acidic drainages from existing mine sites (MEND, 1997; MEND, 1999; McDonald *et al.*, 2006). An important factor governing the chemical stability of neutralization sludges is the neutralization potential (NP) of the final sludge product. Higher NP translates to a greater capacity to neutralize acidic inputs, thus delaying the onset of pH shifts that will result in metal remobilization. Final NP is influenced by the amount, type and efficiency of the reagent through the treatment system. HDS systems that have tight control over flow and pH and can ensure more complete consumption of unreacted lime through sludge recycling are more likely to produce sludges with lower NP (Aubé and Payant, 1997; McDonald *et al.*, 2006).

In contrast, relatively few studies have assessed the redox-dependent solubility of sludges. In repositories that facilitate permanent submergence of sludge materials, suboxic redox conditions, as defined by the onset of Fe(III) reduction, are predicted to form in sludge porewaters shortly after deposition. Similarly, given the fine-grained nature of sludge materials and their tendency to maintain saturation post-deposition, suboxic redox conditions are also predicted to develop in materials deposited subaerially in regions of positive water balance. Given that the composition of many sludges is dominated by phases sensitive to dissolution under conditions of low redox potential (*e.g.*, Fe(III) oxyhydroxides and hydroxysulfates), understanding the redox-dependent solubility of sludge materials is important for the assessment of long-term chemical stability. Field studies that have examined the chemical stability of redox-sensitive Fe-phases (roaster tailings and autoclave products) have shown that such materials are unstable in the suboxic environments typical to permanently saturated settings (McCreadie *et al.*, 1998; Martin and Pedersen, 2002). Sulfate reduction in anoxic porewaters has also been shown to promote under-saturation and dissolution of secondary sulfate minerals (*e.g.*, barite) produced through effluent treatment (Martin *et al.*, 2003).

Metals may be removed from solution through several pathways including precipitation as metal (oxy)hydroxides and co-precipitation/adsorption with hydrous ferric oxides (e.g., FeOOH), Mn-oxyhydroxides (MnOOH), Al hydroxides (Al(OH)₃), and other mixed Fe-Mg-Al-hydroxysulfates (Webster *et al.*, 1998; MEND, 2005; Loomer *et al.*, 2007a; Loomer *et al.*, 2007b). Metal (oxy)hydroxide solubility is highly metal specific. The solubility of ferric hydroxide, for example, is greatly decreased at pH > 5, while other metals such as Zn and Cu require pH ≥ 9 for their respective hydroxides to precipitate (Figure 4-2).

Even for sludges dominated by relatively pure “Fe-oxides”, behaviour cannot be predicted based on simple stoichiometric chemistry of source waters and thermodynamic data. Although the degree of trace metal adsorption onto pure amorphous hydrous Fe(III) oxides has been rigorously examined (Davis and Leckie, 1978; Benjamin and Leckie, 1981), Fe oxides derived from the neutralization of acidic drainages are shown in this study to be poorly crystalline or amorphous, and likely exhibit considerable variability due to the incorporation of structural and adsorbed impurities within the Fe-oxide matrix (Bigham *et al.*, 1990).

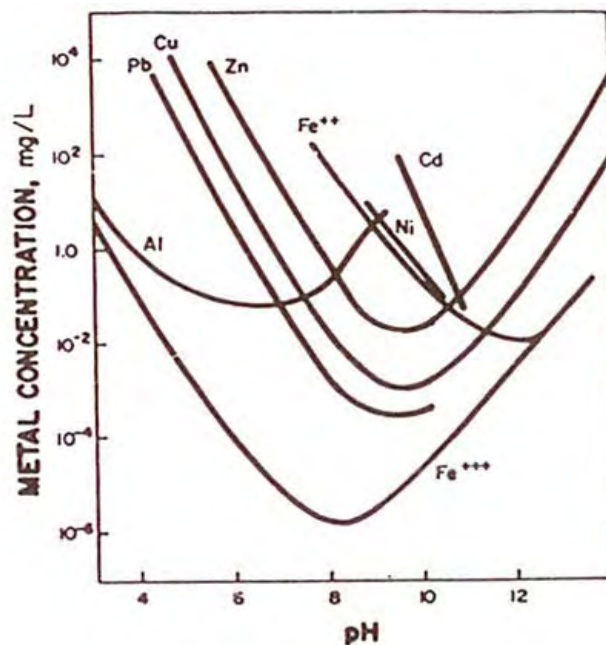


Figure 4-2: Solubility of various metal hydroxides (from Vachon *et al.*, 1987).

Both field and laboratory studies demonstrate that the degree of metal mobility from sludge can decrease with aging; however, the method of disposal will ultimately affect the long-term stability of sludge (MEND, 2005). Factors that affect the geochemical stability of sludges include major element chemistry, pH, redox, complexation, liquid-to-solid ratio, contact time, available alkalinity, biological activity, permeability and water movement.

In the following sections, considerations relevant to the chemical stability of the different sludge types are discussed, and makes reference to the particular depositional environment of each sludge.

4.3.2 Equity Mine (Open Pit Lake)

Of all the sites examined as part of this study, only data for the Equity Mine were available from which to assess *in situ* chemical stability of neutralization sludges. As mentioned in Chapter 2, neutralization sludges produced at Equity Mine are discharged to the neutral-pH surface waters of the Main Zone pit lake. The Main Zone pit lake is ~400 m by 800 m and has a maximum water depth of ~120 m. The discharge of sludge has a pronounced effect of the physical limnology of the Main Zone pit. Specifically, the input of dense oxygen-rich effluents and their rapid sinking act to mix the lake water column and sustain oxygenated bottom waters throughout the year (Figure 4-3). The sludge discharge manifests as a plume of metal-rich particulate matter. This plume, which is revealed by reduced light transmission, is evident from depths extending from ~70 m to the pit bottom (~120 m) (Figure 4-3). The metal-rich sludge inputs are also manifested as elevated levels of total metals (*e.g.*, Zn, Cu, Cd and As) in the pit bottom waters.

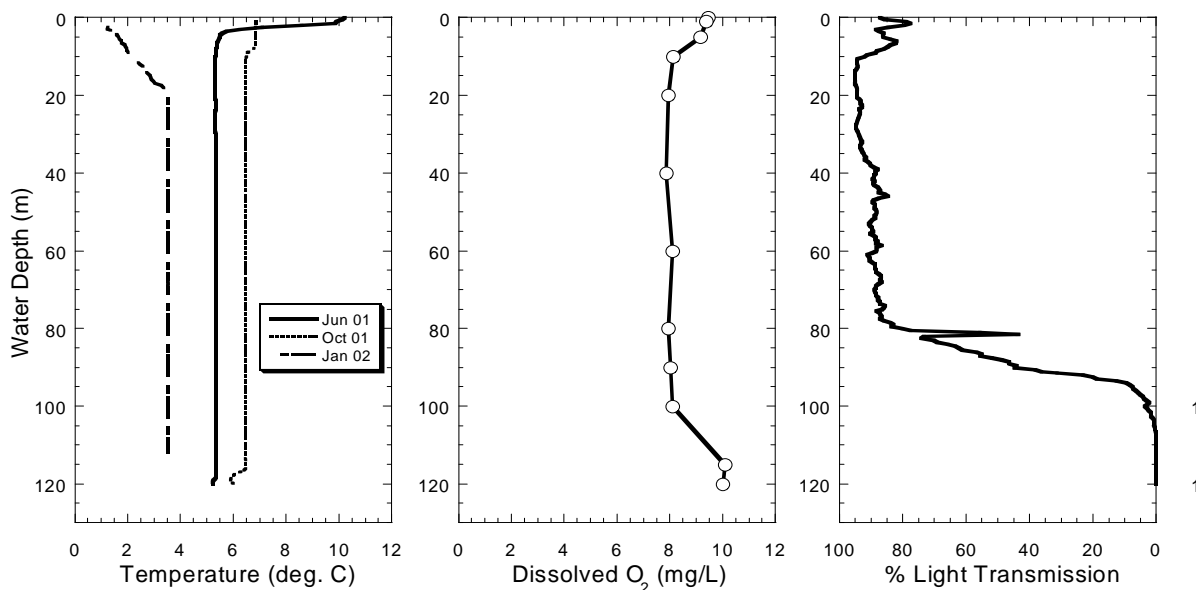


Figure 4-3: Depth distributions of temperature, dissolved oxygen and % light transmission in the Main Zone Pit (June 2001). Temperature profiles for October 2001 and January 2002 are also presented (from McNee *et al.*, 2003).

Despite extremely high concentrations of particulate sludge-derived metals, there is no indication of dissolved metal enrichment in the deep waters of the Main Zone pit. In fact, sludge inputs do not appear to result in increases in dissolved metal levels either in the surface waters or in deep waters.

The data for the Equity Mine demonstrate that the primary trace element bearing phase (Al-Mg-(Fe) hydroxysulfate) is chemically stable in the neutral-pH water column of the Main Zone pit. Such observations demonstrate the importance of site-specific *in situ* evidence to support predictions of sludge chemical stability. In the long term, the chemical stability of the Equity sludge materials will be governed by their behaviour under conditions of low redox potential. Specifically, suboxia is predicted to develop within the sludge deposits that accumulate in the pit bottom. The potential for sludge instability cannot be ascertained with certainty without direct *in situ* measurements of sludge porewaters. However, given that the main trace metal-bearing phase is predicted to host relatively little Fe-hydroxide, these materials will be less susceptible to reductive dissolution processes.

4.3.3 Geco, Brunswick and Samatosum Mines (Subaerial Sludge Cells)

Sludges produced from the Geco, Brunswick and Samatosum HDS processes are currently stored subaerially in sludge cells. Those at Geco and Brunswick mines are located within their respective tailings facilities, while Samatosum employs a separate sludge storage area. In general, sludges deposited without a water cover display a greater degree of densification due to surface evaporation and freeze-thaw effects (Aubé and Zinck, 1999). The degree of densification observed with aging will vary from site to site; however, it was observed for the Geco sludge that after only one year on the dry tailings beach, sludge density increased to 60% solids.

The HDS process at Geco results in extremely efficient use of lime, resulting in a lower final neutralization potential. While this consideration implies enhanced efficiency, it also suggests that these materials are less buffered with respect to acidic inputs (*e.g.*, meteoric water). Although there is no direct information available with regards to the chemical stability of Geco sludge materials, inferences can be made based on information sources provided in this report. As discussed, trace elements (Zn and Cu) in the Geco sludge are predominantly associated with Fe-oxyhydroxide and that this phase is essentially pure with only minor amounts of other constituents (Mg, Al and SO₄). Some degree of crystallinity, as indicated by SAED signatures for ferrihydrite and lepidocrocite, was evident. Crystalline Fe-(oxy)hydroxides are far less susceptible to reductive dissolution in comparison to their amorphous counterparts, and therefore the presence of crystalline compounds may reduce the rate of Fe(III) reduction and

concomitant metal leaching. Analysis of porewater chemistry or proxies (*e.g.*, seepage chemistry) would be required to directly assess the nature of *in situ* chemical stability at the Geco site.

At the Brunswick mine, sludge has also been used as a cover for the closed tailings basin. Covering tailings with sludge may help reduce sulfide oxidation by providing a barrier similar to that of an engineered soil cover (Aubé and Zinck, 1999); however, given the predicted pH-sensitivity of the sludge materials, there is the potential for the sludge materials to re-dissolve through exposure to acidic meteoric waters or acidic tailings drainages if they develop in the future.

At the Samatosum Mine, detailed mineralogical characterization of the HDS demonstrates that the metals of concern (*e.g.*, Zn) are hosted primarily in a Mg- and Fe-rich oxyhydroxide phase. Based on the abundance of trace metal-bearing Fe oxyhydroxides, and its amorphous nature, the chemical stability of the sludge is predicted to be strongly sensitive to redox conditions. Specifically, enhanced chemical instability would be expected under suboxic conditions which promote the reductive dissolution of the Fe oxyhydroxide phases. In this regard, suboxia is most likely to develop in areas of the pile showing permanent or seasonal saturation in pore spaces. In turn, the potential for water saturation within the pile will be strongly dependent on scale, with larger piles showing a greater tendency towards the maintenance of wetted pore spaces. In this regard, the dry climate conditions at the Samatosum site favour the chemical stability of the sludge solids through enhancement of unsaturated (aerobic) conditions.

4.3.4 Britannia and Sullivan Mines (Holding Ponds)

Sludges produced from the Britannia and Sullivan HDS processes are currently stored in holding ponds. In general, sludges deposited without a water cover display a greater degree of densification due to surface evaporation and freeze-thaw effects (Aubé and Zinck, 1999). Pond disposal eventually results in the lowest volume of sludge generated, particularly when the pond is designed to drain water from the base. Under optimal conditions, sludge deposited in a holding pond can densify to two or three times the original solid content. This sort of densification has been observed for the 'old' Sullivan HDS sample, which has been stored in an exfiltration pond for at least 10 years.

Although there is no direct information available with regards to the chemical stability of sludges from the Britannia and Sullivan mines, inferences can be made based on the results of the investigations discussed herein and review of the literature. In general, sludge porewaters can sustain alkaline pH values for decades due to excess alkalinity associated with the sludge solids (MEND, 2005). Such features can minimize the potential for pH-controlled dissolution effects. However, reducing conditions that

develop in these environments also favour the reduction and solubilization of Fe(III) to Fe(II), leading to the mobilization of metals associated with the secondary Fe-phase. The relevance of this process cannot be assessed without direct measures of sludge porewater composition.

With regards to the Sullivan Mines sludge, Zn is primarily associated with an amorphous Fe-Mg oxyhydroxide. Under the reducing conditions that can develop in a holding pond (even without a water cover), this amorphous phase may be more susceptible to reductive dissolution and release of Zn, particularly if neutral conditions are not maintained.

The primary trace metal-bearing phase at the Britannia Mine is an amorphous Cu-Zn (Mg) oxyhydroxide, which is likely to be stable as long as alkaline conditions are maintained ($\text{pH} > 8$). Some degree of chemical instability can be expected if more circum-neutral pH conditions develop due to the pH-dependent solubility controls on Cu-Zn oxyhydroxides. Given the dearth of reducible Fe phases in the Britannia sludge, redox-controlled solubility effects are predicted to be less relevant.

4.3.5 Chisel North Mine (Underground Submerged Storage)

At the Chisel North Mine, the neutralization sludges are deposited subaqueously in the decommissioned underground mine workings. The deposition of sludge in mined out stopes was previously considered to be a less suitable option for long-term environmental management. However, studies conducted at a coal mine site have shown that this disposal method can have a positive impact on mine water quality (Aubé, 2005; MEND, 2005). Specifically, results of the studies suggest that sludge returned to the underground workings may actually reduce the lime required to treat the acidic mine water due to residual alkalinity in the sludge.

As with any subaqueous environment, there is the potential for chemical instability of trace metals associated with reducible Fe/Mn oxyhydroxides, such as those present in the HDS sludge. The potential for this occurrence at Chisel North Mine has not been examined. An assessment of the sludge porewater composition for materials stored in the underground workings at the Chisel North site would be required to provide direct evidence as to the relevance of reductive dissolution processes.

4.4 Recommendations for Future Work

Neutralization sludges are precipitated in oxidizing conditions at high pH (typically pH 8 to 10) to mitigate acidity and remove metals from solution. Once formed, sludge materials may be stored in engineered impoundments or discharged to pit lakes/underground workings in permanently saturated or submerged settings. In these

environments, geochemical conditions with respect to both pH and pE (redox potential) may differ markedly from the conditions of sludge formation. With regards to redox potential, suboxic conditions (as defined by onset to Fe(III) reduction) are predicted to develop within permanently saturated or submerged sludge deposits. Given that the compositions of many sludges are dominated by phases sensitive to dissolution under conditions of low pE (e.g., Fe-Mn oxyhydroxides and hydroxysulfates), understanding the redox-dependent solubility of sludge materials is important for the assessment of long-term chemical stability. Overall, pH and redox controls on sludge behaviour are currently poorly understood.

The reported data for this study increase our understanding of sludge phases, the variability in sludge types, and design requirements and issues of concern in sludge management. However, additional sludge sampling and characterization are needed to gain a better sense of both inter- and intra-mine variability before a model can be developed that predicts sludge types for a given ARD drainage chemistry. Furthermore, an understanding of the link between sludge type and metal mobility under varying depositional environments and management systems is needed to support such a model. Given the site-specific nature of sludge materials, their heterogeneous composition, and largely amorphous nature of the primary trace-element bearing phases, current geochemical model databases cannot be used to provide reliable solubility predictions for these materials under varying pH and redox conditions. Therefore, site-specific studies designed to assess the *in situ* chemical stability of sludge materials must be considered as the most defensible approach to understanding metal leaching behaviour and long-term geochemical stability. In this regard, the assessment of sludge chemical stability would be best assessed via direct measurements of porewater chemistry (piezometers) or suitable proxies (e.g., seepage chemistry immediately downgradient of storage facility). Laboratory studies designed to assess pH- and pE-dependent solubility controls on metal behaviour in sludge materials would also be required to properly constrain metal mobility. Currently, such data are not available for the materials assessed as part of this study.

5. Conclusions

The main conclusions from the analysis are provided below:

- High resolution microscopy techniques (SEM and STEM) were shown to provide an effective means to resolve trace-metal associations in fine-grained and amorphous sludge matrices. With respect to XANES, there is a general absence of suitable model compounds analogous to many of the sludge phases identified in this study, and as a result, the applicability of XANES to discern metal-associations in sludge samples is currently limited;
- Crystalline materials identified by XRD include calcite or Mg-calcite (Britannia, Brunswick, Chisel, Samatosum and Sullivan Mines) and gypsum (Equity, Geco, Samatosum and Sullivan). However, none of these phases were shown to be dominant hosts for precipitated trace metals;
- Five dominant trace metal-bearing phases in the sludge solids were identified: 1) Mg-Al-(Fe) hydroxysulfate (Equity Mine); 2) Fe (oxy)hydroxide (Geco Mine); 3) Cu-Zn oxyhydroxide (Britannia Mine); 4) Zn-Fe-Mn oxyhydroxide (Brunswick and Chisel North mines); and 5) Fe-Mg oxyhydroxide (Samatosum and Sullivan mines). These phases ranged from relatively pure compounds to those characterized by a high degree of heterogeneity;
- For all HDS samples, SAED patterns revealed the presence of poorly crystalline to amorphous phases, while Zn K-edge x-ray absorption near-edge structure (XANES) spectra revealed a mixture of labile (outer-sphere complexes) and less labile (structurally incorporated) Zn species;
- The nature of the trace metal-bearing phases is primarily governed by the composition of the ARD influent solution, with both the concentration and relative proportions of S, Fe, Al, Mg, and Mn being the most relevant. Similarly, elemental abundances in sludge materials can be linked to ARD influent chemistry;
- The link between ARD composition and the nature of the trace metal-bearing phase as presented in this study highlights the potential for the development of a sludge management framework, which may permit prediction of “sludge type” from ARD chemistry. Such a framework could be applied in the pre-mine development phase to highlight potential environmental liabilities associated with sludge storage in various depositional environments. Currently, there is not enough data to support the development of such a model;

- Given the marked contrasts in sludge types, and the wide spectrum of metal-phase associations, the sludge materials would be expected to show varying degrees of chemical stability under various pH and pE conditions; and
- Currently, there is insufficient information from which to assess the chemical stability of the various trace metal-bearing phases identified in this study. This would require the collection of *in situ* porewaters for each sludge type, and laboratory studies designed to assess pH- and pE-dependent solubility controls.

References

- Aubé, B. and Payant, S.C. (1997). The Geco Process: A New High Density Sludge Treatment for Acid Mine Drainage. Proceedings of the Fourth International Conference on Acid Rock Drainage. May 30–June 6, 1997, Vancouver, BC Vol. I:165–180.
- Aubé B. and Zinck J.M. (2003). Lime Treatment of Acid Mine Drainage in Canada; Presented and published at “Brazil-Canada Seminar on Mine Rehabilitation”, Florianópolis, Brazil, December 1-3, 2003.
- Aubé B. and Zinck J.M. (1999). Comparison of AMD Treatment Processes and Their Impact on Sludge Characteristics. In: Goldsack D, Belzile N, Yearwood P, Hall G (eds) Sudbury '99, Mining and the Environment II., Sudbury, ON, Canada September 13-17, 1999, pp 261-270.
- Aubé, B. (2005). The Science of Treating Acid Mine Drainage and Smelter Effluents. Viewed January 7, 2013, <http://www.infomine.com/library/publications/docs/Aube.pdf>
- Bailey, S.L., Paradis, S. and Johnson, S.T. (2000). Geological Setting of the Samatsum and Rea Massive-Sulphide Deposits, Eagle Bay Assemblage, South Central British Columbia. Current Research 2000-A15. Prepared for the Geological Survey of Canada, Project 990002.
- Benjamin, M.M. and Leckie, J.O. (1981). Competitive Adsorption of Cd, Cu, Zn and Pb on Amorphous Iron Oxyhydroxide. *J. Colloid. Inter. Sci.*, 83:410-419.
- Bigham, J.M., Schwertmann, U., Carlson, I. and Murad, E. (1990). A Poorly Crystallized Oxyhydroxysulfate Formed by Bacterial Oxidation of Fe(II) in Acid Mine Waters. *Geochim. Cosmochim. Acta*, 54:2743-2758.
- Britannia Mine Museum (2012), Education Resources. Retrieved May 16, 2013 from <http://britanniamuseum.ca/education/index.html>
- Church, B.N. and Barasko, J.J. (1990). Geology, Lithogeochemistry, and Mineralization in the Buck Creek Area, British Columbia. Mineral Resources Division, Geological Survey Branch, British Columbia Ministry of Energy, Mines, and Petroleum Resources.
- Davis, J.A. and Leckie, J.O. (1978). Surface Ionization and Complexation at the Oxide/Water Interface. II. Surface Properties of Amorphous Iron Oxyhydroxide and Adsorption of Metal Ions. *J. Colloid Inter. Sci.* 67:90-107.
- EPCOR (2005). Britannia Mines Water Treatment Plant – Operations & Maintenance Manual. Prepared by EPCOR Water Services, August 2005.

- Gagne, S., Beaumont-Smith, C.J., Williams-Jones, A.E. and Hynes, A. (2007). Investigation of a Pb-Ag-Au-rich Hangingwall in Lens 4 of the Chisel North mine, Snow Lake, Manitoba (NTS 63K16). In: Report of Activities 2007, Manitoba Science, Technology, Energy and Mines, Manitoba Geological Survey, pp 43–50.
- Gault, A.G. and Jamieson, H.E. (2012). Analysis of Zn K-edge XANES Spectra Collected from Mine Neutralization Sludges. Prepared for Lorax Environmental Services Ltd. June 19, 2012.
- HBMS (2010). Geology and History of the Chisel North Mine, Personal Communication with Hudson Bay Mining and Smelting Co. Limited, 2010.
- Inmet (2010). Samatosum Mine Water Treatment Plant details, Personal Communication with Inmet Mining Corporation, 2010.
- Jamieson, H.E., Shaw, S.C. and Clark, A.H. (1995). Mineralogical Factors Controlling Metal Release From Tailings at Geco, Manitouwadge, Ontario. In: Sudbury '95, Conference on Mining and the Environment, Sudbury, Ontario, May 28 – June 1, 1995.
- Loomer, D.B. (2010) Microscopical Characterization of Mine Waste Sludge Samples Prepared for Skya Fawcett and Alan Martin, Lorax Environmental Ltd., December 2010.
- Loomer, D.B., Flather, D.H. and Al, T.A. (2007a). Determination of Trace-Element Associations in Neutralization Sludges Using High Resolution Microscopy: Implications for the Chemical Stability of Sludge. In: Mine Closure 2007 Conference Proceedings. A. Fourie, M. Tibbett and J. Wiertz (Eds). Santiago, Chile, October 16-19, 2007, pp 829-838.
- Loomer, D.B., McNee, J.J. and Al, T.A. (2007b). Using Scanning Electron Microscopy and Transmission Electron Microscopy to Determine Trace Metal Associations in Neutralization Sludges: Applications for Chemical Stability Assessments. In: Proceedings from the Mining and the Environment IV Conference, Sudbury, Ontario, Canada, October 19-27, 2007.
- Lorax (2009). Solid Phase Characterization of ARD Neutralization Sludges. Prepared for The Mine Neutral Drainage Program (MEND) and The Mining Association of Canada. Prepared by Lorax Environmental Services Ltd., December 2009.
- Martin, A.J. and Pedersen, T.F. (2002). Seasonal and Interannual Mobility of Arsenic in a Lake Impacted by Metal-Mining. *Environ. Sci. Tech.*, 36:1516-1523.
- Martin, A.J., Crusius, J., McNee, J.J. and Yanful, E.K. (2003). The Mobility of Radium-226 and Trace Metals in Pre-oxidized Subaqueous Uranium Mill Tailings. *Appl. Geochem.*, 18:1095-1110.

- Martin A.J., Fawcett S., Kulczycki E., Loomer D., Al T., Rollo A. (2011) Application of High-Resolution Microscopy Methods to the Analysis of Fine-Grained and Amorphous Treatment Sludges, Proceedings Tailings and Mine Waste 2011, Vancouver, Canada, November 7-9, 2011.
- Martin A.J., Loomer D., Fawcett S., Kulczycki E., Rollo A., Al T. (2012) Characterization of ARD Neutralization Sludges: Effect of ARD Influent Chemistry and Treatment Process on Sludge Composition. 9th International Conference on Acid Rock Drainage, Ottawa, Canada, May 20-26, 2012.
- McCreadie, H., Jambor, J.L., Blowes, D.W., Ptacek, C. and Hiller, D. (1998). Geochemical Behaviour of Autoclave-Produced Ferric Arsenates and Jarosite in a Gold-Mine Tailings Impoundment. Waste Characterization and Treatment (W. Petruk, ed.). Proceedings SME Ann. Meet., pp 61-78.
- McDonald, D.M., Webb J.A. and Taylor, J. (2006). Chemical Stability of Acid Rock Drainage Treatment Sludge and Implications for Sludge Management. Environ. Sci. Tech. 40:1984-1990.
- McNee, J. J., Crusius, J., Martin, A. J., Whittle, P., Pieters, R. and Pedersen, T. F. (2003). The Physical, Chemical and Biological Dynamics of Two Contrasting Pit Lakes: Implications for Pit Lake Bio-Remediation. In: Sudbury 2003, Mining and the Environment III. May 25-28, 2003.
- MEND (2005). Review of Disposal, Reprocessing and Reuse Options for Acidic Drainage Treatment Sludge. Prepared for the Mine Environment Neutral Drainage (MEND) program. Prepared by J. Zinck, Natural Resources Canada. MEND Report 3.42.3 (January 2005). Viewed January 07, 2012, <http://www.mend-nedem.org/reports/files/files/3.42.3.pdf>
- MEND (1999). The Effect of Process Parameters and Aging on Lime Sludge Density and Stability. Prepared for the Mine Environment Neutral Drainage (MEND) Program. Prepared by Zinck, J.M., Hogan, C.M., Griffith, W.F. and Laflamme, G. Natural Resources Canada. MEND Report 3.42.2b. February, 1999. Viewed January 7, 2013, <http://www.mend-nedem.org/reports/files/3.42.2b.pdf>
- MEND (1997). Characterization and Stability of Acid Mine Drainage Treatment Sludges. Prepared for the Mine Environment Neutral Drainage (MEND) Program. Prepared by Zinck, J.M., Wilson, L.J., Chen, T.T., Griffith, W., Mikhail, S., and Turcotte, A.M. Natural Resources Canada. MEND Report 3.42.2a. May 1997. Viewed January 7, 2013 at: <http://www.mend-nedem.org/reports/files/3.42.2a.pdf>
- MEND (1994). Acid Mine Drainage - Status of Chemical Treatment and Sludge Management Practices. Prepared for the Mine Environment Neutral Drainage (MEND) Program and the Canadian Centre for Mineral and Energy Technology (CANMET). Prepared by SENES Consultants Ltd. MEND Project 3.32.1. June 1994.

- MINFILE (2009). Equity Silver Mine No. 093L 001. BC Ministry of Energy. Last edited by Gloria Robinson, March 28, 2009. Viewed January 7, 2013, <http://minfile.gov.bc.ca/Summary.aspx?minfilno=093L++001>
- Parkhurst, D.L. and Appelo, C.A.J. (1999). User's Guide to PHREEQC (Version 2) - A Computer Program for Speciation, Batch-Reaction, One-Dimensional Transport, and Inverse Geochemical Calculations. U.S. Geological Survey, Denver, Colorado, p 312.
- Petersen, E.U. (1986). Tin in Volcanogenic Massive Sulphide Deposits: An Example from the Geco Mine, Manitouwadge District, Ontario, Canada. *Economic Geology*, 81:323-342.
- Price, W.A., Schwab, T. and N. Hutt (1995) A Reconnaissance Study of Acid Mine Drainage at the Britannia Mine. Prepared for the British Columbia Ministry of Energy, Mines and Petroleum Resources, March 1995.
- SNC-Lavalin (2004). Willroy-Geco Integrated Water Management Project: Geco WTP and Willroy Water Management Basic Engineering Report. Prepared by SNC-Lavalin for Noranda Inc. – Geco Division, September 2004.
- Taylor, B.E. (2003). Biogenic and Thermogenic Sulfate Reduction in the Sullivan Pb–Zn–Ag Deposit, British Columbia (Canada): Evidence From Micro-Isotopic Analysis of Carbonate and Sulfide in Bedded Ores, *Chemical Geology* 204:215–236.
- Teck (2010). Details regarding the Sullivan Mine Water Treatment Plant, Personal Communication Teck Cominco, October 26, 2010.
- Vachon, D., Siwik, R.S., Schmidt, J., and Wheeland, K. (1987). Treatment of Acid Mine Water and the Disposal of Lime Neutralization Sludge. *Proceedings of Acid Mine Drainage Seminar/Workshop*, Halifax, Nova Scotia, March 23-26, Environment Canada, pp 537-564.
- Webb, S.M. (2005). Sixpack: A Graphical User Interface for XAS Analysis Using IFEFFIT. *Phys. Scripta*, 115:1011-1014.
- Webster, J.G., Swedlund, P.J. and Webster, K.S. (1998). Trace Metal Adsorption onto an Acid Drainage Iron(III) Oxy Hydroxy Sulfate. *Environ. Sci. Tech.* 32:1361-1368.
- Xstrata (2010). Geology and Mineralization of the Brunswick Mine, Personal Communication with Xstrata Zinc Canada, 2010.

Appendices

Appendix A-1 Influent and Effluent Water Chemistry for Equity HDS Process

Equity Silver Mine	Units	Influent (ARD Feed)			Effluent (Clarifier Outflow)			Difference %		Units	Influent (ARD Feed)			Effluent (Clarifier Outflow)		
		06-May-08	07-May-08	08-May-08	06-May-08	07-May-08	08-May-08	Influent	Effluent		06-May-08	07-May-08	08-May-08	06-May-08	07-May-08	08-May-08
Physical Tests																
Conductivity	uS/cm	10300	10010	9540	ND	4960	5180	7.66	4.34	uS/cm	10300	10000	9540	ND	4960	5180
Hardness (as CaCO ₃)	mg/L	ND	ND	ND	ND	ND	ND	NA	NA	mmol/L	ND	ND	ND	ND	ND	ND
pH		2.65	2.65	2.64	7.14	6.95	7.02	0.378	2.70		2.65	2.65	2.64	7.14	6.95	7.02
Anions and Nutrients																
Acidity (as CaCO ₃)	mg/L	8450	7950	8070	ND	ND	ND	6.10	NA	mmol/L	84.4	79.4	80.6	ND	ND	ND
Alkalinity (as CaCO ₃)	mg/L	ND	ND	ND	20.2	20.7	20.0	NA	3.44	mmol/L	ND	ND	ND	0.202	0.207	0.200
Bromide (Br)	mg/L	25.0	25.0	25.0	2.50	2.50	2.50	0.000	0.000	mmol/L	0.313	0.313	0.313	0.0313	0.0313	0.0313
Chloride (Cl)	mg/L	250	250	250	25.0	25.0	25.0	0.000	0.000	mmol/L	7.05	7.05	7.05	0.705	0.705	0.705
Fluoride (F)	mg/L	48.0	64.0	62.0	7.00	3.00	6.20	28.6	80.0	mmol/L	2.53	3.37	3.26	0.368	0.158	0.326
Nitrate (as N)	mg/L	2.50	2.50	2.50	0.610	0.630	0.540	0.000	15.4	mmol/L	0.178	0.178	0.178	0.0436	0.0450	0.0386
Nitrite (as N)	mg/L	0.870	0.850	0.500	0.0620	0.0500	0.0500	54.0	21.4	mmol/L	0.0621	0.0607	0.0357	0.00443	0.00357	0.00357
Sulfate (SO ₄)	mg/L	10900	9430	9300	2840	2980	2650	15.8	11.7	mmol/L	113	98.2	96.8	29.6	31.0	27.6
Dissolved Metals																
Aluminum (Al)-Dissolved	mg/L	815	775	737	0.400	0.400	0.400	10.1	0.000	mmol/L	30.2	28.7	27.3	0.0148	0.0148	0.0148
Antimony (Sb)-Dissolved	mg/L	1.00	1.00	1.00	0.400	0.400	0.400	0.000	0.000	mmol/L	0.00821	0.00821	0.00821	0.00329	0.00329	0.00329
Arsenic (As)-Dissolved	mg/L	5.50	5.50	5.70	0.400	0.400	0.400	3.57	0.000	mmol/L	0.0734	0.0734	0.0761	0.00534	0.00534	0.00534
Barium (Ba)-Dissolved	mg/L	0.0500	0.0500	0.0500	0.0200	0.0200	0.0200	0.000	0.000	mmol/L	0.000364	0.000364	0.000364	0.000146	0.000146	0.000146
Beryllium (Be)-Dissolved	mg/L	0.103	0.0980	0.0910	0.0100	0.0100	0.0100	12.4	0.000	mmol/L	0.0114	0.0109	0.0101	0.00111	0.00111	0.00111
Bismuth (Bi)-Dissolved	mg/L	1.00	1.00	1.00	0.400	0.400	0.400	0.000	0.000	mmol/L	0.00479	0.00479	0.00479	0.00191	0.00191	0.00191
Boron (B)-Dissolved	mg/L	0.500	0.500	0.500	0.200	0.200	0.200	0.000	0.000	mmol/L	0.0462	0.0462	0.0462	0.0185	0.0185	0.0185
Cadmium (Cd)-Dissolved	mg/L	1.15	1.07	1.00	0.0200	0.0200	0.0200	14.0	0.000	mmol/L	0.0102	0.00952	0.00890	0.000178	0.000178	0.000178
Calcium (Ca)-Dissolved	mg/L	340	326	314	598	624	627	7.95	4.73	mmol/L	8.48	8.13	7.83	14.9	15.6	15.6
Chromium (Cr)-Dissolved	mg/L	0.246	0.233	0.244	0.0200	0.0200	0.0200	5.43	0.000	mmol/L	0.00473	0.00448	0.00469	0.000385	0.000385	0.000385
Cobalt (Co)-Dissolved	mg/L	3.84	3.67	3.53	0.0200	0.0200	0.0200	8.41	0.000	mmol/L	0.0652	0.0623	0.0599	0.000339	0.000339	0.000339
Copper (Cu)-Dissolved	mg/L	60.9	59.0	56.7	0.0200	0.0200	0.0200	7.14	0.000	mmol/L	0.958	0.928	0.892	0.000315	0.000315	0.000315
Iron (Fe)-Dissolved	mg/L	941	917	913	0.0600	0.0600	0.0600	3.02	0.000	mmol/L	16.9	16.4	16.3	0.00107	0.00107	0.00107
Lead (Pb)-Dissolved	mg/L	0.250	0.250	0.250	0.100	0.100	0.100	0.000	0.000	mmol/L	0.00121	0.00121	0.00121	0.000483	0.000483	0.000483
Lithium (Li)-Dissolved	mg/L	0.923	0.878	0.836	0.114	0.114	0.111	9.89	2.67	mmol/L	0.133	0.126	0.120	0.0164	0.0164	0.0160
Magnesium (Mg)-Dissolved	mg/L	975	920	862	397	381	356	12.3	10.9	mmol/L	40.1	37.9	35.5	16.3	15.7	14.6
Manganese (Mn)-Dissolved	mg/L	146	139	126	2.66	2.58	2.35	14.7	12.4	mmol/L	2.66	2.53	2.29	0.0484	0.0470	0.0428
Molybdenum (Mo)-Dissolved	mg/L	0.150	0.150	0.150	0.0600	0.0600	0.0600	0.000	0.000	mmol/L	0.00156	0.00156	0.00156	0.000625	0.000625	0.000625
Nickel (Ni)-Dissolved	mg/L	8.04	7.76	7.45	0.100	0.100	0.100	7.62	0.000	mmol/L	0.137	0.132	0.127	0.00170	0.00170	0.00170
Phosphorus (P)-Dissolved	mg/L	26.5	26.0	25.9	0.600	0.600	0.600	2.29	0.000	mmol/L	0.856	0.839	0.836	0.0194	0.0194	0.0194
Potassium (K)-Dissolved	mg/L	10.0	10.0	10.0	4.00	4.00	4.00	0.000	0.000	mmol/L	0.256	0.256	0.256	0.102	0.102	0.102
Selenium (Se)-Dissolved	mg/L	1.00	1.00	1.00	0.400	0.400	0.400	0.000	0.000	mmol/L	0.0127	0.0127	0.0127	0.00507	0.00507	0.00507
Silicon (Si)-Dissolved	mg/L	34.0	32.0	31.5	0.100	0.100	0.100	7.63	0.000	mmol/L	1.21	1.14	1.12	0.00356	0.00356	0.00356
Silver (Ag)-Dissolved	mg/L	0.0500	0.0500	0.0500	0.0200	0.0200	0.0200	0.000	0.000	mmol/L	0.000464	0.000464	0.000464	0.000185	0.000185	0.000185
Sodium (Na)-Dissolved	mg/L	35.0	33.0	32.0	30.7	30.2	29.1	8.96	5.35	mmol/L	1.52	1.44	1.39	1.34	1.31	1.27
Strontium (Sr)-Dissolved	mg/L	2.68	2.58	2.49	3.40	3.41	3.54	7.35	4.03	mmol/L	0.0306	0.0294	0.0284	0.0388	0.0389	0.0404
Thallium (Tl)-Dissolved	mg/L	1.00	1.00	1.00	0.400	0.400	0.400	0.000	0.000	mmol/L	0.00489	0.00489	0.00489	0.00196	0.00196	0.00196
Tin (Sn)-Dissolved	mg/L	0.150	0.150	0.150	0.0600	0.0600	0.0600	0.000	0.000	mmol/L	0.00126	0.00126	0.00126	0.000505	0.000505	0.000505
Titanium (Ti)-Dissolved	mg/L	0.0500	0.0500	0.0500	0.0200	0.0200	0.0200	0.000	0.000	mmol/L	0.00104	0.00104	0.00104	0.000418	0.000418	0.000418
Vanadium (V)-Dissolved	mg/L	0.150	0.150	0.150	0.0600	0.0600	0.0600	0.000	0.000	mmol/L	0.00294	0.00294	0.00294	0.00118	0.00118	0.00118
Zinc (Zn)-Dissolved	mg/L	131	123	115	0.0100	0.0100	0.0100	13.0	0.000	mmol/L	2.00	1.88	1.76	0.000153	0.000153	0.000153

Note:

Blue print are values below the analytical detection limit;

ND = no detected; NA = not applicable;

* Differences are between maximum and minimum values for influent and effluent to demonstrate range in quality.

Appendix A-2 Influent and Effluent Water Chemistry for Geco Mine HDS Process

ALS File No. L836129

Geco Mine	Units	Detection Limit	Influent			Effluent			Difference %		Units	Influent			Effluent		
			14-Apr-08	15-Apr-08	16-Apr-08	14-Apr-08	15-Apr-08	16-Apr-08	Influent	Effluent		14-Apr-08	15-Apr-08	16-Apr-08	14-Apr-08	15-Apr-08	16-Apr-08
Physical Tests																	
Conductivity	uS/cm	2.00	4760	4610	4640	3680	3510	3420	3.20	7.32	uS/cm	4760	4610	4640	3680	3510	3420
Hardness (as CaCO3)	mg/L	ND	1600	1570	1510	2990	2980	2870	5.79	4.10	mg/L	1600	1570	1510	2990	2980	2870
pH		ND	3.12	3.09	2.84	8.15	8.34	7.66	9.40	8.50		3.12	3.09	2.84	8.15	8.34	7.66
TSS	mg/L	3.00	46.0	38.0	6.00	12.0	3.00	3.00	154	120	mg/L	46.0	38.0	6.00	12.0	3.00	3.00
TDS	mg/L	20.0	6380	6070	5730	4690	4580	4440	10.7	5.48	mg/L	6380	6070	5730	4690	4580	4440
Turbidity	NTU	0.500	5.60	4.90	0.800	0.500	0.500	0.600	150	18.2	NTU	5.60	4.90	0.800	0.500	0.500	0.600
Acidity (as CaCO3)	mg/L	5.00	264	242	500	5.00	5.00	5.00	69.5	0.000	mmol/L	2.64	2.42	5.00	0.0500	0.0500	0.0500
Alkalinity (as CaCO3)	mg/L	5.00	5.00	5.00	5.00	26.0	26.0	24.0	0.000	8.00	mmol/L	0.0500	0.0500	0.0500	0.260	0.260	0.240
Bromide (Br)	mg/L	0.0500	0.0500	0.0500	0.0500	0.0500	0.0500	0.0500	0.000	0.000	mmol/L	0.000626	0.000626	0.000626	0.000626	0.000626	0.000626
Chloride (Cl)	mg/L	0.100	7.11	6.19	7.96	8.08	7.49	7.68	25.0	7.58	mmol/L	0.201	0.175	0.225	0.228	0.211	0.217
Fluoride (F)	mg/L	0.0500	8.90	8.83	7.89	6.42	5.65	6.18	12.0	12.8	mmol/L	0.468	0.465	0.415	0.338	0.297	0.325
Nitrate (as N)	mg/L	0.0500	0.0500	0.160	0.270	0.0500	0.210	0.230	138	129	mmol/L	0.00357	0.0114	0.0193	0.00357	0.0150	0.0164
Nitrite (as N)	mg/L	0.0500	0.0500	0.0500	0.0500	0.0500	0.0500	0.0500	0.000	0.000	mmol/L	0.00357	0.00357	0.00357	0.00357	0.00357	0.00357
Ammonia (as N)	mg/L	0.0200	20.9	18.4	19.0	19.5	18.0	18.1	12.7	8.00	mmol/L	1.49	1.31	1.36	1.39	1.29	1.29
Total Dissolved Phosphate As P	mg/L	0.100	0.100	0.100	0.100	0.100	0.100	0.100	0.000	0.000	mmol/L	0.00323	0.00323	0.00323	0.00323	0.00323	0.00323
Sulfate (SO4)	mg/L	0.100	4640	4550	4570	3550	3180	3500	1.96	11.0	mmol/L	48.3	47.4	47.6	37.0	33.1	36.4
Dissolved Metals																	
Aluminum (Al)-Dissolved	mg/L	0.00400	6.38	14.0	11.3	0.0200	0.0200	0.00400	74.8	133	mmol/L	0.236	0.519	0.419	0.000741	0.000741	0.000148
Antimony (Sb)-Dissolved	mg/L	0.00600	0.0200	0.00600	0.00500	0.0200	0.00600	0.00500	120	120	mmol/L	0.000164	0.0000493	0.0000411	0.000164	0.0000493	0.0000411
Arsenic (As)-Dissolved	mg/L	0.00300	0.0150	0.00300	0.00300	0.0150	0.00300	0.00300	133	133	mmol/L	0.000200	0.0000400	0.0000400	0.000200	0.0000400	0.0000400
Barium (Ba)-Dissolved	mg/L	0.00200	0.0350	0.0400	0.0420	0.0440	0.00400	0.110	18.2	186	mmol/L	0.000255	0.000291	0.000306	0.000320	0.000291	0.000801
Beryllium (Be)-Dissolved	mg/L	0.00100	0.0100	0.00100	0.00200	0.0100	0.00100	0.00200	164	164	mmol/L	0.00111	0.000111	0.000222	0.00111	0.000111	0.000222
Boron (B)-Dissolved	mg/L	0.0100	0.0500	0.0520	0.0520	0.0500	0.0390	0.0480	3.92	24.7	mmol/L	0.00462	0.00481	0.00481	0.00462	0.00361	0.00444
Cadmium (Cd)-Dissolved	mg/L	0.000100	0.0400	0.0413	0.0330	0.0100	0.000100	0.00200	22.3	196	mmol/L	0.000356	0.000367	0.000294	0.0000890	0.0000890	0.0000178
Calcium (Ca)-Dissolved	mg/L	0.0500	339	337	333	868	880	855	1.79	2.88	mmol/L	8.46	8.41	8.31	21.7	22.0	21.3
Chromium (Cr)-Dissolved	mg/L	0.00300	0.0150	0.00600	0.00300	0.0150	0.00300	0.00300	133	133	mmol/L	0.000288	0.000115	0.000577	0.000288	0.000577	0.000577
Cobalt (Co)-Dissolved	mg/L	0.000500	0.0130	0.0141	0.0140	0.0100	0.000900	0.00200	8.12	167	mmol/L	0.000221	0.000239	0.000238	0.000170	0.0000153	0.0000339
Copper (Cu)-Dissolved	mg/L	0.00200	0.316	0.311	0.272	0.0290	0.0240	0.0220	15.0	27.5	mmol/L	0.00497	0.00489	0.00428	0.000456	0.000378	0.000346
Iron (Fe)-Dissolved	mg/L	0.0100	1160	917	1170	0.0300	0.0760	0.0100	24.2	153	mmol/L	20.8	16.4	21.0	0.000537	0.00136	0.000179
Lead (Pb)-Dissolved	mg/L	0.00100	0.0160	0.0130	0.0110	0.0100	0.00100	0.00200	37.0	164	mmol/L	0.0000772	0.0000627	0.0000531	0.0000483	0.00000483	0.00000965
Magnesium (Mg)-Dissolved	mg/L	0.0500	184	178	165	199	191	179	10.9	10.6	mmol/L	7.57	7.32	6.79	8.19	7.86	7.36
Manganese (Mn)-Dissolved	mg/L	0.00200	5.13	8.57	8.11	0.223	0.259	0.263	50.2	16.5	mmol/L	0.0934	0.156	0.148	0.00406	0.00471	0.00479
Mercury (Hg)-Dissolved	mg/L	0.000100	0.000100	0.00500	ND	0.000100	0.000100	ND	192	0.000	mmol/L	0.00000499	0.0000249	ND	0.00000499	0.00000499	ND
Molybdenum (Mo)-Dissolved	mg/L	0.00200	0.0100	0.00200	0.00200	0.000100	0.00200	0.00200	133	181	mmol/L	0.000104	0.0000208	0.0000208	0.0000104	0.0000208	0.0000208
Nickel (Ni)-Dissolved	mg/L	0.00300	0.0190	0.0200	0.0190	0.0100	0.00300	0.00300	5.13	108	mmol/L	0.000324	0.000341	0.000324	0.000170	0.0000511	0.0000511
Phosphorus (P)-Dissolved	mg/L	0.0500	0.0190	0.0500	0.00200	0.0150	0.0500	0.0200	185	108	mmol/L	0.000613	0.00161	0.000646	0.000484	0.00161	0.000646
Potassium (K)-Dissolved	mg/L	0.0500	49.5	48.8	44.7	55.1	52.4	47.9	10.2	14.0	mmol/L	1.27	1.25	1.14	1.41	1.34	1.23
Selenium (Se)-Dissolved	mg/L	0.00400	0.0200	0.00400	0.00400	0.0200	0.00400	0.00400	133	133	mmol/L	0.000253	0.0000507	0.0000507	0.000253	0.0000507	0.0000507
Silicon (Si)-Dissolved	mg/L	0.0100	9.60	11.2	6.47	0.109	0.110	0.185	53.5	51.7	mmol/L	0.342	0.399	0.230	0.00388	0.00392	0.00659
Silver (Ag)-Dissolved	mg/L	0.000100	0.0100	0.000100	0.00200	0.0100	0.000100	0.00200	196	196	mmol/L	0.0000927	0.00000927	0.0000185	0.0000927	0.00000927	0.0000185
Sodium (Na)-Dissolved	mg/L	0.0500	32.3	30.0	27.3	34.7	34.8	31.8	16.8	9.01	mmol/L	1.40	1.30	1.19	1.51	1.51	1.38
Strontium (Sr)-Dissolved	mg/L	0.00500	0.939	1.35	1.00	1.69	1.52	1.49	35.9	12.6	mmol/L	0.0107	0.0154	0.0114	0.0193	0.0173	0.0170
Thallium (Tl)-Dissolved	mg/L	0.000300	0.0100	0.000300	0.00300	0.0100	0.000300	0.00300	188	188	mmol/L	0.0000489	0.00000147	0.0000147	0.0000489	0.00000147	0.0000147
Vanadium (V)-Dissolved	mg/L	0.00200	0.0100	0.00200	0.00400	0.0100	0.00200	0.00400	133	133	mmol/L	0.000196	0.0000393	0.0000785	0.000196	0.0000393	0.0000785
Zinc (Zn)-Dissolved	mg/L	0.00500	9.43	15.0	12.8	0.0170	0.00800	0.0300	45.6	116	mmol/L	0.144	0.229	0.196	0.000260	0.000122	0.000459

Note:
 Blue print are values below the analytical detection limit;
 ND = no detected;
 * Differences are between maximum and minimum values for influent and effluent to demonstrate range in quality.

Appendix A-3 Influent and Effluent Water Chemistry for Britannia Mine HDS Process

ALS File No. L836129

Britannia Mine	Units	Detection Limit	Influent	Effluent	Units	Influent	Effluent
			30-Oct-09	30-Oct-09		30-Oct-09	30-Oct-09
Physical Tests							
Conductivity	uS/cm	2.00	2100	2170	uS/cm	2100	2170
Hardness (as CaCO ₃)	mg/L	1.00	1290	1470	mg/L	12.9	14.7
pH	pH	0.100	4.05	7.47	pH	4.05	7.47
Anions and Nutrients							
Acidity (as CaCO ₃)	mg/L	1.00	235	15.0	mmol/L	2.35	0.150
Alkalinity, Bicarbonate (as CaCO ₃)	mg/L	1.00	1.00	38.7	mmol/L	0.00999	0.387
Alkalinity, Carbonate (as CaCO ₃)	mg/L	1.00	1.00	1.00	mmol/L	0.00999	0.00999
Alkalinity, Hydroxide (as CaCO ₃)	mg/L	1.00	1.00	1.00	mmol/L	0.00999	0.00999
Alkalinity, Total (as CaCO ₃)	mg/L	1.00	1.00	38.7	mmol/L	0.00999	0.387
Bromide (Br)	mg/L	1.00	1.00	1.00	mmol/L	0.0282	0.0282
Chloride (Cl)	mg/L	10.0	10.0	14.0	mmol/L	0.526	0.737
Fluoride (F)	mg/L	0.400	1.01	0.860	mmol/L	0.0721	0.0614
Nitrate (as N)	mg/L	0.100	0.100	0.100	mmol/L	0.00714	0.00714
Nitrite (as N)	mg/L	0.0200	0.0200	0.0200	mmol/L	0.00143	0.00143
Ammonia as N	mg/L	0.00500	0.0303	0.0405	mmol/L	0.000379	0.000507
Total Dissolved Phosphate As P	mg/L	0.00200	0.00200	0.00200	mmol/L	0.0000646	0.0000646
Sulfate (SO ₄)	mg/L	10.0	1320	1310	mmol/L	13.7	13.6
Dissolved Metals							
Aluminum (Al)-Dissolved	mg/L	0.00500	19.0	0.502	mmol/L	0.704	0.0186
Antimony (Sb)-Dissolved	mg/L	0.000500	0.000500	0.000500	mmol/L	0.00000411	0.00000411
Arsenic (As)-Dissolved	mg/L	0.000500	0.000500	0.000500	mmol/L	0.00000667	0.00000667
Barium (Ba)-Dissolved	mg/L	0.000250	0.00751	0.00529	mmol/L	0.0000547	0.0000385
Beryllium (Be)-Dissolved	mg/L	0.00250	0.00250	0.00250	mmol/L	0.000277	0.000277
Bismuth (Bi)-Dissolved	mg/L	0.00250	0.00250	0.00250	mmol/L	0.0000120	0.0000120
Boron (B)-Dissolved	mg/L	0.0500	0.171	0.157	mmol/L	0.0158	0.0145
Cadmium (Cd)-Dissolved	mg/L	0.0000850	0.0887	0.00118	mmol/L	0.000789	0.0000105
Calcium (Ca)-Dissolved	mg/L	0.0500	411	502	mmol/L	10.3	12.5
Chromium (Cr)-Dissolved	mg/L	0.00250	0.00250	0.00250	mmol/L	0.0000481	0.0000481
Cobalt (Co)-Dissolved	mg/L	0.000500	0.0524	0.000500	mmol/L	0.000889	0.00000848
Copper (Cu)-Dissolved	mg/L	0.000500	17.5	0.00354	mmol/L	0.275	0.0000557
Iron (Fe)-Dissolved	mg/L	0.0300	0.555	0.0300	mmol/L	0.00994	0.000537
Lead (Pb)-Dissolved	mg/L	0.000250	0.0524	0.000250	mmol/L	0.000253	0.0000121
Lithium (Li)-Dissolved	mg/L	0.0250	0.0530	0.0520	mmol/L	0.00764	0.00749
Magnesium (Mg)-Dissolved	mg/L	0.100	63.7	52.8	mmol/L	2.62	2.17
Manganese (Mn)-Dissolved	mg/L	0.000250	4.20	0.432	mmol/L	0.0764	0.00786
Molybdenum (Mo)-Dissolved	mg/L	0.000250	0.000250	0.000250	mmol/L	0.00000261	0.00000261
Nickel (Ni)-Dissolved	mg/L	0.00250	0.0403	0.00250	mmol/L	0.000687	0.0000426
Phosphorus (P)-Dissolved	mg/L	0.300	0.300	0.300	mmol/L	0.00969	0.00969
Potassium (K)-Dissolved	mg/L	2.00	2.00	2.00	mmol/L	0.0512	0.0512
Selenium (Se)-Dissolved	mg/L	0.000500	0.000500	0.000500	mmol/L	0.00000633	0.00000633
Silicon (Si)-Dissolved	mg/L	0.0500	14.5	1.12	mmol/L	0.516	0.0399
Silver (Ag)-Dissolved	mg/L	0.000500	0.000500	0.000500	mmol/L	0.00000464	0.00000464
Sodium (Na)-Dissolved	mg/L	2.00	9.40	18.1	mmol/L	0.409	0.787
Strontium (Sr)-Dissolved	mg/L	0.000500	2.05	2.17	mmol/L	0.0234	0.0248
Thallium (Tl)-Dissolved	mg/L	0.000500	0.000500	0.000500	mmol/L	0.00000245	0.00000245
Tin (Sn)-Dissolved	mg/L	0.000500	0.000500	0.000500	mmol/L	0.00000421	0.00000421
Titanium (Ti)-Dissolved	mg/L	0.0100	0.0100	0.0110	mmol/L	0.000209	0.000230
Uranium (U)-Dissolved	mg/L	0.0000500	0.000377	0.0000500	mmol/L	0.00000158	0.000000210
Vanadium (V)-Dissolved	mg/L	0.00500	0.00500	0.00500	mmol/L	0.0000982	0.0000982
Zinc (Zn)-Dissolved	mg/L	0.00500	17.9	0.0121	mmol/L	0.274	0.000185

Note: Blue print are values below the analytical detection limit

Appendix A-4 Influent and Effluent Water Chemistry for Brunswick Mine HDS Process

ALS File No. L853002

Brunswick Mine	Units	Detection Limit	Influent			Effluent			Difference %		Units	Influent			Effluent		
			05-Jan-10 (8:00 am)	05-Jan-10 (9:30 am)	05-Jan-10 (11:00 am)	05-Jan-10 (8:10 am)	05-Jan-10 (9:40 am)	05-Jan-10 (11:10 am)	Influent	Effluent		05-Jan-10 (8:00 am)	05-Jan-10 (9:30 am)	05-Jan-10 (11:00 am)	05-Jan-10 (8:10 am)	05-Jan-10 (9:40 am)	05-Jan-10 (11:10 am)
Physical Tests																	
Hardness (as CaCO3)	mg/L	2.20	742	755	745	946	944	960	1.74	1.68	mg/L	7.41	7.54	7.44	9.45	9.43	9.59
pH	pH	0.100	6.75	6.83	6.79	8.59	8.45	8.47	1.18	1.64	pH	6.75	6.83	6.79	8.59	8.45	8.47
Anions and Nutrients																	
Alkalinity, Total (as CaCO3)	mg/L	2.00	131	135	132	159	158	158	3.01	0.631	mmol/L	1.31	1.35	1.32	1.59	1.58	1.58
Bromide (Br)	mg/L	2.50	2.50	5.00	5.00	0.500	2.50	5.00	66.7	164	mg/L	0.0313	0.0626	0.0626	0.00626	0.0313	0.0626
Chloride (Cl)	mg/L	25.0	108	99.0	99.0	98.5	102	99.0	8.70	3.49	mg/L	3.05	2.79	2.79	2.78	2.88	2.79
Fluoride (F)	mg/L	0.0300	0.871	0.871	0.850	0.820	0.803	0.860	2.44	6.86	mg/L	0.0458	0.0458	0.0447	0.0432	0.0423	0.0453
Nitrate (as N)	mg/L	0.250	0.510	0.800	0.680	0.849	0.820	1.01	44.3	20.8	mg/L	0.0364	0.0571	0.0485	0.0606	0.0585	0.0721
Nitrite (as N)	mg/L	0.0500	0.0500	0.100	0.100	0.0670	0.0500	0.100	66.7	66.7	mg/L	0.00357	0.00714	0.00714	0.00478	0.00357	0.00714
Sulfate (SO4)	mg/L	25.0	3670	3440	3430	3540	3690	3430	6.76	7.30	mg/L	38.2	35.8	35.7	36.9	38.4	35.7
Dissolved Metals																	
Aluminum (Al)-Dissolved	mg/L	0.0200	0.0200	0.0200	0.0200	0.0200	0.0200	0.0200	0.000	0.000	mg/L	0.000741	0.000741	0.000741	0.000741	0.000741	0.000741
Antimony (Sb)-Dissolved	mg/L	0.00200	0.0144	0.0141	0.0154	0.0145	0.0150	0.0156	8.81	7.31	mg/L	0.000118	0.000116	0.000126	0.000119	0.000123	0.000128
Arsenic (As)-Dissolved	mg/L	0.00200	0.00200	0.00200	0.00200	0.00200	0.00200	0.00200	0.000	0.000	mg/L	0.0000267	0.0000267	0.0000267	0.0000267	0.0000267	0.0000267
Barium (Ba)-Dissolved	mg/L	0.00100	0.0260	0.0257	0.0265	0.0184	0.0186	0.0192	3.07	4.26	mg/L	0.000189	0.000187	0.000193	0.000134	0.000135	0.000140
Beryllium (Be)-Dissolved	mg/L	0.0100	0.0100	0.0100	0.0100	0.0100	0.0100	0.0100	0.000	0.000	mg/L	0.00111	0.00111	0.00111	0.00111	0.00111	0.00111
Bismuth (Bi)-Dissolved	mg/L	0.0100	0.0100	0.0100	0.0100	0.0100	0.0100	0.0100	0.000	0.000	mg/L	0.0000479	0.0000479	0.0000479	0.0000479	0.0000479	0.0000479
Boron (B)-Dissolved	mg/L	0.200	0.200	0.200	0.200	0.200	0.200	0.200	0.000	0.000	mg/L	0.0185	0.0185	0.0185	0.0185	0.0185	0.0185
Cadmium (Cd)-Dissolved	mg/L	0.000340	0.0536	0.0534	0.0536	0.00359	0.00357	0.00375	0.374	4.92	mg/L	0.000477	0.000475	0.000477	0.0000319	0.0000318	0.0000334
Calcium (Ca)-Dissolved	mg/L	0.250	117	119	117	212	212	216	1.69	1.87	mg/L	2.92	2.97	2.92	5.29	5.29	5.39
Chromium (Cr)-Dissolved	mg/L	0.0100	0.0100	0.0100	0.0100	0.0100	0.0100	0.0100	0.000	0.000	mg/L	0.000192	0.000192	0.000192	0.000192	0.000192	0.000192
Cobalt (Co)-Dissolved	mg/L	0.00200	0.264	0.268	0.263	0.00660	0.00650	0.00640	1.88	3.08	mg/L	0.00448	0.00455	0.00446	0.000112	0.000110	0.000109
Copper (Cu)-Dissolved	mg/L	0.00200	0.788	0.785	0.790	0.0350	0.0370	0.0360	0.635	5.56	mg/L	0.0124	0.0124	0.0124	0.000551	0.000582	0.000567
Iron (Fe)-Dissolved	mg/L	0.150	31.0	31.4	33.5	0.150	0.150	0.150	7.75	0.000	mg/L	0.555	0.562	0.600	0.00269	0.00269	0.00269
Lead (Pb)-Dissolved	mg/L	0.00100	0.00100	0.00100	0.00100	0.00100	0.00100	0.00100	0.000	0.000	mg/L	0.00000483	0.00000483	0.00000483	0.00000483	0.00000483	0.00000483
Lithium (Li)-Dissolved	mg/L	0.100	0.100	0.100	0.100	0.100	0.100	0.100	0.000	0.000	mg/L	0.0144	0.0144	0.0144	0.0144	0.0144	0.0144
Magnesium (Mg)-Dissolved	mg/L	0.500	109	111	110	101	101	103	1.82	1.96	mg/L	4.48	4.57	4.53	4.16	4.16	4.24
Manganese (Mn)-Dissolved	mg/L	0.00100	25.0	25.2	25.1	6.29	6.34	6.46	0.797	2.67	mg/L	0.455	0.459	0.457	0.114	0.115	0.118
Molybdenum (Mo)-Dissolved	mg/L	0.00100	0.00310	0.00360	0.00320	0.00840	0.00780	0.00770	14.9	8.70	mg/L	0.0000323	0.0000375	0.0000333	0.0000875	0.0000813	0.0000802
Nickel (Ni)-Dissolved	mg/L	0.0100	0.0670	0.0660	0.0660	0.0100	0.0100	0.0100	1.50	0.000	mg/L	0.00114	0.00112	0.00112	0.000170	0.000170	0.000170
Phosphorus (P)-Dissolved	mg/L	1.50	1.50	1.50	1.50	1.50	1.50	1.50	0.000	0.000	mg/L	0.0484	0.0484	0.0484	0.0484	0.0484	0.0484
Potassium (K)-Dissolved	mg/L	10.0	21.0	21.0	21.0	21.0	21.0	21.0	0.000	0.000	mg/L	0.537	0.537	0.537	0.537	0.537	0.537
Selenium (Se)-Dissolved	mg/L	0.000500	0.00360	0.00357	0.00321	0.00361	0.00340	0.00353	11.5	5.99	mg/L	0.0000456	0.0000452	0.0000407	0.0000457	0.0000431	0.0000447
Silicon (Si)-Dissolved	mg/L	0.250	3.98	4.01	4.00	0.680	0.680	0.670	0.751	1.48	mg/L	0.142	0.143	0.142	0.0242	0.0242	0.0239
Silver (Ag)-Dissolved	mg/L	0.000200	0.0123	0.0175	0.00955	0.000530	0.000980	0.000770	58.8	59.6	mg/L	0.000114	0.000162	0.0000885	0.00000491	0.00000909	0.00000714
Sodium (Na)-Dissolved	mg/L	10.0	1830	1860	1830	1830	1820	1840	1.63	1.09	mg/L	79.6	80.9	79.6	79.6	79.2	80.0
Strontium (Sr)-Dissolved	mg/L	0.00200	0.241	0.248	0.244	0.297	0.295	0.301	2.86	2.01	mg/L	0.00275	0.00283	0.00278	0.00339	0.00337	0.00344
Thallium (Tl)-Dissolved	mg/L	0.00200	0.00930	0.00950	0.00950	0.00780	0.00770	0.00790	2.13	2.56	mg/L	0.0000455	0.0000465	0.0000465	0.0000382	0.0000377	0.0000387
Tin (Sn)-Dissolved	mg/L	0.00200	0.00200	0.00200	0.00200	0.00200	0.00200	0.00200	0.000	0.000	mg/L	0.0000168	0.0000168	0.0000168	0.0000168	0.0000168	0.0000168
Titanium (Ti)-Dissolved	mg/L	0.0500	0.0500	0.0500	0.0500	0.0500	0.0500	0.0500	0.000	0.000	mg/L	0.00104	0.00104	0.00104	0.00104	0.00104	0.00104
Uranium (U)-Dissolved	mg/L	0.000200	0.000220	0.000200	0.000200	0.000390	0.000350	0.000370	9.52	10.8	mg/L	0.00000924	0.00000840	0.00000840	0.00000164	0.00000147	0.00000155
Vanadium (V)-Dissolved	mg/L	0.0200	0.0200	0.0200	0.0200	0.0200	0.0200	0.0200	0.000	0.000	mg/L	0.000393	0.000393	0.000393	0.000393	0.000393	0.000393
Zinc (Zn)-Dissolved	mg/L	0.0200	72.2	72.7	73.7	0.191	0.209	0.199	2.06	9.00	mg/L	1.10	1.11	1.13	0.00292	0.00320	0.00304

Note:
 Blue print are values below the analytical detection limit;
 * Differences are between maximum and minimum values for influent and effluent to demonstrate range in quality.

Appendix A-5 Influent and Effluent Water Chemistry for Chisel North Mine HDS Process

ALS File No. L855616

Chisel North Mine	Units	Detection Limit	Influent			Effluent			Difference %		Units	Influent			Effluent		
			13-Jan-10	14-Jan-10	15-Jan-10	13-Jan-10	14-Jan-10	15-Jan-10	Influent	Effluent		13-Jan-10	14-Jan-10	15-Jan-10	13-Jan-10	14-Jan-10	15-Jan-10
Physical Tests																	
Conductivity	uS/cm	2.00	6330	6410	6280	6360	6380	6330	2.05	0.787	uS/cm	6330	6410	6280	6360	6380	6330
Hardness (as CaCO3)	mg/L	1.00	2430	2420	2380	2670	2660	2600	2.08	2.66	mmol/L	24.3	24.2	23.8	26.7	26.6	26.0
pH	pH	0.100	4.69	4.63	5.14	7.34	7.35	7.48	10.4	1.89	pH	4.69	4.63	5.14	7.34	7.35	7.48
Anions and Nutrients																	
Bromide (Br)	mg/L	1.00	14.8	12.3	14.9	12.5	15.8	15.2	19.1	23.3	mmol/L	0.185	0.154	0.186	0.156	0.198	0.190
Chloride (Cl)	mg/L	10.0	1610	1490	1510	1480	1600	1490	7.74	7.79	mmol/L	45.4	42.0	42.6	41.7	45.1	42.0
Fluoride (F)	mg/L	0.0300	0.712	0.690	0.769	0.767	0.779	0.856	10.8	11.0	mmol/L	0.0375	0.0363	0.0405	0.0404	0.0410	0.0451
Nitrate (as N)	mg/L	0.100	1.19	1.43	1.20	1.10	1.30	1.12	18.3	16.7	mmol/L	0.0850	0.102	0.0857	0.0785	0.0928	0.0800
Nitrite (as N)	mg/L	0.0200	0.0400	0.0500	0.0500	0.0500	0.0200	0.0500	22.2	85.7	mmol/L	0.00286	0.00357	0.00357	0.00357	0.00143	0.00357
Sulfate (SO4)	mg/L	10.0	1450	1330	1350	1310	1430	1320	8.63	8.76	mmol/L	15.1	13.8	14.1	13.6	14.9	13.7
Dissolved Metals																	
Aluminum (Al)-Dissolved	mg/L	0.0200	0.793	0.760	0.784	0.0200	0.0200	0.0200	4.25	0.000	mmol/L	0.0294	0.0282	0.0291	0.000741	0.000741	0.000741
Antimony (Sb)-Dissolved	mg/L	0.00200	0.00200	0.00200	0.00200	0.00200	0.00200	0.00200	0.000	0.000	mmol/L	0.0000164	0.0000164	0.0000164	0.0000164	0.0000164	0.0000164
Arsenic (As)-Dissolved	mg/L	0.0100	0.0110	0.0200	0.0173	0.0100	0.0100	0.0100	58.1	0.000	mmol/L	0.000147	0.000267	0.000231	0.000133	0.000133	0.000133
Barium (Ba)-Dissolved	mg/L	0.00100	0.0935	0.0920	0.0979	0.201	0.213	0.194	6.21	9.34	mmol/L	0.000681	0.000670	0.000713	0.00146	0.00155	0.00141
Beryllium (Be)-Dissolved	mg/L	0.0100	0.0100	0.0100	0.0100	0.0100	0.0100	0.0100	0.000	0.000	mmol/L	0.00111	0.00111	0.00111	0.00111	0.00111	0.00111
Bismuth (Bi)-Dissolved	mg/L	0.0100	0.0100	0.0100	0.0100	0.0100	0.0100	0.0100	0.000	0.000	mmol/L	0.0000479	0.0000479	0.0000479	0.0000479	0.0000479	0.0000479
Boron (B)-Dissolved	mg/L	0.200	0.510	0.510	0.560	0.470	0.470	0.510	9.35	8.16	mmol/L	0.0472	0.0472	0.0518	0.0435	0.0435	0.0472
Cadmium (Cd)-Dissolved	mg/L	0.000340	0.0808	0.0801	0.0832	0.00179	0.00180	0.00177	3.80	1.68	mmol/L	0.000719	0.000713	0.000740	0.0000159	0.0000160	0.0000157
Calcium (Ca)-Dissolved	mg/L	0.0500	663	658	642	767	762	743	3.22	3.18	mmol/L	16.5	16.4	16.0	19.1	19.0	18.5
Chromium (Cr)-Dissolved	mg/L	0.0100	0.0100	0.0100	0.0100	0.0100	0.0100	0.0100	0.000	0.000	mmol/L	0.000192	0.000192	0.000192	0.000192	0.000192	0.000192
Cobalt (Co)-Dissolved	mg/L	0.00200	0.159	0.158	0.163	0.00260	0.00300	0.00270	3.12	14.3	mmol/L	0.00270	0.00268	0.00277	0.0000441	0.0000509	0.0000458
Copper (Cu)-Dissolved	mg/L	0.00200	0.228	0.222	0.228	0.00200	0.00200	0.00200	2.67	0.000	mmol/L	0.00359	0.00349	0.00359	0.0000315	0.0000315	0.0000315
Iron (Fe)-Dissolved	mg/L	0.0300	44.8	44.4	46.8	0.0300	0.0300	0.0300	5.26	0.000	mmol/L	0.802	0.795	0.838	0.000537	0.000537	0.000537
Lead (Pb)-Dissolved	mg/L	0.00100	0.00100	0.00150	0.00100	0.00100	0.00100	0.00100	40.0	0.000	mmol/L	0.00000483	0.00000724	0.00000483	0.00000483	0.00000483	0.00000483
Lithium (Li)-Dissolved	mg/L	0.100	0.100	0.100	0.100	0.110	0.100	0.110	0.000	9.52	mmol/L	0.0144	0.0144	0.0144	0.0158	0.0144	0.0158
Magnesium (Mg)-Dissolved	mg/L	0.100	188	189	188	183	184	181	0.531	1.64	mmol/L	7.74	7.78	7.74	7.53	7.57	7.45
Manganese (Mn)-Dissolved	mg/L	0.00100	4.90	4.89	5.08	0.357	0.356	0.350	3.81	1.98	mmol/L	0.0892	0.0890	0.0925	0.00650	0.00648	0.00637
Molybdenum (Mo)-Dissolved	mg/L	0.00100	0.00100	0.00100	0.00100	0.00100	0.00100	0.00100	0.000	0.000	mmol/L	0.0000104	0.0000104	0.0000104	0.0000104	0.0000104	0.0000104
Nickel (Ni)-Dissolved	mg/L	0.0100	0.109	0.106	0.112	0.0100	0.0100	0.0100	5.50	0.000	mmol/L	0.00186	0.00181	0.00191	0.000170	0.000170	0.000170
Phosphorus (P)-Dissolved	mg/L	0.300	0.300	0.300	0.300	0.300	0.300	0.300	0.000	0.000	mmol/L	0.00969	0.00969	0.00969	0.00969	0.00969	0.00969
Potassium (K)-Dissolved	mg/L	2.00	26.1	26.1	23.1	26.0	34.0	22.1	12.2	42.4	mmol/L	0.668	0.668	0.591	0.665	0.870	0.565
Selenium (Se)-Dissolved	mg/L	0.000500	0.00232	0.00230	0.00191	0.00225	0.00218	0.00185	19.4	19.5	mmol/L	0.0000294	0.0000291	0.0000242	0.0000285	0.0000276	0.0000234
Silicon (Si)-Dissolved	mg/L	0.0500	6.09	6.08	6.01	0.338	0.341	0.326	1.32	4.50	mmol/L	0.217	0.216	0.214	0.0120	0.0121	0.0116
Silver (Ag)-Dissolved	mg/L	0.000200	0.000200	0.000200	0.000200	0.000200	0.000350	0.000200	0.000	54.5	mmol/L	0.00000185	0.00000185	0.00000185	0.00000185	0.00000324	0.00000185
Sodium (Na)-Dissolved	mg/L	2.00	414	414	410	413	417	402	0.971	3.66	mmol/L	18.0	18.0	17.8	18.0	18.1	17.5
Strontium (Sr)-Dissolved	mg/L	0.00200	9.26	9.12	9.30	8.91	8.91	8.57	1.95	3.89	mmol/L	0.106	0.104	0.106	0.102	0.102	0.0978
Thallium (Tl)-Dissolved	mg/L	0.00200	0.00200	0.00200	0.00200	0.00200	0.00200	0.00200	0.000	0.000	mmol/L	0.00000979	0.00000979	0.00000979	0.00000979	0.00000979	0.00000979
Tin (Sn)-Dissolved	mg/L	0.00200	0.00200	0.00200	0.00200	0.00200	0.00200	0.00200	0.000	0.000	mmol/L	0.0000168	0.0000168	0.0000168	0.0000168	0.0000168	0.0000168
Titanium (Ti)-Dissolved	mg/L	0.0100	0.0100	0.0100	0.0100	0.0100	0.0100	0.0100	0.000	0.000	mmol/L	0.000209	0.000209	0.000209	0.000209	0.000209	0.000209
Uranium (U)-Dissolved	mg/L	0.000200	0.000530	0.000530	0.000620	0.000200	0.000200	0.000200	15.7	0.000	mmol/L	0.00000223	0.00000223	0.00000260	0.00000840	0.00000840	0.00000840
Vanadium (V)-Dissolved	mg/L	0.0200	0.0200	0.0200	0.0200	0.0200	0.0200	0.0200	0.000	0.000	mmol/L	0.000393	0.000393	0.000393	0.000393	0.000393	0.000393
Zinc (Zn)-Dissolved	mg/L	0.0200	70.3	69.3	70.1	0.278	0.276	0.301	1.43	8.67	mmol/L	1.08	1.06	1.07	0.00425	0.00422	0.00460

Note:
 Blue print are values below the analytical detection limit;
 * Differences are between maximum and minimum values for influent and effluent to demonstrate range in quality.

Appendix A.6 Influent and Effluent Water Chemistry for Samatosum Mine HDS Process

Maxxam ID: R85688
 Maxxam COC No.: F89087

Samatosum Mine	Units	Detection Limit	Influent	Effluent	Units	Influent	Effluent
			12-Nov-09	12-Nov-09		12-Nov-09	12-Nov-09
Physical Tests							
Conductivity	uS/cm	1.00	5540	4900	uS/cm	5540	4900
Dissolved Hardness (as CaCO ₃)	mg/L	0.500	2520	3380	mmol/L	25.2	33.8
pH	pH Units		2.90	8.80	pH Units	2.90	8.80
Total Dissolved Solids	mg/L	10.0	5900	5500	mg/L	5900	5500
Turbidity	NTU	0.100	37.4	4.80	NTU	37.4	4.80
Anions and Nutrients							
Acidity (pH 4.5) (as CaCO ₃)	mg/L	0.500	930	0.500	mmol/L	9.29	0.00500
Acidity (pH 8.3) (as CaCO ₃)	mg/L	0.500	1380	0.500	mmol/L	13.8	0.00500
Alkalinity (Total as CaCO ₃)	mg/L	0.500	0.500	33.0	mmol/L	0.00500	0.330
Alkalinity (PP as CaCO ₃)	mg/L	0.500	0.500	4.50	mmol/L	0.00500	0.0450
Bicarbonate (HCO ₃)	mg/L	0.500	0.500	30.0	mmol/L	0.00819	0.492
Carbonate (CO ₃)	mg/L	0.500	0.500	5.40	mmol/L	0.00833	0.0900
Bromide (Br)	mg/L	0.400	0.400	0.400	mmol/L	0.00501	0.00501
Dissolved Chloride (Cl)	mg/L	0.500	1.60	1.40	mmol/L	0.0451	0.0395
Fluoride (F)	mg/L	0.0100	3.20	1.28	mmol/L	0.168	0.0674
Nitrate (N)	mg/L	0.0200	1.60	0.0400	mmol/L	0.114	0.00286
Nitrite (N)	mg/L	0.00500	0.240	0.00500	mmol/L	0.0171	0.000357
Ammonia (N)	mg/L	0.00500	0.352	0.0760	mmol/L	0.0251	0.00543
Dissolved Phosphorus (P)	mg/L	0.00200	4.01	0.00300	mmol/L	0.129	0.0000969
Dissolved Sulphate (SO ₄)	mg/L	50.0	4100	2900	mmol/L	42.7	30.2
Dissolved Organic Carbon (C)	mg/L	0.500	2.70	2.20	mmol/L	0.225	0.183
Dissolved Metals							
Dissolved Aluminum (Al)	mg/L	0.00100	11.8	0.00400	mmol/L	0.437	0.000148
Dissolved Antimony (Sb)	mg/L	0.000100	0.0180	0.00100	mmol/L	0.000148	0.00000821
Dissolved Arsenic (As)	mg/L	0.000100	0.652	0.000900	mmol/L	0.00870	0.0000120
Dissolved Barium (Ba)	mg/L	0.000100	0.0101	0.00510	mmol/L	0.0000735	0.0000371
Dissolved Beryllium (Be)	mg/L	0.0000500	0.000400	0.0000500	mmol/L	0.0000444	0.00000555
Dissolved Bismuth (Bi)	mg/L	0.0000300	0.0000300	0.0000300	mmol/L	0.000000144	0.000000144
Dissolved Boron (B)	mg/L	0.300	0.300	0.300	mmol/L	0.0277	0.0277
Dissolved Cadmium (Cd)	mg/L	0.0000300	0.184	0.000160	mmol/L	0.00164	0.00000142
Dissolved Calcium (Ca)	mg/L	0.0500	343	793	mmol/L	8.56	19.8
Dissolved Chromium (Cr)	mg/L	0.000500	0.0720	0.000500	mmol/L	0.00138	0.00000962
Dissolved Cobalt (Co)	mg/L	0.0000300	0.488	0.000300	mmol/L	0.00828	0.00000509
Dissolved Copper (Cu)	mg/L	0.000300	3.88	0.00190	mmol/L	0.0611	0.0000299
Dissolved Iron (Fe)	mg/L	0.00500	370	0.0100	mmol/L	6.63	0.000179
Dissolved Lead (Pb)	mg/L	0.0000300	0.144	0.0000500	mmol/L	0.000695	0.000000241
Dissolved Lithium (Li)	mg/L	0.00300	0.00300	0.00500	mmol/L	0.000432	0.000720
Dissolved Magnesium (Mg)	mg/L	0.0500	405	339	mmol/L	16.7	13.9
Dissolved Manganese (Mn)	mg/L	0.000300	11.4	0.0371	mmol/L	0.208	0.000675
Dissolved Molybdenum (Mo)	mg/L	0.000300	0.0136	0.0117	mmol/L	0.000142	0.000122
Dissolved Nickel (Ni)	mg/L	0.000100	1.40	0.00110	mmol/L	0.0239	0.0000187
Dissolved Phosphorus (P)	mg/L	0.0100	3.49	0.0100	mmol/L	0.113	0.000323
Dissolved Potassium (K)	mg/L	0.0500	1.17	1.41	mmol/L	0.0299	0.0361
Dissolved Selenium (Se)	mg/L	0.000200	0.00520	0.00350	mmol/L	0.0000659	0.0000443
Dissolved Silicon (Si)	mg/L	0.500	6.30	0.500	mmol/L	0.224	0.0178
Dissolved Silver (Ag)	mg/L	0.0000300	0.000850	0.0000300	mmol/L	0.00000788	0.000000278
Dissolved Sodium (Na)	mg/L	0.0500	3.48	4.35	mmol/L	0.151	0.189
Dissolved Strontium (Sr)	mg/L	0.000300	2.77	3.66	mmol/L	0.0316	0.0418
Dissolved Thallium (Tl)	mg/L	0.0000100	0.00128	0.000390	mmol/L	0.00000626	0.00000191
Dissolved Tin (Sn)	mg/L	0.0000500	0.0000500	0.0000500	mmol/L	0.000000421	0.000000421
Dissolved Titanium (Ti)	mg/L	0.00300	0.00900	0.00300	mmol/L	0.000188	0.0000627
Dissolved Uranium (U)	mg/L	0.0000100	0.0696	0.00344	mmol/L	0.000292	0.0000145
Dissolved Vanadium (V)	mg/L	0.00100	0.0230	0.00100	mmol/L	0.000451	0.0000196
Dissolved Zinc (Zn)	mg/L	0.000500	64.1	0.00160	mmol/L	0.980	0.0000245

Note: Blue print are values below the analytical detection limit

Appendix A.7 Influent and Effluent Water Chemistry for Sullivan Mine HDS Process

ALS File No. L889787

Sullivan Mine	Units	Detection Limit	Influent					Effluent				
			16-May-10	17-May-10	18-May-10	19-May-10	20-May-10	16-May-10	17-May-10	18-May-10	19-May-10	20-May-10
Physical Tests												
Conductivity	uS/cm	2.0	5060	5100	5170	5200	5230	4670	4680	4750	4690	4610
Hardness (as CaCO3)	mg/L	1.4	3340	3400	3450	3540	3550	3820	3750	3790	3750	3750
pH	pH	0.10	3.10	3.16	3.21	3.22	3.22	8.60	8.62	8.64	8.51	8.58
Anions and Nutrients												
Acidity (as CaCO3)	mg/L	1.0	862	843	811	810	795	1.00	1.00	1.00	1.00	1.00
Alkalinity, Total (as CaCO3)	mg/L	2.0	2.00	2.00	2.00	2.00	2.00	39.9	40.4	40.0	38.1	39.0
Bromide (Br)	mg/L	5.0	5.00	5.00	5.00	5.00	5.00	5.00	5.00	5.00	5.00	5.00
Chloride (Cl)	mg/L	50	50.0	50.0	50.0	50.0	50.0	50.0	50.0	50.0	50.0	50.0
Fluoride (F)	mg/L	0.30	2.34	2.24	2.17	2.23	2.23	1.22	1.20	1.17	1.07	1.03
Nitrate (as N)	mg/L	0.50	0.500	0.500	0.500	0.500	0.500	0.500	0.500	0.500	0.570	0.500
Nitrite (as N)	mg/L	0.10	0.100	0.100	0.100	0.100	0.100	0.100	0.100	0.100	0.100	0.100
Ammonia as N	mg/L	0.10	0.323	2.48	0.320	0.352	2.73	2.76	2.16	2.38	2.44	2.45
Sulfate (SO4)	mg/L	50	4010	4070	4120	4150	4200	3680	3690	3730	3720	3720
Dissolved Metals												
Aluminum (Al)-Dissolved	mg/L	0.010	26.8	18.9	18.4	19.0	18.5	0.0350	0.0300	0.0280	0.0120	0.0110
Antimony (Sb)-Dissolved	mg/L	0.0010	0.00200	0.00100	0.00100	0.00200	0.00200	0.00100	0.00100	0.00100	0.00100	0.00100
Arsenic (As)-Dissolved	mg/L	0.0010	0.00200	0.00160	0.00170	0.00200	0.00200	0.00100	0.00100	0.00100	0.00100	0.00100
Barium (Ba)-Dissolved	mg/L	0.00050	0.0148	0.0125	0.0130	0.0129	0.0127	0.0131	0.0125	0.0130	0.0137	0.0148
Beryllium (Be)-Dissolved	mg/L	0.0050	0.0100	0.00500	0.00500	0.0100	0.0100	0.00500	0.00500	0.00500	0.00500	0.00500
Bismuth (Bi)-Dissolved	mg/L	0.0050	0.0100	0.00500	0.00500	0.0100	0.0100	0.00500	0.00500	0.00500	0.00500	0.00500
Boron (B)-Dissolved	mg/L	0.10	0.200	0.120	0.120	0.200	0.200	0.100	0.100	0.100	0.100	0.100
Cadmium (Cd)-Dissolved	mg/L	0.00017	0.0630	0.0522	0.0500	0.0516	0.0499	0.000210	0.000180	0.000170	0.000170	0.000170
Calcium (Ca)-Dissolved	mg/L	0.10	320	318	323	342	329	755	743	750	781	775
Chromium (Cr)-Dissolved	mg/L	0.0050	0.0100	0.00500	0.00500	0.0100	0.0100	0.00500	0.00500	0.00500	0.00500	0.00500
Cobalt (Co)-Dissolved	mg/L	0.0010	0.0910	0.0760	0.0748	0.0777	0.0767	0.00100	0.00100	0.00100	0.00100	0.00100
Copper (Cu)-Dissolved	mg/L	0.0010	0.103	0.0843	0.0824	0.0855	0.0829	0.00100	0.00100	0.00100	0.00100	0.00100
Iron (Fe)-Dissolved	mg/L	0.060	249	252	256	263	264	0.0600	0.0600	0.0600	0.0600	0.0600
Lead (Pb)-Dissolved	mg/L	0.00050	0.0276	0.0244	0.0247	0.0259	0.0257	0.000500	0.000500	0.000500	0.000500	0.000500
Lithium (Li)-Dissolved	mg/L	0.050	0.140	0.127	0.133	0.140	0.130	0.129	0.123	0.128	0.128	0.131
Magnesium (Mg)-Dissolved	mg/L	0.20	618	632	642	653	662	469	461	466	438	440
Manganese (Mn)-Dissolved	mg/L	0.00050	56.8	40.0	40.8	44.2	44.2	1.13	1.02	0.927	0.555	0.537
Molybdenum (Mo)-Dissolved	mg/L	0.00	0	0	0	0	0	0	0	0	0	0
Nickel (Ni)-Dissolved	mg/L	0.0050	0.140	0.114	0.112	0.116	0.114	0.00500	0.00500	0.00500	0.00500	0.00500
Phosphorus (P)-Dissolved	mg/L	0.60	0.600	0.600	0.600	0.600	0.600	0.600	0.600	0.600	0.600	0.600
Potassium (K)-Dissolved	mg/L	4.0	26.4	25.8	26.1	26.1	26.2	25.7	25.0	24.9	24.5	25.0
Selenium (Se)-Dissolved	mg/L	0.010	0.0200	0.0100	0.0100	0.0200	0.0200	0.0100	0.0100	0.0100	0.0100	0.0100
Silicon (Si)-Dissolved	mg/L	0.10	16.3	16.0	15.9	15.8	15.7	0.690	0.700	0.730	0.760	0.780
Silver (Ag)-Dissolved	mg/L	0.00010	0.000200	0.000100	0.000100	0.000200	0.000200	0.000100	0.000100	0.000100	0.000100	0.000100
Sodium (Na)-Dissolved	mg/L	4.0	36.8	35.7	35.9	36.2	36.0	35.6	34.3	34.0	33.4	33.8
Strontium (Sr)-Dissolved	mg/L	0.0010	1.74	1.68	1.72	1.85	1.88	2.28	2.14	2.19	2.27	2.36
Thallium (Tl)-Dissolved	mg/L	0.0010	0.00200	0.00100	0.00100	0.00200	0.00200	0.00100	0.00100	0.00100	0.00100	0.00100
Tin (Sn)-Dissolved	mg/L	0.0010	0.00200	0.00100	0.00100	0.00200	0.00200	0.00100	0.00100	0.00100	0.00100	0.00100
Titanium (Ti)-Dissolved	mg/L	0.020	0.0250	0.0250	0.0260	0.0250	0.0250	0.0280	0.0280	0.0270	0.0290	0.0280
Uranium (U)-Dissolved	mg/L	0.00010	0.0151	0.0139	0.0142	0.0148	0.0142	0.00112	0.00100	0.000940	0.000730	0.000670
Vanadium (V)-Dissolved	mg/L	0.010	0.0200	0.0100	0.0100	0.0200	0.0200	0.0100	0.0100	0.0100	0.0100	0.0100
Zinc (Zn)-Dissolved	mg/L	0.010	70.2	48.3	47.3	49.5	48.4	0.0100	0.0100	0.0120	0.0100	0.0100

Note:

Blue print are values below the analytical detection limit;

* Differences are between maximum and minimum values for influent and effluent to demonstrate range in quality.

Appendix A.7 Influent and Effluent Water Chemistry for Sullivan Mine HDS Process

ALS File No. L889787

Sullivan Mine	Difference %		Units	Influent					Effluent				
	Influent	Effluent		16-May-10	17-May-10	18-May-10	19-May-10	20-May-10	16-May-10	17-May-10	18-May-10	19-May-10	20-May-10
Physical Tests													
Conductivity	3.30	2.99	uS/cm	5060	5100	5170	5200	5230	4670	4680	4750	4690	4610
Hardness (as CaCO3)	6.10	1.85	mmol/L	33.4	34.0	34.5	35.4	35.5	38.2	37.5	37.9	37.5	37.5
pH	3.80	1.52	pH	3.10	3.16	3.21	3.22	3.22	8.60	8.62	8.64	8.51	8.58
Anions and Nutrients													
Acidity (as CaCO3)	8.09	0.000	mmol/L	8.61	8.42	8.10	8.09	7.94	0.00999	0.00999	0.00999	0.00999	0.00999
Alkalinity, Total (as CaCO3)	0.000	5.86	mmol/L	0.0200	0.0200	0.0200	0.0200	0.0200	0.399	0.404	0.400	0.381	0.390
Bromide (Br)	0.000	0.000	mmol/L	0.0626	0.0626	0.0626	0.0626	0.0626	0.0626	0.0626	0.0626	0.0626	0.0626
Chloride (Cl)	0.000	0.000	mmol/L	1.41	1.41	1.41	1.41	1.41	1.41	1.41	1.41	1.41	1.41
Fluoride (F)	7.54	16.9	mmol/L	0.123	0.118	0.114	0.117	0.117	0.0642	0.0632	0.0616	0.0563	0.0542
Nitrate (as N)	0.000	13.1	mmol/L	0.0357	0.0357	0.0357	0.0357	0.0357	0.0357	0.0357	0.0357	0.0407	0.0357
Nitrite (as N)	0.000	0.000	mmol/L	0.00714	0.00714	0.00714	0.00714	0.00714	0.00714	0.00714	0.00714	0.00714	0.00714
Ammonia as N	158	24.4	mmol/L	0.0231	0.177	0.0228	0.0251	0.195	0.197	0.154	0.170	0.174	0.175
Sulfate (SO4)	4.63	1.35	mmol/L	41.7	42.4	42.9	43.2	43.7	38.3	38.4	38.8	38.7	38.7
Dissolved Metals													
Aluminum (Al)-Dissolved	37.2	104	mmol/L	0.993	0.700	0.682	0.704	0.686	0.00130	0.00111	0.00104	0.000445	0.000408
Antimony (Sb)-Dissolved	66.7	0.000	mmol/L	0.0000164	0.00000821	0.00000821	0.0000164	0.0000164	0.00000821	0.00000821	0.00000821	0.00000821	0.00000821
Arsenic (As)-Dissolved	22.2	0.000	mmol/L	0.0000267	0.0000214	0.0000227	0.0000267	0.0000267	0.0000133	0.0000133	0.0000133	0.0000133	0.0000133
Barium (Ba)-Dissolved	16.8	16.8	mmol/L	0.000108	0.0000910	0.0000947	0.0000939	0.0000925	0.0000954	0.0000910	0.0000947	0.0000998	0.000108
Beryllium (Be)-Dissolved	66.7	0.000	mmol/L	0.00111	0.000555	0.000555	0.00111	0.00111	0.000555	0.000555	0.000555	0.000555	0.000555
Bismuth (Bi)-Dissolved	66.7	0.000	mmol/L	0.0000479	0.0000239	0.0000239	0.0000479	0.0000479	0.0000239	0.0000239	0.0000239	0.0000239	0.0000239
Boron (B)-Dissolved	50.0	0.000	mmol/L	0.0185	0.0111	0.0111	0.0185	0.0185	0.00925	0.00925	0.00925	0.00925	0.00925
Cadmium (Cd)-Dissolved	23.2	21.1	mmol/L	0.000560	0.000464	0.000445	0.000459	0.000444	0.00000187	0.00000160	0.00000151	0.00000151	0.00000151
Calcium (Ca)-Dissolved	7.27	4.99	mmol/L	7.98	7.93	8.06	8.53	8.21	18.8	18.5	18.7	19.5	19.3
Chromium (Cr)-Dissolved	66.7	0.000	mmol/L	0.000192	0.0000962	0.0000962	0.000192	0.000192	0.0000962	0.0000962	0.0000962	0.0000962	0.0000962
Cobalt (Co)-Dissolved	19.5	0.000	mmol/L	0.00154	0.00129	0.00127	0.00132	0.00130	0.0000170	0.0000170	0.0000170	0.0000170	0.0000170
Copper (Cu)-Dissolved	22.2	0.000	mmol/L	0.00162	0.00133	0.00130	0.00135	0.00130	0.0000157	0.0000157	0.0000157	0.0000157	0.0000157
Iron (Fe)-Dissolved	5.85	0.000	mmol/L	4.46	4.51	4.58	4.71	4.73	0.00107	0.00107	0.00107	0.00107	0.00107
Lead (Pb)-Dissolved	12.3	0.000	mmol/L	0.000133	0.000118	0.000119	0.000125	0.000124	0.00000241	0.00000241	0.00000241	0.00000241	0.00000241
Lithium (Li)-Dissolved	9.74	6.30	mmol/L	0.0202	0.0183	0.0192	0.0202	0.0187	0.0186	0.0177	0.0184	0.0184	0.0189
Magnesium (Mg)-Dissolved	6.88	6.84	mmol/L	25.4	26.0	26.4	26.9	27.2	19.3	19.0	19.2	18.0	18.1
Manganese (Mn)-Dissolved	34.7	71.1	mmol/L	1.03	0.728	0.743	0.805	0.805	0.0206	0.0186	0.0169	0.0101	0.00977
Molybdenum (Mo)-Dissolved	66.67	0.00	mmol/L	0.0	0.0	0.0	0.0	0.0	0.0	0.0	0.0	0.0	0.0
Nickel (Ni)-Dissolved	22.2	0.000	mmol/L	0.00239	0.00194	0.00191	0.00198	0.00194	0.0000852	0.0000852	0.0000852	0.0000852	0.0000852
Phosphorus (P)-Dissolved	0.000	0.000	mmol/L	0.0194	0.0194	0.0194	0.0194	0.0194	0.0194	0.0194	0.0194	0.0194	0.0194
Potassium (K)-Dissolved	2.30	4.78	mmol/L	0.675	0.660	0.668	0.668	0.670	0.657	0.639	0.637	0.627	0.639
Selenium (Se)-Dissolved	66.7	0.000	mmol/L	0.000253	0.000127	0.000127	0.000253	0.000253	0.000127	0.000127	0.000127	0.000127	0.000127
Silicon (Si)-Dissolved	3.75	12.2	mmol/L	0.580	0.570	0.566	0.563	0.559	0.0246	0.0249	0.0260	0.0271	0.0278
Silver (Ag)-Dissolved	66.7	0.000	mmol/L	0.00000185	0.000000927	0.000000927	0.00000185	0.00000185	0.000000927	0.000000927	0.000000927	0.000000927	0.000000927
Sodium (Na)-Dissolved	3.03	6.38	mmol/L	1.60	1.55	1.56	1.57	1.57	1.55	1.49	1.48	1.45	1.47
Strontium (Sr)-Dissolved	11.2	9.78	mmol/L	0.0199	0.0192	0.0196	0.0211	0.0215	0.0260	0.0244	0.0250	0.0259	0.0269
Thallium (Tl)-Dissolved	66.7	0.000	mmol/L	0.00000979	0.00000489	0.00000489	0.00000979	0.00000979	0.00000489	0.00000489	0.00000489	0.00000489	0.00000489
Tin (Sn)-Dissolved	66.7	0.000	mmol/L	0.0000168	0.00000842	0.00000842	0.0000168	0.0000168	0.00000842	0.00000842	0.00000842	0.00000842	0.00000842
Titanium (Ti)-Dissolved	3.92	7.14	mmol/L	0.000522	0.000522	0.000543	0.000522	0.000522	0.000585	0.000585	0.000564	0.000606	0.000585
Uranium (U)-Dissolved	8.28	50.3	mmol/L	0.0000634	0.0000584	0.0000597	0.0000622	0.0000597	0.00000471	0.00000420	0.00000395	0.00000307	0.00000281
Vanadium (V)-Dissolved	66.7	0.000	mmol/L	0.000393	0.000196	0.000196	0.000393	0.000393	0.000196	0.000196	0.000196	0.000196	0.000196
Zinc (Zn)-Dissolved	39.0	18.2	mmol/L	1.07	0.739	0.723	0.757	0.740	0.000153	0.000153	0.000184	0.000153	0.000153

Note:

Blue print are values below the analytical detection limit:

* Differences are between maximum and minimum values for influent and effluent to demonstrate range in quality.

Appendix B-1: Solid Phase Elements in Neutralization Sludge Samples

Element	Unit	Equity		Geco	Britannia	Brunswick	Chisel North	Samatosum	Sullivan	
		EQM-1 (LDS)	EQM-2	GM	Brit. M	Brun. M	CNM	Sama. M	Sull. M new	Sull. M old
Al	%	1.9	4.02	0.26	5.56	0.19	0.21	0.52	1.45	3.75
Ca	%	16.5	13.9	10	13.2	15.8	14.6	11.5	8.49	3.42
Fe	%	4.1	4.34	26.2	0.69	10.99	9.42	10.63	11.49	15.31
Mg	%	1.4	2.49	0.34	3.45	0.94	2.31	6.14	6.78	6.85
P	%	0.14	0.13	0.001	0.008	0.002	0.007	0.13	0.008	0.022
K	%	0.004	<0.01	<0.01	<0.01	0.01	0.01	<0.01	<0.01	<0.01
Si	%	0.2	0.29	0.35	ND	ND	ND	ND	ND	ND
Na	%	<0.02	0.006	0.005	0.006	0.4	0.11	0.004	<0.01	<0.001
S	%	ND	11.6	7.36	1.13	1.61	1.06	6.02	3.5	1.64
Ti	%	0.01	0.001	0.002	0.002	0.003	0.004	0.002	0.003	0.002
LOI	%	15	ND	ND	36.2	32.4	35.2	31.2	34.0	34.0
As	ppm	572	267	<0.5	6.7	19.8	3	168	3.8	11
Sb	ppm	ND	2.9	<0.1	0.1	52.2	<0.1	5.9	1.1	7.0
Ba	ppm	2.0	1.0	5.0	9.0	56	152	10	19	14
Bi	ppm	ND	<0.1	<0.1	<0.1	0.1	<0.1	<0.1	<0.1	0.1
B	ppm	ND	<20	<20	5.56	0.19	0.21	0.52	<20	<20
Cd	ppm	ND	58.2	6.8	262	85.1	150	57.1	37	84.3
Cr	ppm	15.7	12.0	2.0	3.0	2.0	6.0	23.0	3.0	1.0
Co	ppm	80.9	184	4.2	143	447	292	161	49.2	105
Cu	ppm	4,900	2,693	72.7	50,340	1,470	430	1,430	54	117
Ga	ppm	ND	<1	<1	<1	<1	<1	<1	1	2
Au	ppm	ND	1.8	2.1	1.4	1,667	2.5	8.5	2.0	11.1
La	ppm	ND	5.0	24.0	51.0	7.0	101	5.0	119	250
Pb	ppm	12.9	0.3	2.6	150	392	5.5	45.4	440	3,569
Mn	ppm	6,400	6,956	1,880	11,400	27,700	9,140	4,435	21,700	20,600
Hg	ppm	ND	<0.01	<0.01	<0.01	0.1	0.02	0.02	0.01	0.06
Mo	ppm	ND	0.5	0.3	0.4	0.9	0.3	1.3	0.6	0.9
Ni	ppm	460	368	9.2	112	102	201	511	73.5	170
Sc	ppm	ND	5.0	0.2	1.7	0.3	0.3	2.8	1.7	6.1
Se	ppm	ND	1.3	0.9	3.4	5.2	5.5	1.6	2.3	5.3
Ag	ppm	ND	<0.1	<0.1	0.2	109	<0.1	0.3	<0.1	0.3
Sr	ppm	432	405	120	346	99.0	866	430	130	48.0
Tl	ppm	ND	<0.1	<0.1	<0.1	2.6	<0.1	0.2	0.003	2.0
Th	ppm	ND	1.3	0.3	<0.1	0.1	0.1	2.5	5.4	37.5
W	ppm	ND	<0.1	<0.1	<0.1	<0.1	<0.1	<0.1	<0.1	0.2
U	ppm	ND	7.7	3.1	3.0	0.9	1.4	18.9	9.9	31.2
V	ppm	18.6	18	2.0	15.0	21.0	<2	23.0	3.0	2.0
Zn	ppm	7,500	6,317	2,743	52,800	122,600	131,800	20,400	29,100	53,600

Notes: ND = no data; LOI = loss on ignition

Appendix B-2: Molar Concentrations of Solid Phase Elements in Neutralization Sludge Samples

Element	Unit	Equity		Geco	Britannia	Brunswick	Chisel North	Samatosum	Sullivan	
		EQM-1 (LDS)	EQM-2	GM	Brit. M	Brun. M	CNM	Sama. M	Sull. M new	Sull. M old
Al	mmol/kg	704	1490	96.4	2061	70.4	77.8	193	537	1390
Ca	mmol/kg	4117	3468	2495	3294	3942	3643	2869	2118	853
Fe	mmol/kg	734	777	4692	124	1968	1687	1903	2057	2742
Mg	mmol/kg	576	1024	140	1419	387	950	2526	2790	2818
P	mmol/kg	45.2	42.0	0.323	2.58	0.646	2.26	42.0	2.58	7.10
K	mmol/kg	1.02	2.56	2.56	2.56	2.56	2.56	2.56	2.56	2.56
Si	mmol/kg	71.2	103	125	ND	ND	ND	ND	ND	ND
Na	mmol/kg	8.70	2.61	2.17	2.61	174	47.8	1.74	4.35	0.435
S	mmol/kg	ND	3618	2295	352	502	331	1877	1092	511
Ti	mmol/kg	2.09	0.209	0.418	0.418	0.627	0.836	0.418	0.627	0.418
LOI										
As	mmol/kg	7.63	3.56	0.00667	0.0894	0.264	0.0400	2.24	0.0507	0.147
Sb	mmol/kg	ND	0.0238	0.000821	0.000821	0.429	0.000821	0.0485	0.00903	0.0575
Ba	mmol/kg	0.0146	0.00728	0.0364	0.0655	0.408	1.11	0.0728	0.138	0.102
Bi	mmol/kg	ND	0.000479	0.000479	0.000479	0.000479	0.000479	0.000479	0.000479	0.000479
B	mmol/kg	ND	1.85	1.85	0.514	0.0176	0.0194	0.0481	1.85	1.85
Cd	mmol/kg	ND	0.518	0.0605	2.33	0.757	1.33	0.508	0.329	0.750
Cr	mmol/kg	0.302	0.231	0.0385	0.0577	0.0385	0.115	0.442	0.0577	0.0192
Co	mmol/kg	1.37	3.12	0.0713	2.43	7.58	4.95	2.73	0.835	1.78
Cu	mmol/kg	77.1	42.4	1.14	792	23.1	6.77	22.5	0.850	1.84
Ga	mmol/kg	ND	0.0143	0.0143	0.0143	0.0143	0.0143	0.0143	0.0143	0.0287
Au	mmol/kg	ND	0.00914	0.0107	0.00711	8.46	0.0127	0.0431	0.0102	0.0563
La	mmol/kg	ND	0.0360	0.173	0.367	0.0504	0.727	0.0360	0.857	1.80
Pb	mmol/kg	0.0623	0.00145	0.0125	0.724	1.89	0.0265	0.219	2.12	17.2
Mn	mmol/kg	116	127	34.2	208	504	166	80.7	395	375
Hg	mmol/kg	ND	0.0000499	0.0000499	0.0000499	0.000499	0.0000997	0.0000997	0.0000499	0.000299
Mo	mmol/kg	ND	0.00521	0.00313	0.00417	0.00938	0.00313	0.0135	0.00625	0.00938
Ni	mmol/kg	7.84	6.27	0.157	1.91	1.74	3.42	8.71	1.25	2.90
Sc	mmol/kg	ND	0.111	0.00445	0.0378	0.00667	0.00667	0.0623	0.0378	0.136
Se	mmol/kg	ND	0.0165	0.0114	0.0431	0.0659	0.0697	0.0203	0.0291	0.0671
Ag	mmol/kg	ND	0.000927	0.000927	0.00185	1.01	0.000927	0.00278	0.000927	0.00278
Sr	mmol/kg	4.93	4.62	1.37	3.95	1.13	9.88	4.91	1.48	0.548
Tl	mmol/kg	ND	0.000489	0.000489	0.000489	0.0127	0.000489	0.000979	0.0000147	0.00979
Th	mmol/kg	ND	0.00560	0.00129	0.000431	0.000431	0.000431	0.0108	0.0233	0.162
W	mmol/kg	ND	0.000544	0.000544	0.000544	0.000544	0.000544	0.000544	0.000544	0.00109
U	mmol/kg	ND	0.0323	0.0130	0.0126	0.00378	0.00588	0.0794	0.0416	0.131
V	mmol/kg	0.365	0.353	0.0393	0.294	0.412	0.0393	0.451	0.0589	0.0393
Zn	mmol/kg	115	96.6	42.0	808	1875	2016	312	445	820

Notes: ND = no data; LOI = loss on ignition